School of Science and Engineering
Department of Civil Engineering

Laboratory Stiffness Characterization of Western Australia Asphalt Mixtures

Gunawan Wibisono

This thesis is presented for the Degree of
Doctor of Philosophy
of
Curtin University

May 2014

DECLARATION

To the best of my knowledge and belief this thesis contains no material previously published by any other person except where due acknowledgement has been made.

This thesis contains no material which has been accepted for the award of any other degree or diploma in any university.

Signature

Gunawan Wibisono

Date: May 2014

ABSTRACT

Stiffness is an important input in mechanistic-empirical design method to determine the required thickness of the asphalt pavement. In terms of stiffness of Western Australian asphalt mixtures, a limited number of publications were available. The Western Australia road network is prevalent to early damage such as fatigue cracking and permanent deformation. Hence, a study on stiffness is essential when material suitability and environmental effects have a significant impact on asphalt pavement design. This study presents results from an experimental work on the stiffness characterization of hot mix asphalt for Western Australian mixtures. Five dense-graded mixtures with varying nominal maximum aggregate sizes, asphalt grades, and air voids were designed using Main Roads Western Australia Specification. Laboratory stiffness tests were determined from creep, resilient modulus, flexural fatigue, and dynamic modulus of the mixtures. In addition MEPDG Witczak and Hirsch predictive models were used to compare the measured and predictive dynamic modulus master curve. It can be summarised from creep test, both mixes AC14-320 and AC20-320 are classified suitable for medium and heavy traffic application, respectively. The AC20-320 has the highest resistant to permanent deformation. The resilient modulus values for WA mixes in this research are acceptable and the values were still within the lower part of Austroads presumptive values range. The AC20-320 had the highest resilient modulus due to the higher particle-to-particle contact in the mixture. Since there was limited data for beam fatigue test, mix AC14-320 had the highest flexural stiffness despite a considerable variability in the results. A study on the dynamic modulus of WA asphalt mixtures demonstrated mixes with higher binder grade, higher nominal maximum aggregate size, and lower air voids were stiffer than other mixes. Both the Witczak and Hirsch models were able to indicate the dynamic values with considerable reliability. It can be concluded that the WA mixtures satisfied stiffness criteria for asphalt pavement construction.

ACKNOWLEDGEMENT

I would like to thank my supervisor, Prof Hamid R Nikraz, for his help and guidance throughout my study. I would like to express my gratitude for Curtin Pavement Research Group (Curtin-PRG): Dr Peerapong Jitsangiam, A/Prof Collin Leek, Dr Komsun Siripun, Mr Darren Isaac, Mr Mark Whittaker, and Mr Ashley Hughes. Also, I would like to thank Directorate General of Higher Education Indonesia for the scholarships, and Universitas Riau as my home base university in Indonesia for its kind supports. I thank all my friends in Perth: Dr Hendra Jitno, Dr Edy Saputra, Dr Isnandar Slamet, Dr Yusep Muslih Purwana, Dr Johny Latuny, Mr M Arief Budiharjo, Mr Muhammad Karami, Mr Bowo Cahyono, Mr Agus Ika Putra, Mr Afiq Julaihi and Mr Yogie Rinaldi Ginting for their encouragement and friendships. Last but not least, I thank my parents, parents in law, family and wife, Dr Monita Olivia MSc, who always supporting me during this PhD journey.

LIST OF PUBLICATIONS

The following publications were produced during my PhD research.

1. Wibisono, G, Nikraz, HR, Jitsangiam, P, and Isaac, D, 2013, "Dynamic Modulus of Western Australia Asphalt Wearing Course", in Proceedings of the 9th International Conference on Geo-technical & Transportation Engineering (GEOTROPIKA) and The 1st International Conference on Construction and Building Engineering (ICONBUILD), October 2013, Johor.

2. Wibisono, G and Nikraz, HR, 2014, "Dynamic Modulus of Western Australia Asphalt Wearing Course", Jurnal Teknologi Malaysia, Volume 71 No.3, DOI: http://dx.doi.org/10.11113/jt.v71.3759.

TABLE OF CONTENTS

DECLARATION i
ABSTRACT ii
ACKNOWLEDGEMENTS iii
LIST OF PUBLICATIONS iv
TABLE OF CONTENTS v
LIST OF FIGURES viii
LIST OF TABLES xi
LIST OF SYMBOLS xiii
LIST OF ABBREVIATIONS xv
1 INTRODUCTION 1
1.1 Background 1
1.2 Research Significance 2
1.3 Scope and Research Objectives 3
1.4 Thesis Structure 3
2 LITERATURE REVIEW 6
2.1 Introduction 6
2.2 Asphalt Binder 8
2.2.1 Bitumen 8
2.2.2 Aggregates 9
2.2.3 Air Voids 12
2.2.4 Filler 12
2.3 Asphalt Pavement Distress 13
2.3.1 Major Distress Mechanisms 13
2.3.2 Fatigue Cracking 14
2.3.3 Permanent Deformation or Rutting 16
2.3.4 Stripping (Moisture Damage) 19
2.3.5 Thermal Cracking 21
2.4 Structural Design Of Flexible Pavement 22
2.4.1 Overview of the Austroads Guide to Pavement Technology 2008 24
2.4.2 Overview of MEPDG 2004 27
2.5 Asphalt Stiffness Prediction 31
2.5.1 The Importance of Asphalt Stiffness 31
2.5.2 Factors Affecting Asphalt Stiffness 33
2.5.3 Asphalt Performance and Stiffness 37

2.5.3.1 Creep 38
2.5.3.2 Resilient Modulus 39
2.5.3.3 Flexural Stiffness (Modulus) 43
2.5.3.4 Dynamic Modulus 43
2.5.4 Asphalt Stiffness Prediction 50
2.5.4.1 Fatigue Life 50
2.5.4.2 Dynamic Modulus Predictive Models 55
2.5.4.3 Statistical Assessment of Dynamic Modulus Predictive Models 58
2.6 Summary 60
2.6.1 Research Needs 60
2.6.2 Research Objectives 61
3 RESEARCH METHODOLOGY 62
3.1 Introduction 62
3.2 Material Properties 63
3.2.1 Bitumen 63
3.2.2 Aggregates 63
3.2.3 Hydrated Lime 65
3.2.4 Baghouse Dust 66
3.3 Mixture Proportions 66
3.4 Specimen Fabrication 68
3.4.1 Batching 68
3.4.2 Mixing 68
3.4.3 Conditioning 70
3.4.4 Compaction 70
3.4.4.1 Marshall Compaction 70
3.4.4.2 Gyratory Compaction 72
3.4.4.3 Slab Compactor 73
3.5 Asphalt Performance and Stiffness Characterization 75
3.5.1 Volumetric Properties 75
3.5.2 Experimental Design 75
3.5.3 Creep Test 77
3.5.4 Indirect Tensile Test (ITT) 79
3.5.5 Beam Fatigue Test 82
3.5.6 Dynamic Modulus Test 84
4 RESULTS AND DISCUSSION 90
4.1 Introduction 90
4.2 Aggregate Properties 90

4.2.1 Physical Properties 90
4.2.2 Gradation 91
4.2.3 Volumetric Properties 93
4.3 Asphalt Performance and Stiffness Characterization 94
4.3.1 Creep 94
4.3.2 Resilient Modulus 96
4.3.3 Flexural Fatigue 98
4.3.4 Dynamic Modulus (|*E**|) of Western Australian Asphalt Mixture 100
4.3.4.1 Dynamic Modulus 101
4.3.4.2 Construction of |*E**| master curve 104
4.3.4.3 Evaluation of factors influencing measured |*E**| values 109
4.3.4.4 Phase angle and black space 114
4.3.4.5 Comparison of predicted and measured dynamic modulus master curve 116
4.3.4.6 Statistical analysis of predicted and measured values of dynamic modulus 128
4.3.4.7 Comparison of dynamic modulus with resilient modulus 136
5 CONCLUSIONS AND RECOMMENDATIONS 138
5.1 Introduction 138
5.2 Conclusions 138
5.3 Recommendations 140
6 REFERENCES 142
APPENDICES

LIST OF FIGURES

Figure 1.1	Thesis map	5
Figure 2.1	Layout of literature review	7
Figure 2.2	Aggregate interlock mechanism (Somayaji 2001)	10
Figure 2.3	Comparison of asphalt gradation (Austroads 2002)	10
Figure 2.4	Critical stresses and strains in an asphalt pavement (Powell et al. 1984)	14
Figure 2.5	Bottom-up fatigue cracking (NCHRP 2004b)	15
Figure 2.6	Top-down fatigue cracking (NCHRP 2004b)	16
Figure 2.7	Permanent deformation (Read and Whiteoak 2003)	17
Figure 2.8	Types and mechanisms of rutting in flexible pavements in MEPDG 2004, (a) one-dimensional densification or vertical compression, (b) lateral displacement or two dimensional plastic movement (NCHRP 2004b)	17
Figure 2.9	Thermal cracking mechanism (Read and Whiteoak 2003)	21
Figure 2.10	Sample interconversion between dynamic modulus and creep compliance (Yin et al. 2010)	22
Figure 2.11	Fundamental pavement responses as a function of load, material properties and layer thicknesses – the mechanistic aspect (Haas and Tighe 2007)	23
Figure 2.12	Correlated pavement performance from mechanistic responses – the empirical aspect (Haas and Tighe 2007)	23
Figure 2.13	Pavement response model (Austroads 2008c)	25
Figure 2.14	Design procedure for flexible pavements (Austroads 2008c)	26
Figure 2.15	Overall design process for flexible pavements (NCHRP 2004b)	28
Figure 2.16	Pavement strains under traffic loading (Austroads 2006b)	31
Figure 2.17	The load spreading principle (Nunn 1998)	32
Figure 2.18	Conceptual stiffness and strength criteria (Pellinen 2004)	33
Figure 2.19	Asphalt damage dependence on temperature and loading rate (Lytton 2009)	35
Figure 2.20	Strains under repeated load (Huang 2004)	40
Figure 2.21	Dynamic modulus (Witczak and Bari 2004)	44
Figure 2.22	Asphalt mixture stress-strain responses under a sinusoidal load for different viscoelastic behaviour (Biligiri, Kaloush and Uzan 2010)	46
Figure 2.23	Samples of fitted master curve for various mixes used in the study (Zhu et al. 2011).	48
Figure 2.24	The influence of asphalt layer thickness on fatigue life (Said et al. 2011)	51
Figure 2.25	Laboratory fatigue and field fatigue considerations (Rajbongshi 2009)	54
Figure 2.26	Illustration of bias and precision (Tran 2005)	59
Figure 3.1	Layout of the research plan.	62
Figure 3.2	Grading curves of each nominal maximum aggregate size.	65

Figure 3.3	Grading envelopes of MRWA specifications	67
Figure 3.4	Planetary mixer with 6 kg mixing capacity	69
Figure 3.5	Loose asphalt concrete after mixing process	69
Figure 3.6	Splitting: (a) quartering mixtures, (b) quarter samples for conditioning	70
Figure 3.7	Marshall Test: (a) Marshall test rig, (b) specimen under stability and flow test	71
Figure 3.8	Gyratory compaction: (a) Gyratory compactor, (b) Gyratory mould	72
Figure 3.9	Variation of air voids with gyration cycles	73
Figure 3.10	Slab compactor: (a) rolling compactor, (b) specimen under compaction	74
Figure 3.11	Beam fatigue test: (a) Autosaw machine, (b) beam samples	77
Figure 3.12	Creep test set up	78
Figure 3.13	Typical creep test result.	79
Figure 3.14	Indirect tensile test; IPC UTM-14 apparatus and environmental chamber	80
Figure 3.15	Indirect tensile (resilient modulus) test set up	80
Figure 3.16	Typical indirect tensile test result	81
Figure 3.17	Beam fatigue test set up	83
Figure 3.18	Typical result of beam fatigue test	84
Figure 3.19	Dynamic modulus test set up with three on-specimen LVDTs	85
Figure 3.20	Dynamic modulus gauge point fixing jig	86
Figure 3.21	Example of dynamic modulus test result	86
Figure 3.22	Typical dynamic modulus data at various temperature and loading frequencies	89
Figure 4.1	Grading of AC10-170 and AC10-320	92
Figure 4.2	Grading of AC14-320	92
Figure 4.3	Grading of AC20-320	93
Figure 4.4	Plot of average minimum slopes and cycles at minimum slope with variation of air voids	95
Figure 4.5	Resilient modulus values with various maximum aggregate sizes and air void contents	97
Figure 4.6	Flexural stiffness vs loading cycles for mix AC10-320	99
Figure 4.7	Typical shift factors for mixes AC10-320, AC14-320 and AC20-320	105
Figure 4.8	Effect of air voids on dynamic modulus for mix AC-170	109
Figure 4.9	Effect of air voids on dynamic modulus for mix AC10-320	110
Figure 4.10	Effect of maximum aggregate size, binder type and binder conditioning on dynamic modulus for 5% air voids mixtures a) Original binder, b) RTFOT binder	112
Figure 4.11	Effect of maximum size, aggregate binder type and binder conditioning on dynamic modulus for 7% air voids mixtures a) Original binder, b) RTFOT binder	113
Figure 4.12	Measured phase angle master curves for 5% air void content	114

Figure 4.13	Measured phase angle master curves for 7% air void content	115
Figure 4.14	Black space diagram for all mixtures	116
Figure 4.15	Comparison of developed master curves with Witczak's predictive equation for mixes AC10-170	119
Figure 4.16	Comparison of developed master curves with Witczak's predictive equation for mixes AC10-320	120
Figure 4.17	Comparison of developed master curves with Witczak's predictive equation for mixes AC14-320	121
Figure 4.18	Comparison of developed master curves with Witczak's predictive equation for mixes AC20-320	122
Figure 4.19	Comparison of developed master curves with Hirsch's predictive equation for mixes AC10-170	124
Figure 4.20	Comparison of developed master curves with Hirsch's predictive equation for mixes AC10-320	125
Figure 4.21	Comparison of developed master curves with Hirsch's predictive equation for mixes AC14-320	126
Figure 4.22	Comparison of developed master curves with Hirsch's predictive equation for mixes AC20-320	127
Figure 4.23	Comparison of measured and predicted dynamic modulus by Witczak equation	129
Figure 4.24	Comparison of measured and predicted dynamic modulus by modified Witczak equation	131
Figure 4.25	Comparison of measured and predicted dynamic modulus by Hirsch equation	133
Figure 4.26	Comparison between resilient modulus and dynamic modulus	137

LIST OF TABLES

Table 2.1	Bitumen classes (Austroads 2006a)	9
Table 2.2	Typical mix sizes for various applications (Austroads 2006a)	11
Table 2.3	Distress modes for flexible pavement (Austroads 2008c)	14
Table 2.4	The effect of material and other variables on rutting susceptibility adapted from Sousa, Craus and Monismith, 1991 (Al-Khateeb and Basheer 2009)	18
Table 2.5	Material properties and external factors that can affect the bitumen/aggregate bond (Read and Whiteoak 2003)	20
Table 2.6	Summary comparison of the mechanistic-empirical approaches	30
Table 2.7	Factors affecting stiffness of asphalt and effect of increasing factor values (Austroads 2008c)	34
Table 2.8	Typical laboratory minimum dynamic creep slopes in μm/m/cycle (Austroads 2008e)	39
Table 2.9	Modulus (MPa) of typical Australian dense graded asphalts determined on laboratory-manufactured samples using the indirect tensile test procedure and standard test conditions and 5% air voids (Austroads 2008c)	41
Table 2.10	Typical laboratory resilient modulus values in MPa (Austroads 2008e)	42
Table 2.11	Summary of temperature and frequencies used in some studies	47
Table 2.12	Suggested reliability factors (RF) for asphalt fatigue (Austroads 2008c)	53
Table 2.13	Criteria for goodness of fit	60
Table 3.1	Physical and chemical properties of bitumen (Austroads 2008b)	64
Table 3.2	Physical properties of crushed aggregates (Main Roads Western Australia 2006)	64
Table 3.3	Sieve analysis results for each nominal maximum aggregate size	65
Table 3.4	Physical and chemical properties of hydrated lime*	66
Table 3.5	MRWA grading specification	67
Table 3.6	Volumetric properties of Western Australian mix design	75
Table 3.7	Details of the test specimens	76
Table 3.8	Test program for characterization of asphalt stiffness	76
Table 4.1	Physical properties of coarse and fine aggregates	90
Table 4.2	Aggregate grading combinations	91
Table 4.3	Volumetric properties of Western Australian mixtures	94
Table 4.4	Summary of dynamic creep results	95
Table 4.5	Resilient modulus results from laboratory tests (test temperature of 25^{o}C)	98
Table 4.6	Summary of beam fatigue test	100

Table 4.7	Typical values of dynamic modulus $\|E^*\|$ and phase angle (ϕ) for each different air void content of mix AC10-170	102
Table 4.8	Typical values of dynamic modulus $\|E^*\|$ and phase angle (ϕ) for each different air void content of mix AC10-320	103
Table 4.9	Typical values of dynamic modulus $\|E^*\|$ for each mixture (origin and RTFOT)	104
Table 4.10	Shift factor regressions (AASHTO 2010a)	106
Table 4.11	Shift factor regressions for original binder (AASHTO 2010b)	106
Table 4.12	Shift factor regressions for RTFOT binder (AASHTO 2010b)	106
Table 4.13	Asphalt bitumen properties at various temperatures (original binder)	107
Table 4.14	Asphalt bitumen properties at various temperatures (RTFOT)	107
Table 4.15	Sigmoidal function coefficients for $\|E^*\|$ master curve (AASHTO 2010b)	107
Table 4.16	Sigmoidal function coefficients for $\|E^*\|$ master curve for original binder (AASHTO 2010b)	108
Table 4.17	Sigmoidal function coefficients for $\|E^*\|$ master curve for RTFOT binder (AASHTO 2010b)	108
Table 4.18	Input aggregate gradation for the Witczak predictive model	130
Table 4.19	Performance analysis of mixtures predicted using Witczak's equation	135
Table 4.20	Performance analysis of mixtures predicted using Hirsch's equation	135

LIST OF SYMBOLS

A	regression intercept [dimensionless]
A'	adjusted A (adjusted from loading frequency) [dimensionless]
a_T	shift factor as a function of temperature [dimensionless]
C	laboratory to field adjustment factor [dimensionless]
E	stiffness of the material [M L^{-1} T^{-2}]
$\|E^*\|$	dynamic or complex modulus [M L^{-1} T^{-2}]
f	loading frequency [T^{-1}]
f_s	dynamic shear loading frequency [T^{-1}]
$\|G^*\|_{binder}$	dynamic or complex shear modulus [M L^{-1} T^{-2}]
h_{ac}	total thickness of the asphalt layers [L]
k_1, k_2, k_3	laboratory regression coefficients [dimensionless]
M_R	resilient modulus [M L^{-1} T^{-2}]
N_f	number of repetitions of fatigue cracking [dimensionless]
t	time of loading at a given temperature of interest [T]
T_i	time lag between stress and strain [T]
T_p	period of applied stress [T]
t_r	time of loading at the reference temperature [Θ]
T	temperature of interest [Θ]
T_R	temperature at which the viscosity was estimated (in Rankine scale) [Θ]
V_a	air voids [dimensionless]
V_{beff}	effective binder content [dimensionless]
VTS	regression slope of viscosity temperature susceptibility [dimensionless]
VTS'	adjusted VTS (adjusted from loading frequency) [dimensionless]
P_C	contact factor
VMA	void in the mineral aggregate [dimensionless]
VFA	void filled with asphalt [dimensionless]
α	fitting parameters of sigmoidal functions [dimensionless]
β	parameters describing the shape of sigmoidal functions [dimensionless]
β_1, β_2, β_3	calibration parameters [dimensionless]
δ	fitting parameters of sigmoidal functions [dimensionless]
δ_b	phase angle of bitumen [dimensionless]
ε_0	peak (maximum) recoverable axial strain [dimensionless]
ε_r	plastic strain [dimensionless]
ε_t	tensile strain at the critical location [dimensionless]
ϕ	phase angle of asphalt concrete [dimensionless]

γ	parameters describing the shape of the sigmoidal function [dimensionless]
η	bitumen viscosity [M L^{-1} T^{-1}]
$\eta_{fs,T}$	viscosity of asphalt binder as a function of both loading frequency (f_s) and temperature (T) [M L^{-1} T^{-1}]
σ_d	axial stress in an unconfined compression test [M L^{-1} T^{-2}]
σ_0	peak (maximum) stress [M L^{-1} T^{-2}]
ω	angular velocity [T^{-1}]

LIST OF ABBREVIATIONS

AASHTO	American Association of State Highway and Transportation Officials
AC	Asphalt Concrete
APRG	Austroads Pavement Reference Groups
BBR	Bending Beam Rheometer
BC	Base Course
CBR	California Bearing Ratio
CDAS	Control Data Acquisition System
DSR	Dynamic Shear Rheometer
FWD	Falling Weight Deflectometer
GPC	Gel Permeation Chromatography
HMA	Hot Mix Asphalt
IC	Intermediate Course
INDOT	Indiana Department of Transportation
IRI	International Roughness Index
ITT	Indirect Tensile Test
LVDT	Linear Variable Displacement Transducers
MATTA	Material Testing Apparatus
MBV	Methylene Blue Value
MEPDG	Mechanistic Empirical Pavement Design Guide
MRWA	Main Roads Western Australia
NAASRA	National Association of Australian State Road Authorities
NCHRP	National Cooperative Highway Research Program
NMAS	Nominal Maximum Aggregate Size
PMB	Polymer Modified Binder
RTFOT	Rolling Thin Film Oven Test
VFA	Voids Filled with Asphalt
VMA	Voids in Mineral Aggregates
VTS	Viscosity Temperature Susceptibility
RF	Realiability Factors
SAR	Standard Axle Repetitions
SBS	Styrene Butadiene Styrene
SSD	Saturate Surface Dry
TFOT	Thin Film Oven Test
WC	Wearing Course
WMAPT	Weighted Mean Annual Pavement Temperature

1 INTRODUCTION

1.1 Background

Recent years have seen traffic increase in many countries, as a result of which transportation infrastructure is under pressure to meet service demands. The cost of building new pavement and maintaining existing roads has increased significantly, despite a decrease in infrastructure budgets. Australian governments at the national, state and local levels have dedicated a significant amount of budget annually towards road-related expenditure. This expenditure has increased by an average of more than 8% per year in the last decade and reached $12 billion in the 2006–2007 fiscal years (Bureau of Infrastructure, Transport and Regional Economics 2009). In Western Australia (WA), almost 40% or a major portion of the road-related spending is directed toward road network maintenance (Main Roads Western Australia 2008). Therefore, roads should be properly designed and built in order to address excessive traffic demand, support national economic activities, and accommodate limited public funds by lowering maintenance costs. This can be achieved by applying good principles, implementing proven new concepts and technologies, and researching better materials and methods.

The flexible pavement is mostly used in many countries as an infrastructure component, and in Australia alone, it comprises approximately 300,000 km road network (Jitsangiam, Nikraz and Leek, 2010). Basically, the flexible pavement is made up of several layers, i.e. wearing surface, base, sub base, and subgrade layer, with a combination of materials, such as aggregates, binders, air and any other additive components (Malick and El-Korchi 2009). The structural flexible pavement is designed based on guides and standards and in Australia, the guidelines is prepared by Austroads, the association of Australian and New Zealand road transport and traffic authorities. The guidelines have been improved to alleviate the shortcomings and problems with the previous design approach in project level. Currently, the newly 2008 series of Austroads Guide to Pavement Technology has adopted a mechanistic-empirical approach by incorporating the mechanical properties of the asphalt materials and their associated failure mechanisms such as fatigue cracking, permanent deformation, and creep. A mechanistic-empirical analysis is a principle to design the flexible pavement, which the prediction of pavement responses and performance requires fundamental properties of layer materials. The method is widely used now in many countries to ensure the application of pavement designs with appropriate thickness and stiffness characteristics to prevent premature failure and ensure good long-term performance.

Nevertheless, the structural pavement design faces a new challenge in implementing its application in Western Australia. Western Australia has mild temperate weather with a significant effect on pavement integrity. High temperatures on summer days make asphalt pavement more prone to permanent deformation, and persistent damage is expected during the very rainy winter. A fatigue cracking is reported more prevalent in Western Australia than in other states (Jitsangiam, Nikraz and Leek 2010), and a general structural design approach (Austroads) cannot be applied precisely for this particular state. It becomes important to design the flexible pavement in WA with adequate stiffness or load spreading ability to avoid premature fatigue cracking. The stiffness, a measure of a material's elasticity characteristics and is determined using a stress-strain curve such as with Young's Modulus (Lytton 2009), is an important property in a mechanistic-empirical structural design approach. The stiffness is used to calculate primary pavement responses (deflections, stresses and strains) and distress mechanisms (fracture and flow) of pavements. Fracture or cracking distress is caused by mechanical loading from repetitive traffic, and thermal loading from changes of temperature. Flow or permanent deformation is caused by shear flow where asphalt binder becomes too soft to carry loads at high temperatures (Kim et al. 2009). The stiffness is characterized by complex modulus, resilient modulus, flexural modulus and dynamic modulus. Increasing the asphalt stiffness eventually results in an increase in the load spreading ability, structural strength and expected design life of the pavement. There is little data available from Western Australia-based laboratory measurements (Butcher and Van Loon 2003, Hubner and Jameson 2008), hence, there is a need to investigate the stiffness characteristics of Western Australian asphalt mixture made from local materials and under local conditions.

1.2 Research Significance

Main Roads Western Australia uses its own design guide to accommodate the local conditions and material availability. Environmental effects have a significant impact on asphalt pavement design, based on commonly-occurring pavement distress seen in Western Australia. This is where the stiffness of asphalt pavement becomes a major issue since accurate measurements using these characteristics are still limited. It is therefore essential to obtain data on the typical asphalt modulus of WA pavement using local materials and environmental conditions, and to quantify the potential damage from major pavement distress mechanisms in WA. Further evaluation of data precision by any reliable statistical method is beneficial, to limit the uncertainty of laboratory measurements. To make the data viable in application, a correlation between the laboratory and field measurement must be established. The results can be used to verify and add to the asphalt modulus values listed in

the Australian pavement design guide. This will eventually contribute to the development of a mechanistic empirical pavement design guide and help asphalt industries in Western Australia to properly and efficiently design hot mix asphalt pavements.

1.3 Scope and Research Objectives

The main objective of this research is to study the stiffness characterization of typical Western Australian dense graded asphalt mixtures based on laboratory tests. The detailed objectives of this research are as follows:

a) To measure creep values as a means of characterizing permanent deformation for typical Western Australian mixtures.
b) To investigate resilient modulus for typical Western Australian mixtures and compare the laboratory data to the modulus values listed in the Austroads 2008.
c) To determine flexural fatigue by measuring beam fatigue for typical Western Australian mixtures.
d) To establish the dynamic modulus /E^*/ values for typical asphalt mixes used in Western Australia by measuring the laboratory dynamic modulus and phase angle using normal and Rolling Thin Film Oven Test (RTFOT) aged binders. In addition, the /E^*/ master curves are generated and factors influencing the measured /E^*/ are evaluated.
e) To compare the predicted and measured dynamic modulus master curve using the Mechanistic Empirical Pavement Design Guide (MEPDG) Witczak and Hirsch's predictive models. Validation of the Witczak and Hirsch's model predicted data /E^*/ with laboratory /E^*/ is investigated. Statistical evaluation of Witczak and Hirsch predictive equations is conducted.

1.4 Thesis Structure

There are five chapters in the thesis as can be seen in Figure 1.1.

Chapter 1 presents the background, research significance, objectives of the thesis, and scope of the work.

Chapter 2 gives an overview of asphalt binder in general, the major distress mechanisms of asphalt pavement, fatigue cracking, the pavement design guide, the dynamic modulus master curve, and the comparison and verification of stiffness performance. The aim is to review the stiffness characterization and performance of asphalt mixtures.

Chapter 3 presents the material properties, mix design for Western Australian hot mix asphalt (HMA) mixtures, and the performance testing methods. The aim is to present the research design and laboratory experiments that have been carried out to investigate the stiffness characterization of asphalt mixtures.

Chapter 4 describes and discusses the results of the experimental work and comparison between the measured and predicted values using predictive models. The aim is to display and analyse the data from the experimental work.

Chapter 5 summarizes the results and discussions, and gives recommendations for future work.

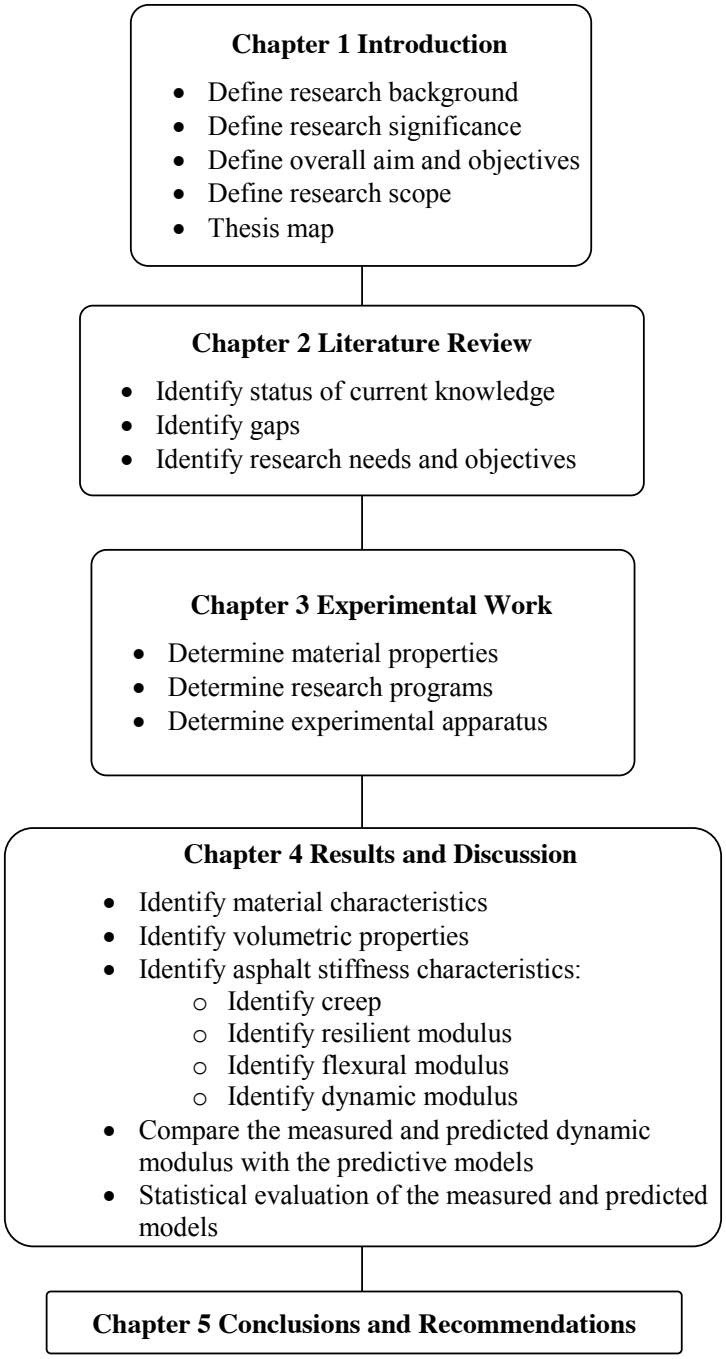

Figure 1.1 Thesis map

2 LITERATURE REVIEW

2.1 Introduction

Asphalt is a viscoelastic material used for the surface course in a flexible pavement. This material has characteristics between viscous and elastic under various environmental conditions and modes of loading. The viscoelastic properties of asphalt make it sensitive to some distress mechanisms such as fatigue cracking and permanent deformation. Previous studies have concluded that the ideal pavement surface must conform to some criteria. Firstly, it must display high elastic stiffness to ensure good load spreading. Secondly, it must have high fatigue strength to prevent the initiation and propagation of cracks due to repetitive loading by traffic. Finally, it must have high resistance to permanent deformation to ensure the layers do not undergo rutting.

This chapter presents an overview of asphalt, major distress mechanisms, flexible pavement design methods and asphalt stiffness characteristics. The review starts with asphalt and its major components such as bitumen, aggregates, lime and filler. Then, some major pavement distresses such as fatigue cracking, permanent deformation, thermal cracking, and stripping are discussed. In order to understand the mechanistic-empirical approach in designing flexible pavement, both Austroads Guide to Pavement Technology Part 2: Pavement Structural Design or Austroads 2008 (Austroads 2008c), and AASHTO Guide for Mechanistic-Empirical Design of New and Rehabilitated Pavement Structures Chapter 3: Design of New and Reconstructed Flexible Pavements or Mechanistic-Empirical Pavement Design Guide (MEPDG) 2004 (NCHRP 2004b) are discussed. Since stiffness is the key issue in this study, asphalt stiffness is reviewed, including its significance, influential factors, laboratory characterization, predictive models and statistical validation. The final section summarizes the research needs and research objectives of the thesis. The layout of this chapter is shown in Figure 2.1.

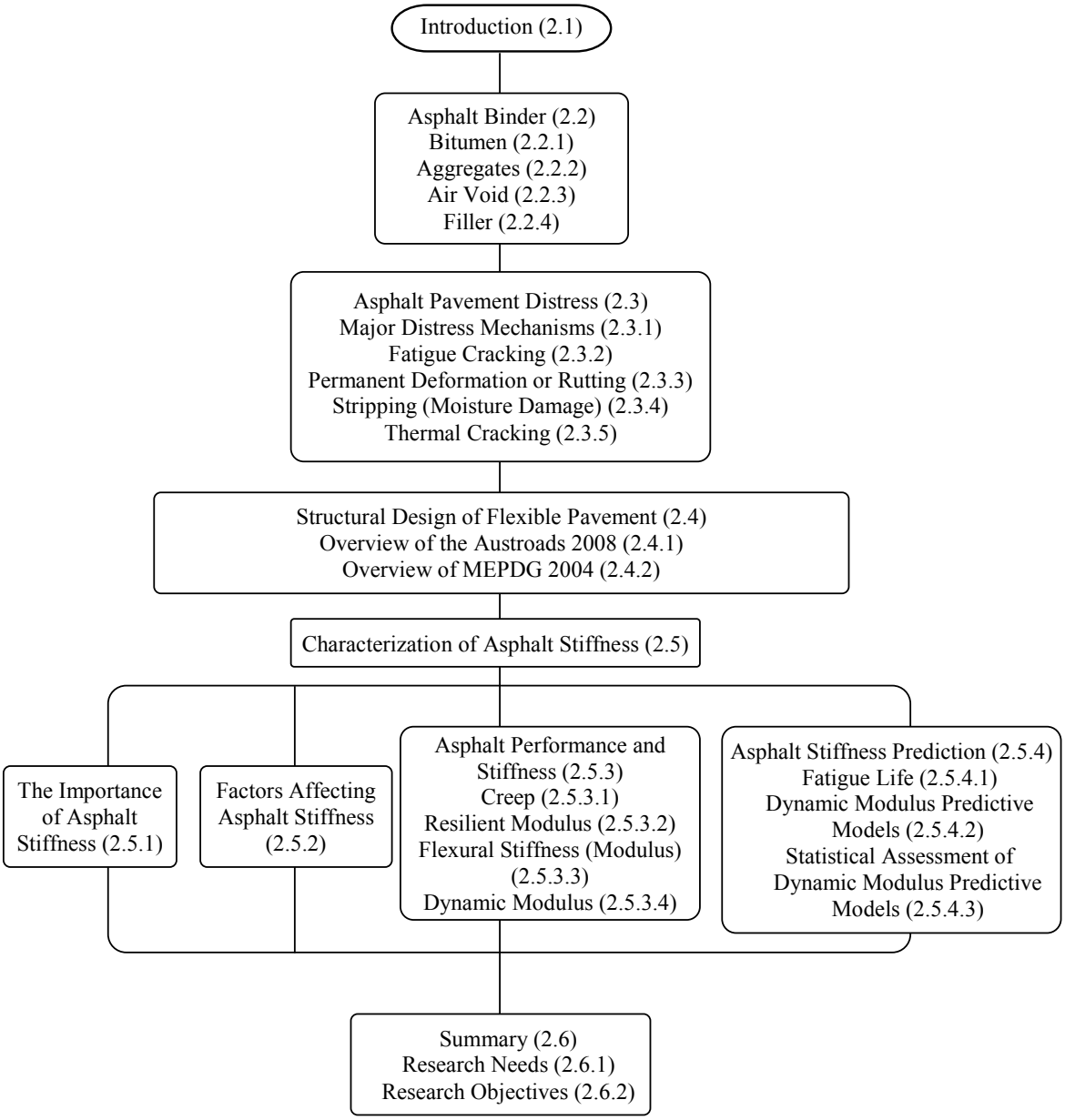

Figure 2.1 Layout of literature review

2.2 Asphalt Binder

2.2.1 Bitumen

Bitumen is mainly composed of various hydrocarbons with minor chemical compounds such as sulphur, nitrogen, oxygen and trace metals. The bitumen constitutes of four broad chemicals, namely asphalthenes that determine the viscous component of bitumen; maltenes; resins; and aromatics that influence the ageing of bitumen (Read and Whiteoak 2003, Somayaji 2001). The consistency of bitumen changes from solid to semisolid due to temperature. At low temperatures, bitumen has a high viscosity since the molecules are motionless. Conversely, as the temperature rises the bitumen viscosity decreases and molecules flow or move freely. This reversible viscosity at different temperatures classifies bitumen as a thermoplastic material.

Bitumen is used in asphalt to hold aggregate particles together by forming a thin film around the particles' surface. Some important properties, namely the physical properties, performance and durability and sensitivity of bitumen need to be considered in asphalt pavement design (Austroads 2008a, Lancaster 2000, Somayaji 2001). The defined physical properties of bituminous binder are consistency, viscosity, specific gravity, solubility and volatility. Second, the performance properties include stiffness at various service temperatures, cohesion, and adhesion. The stiffness relates to the ability of bitumen to provide asphalt with high bearing capacity and adequate resistance to fatigue and permanent deformation. Bitumen must be cohesive enough to bind the minerals and adhesive enough to prevent mineral erosion (fretting). Third, the durability and sensitivity of bitumen to ageing, hardening and weathering occurs in application. Durability is defined as the ability of bitumen to sustain rheology, cohesion and adhesion with time under the threat of hardening due to oxidation from exposure to heat and air (Austroads 2006a). In addition, other properties such as health and safety, environment, and handling are also important in application.

The bitumen used in Australia from the 1960s until the last few years was a product derived from Middle Eastern crude oils. The rationalization of local refineries has encouraged the import of bitumen from several refineries in Asia for domestic pavement applications (Austroads 2008a). There are three types of bitumen, classified according to their origin and application, namely residual bitumen, multigrade bitumen and polymer-modified binder. Residual bitumen is also divided into three grades, namely Class 170, Class 320 and Class 600 (Austroads 2006a, Austroads 2008b). Bitumen Class 170 is best suited for making workable and durable mixes for low traffic applications and cool climate zones. Class 320 is

the bitumen most commonly used in asphalt manufacture because it offers great resistance to rutting and deformation at high temperatures. Class 600 bitumen provides high stiffness in base course and heavy-duty asphalt base layers. Both multigrade bitumen and polymer-modified binder (PMB) are used in Australia for specific purposes. Multigrade bitumen increases temperature susceptibility, while the polymer-modified binder improves binder toughness, elasticity or temperature susceptibility. The residual bitumen grades and properties are presented in Table 2.1.

Table 2.1 Bitumen classes (Austroads 2006a)

Class	Viscosity (Pa.s)	Approximate penetration at 25°C
170	140–200	85–100
320	260–380	50–65
600	500–700	30–40

It is necessary to use bitumen that meets construction purposes because its viscosity must be within the optimum range of the area's annual temperature span. Soft-grade asphalt is more suitable for use in cold climates, while hard-grade asphalt performs better than the soft-grade class in hot climates. In Australia, Class 170 and Class 320 bitumen are normally used in pavement manufacture as sprayed seals and hot mix asphalt. Class 600, multigrade bitumen and polymer-modified binder are more preferable for other purposes, such as increasing surface stresses at high temperature and traffic loads, and providing additional flexibility in weak pavements.

2.2.2 Aggregates

Asphalt pavement consists of 90–95% by weight of aggregates of various sizes and proportions. The aggregate framework distributes external loads through point-to-point contact among the aggregate particles. This mechanism is known as internal friction or aggregate interlock (Figure 2.2). Furthermore, this particle interlock determines asphalt performance under major distress mechanisms such as fatigue cracking, permanent deformation and thermal cracking.

The aggregate interlock mechanism is affected by aggregate quality, shape, stiffness, quantity and gradation in asphalt mixtures (Somayaji 2001). Aggregates for asphalt must hard, tough and able to withstand disintegration under atmospheric pressure and chemical action. Angular particles have a more stable shape and texture than round particles. Round particles tend to slide over each other and become less effective in load transfer. High stiffness aggregates are more desirable than soft aggregates due to their high resistance under

the load. Due to the high quantity of aggregates in pavement (90%), the bitumen quantity becomes an important factor in determining the ability of the pavement to resist movement under the load through the aggregate network. Moreover, aggregate grading controls the amount of bitumen in the mixture. The type of grading selection, such as open graded, intermediate graded, and dense graded, becomes important in ensuring the development of particle interlocking (Austroads 2002). Figure 2.3 shows the comparison of asphalt gradation.

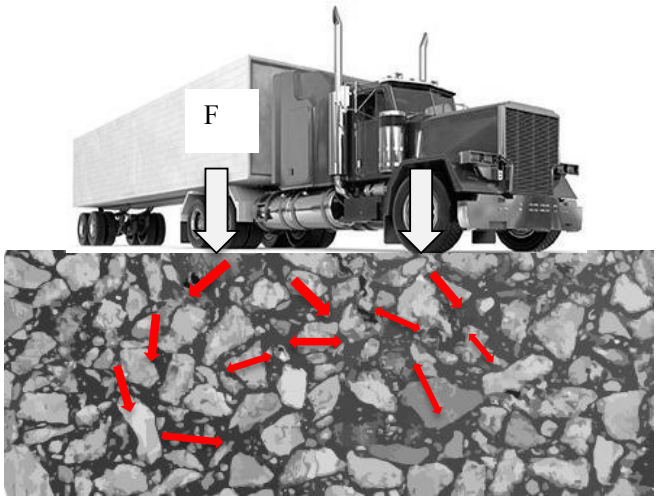

Figure 2.2 Aggregate interlock mechanism (Somayaji 2001)

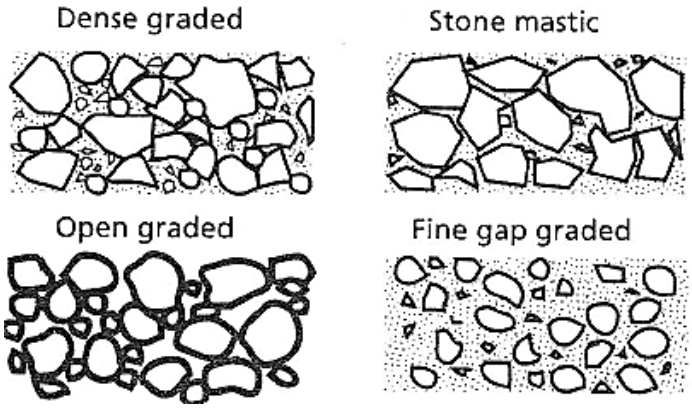

Figure 2.3 Comparison of asphalt gradation (Austroads 2002)

The choice of gradation determines the long-term performance of hot mix asphalt (HMA) with regard to factors such as permanent deformation and dynamic modulus. A large

nominal maximum aggregate size (NMAS) was reported to be more resistant to permanent deformation than small size aggregates (Brown and Basset 1990). By engineering the aggregate gradation such as by modifying the 'n' exponent (n = 0.45–0.55) in Fuller Equation gradations, mixtures with high permanent deformation resistance could be obtained (Yaghoubi and Mansourkhaki 2010). Tashman and Elangovan (2007) have reported a lower dynamic modulus master curve at high temperature than at normal temperature. This is because the asphalt has the ability to change its phase and lose its stiffness at high temperature, causing the dynamic modulus become solely a function of aggregate interlocking.

The NMAS limits the available maximum particle size in applications. This is due to the position, thickness and the requirement for meeting asphalt layer specifications (Austroads 2006a). The selected nominal sizes for various applications of asphalt course are given in Table 2.2. According to Austroads (2006a), the three courses that are normally used in flexible pavement are wearing/surface course (WC), intermediate course (IC), and base course (BC). The WC serves as a structural overlay, and form structural medium with the IC. The IC is the layer underneath the WC. The element that provides structural strength to the pavement is the BC.

Table 2.2 Typical mix sizes for various applications (Austroads 2006a)

Application	Typical mix size
Dense graded wearing course	
Lightly trafficked pavements	7 mm or 10 mm
Medium to heavily trafficked pavements	10 mm or 14 mm
Highway pavements	Generally 14 mm (also 10 mm)
Heavy-duty industrial pavements	14 mm or 20 mm
Dense graded intermediate course	Normally 10 mm, 14 mm, or 20 mm. In general it is better to use the largest size practicable.
Dense graded base course	Normally 20 mm. 28 mm and 40 mm may also be used depending on layer thickness and availability, although larger sizes require careful handling to avoid segregation.
Dense graded corrective course	5 mm, 7 mm, 10 mm, 14 mm or 20 mm
Open graded wearing course	10 mm or 14 mm
Open graded base course (drainage layers)	28 mm or 40 mm
Fine gap graded asphalt	Generally 10 mm (also 7 mm or 14 mm)
Stone mastic asphalt wearing course	Generally 10 mm or 14 mm (also 7 mm)
Stone mastic asphalt base course	Generally 20 mm
Minor patching	10 mm (also 5 mm, 7 mm, 14 mm and 20 mm) All sizes as appropriate

2.2.3 Air Voids

Asphalt mixture consists of bitumen, aggregates and air voids that are designed through volumetric properties. Air voids are a component of the volumetric properties, instead of voids in mineral aggregates (VMA) and voids filled with asphalt (VFA). Air void is defined as the total volume of all small pockets of air between the coated aggregate particles throughout a compacted paving mixture. An asphalt mixture usually has an air void content of 3–5% (Cominsky et al. 1998). In asphalt mixture design, it is common to limit air voids to the lowest practical value, in order to reduce ageing and stripping. Arambula, Masad and Martin (2007) suggested a new asphalt mixture design and compaction method capable of producing uniform air voids and making the asphalt layer least susceptible to moisture. X-ray computed tomography (CT) assessment revealed that the mixes with the greatest range of air void content were more resistant to moisture damage.

The volumetric properties, namely air voids, VMA and VFA, can ensure the stability and durability of asphalt mixtures under fatigue cracking, rutting, thermal cracking and ageing. In one study aimed at optimizing volumetric properties, the optimum air void value for Superpave mixtures in Kansas was found to be approximately 4%. In order to avoid distress failure, the air void value should be no lower than 2% nor higher than 6% (Hossain and Chen 2002). A very low air void content, i.e. less than 1%, was used for Superpave mixtures in Taiwan (Wang, Kennedy and McGennis 2000). This is certainly detrimental, since a very low air void content makes asphalt highly prone to permanent deformation. In application, it is imperative to maintain the air void value in order to prevent excessive plastic deformation from actual traffic compaction. In this case, the Indiana Department of Transportation (INDOT) suggested a new approach to overcome the problem associated with low air voids (less than 2%) in plant- produced mixtures. Materials with low air void content can be used for in situ applications, as long as the placed materials have adequate stiffness to ensure that the whole pavement performs effectively under loading conditions (McDaniel et al. 2005).

2.2.4 Filler

Filler which passes a 0.075 mm sieve is required to improve the gradation of materials. Materials such as rock dust, fly ash, lime, Portland cement and cement kiln dust are normally added to asphalt mixtures as filler, and function as part of the aggregate and overall particle size distribution of the mix, as well as increasing binder volume. The fineness of the filler determines its role in the asphalt mixture. According to Austroads (2007), the filler portion of asphalt mixture has several purposes, such as increasing the stability of the mix and the

stiffness of the binder, increasing the binder content, and influencing the voids in the total aggregate. Two types of mineral filler, i.e. natural and imported fillers, are used in applications. Well-known natural fillers include rock dust and baghouse or cyclone dust, while the commercially available fillers include hydrated lime, ground limestone, Portland cement, ground-granulated blast-furnace slag and fly ash. The commercially available fillers must comply with the filler requirements set out in AS 2150-2005 (Standards Australia 2005) or other asphalt specifications. Austroads (2006a) suggests that the required characteristics of mineral filler for asphalt pavement are particle size distribution, dry compacted voids content, moisture content, particle density, chemical composition, water solubility, loss on ignition and presence of clay or other contaminants.

Several studies have been conducted to investigate the effect of filler inclusion in asphalt pavement, showing that fillers can reduce the required amount of asphalt, increase stability, improve the bond between aggregates and asphalt, and fill the voids (Mamlouk and Zaniewski 1999). Also, filler inclusion in asphalt significantly reduces the by-product accumulating in the environment. Huang et al. (2010) investigated some types of cementitious fillers and hydrated lime with diverse fineness and found that cementitious fillers enhance moisture resistance due to the stiffening effect between particles. The finer hydrated lime is clearly advantageous in resisting moisture damage. Fly ash and bottom ash are also popular choices as aggregate and mineral filler for stone mastic asphalt (Xue et al. 2009). Addition of 8–16% fly ash/bottom ash to asphalt increases the dynamic stability, water sensitivity and fatigue life of asphalt pavement in the long term. By contrast, dust content is not advantageous in HMA since a 2% increase in dust may be more detrimental than a 0.7% reduction of asphalt content. Excessive dust content enhances cracking of the HMA (Villiers et al. 2008).

2.3 Asphalt Pavement Distress

2.3.1 Major Distress Mechanisms

Distress in the structure of asphalt under service load results from excessive stress, strain and deflection. There are three major distresses identified and considered in asphalt mixture design, including fatigue cracking, rutting and thermal cracking. Fatigue cracking due to repeated bending, rutting due to accumulation of permanent deformation, and thermal cracking are common asphalt failures, and are due to poor mix design, uneven load distribution, inappropriate construction, or environmental conditions. Fatigue cracks result from high asphalt loading and ageing, permanent deformation is caused by the binder losing

its elasticity at high temperatures, and brittleness and shrinking of asphalt is caused by low temperatures. Table 2.3 details the distress modes for flexible pavement.

Table 2.3 Distress modes for flexible pavement (Austroads 2008c)

Distress mode	Likely causes	Materials affected
Rutting	Traffic-associated: densification, shoving	All bound but sound cemented materials
Cracking	Traffic-associated: - single or low repetitions of high load - many repetitions of normal load Non-traffic- associated: - thermal cycling - reflection of shrinkage cracks from underlying materials - swelling of subgrade materials	Asphalt, cemented materials, granular materials
Roughness	Variability of density, material properties	

2.3.2 Fatigue Cracking

Repeated tensile stress/strain at the bottom of the asphalt mix layer due to traffic loading is a primary cause of fatigue cracking. This mechanism receives more attention than other distress mechanisms since it occurs more frequently in practice. In theory, the initiation of cracking commences under or adjacent to wheel loads. The cracks depend on the location of the maximum horizontal tensile stresses and strains in the pavement layer. Asphalt thickness and base stiffness can affect the level of fatigue cracking by limiting the excessive elastic strain from repeated wheel loads. Figure 2.4 shows the position of typical critical stresses and strains in asphalt pavement.

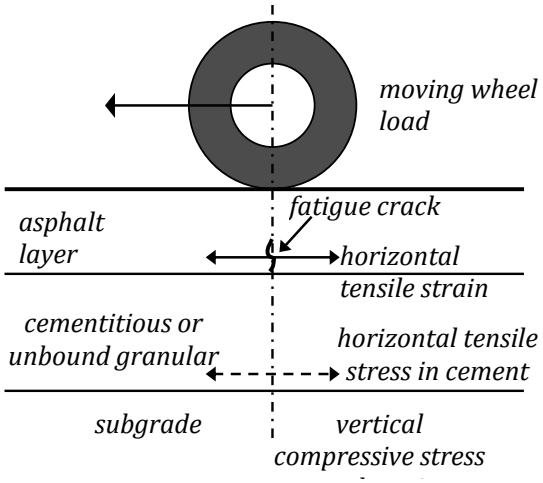

Figure 2.4 Critical stresses and strains in an asphalt pavement (Powell et al. 1984)

There are two types of common fatigue cracking based on pavement thickness recognized in application and included in the MEPDG 2004, namely bottom-up fatigue cracking and top-down fatigue cracking (NCHRP 2004b). Both cracks are usually initiated by maximum tensile strains in the top or bottom layer. The magnitude and potential location of both types of crack depend on some determining factors such as pavement structure and wheel/tyre loading configurations. In a study about fatigue cracking, the non-uniformity tyre-pavement contact pressure distribution was analysed using a three-dimensional finite element program. The study found that both longitudinal and low latitudinal tyre-pavement stresses influence the maximum tensile strains in the asphalt layer (Hu and Walubita 2009).

Bottom-up fatigue cracks form as short longitudinal cracks in the surface layer (Figure 2.5). Under repeated traffic loading, the cracks start at the bottom of the asphalt layer before propagating to the surface. These cracks develop quickly and become interconnected to form chicken wire or alligator cracking. This type of failure occurs due to the thickness of the asphalt layer being insufficient for the magnitude and repetition of wheel loads, high wheel loads and tyre pressures, soft areas in the subgrade, and a weak aggregate base due to inadequate compaction or high moisture content.

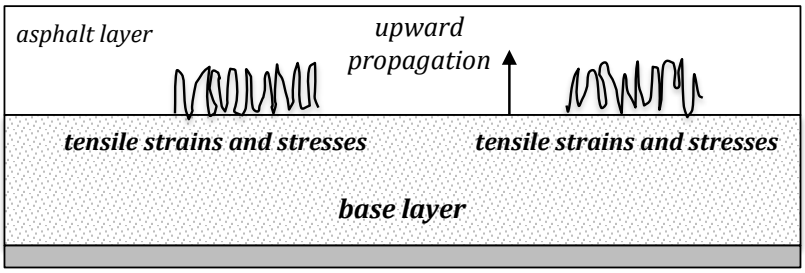

Figure 2.5 Bottom-up fatigue cracking (NCHRP 2004b)

Figure 2.6 shows top-down fatigue cracking caused by conditions on the surface being favourable for the initiation of cracking. Cracks occur at the asphalt surface and propagate downward. Some causes have been identified, such as the oxidation of asphalt making the layer hard and brittle, micro-cracks from surface rolling, and a surface texture that leads to crack initiation (Brown 2000). Furthermore, severe ageing of asphalt layer and high contact pressure are prone to induce cracks.

The classical fatigue cracking or bottom-up mechanism is a common pavement distress mechanism in the USA and France where a thin layer of asphalt is used. The bottom-up fatigue cracking in pavement thickness design occurs in practice when the asphalt layer is

less than 160 mm (Brown 2000). Similar conditions have been observed in the Netherlands, where more than 75% of road sections failed due to full-depth cracking or bottom-up cracking due to the asphalt layer having a thickness of less than 160 mm (Merril, van Dommelen and Gaspar 2006).

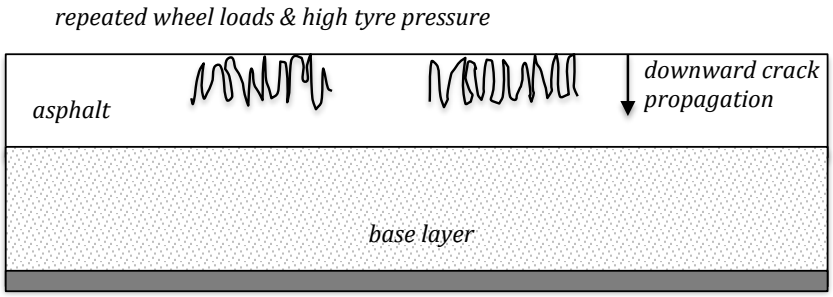

Figure 2.6 Top-down fatigue cracking (NCHRP 2004b)

In Western Australia, most roads use a thin pavement layer with a thickness less than 140 mm or 60–120 mm (Rickards 2009, Austroads 2008c). Although the use of a thin layer ensures noise reduction and efficient production over small areas, this type of pavement is more prone to classical fatigue cracking (bottom-up) early in its life (Jitsangiam, Nikraz, and Leek 2010). According to Rickards (2011), this type of failure occurs due to high strain levels and the disproportionate application of loads at high temperatures. This is a common type of failure in the warmer parts of Australia, such as Western Australia. In fact, Austroads 2008 has included fatigue cracking as a major mechanism to be taken into account during pavement design; however, specific types of fatigue cracking and their effect on pavement structural design have not yet been specifically defined in the design guidelines. Because Western Australian pavement might undergo this type of failure, it is important to investigate the mechanisms of fatigue cracking through laboratory testing, field studies and numerical modelling.

2.3.3 Permanent Deformation or Rutting

Permanent deformation or rutting is a plastic deformation of asphalt that develops gradually as the number of load repetitions accumulates. The deformation results from unrecoverable strain on inelastic bituminous and granular materials in the subgrade under continuous traffic loading. This mechanism is important since it mainly occurs at high temperatures and with slow moving traffic. When there is a temperature gradient between the asphalt layers on hot days, with higher temperatures at the surface than deeper down, the structure undergoes

plastic deformation from the surface to the subgrade. Rutting leads to poor ride quality and increased driving hazards due to skidding and steering problems. Permanent deformation is illustrated in Figure 2.7.

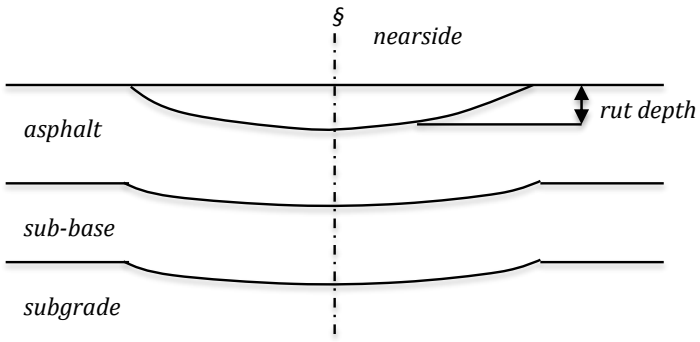

Figure 2.7 Permanent deformation (Read and Whiteoak 2003)

MEPDG 2004 classifies two causes of permanent deformation, i.e. one-dimensional densification consolidation (vertical compression) and lateral flow (plastic movement). The first type is related to material densification with excessive air voids and poor compaction causing a slump to form near the centre of the wheel path. This type of deformation is low to moderate in level of severity. The latter type is caused by shear failure, which is accompanied by vertical and lateral flow (downward and upward) of the material. This type is moderate to high in level of rutting severity and is difficult to measure (Figure 2.8).

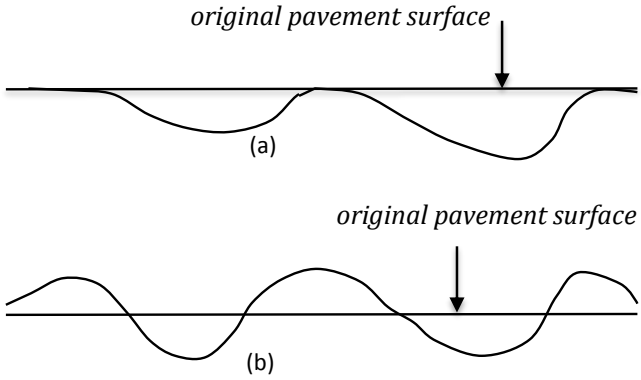

Figure 2.8 Types and mechanisms of rutting in flexible pavements in MEPDG 2004, (a) one-dimensional densification or vertical compression, (b) lateral displacement or two dimensional plastic movement (NCHRP 2004b)

The premature rutting of asphalt pavement is also a major concern in flexible pavement because it is difficult to model the mechanism appropriately. This mechanism causes premature failure in asphalt pavement, with some road authorities in the US, such as the Texas Department of Transportation, reporting severe rutting in some road sections after only a year service (Zhou et al. 2003). Generally, the thickness of the asphalt mixture used in Texas ranges from 100 mm to 380 mm. However, after a year of service, some road sections displayed severe rutting more than 20 mm deep. Other road sections failed after three years of service. The non-uniform distribution of rutting in some sections made this type of mechanism unpredictable in the early stages. Some discrepancies in the prediction of rutting in pavement design and evaluation were reported. In a study of permanent deformation at high temperature, the viscoelastic nature of asphalt at high temperature was shown to affect the dynamic modulus, making the asphalt more susceptible to premature rutting (Ghareib and Ahmed 2009). An unrealistic prediction was also noticed in a lab study where uniform elevated temperature was applied through the asphalt layers. It was argued that it was difficult to model a temperature gradient through asphalt layers (Merril, van Dommelen and Gaspar 2006). The observed permanent deformation occurred solely on the asphalt surface and not in every layer.

Material characteristics and other variables have been shown to have a considerable effect on rutting susceptibility in asphalt. Table 2.3 summarizes various parameters that affect rutting.

Table 2.4 The effect of material and other variables on rutting susceptibility adapted from Sousa, Craus and Monismith, 1991 (Al-Khateeb and Basheer 2009)

Category	Parameter	Direction of change	Expected effect on rutting potential
Aggregate properties	Surface texture	Smooth to rough	Decrease
	Gradation	Gap to continuous	Decrease
	Shape	Round to angular	Decrease
	Size	Increase NMAS*	Decrease
Binder properties	Stiffness	Increase	Decrease
Mixture volumetric properties	Binder content	Increase	Decrease
	Air void content	Increase	Increase
	VMA	Increase	Increase
	Compaction method	Varies	Varies
Environmental or operating conditions	Temperature	Increase	Increase
	State of stress or strain	Increase in tyre pressure	Increase
	Number of load repetitions	Increase	Increase
	Water	Dry to wet	Increase (with moisture sensitive mix)
	Thickness		Decrease

*NMAS: Nominal Maximum Aggregate Size

Table 2.4 shows some critical parameters determining rutting susceptibility such as aggregate properties, binder properties, volumetric properties and environmental conditions. It was reported that mixtures with large NMAS or coarse aggregates have better rutting resistance due to good particle interlocking (Moghaddam, Karim and Abdelaziz. 2011). In a similar study, high binder content in the mixtures was found to reduce the risk of rutting. Inclusion of fibres and polymers such as styrene butadiene styrene (SBS) could increase stiffness, reducing the rate of deformation and energy loss at high temperature. This certainly has a more positive impact on the rutting resistance of asphalt pavement (Kumar and Veeraragavan 2011).

Rutting is included in the pavement design procedures in the Austroads 2008 to model permanent deformation. However, there is no model that can precisely predict actual permanent deformation under the passage of traffic and time. The Guide explains that it is difficult to estimate rutting because of its weather dependent behaviour. Permanent deformation normally only occurs on rare occasions when asphalt is exposed to highly elevated temperatures. The mild-temperate Mediterranean weather in Western Australia, with a warm winter and extremely high temperatures in summer, means that asphalt pavement is more prone to premature rutting. In order to understand premature rutting in Western Australian asphalt pavement, it is imperative to study this type of distress, both to characterize the distress and model the deformation.

2.3.4 Stripping (Moisture Damage)

Stripping or moisture damage is an important source of pavement distress due to the susceptibility of the asphalt mix to water damage. In asphalt mixtures, the asphalt is used as a binder or adhesive for the aggregate particles. A loss or failure of the bond between asphalt and the aggregate surface due to the presence of moisture between them is called stripping (Read and Whiteoak 2003). Moisture can lead to the reduction of adhesion, interlock and internal friction between aggregate particles, resulting in the reduction of stiffness in the asphalt pavement. The mechanism behind the bond/adhesion between aggregate and asphalt binder and its failure is explained by the surface energy concept. An adhesive bond is formed when the aggregate with its unbalanced surface charge is coated with a liquid of the opposite polarity. In this case, water can displace asphalt binder as the preferred coating since water meets the surface energy requirements of aggregates, causing stripping.

Aggregate-asphalt binder adhesion is mainly influenced by aggregate properties, although the asphalt properties, mixture properties and external factors may intensify the problem.

Table 2.5 displays material properties and external factors that can affect the asphalt/aggregates bond.

Studies on asphalt mixtures using anti-stripping additives or cementitious fillers like fly ash, cement kiln dust and hydrated lime to reduce stripping have been carried out by various researchers (Berthelot et al. 2010, Hossain, Zaman and Hobson 2010, Huang et al. 2010). Anti-stripping additives such as amine-based materials do not change the mechanical workability and the rheology of the bitumen; hence they can be used in asphalt mixtures. Cementitious fillers such as lime can improve structural performance by increasing the dynamic modulus values, decreasing strains and increasing the phase angle. Fine hydrated lime has been reported as being more effective in mitigating stripping. Other types of additives such ash fly ash and cement kiln dust have strong chemical activity and a stiffening effect that can improve moisture resistance.

Table 2.5 Material properties and external factors that can affect the bitumen/aggregate bond (Read and Whiteoak 2003)

Aggregate properties	Asphalt properties	Mixture properties	External factors
Mineralogy	Rheology	Void content	Rainfall
Surface texture	Electrical polarity	Permeability	Humidity
Porosity	Constitution	Asphalt content	Water pH
Dust		Asphalt film thickness	Presence of salts
Durability		Filler type	Temperature
Surface area		Aggregate grading	Temperature cycling
Absorption		Type of mixture	Traffic
Moisture content			Design
Shape			Workmanship
Weathering			Drainage

The type of aggregate used in asphalt mixtures is a primary concern due to the differences in degree of affinity for asphalt. Siliceous quartz and granite are common types of aggregates used in asphalt mixtures and can be classified as acidic rocks due to their high silicon oxide content. The acidic type of aggregate has less affinity and is difficult to coat with asphalt compared to basic rocks like limestone and basalt. In general, granite is the most available aggregate in Western Australia for asphalt mixtures. Granite is siliceous, has low affinity and is hydrophilic (water-loving). This can cause stripping that affects the overall stiffness of asphalt pavement. Hence, it is important to investigate stripping in asphalt mixtures used in Western Australia.

2.3.5 Thermal Cracking

Thermal cracking is a common problem in cold climates and in areas with large variations in daily temperature. Asphalt is more prone to thermal cracking when the asphalt surface has low strength and ductility at low temperatures. The cracks develop from thermal stresses due to low temperature and thermal cycles, i.e. repeated low and high temperature cycles. Temperature changes significantly influence asphalt mechanical properties. Since asphalt is viscoelastic, it becomes too stiff to withstand thermally induced stress at low temperatures. Thermal cracks widen and propagate into the underlying layers of the pavement, leading to water infiltration, loss of smoothness and ultimately structural failure of the pavement (Bae et al. 2007, Isacsson and Zeng 1998).

There are two forms of thermal cracking. In the first form, the stresses are induced by asphalt contraction as it cools, and the magnitude of the stresses varies according to depth. This results in crack propagation downwards from the surface (
Figure 2.9). In the second form of cracking, thermal fatigue cracking occurs under repetitive cycles of high stress due to a drop in temperature at night and low stress due to a warm asphalt temperature. The binder hardens with age, particularly at high temperatures, reducing its capacity to withstand thermal stresses caused by cool temperatures at night (Read and Whiteoak 2003).

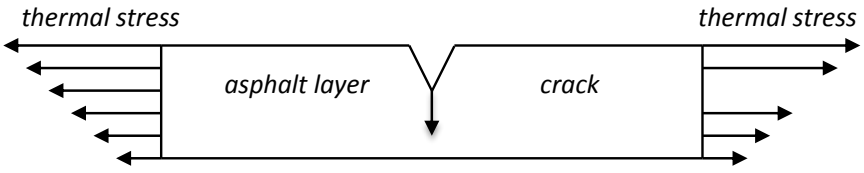

Figure 2.9 Thermal cracking mechanism (Read and Whiteoak 2003)

Asphalt performance at very low temperatures and fast cooling rates can be measured using unit response functions such as creep compliance, relaxation modulus and complex modulus. Creep compliance has been shown to be a sensitive predictor of thermal cracking (Yin, Chehab and Stoffels 2006). However, since the determination of the thermal cracking response requires expensive instruments and wide-ranging tests, an interconversion method can be used to obtain the creep function from the other uniaxial stress values (Yin et al. 2010). In this case, the creep compliance can be determined from the dynamic modulus values (E*). Figure 2.10 illustrates the interconversion method using these values.

Thermal cracking prediction is not included as an input parameter in the Austroads 2008. This is mainly due to the assumption that there are no specific low temperature regions in Australia, except for minor snow areas in Victoria during winter. Hence, it is imperative to investigate thermal cracking by identifying the degree of severity of this type of distress in asphalt pavement.

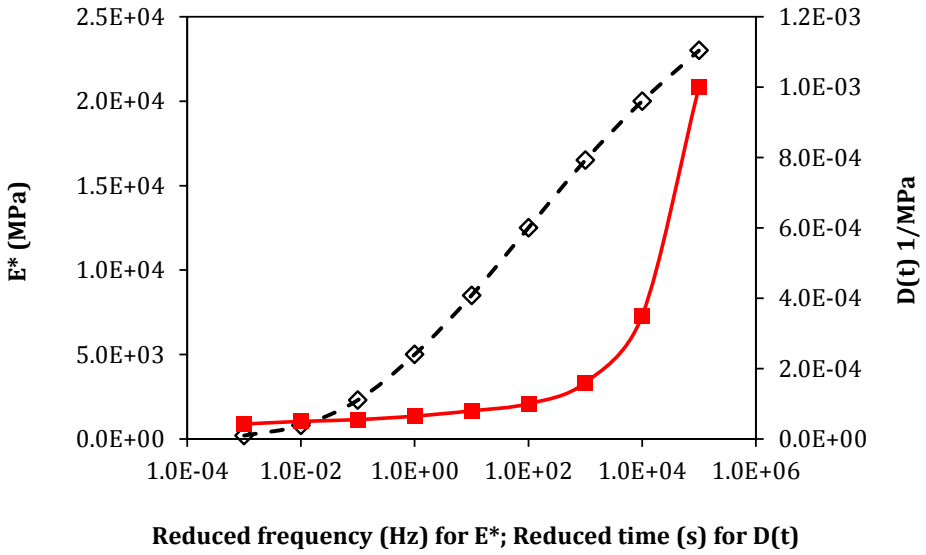

Figure 2.10 Sample interconversion between dynamic modulus and creep compliance (Yin et al. 2010)

2.4 Structural Design of Flexible Pavement

There are two approaches the structural design of flexible pavement (Mallick and El-Korchi 2009). Firstly, there is the empirical method using statistical regression with empirical data based on the soil classification and subgrade type. The most widely used empirical methods are the California Bearing Ratio (CBR) and American Association of State Highway and Transportation Officials (AASHTO) methods, which are used in many countries. The empirical method is basically less time-consuming and user-friendly due to the availability of data from in-service pavements or experiments. Due to its limitations in accommodating traffic, environmental conditions and materials, this approach is no longer recommended for the design of cost-effective pavement materials.

The second method is the mechanistic-empirical method consisting of two separate procedures, i.e. mechanistic analytical and empirical. The mechanistic part relates to pavement response under load or determination of stress-strain. The empirical part relates

pavement performance to major distress mechanisms such as fatigue cracking or permanent deformation. Figures 2.11 and 2.12 illustrate the mechanistic and empirical aspects respectively. Some pavement responses that can be included in structural design are displayed in Figure 2.11, while Figure 2.12 shows the empirical aspect or the correlated pavement performance from mechanistic responses.

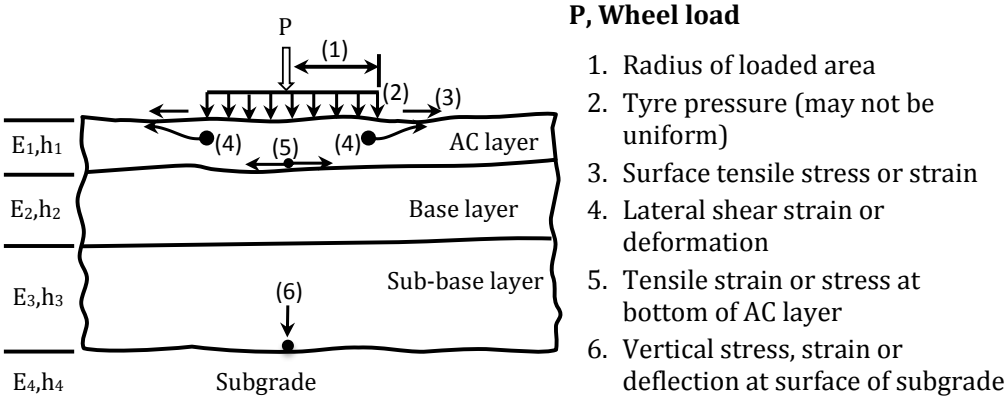

Figure 2.11 Fundamental pavement responses as a function of load, material properties and layer thicknesses – the mechanistic aspect (Haas and Tighe 2007)

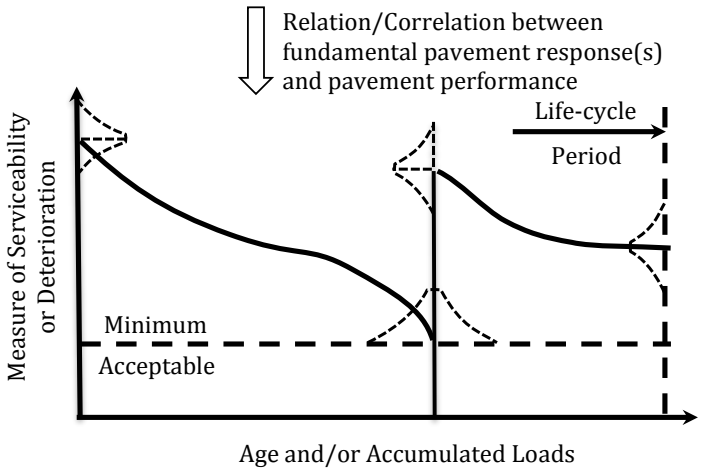

Figure 2.12 Correlated pavement performance from mechanistic responses – the empirical aspect (Haas and Tighe 2007)

Many countries have adopted the mechanistic-empirical method as it is more viable, allowing the incorporation of materials, environmental conditions and traffic load with or without experiments. In this thesis, two mechanistic-empirical methods were summarized,

including the Austroads 2008 method, and MEPDG 2004 from the National Cooperative Highway Research Program (NCHRP) USA. The philosophical background, methods, tests and design procedures of each are briefly reviewed in this section.

2.4.1 Overview of the Austroads Guide to Pavement Technology 2008

The guide for the design of flexible pavement was initially published in 1987 by the National Association of Australian State Road Authorities (NAASRA) and reissued by Austroads in 1992. Since then, the Guide was revised in 2004, and then again in 2008. The most recent revision of the Guide adopted the mechanistic-empirical method that makes it possible for Austroads member authorities to design flexible pavements which contain one or more layers of bound material (asphalt) for wide-ranging loading types and configurations. A purely empirical design is also included in the Guide for granular pavements with thin bituminous surfacing (less than 40mm thickness) over granular material. The document was published as the Guide to Pavement Technology Part 2: Pavement Structural Design or Austroads 2008 (Austroads 2008c). The Austroads 2008 aims to determine the most cost-effective pavement thickness and composition to provide a satisfactory level of service for traffic. In the mechanistic theory adopted by Austroads, the material behaviour response takes into consideration the properties relating to the level of traffic (equivalent standard axle) and the environmental conditions (air temperature and level of moisture). The properties are the stress-strain relationship (linear or non-linear), time dependency of the strain under a constant stress level (viscous or not viscous), and the material's ability to recover strain after stress removal (plastic or elastic) (Urbaez and Erskine 2011).

The mechanistic-empirical procedure is subject to normal road traffic loading that considers a full standard axle in calculating the critical strains. This allows the Guide to accommodate a substantial increase in traffic volumes and high tyre pressures by providing thicker pavement construction and high stiffness material in asphalt pavement. Figure 2.13 shows the idealized loading situation and critical locations of the strains in the assumed model.

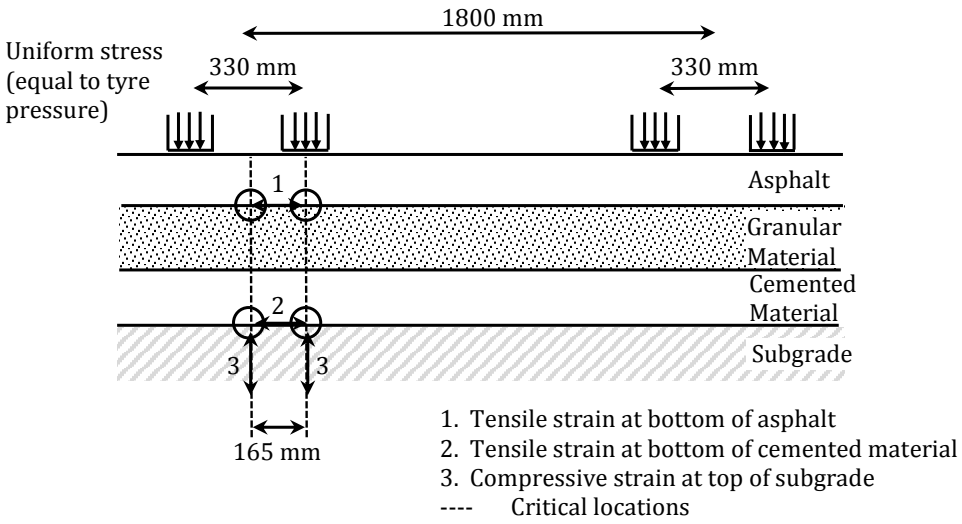

Figure 2.13 Pavement response model (Austroads 2008c)

The Austroads 2008 highlights the following aspects of the model illustrated in Figure 2.13 as follows. First, the pavement materials are homogeneous, elastic and isotropic, excluding unbound granular materials and subgrade. Second, a linear elastic model such as CIRCLY developed by Mincad Systems in 2004 is used to determine the response to load. Third, the critical responses considered include the horizontal tensile strain at the bottom of the asphalt and cemented layer, and vertical compressive strain at the top of the subgrade layer. Fourth, the standard axle consists of a dual-wheeled single axle applying a load of 80 kN with critical responses within the pavement depending on the vertical axis of the wheels. Fifth, the contact stress is taken to be 750 kPa. Other contact stress relates to a tyre pressure in the range of 500–100 kPa considered normal for highway traffic.

The mechanistic design procedure from Austroads 2008 for moderate to heavily trafficked pavement consists of several steps that can be grouped into three stages, i.e. design inputs, analysis and interpretation of the results (Austroads 2008c). The mechanistic procedure is shown in Figure 2.14. The first stage involves assessment of the input variables such as materials, traffic and environment. The trial pavement and desired project reliability are selected and analysed in this stage, and the elastic parameters such as design asphalt modulus and Poisson's Ratio, the fatigue criteria for asphalt, and the design number of standard axle repetitions (SAR) for each relevant distress mode are determined. The design asphalt modulus is the resilient modulus using the tensile strength test and bitumen modulus using the Shell nomograph. A brief review of resilient modulus can be seen in section 2.5.3.2.

The second stage involves the analysis of the trial pavement to determine the allowable traffic. In this stage, critical locations in the pavement for strain calculation are determined using CIRCLY by assuming the material is linear-elastic. The output is the maximum horizontal tensile strain of the cemented/asphalt layer or maximum compressive strain of the subgrade materials. The final stage consists of results interpretation. The allowable number of SAR for the relevant distress modes in trial pavement is compared with the design number of SAR in the first stage. The trial pavement is acceptable once the allowable number of SAR exceeds the design number of SAR. If this is unacceptable, the design must be repeated.

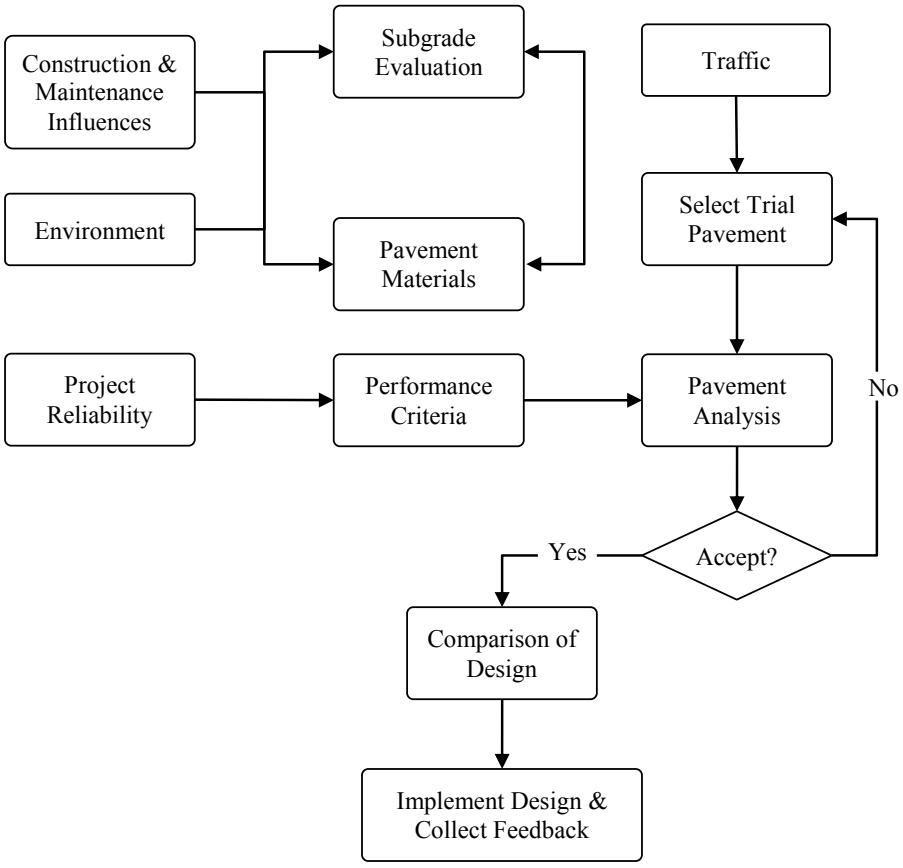

Figure 2.14 Design procedure for flexible pavements (Austroads 2008c)

The Austroads 2008 includes more detailed traffic load distributions in terms of SAR for urban and rural roads than the previous Guide. It also incorporates high tyre pressure and heavy vehicle loads in the calculations in order to enable more accurate prediction of thicker and stiffer asphalt pavement. However, several limitations need to be addressed in order to

modify the mechanistic-empirical pavement design procedure. The first is to optimize the impact of the critical strains in the pavement layer; the response model could use a full single axle with dual tyres as opposed to a half axle. The second is to revise the modified Shell fatigue relationship used in the Guide to predict the remaining life of the asphalt pavement, since the equation only predicts a general fatigue life without specifically defining whether the fatigue cracking type is top-down or bottom-up. The third is to determine the asphalt modulus in each period taking into consideration the thickness and temperature of each asphalt layer and location within the pavement structure. The fourth is to include traffic distribution in various seasons, such as low traffic volume in winter and high traffic volume in summer. The fifth is to include environmental factors in the mechanistic-empirical method by incorporating a minimum of six seasons in Australia rather than generalizing this parameter into only one season, since this has a significant impact on material stiffness throughout the year (Urbaez and Erskine 2011).

2.4.2 Overview of MEPDG 2004

The Mechanistic-Empirical Design of New and Rehabilitated Pavement Structures was developed through the National Cooperative Highway Research Program (NCHRP) under the Transportation Research Board, United States in 2004 in order to replace the previous American Association of State Highway and Transportation Officials (AASHTO) design. The Mechanistic-Empirical Pavement Design Guide or MEPDG 2004 (NCHRP 2004a and 2004b) provides procedures for designing new and reconstructed flexible pavements. The Guide states that the methodology in the design process is more applicable for conventional dense graded flexible pavements than modified pavement materials such as stone matrix, polymer or recycled aggregate asphalt mixtures.

The flexible pavement design process as summarized from the MEPDG 2004 Guide comprises three stages, starting with the development of input values and evaluation. The input values consist of traffic loads, materials, climate, pavement type and other features. The second stage involves the structural analysis of trial designs including performance modelling. The performance criteria and desired level of reliability for the performance indicators such as acceptable limit of rutting, fatigue cracking, thermal cracking and International Roughness Index (IRI) are assigned. During this stage, the pavement responses are calculated using multilayer elastic theory or finite element analysis for each axle type, load and damage to obtain the stress, strain and displacement within the pavement layers. The critical locations within the pavement layer where the stresses/strains are at their most extreme values are determined. The accumulated distress or damage at the end of each

analysis period is also calculated in this stage. A prediction of key distresses throughout the design life is taken using calibrated mechanistic-empirical performance models. The performance criteria must be fulfilled, otherwise the design should be modified until it eventually meets the performance criteria. The final stage is an evaluation of viable alternatives including life-cycle analysis, culminating in a final strategy or design selection. A brief flowchart of the design process for flexible pavements is shown in Figure 2.15.

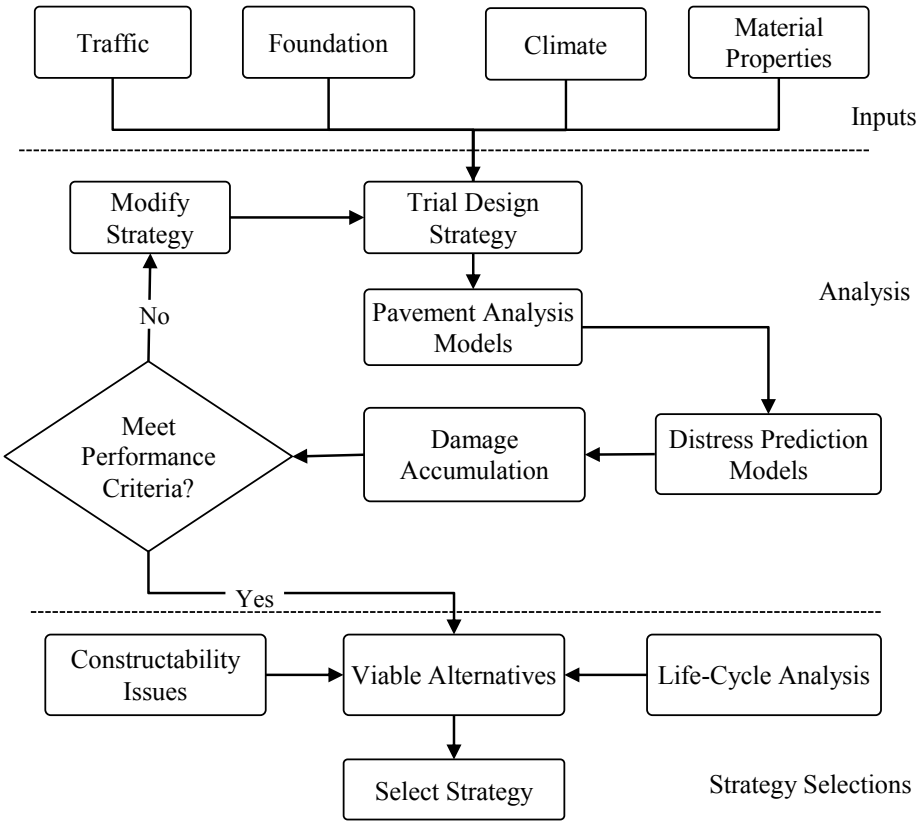

Figure 2.15 Overall design process for flexible pavements (NCHRP 2004b)

The trial design inputs become a major concern in MEPDG 2004 (NCHRP 2004a) since they must satisfy all performance criteria, i.e. permanent deformation, fatigue cracking, thermal cracking and IRI, over the analysis period. A realistic design depends on the quantity of data obtained including in situ material properties, traffic, climate, subgrade properties and construction duration. Some obstacles such as limited final information on the specific project and the actual materials used force engineers to collect a large amount of data and carry out sensitivity analyses to determine the pavement performance. From this point of view, the designer is allowed to select design inputs based on three levels of data quality. Level 1 has the highest level of accuracy with the material properties from laboratory testing

incorporating material properties, traffic and environmental conditions at the site. Level 2 uses correlations equations or material properties and regional factors from the available test data as input design. Level 3 has the lowest accuracy since it only uses typical local values or default values and generalizes the specific project site.

Various challenges and issues regarding the implementation of MEPDG 2004 have been identified as a result of research and application. It is imperative to overcome the following issues regarding data, performance design criteria, testing equipment, software requirement, validation of distress models, project database and training for pavement designers. Based on studies from several states (Li et al. 2011), there are some conditions that need to be standardized, such as sensitivity analysis of pavement responses used in MEPDG 2004 design inputs, evaluation of materials and traffic inputs, acceptable performance criteria and calibration of local materials, climate and traffic conditions.

Both Austroads 2008 and MEPDG 2004 Guides show that the mechanistic-empirical approach is currently the most appropriate method of designing flexible pavement despite variability in local environment conditions and traffic load. Table 2.6 summarizes the difference between mechanistic-empirical approaches adopted by Austroads 2008 and MEPDG 2004.

Table 2.6 Summary comparison of the mechanistic-empirical approaches

Item	Mechanistic-Empirical Approach	
	Austroads 2008, Australia (Austroads 2008c)	MEPDG 2004, USA (NCHRP 2004b)
Concept	Mechanistic-empirically based	Mechanistic-empirically based
Pavement materials	Asphalt layer more than 40 mm thick	Conventional flexible pavement, deep strength pavement, full depth pavement, semi-rigid pavement
Environment effects	Temperature, moisture	Temperature, moisture
Design input levels	None	Three (3)
Asphalt modulus design	Resilient Modulus Bitumen properties and mix volumetric	Dynamic Modulus
Laboratory testing	Rigorous and lengthy	Laborious, time consuming, expensive and requires skilled personnel
Mechanistic failure load-response parameter (critical pavement response variables)	a) Maximum horizontal strain at the bottom of asphalt/cemented layer b) Maximum vertical compressive strain at the top of the layer c) None/not considered in model for unbound granular layer	a) Maximum tensile horizontal strain at the bottom of asphalt layer (fatigue cracking) b) Maximum compressive vertical stresses/strains within asphalt layer (rutting) c) Maximum compressive vertical stresses/strains within the base/sub-base layers (rutting of unbound layers) d) Maximum compressive vertical stresses/strains at the top of the subgrade (subgrade rutting)
Assumption to analyse response to load (pavement representation)	Linear elastic	a) Linear-elastic b) Non-linear
Design format	CIRCLY (linear elastic material)	JULEA (linear elastic material) DSC2D (non linear material)
Distress modes	a) Fatigue cracking b) Permanent deformation	a) Fatigue cracking (top-down and bottom-up) b) Permanent deformation (asphalt layer, unbound layer, subgrade) c) Thermal cracking d) Smoothness (International Roughness Index or IRI)
Distress/performance prediction	a) Fatigue life $N = RF\left(\frac{6918(0.85V_b + 1.08)}{S_{mix}^{0.36} \cdot \mu_\varepsilon}\right)^5$ b) Permanent deformation $N = \left(\frac{9300}{\mu_\varepsilon}\right)^7$	a) Fatigue cracking $N_f = 0.00432 \cdot k'_1 C\left(\frac{1}{\varepsilon_t}\right)^{3.9492}\left(\frac{1}{E}\right)^{1.281}$ for the bottom-up cracking: $k'_1 = \left(\frac{1}{0.000398 + \frac{0.003602}{e^{11.02-3.49 \cdot hac}}}\right)$ for the top-down cracking: $k'_1 = \left(\frac{1}{0.01 + \frac{12.00}{1+e^{15.676-2.8186 \cdot hac}}}\right)$ b) Permanent deformation $\frac{\varepsilon_p}{\varepsilon_r} = k_1 \cdot 10^{-3.4488} T^{1.5606} N^{0.479244}$ c) Thermal Cracking $C_f = \beta_1 N\left(\frac{\log C/h_{ac}}{\sigma}\right)$

2.5 Asphalt Stiffness Prediction

2.5.1 The Importance of Asphalt Stiffness

Asphalt is a viscoelastic material with behaviour in between the viscous or elastic states according to temperature. It becomes a viscous liquid at high temperatures, while at low temperature it becomes an elastic (brittle) solid. In 1954, Van der Poel used stiffness modulus (asphalt modulus), which is equivalent to the elastic modulus of solids, as a term to describe the viscoelastic properties of asphalt (Read and Whiteoak 2003). Asphalt stiffness is a major characteristic used to predict material performance in pavement structures. Inadequate stiffness causes early degradation when pavements are subjected to major distresses such as permanent deformation and fatigue cracking. Conversely, adequate stiffness improves the load spreading ability, increases the structural strength and lengthens the expected design life of the pavement.

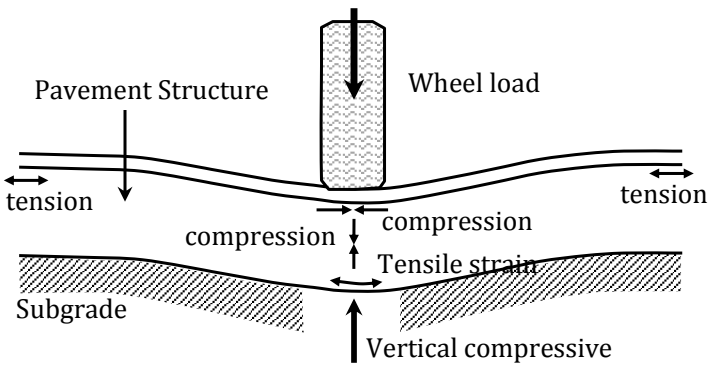

Figure 2.16 Pavement strains under traffic loading (Austroads 2006b)

The asphalt layer is used to distribute traffic loading stresses to the sub-base and subgrade (Figure 2.16). Asphalt stiffness is greater when it is subject to compressive loading rather than tensile loading. The stress has to be distributed in such way as to ensure that there is no deformation, overstress and repeated levels of critical tensile stress leading to fatigue on the subgrade. Under this condition, stiffness is defined as the resistance to bending and load spreading ability. Stiffness is also referred to as a function of the binder response to loading. This property comes from interparticle friction, the viscosity of the asphalt, cohesion within the mass, and adhesion between binder and aggregate. The load spreading principle is illustrated in Figure 2.17.

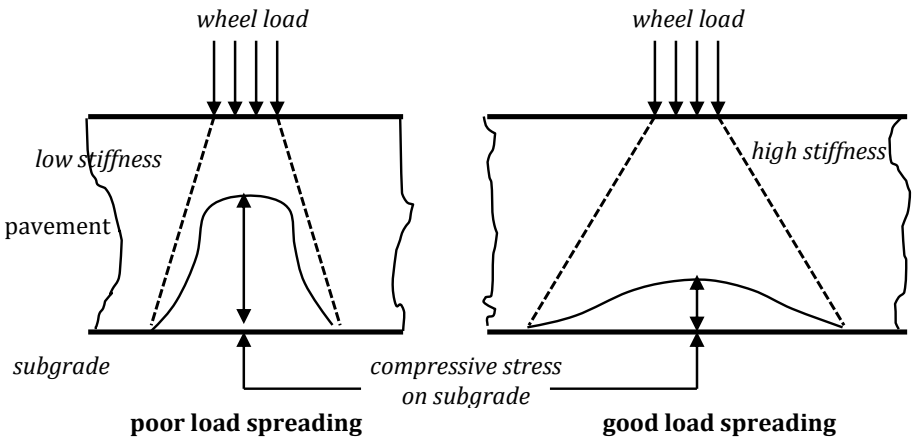

Figure 2.17 The load spreading principle (Nunn 1998)

As can be seen in Figure 2.17, it is assumed that both low and high stiffness materials have the same thicknesses. When the load is applied to both types of materials, the material with low stiffness shows poorer load spreading than the high stiffness material. The poor load spreading causes the underneath layer to have a high stress value (Read and Whiteoak 2003). The underlying layer would be able to tolerate the stress if the layer thickness were increased to produce an acceptable pressure value at the underside. The application of innovative asphalt mixtures such as elastomer-bitumen would reduce the total thickness of the asphalt layers by 120mm without sacrificing the overall stiffness (Sybilski and Bankowski 2002). However, in order to achieve ideal conditions in asphalt pavement, the use of a high stiffness material with low pressure and good load spreading for the underneath layer is preferable. It is believed that asphalt stiffness not only results from a good understanding of the load spreading mechanism, but also by providing a stiffer/stronger mix to improve the confinement. Stiffness is important when asphalt thickness becomes a major issue. If the pavement is much less stiff, the noise generated will be reduced.

Asphalt stiffness can be determined either in a laboratory or directly in the field. Several methods have been developed and utilized to measure asphalt concrete modulus in the laboratory, and have become a part of the asphalt performance-based mix design and mechanistic pavement design processes. The tests can be a uniaxial or triaxial tension and compression test, a shear test, a bending or torsion test, or an indirect tension test (Lytton 2009). The indirect tensile strength or resilient modulus test and flexural beam (bending) test are commonly used in the Austroads mix design guide. Asphalt stiffness is measured using

the specially designed Material Testing Apparatus (MATTA). Further detail will be given on laboratory asphalt stiffness characterization in section 2.5.3.

Asphalt pavement must be designed strictly according to Austroads 2008 and MEPDG 2004 to meet strength and stiffness requirements. Currently, there are no specific correlations or relationship criteria between the strength and stiffness of asphalt pavement that can be used as a guideline in designing the appropriate thickness from the prediction of major distresses. An attempt to correlate stiffness and strength as performance criteria of the asphalt mixture has been suggested by Pellinen (2004). The idea is to identify the correlation between certain conditions of strength and stiffness and its associated probable distresses in order to optimize pavement performance design. Stiffness can be characterized from creep, flexural modulus and dynamic modulus values. Strength is based on indirect tensile test (ITT) as a surrogate property for shear strength (Christensen and Bonaquist 2002). Figure 2.18 shows the conceptual criteria for stiffness and strength.

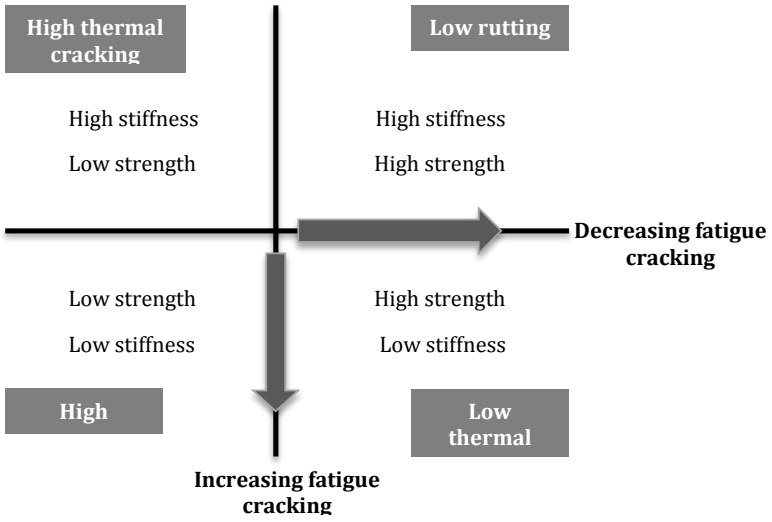

Figure 2.18 Conceptual stiffness and strength criteria (Pellinen 2004)

2.5.2 Factors Affecting Asphalt Stiffness

Stiffness results from the friction between aggregates, viscosity of the bitumen binder under operating conditions and cohesion within the mass from the binder, and the adhesion between binder and aggregate. Mix composition, binder type, binder content, air voids, temperature, rate of loading and age are identified as some important factors affecting

asphalt stiffness (Austroads 2008c). The factors and the effect of increasing factor values are shown in Table 2.7 and described in the following section.

Table 2.7 Factors affecting stiffness of asphalt and effect of increasing factor values (Austroads 2008c)

Factor	Effect of increasing factor on asphalt stiffness
Proportion of coarse angular particles	Increase
Density	Increase
Stress level	No change
Age	Increase
Extent of cracking	Decrease
Efficiency of mixing	Increase
Bitumen content	Increase then decrease
Bitumen class	Increase
Bitumen viscosity	Increase
Per cent air voids	Decrease
Temperature	Decrease
Rate of loading	Increase

Mix composition

Mix composition is influenced by aggregate angularity and grading, binder type, binder content and air voids. In general, dense graded aggregates increase mix stiffness due to packing and aggregate interlocking from the combination of aggregates of various sizes. Aggregate angularity may increase the stiffness due to rough fractured faces (Prowell, Zhang and Brown 2005).

Binder type and content

Binder type influences the asphalt stiffness at a variety of temperatures and rates of loading. According to Austroads (2006a), modified binders such as multigrade bitumen and polymer-modified bitumen are created to be less susceptible to temperature changes and provide greater flexibility than conventional binders. For example, a binder made from a combination of styrene butadiene styrene (SBS) polymer and crumb rubber was more resilient and flexible over a wide range of temperatures due to a reduction in energy loss at high temperature (Kumar and Veeraragavan 2011). Binder content is expressed as a percentage of the total weight of the mix or of the aggregate (Monismith, Epps and Finn 1985). A low percentage of binder increases the cohesion and strength of the mix. However, when there is an increase in binder content, there will be a reduction of the frictional contact between aggregate particles that influences the overall stiffness and stability of asphalt.

Air voids

Air voids are another parameter affecting asphalt stiffness, as discussed in section 2.2.3. The air voids must be small and well-dispersed in order to act as microcrack arresters and provide spaces to expand into at high temperatures. Increasing the air voids will accelerate the growth of microcracks and introduce permeability issues, while decreasing the air voids creates bleeding and encourages plastic deformations (Lytton 2009). The voids are controlled by asphalt content, degree of compaction during construction and additional compaction under traffic. Previous research (Brown 1990) has indicated that a typical mix design contains 4% air voids. To avoid permanent deformation (rutting), the air voids should fall within a range of 3–8%. It is also advisable to ensure that the air voids are at the optimum level for the binder content, as allowing the air voids to fall outside of the optimum range for the binder content can lead to a decrease in the stiffness of the mix.

Temperature

Temperature and rate of loading have a significant effect on asphalt stiffness. Due to its viscoelastic nature, when asphalt is loaded slowly at any given temperature, there will be low deformation. At a higher loading rate, the asphalt tends to be stiffer and subject to fracture. However, at any given strain rate of loading, there is a particular temperature where the material can relax quickly to prevent stress accumulating in the sample. The relationship of strain rate to temperature is shown in Figure 2.19. When the asphalt is under the stress free temperature and strain rate line, it undergoes plastic flow, while above the line it experiences fracture and microcracking healing.

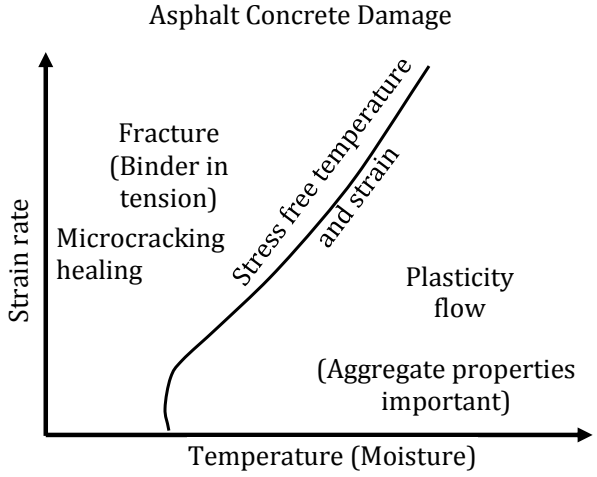

Figure 2.19 Asphalt damage dependence on temperature and loading rate (Lytton 2009)

Oxidation

Hardening due to oxidation is considered important in the ageing of bitumen. Bitumen stiffness increases with age because of hardening due to oxidation and volatilization. Oxidation is a chemical reaction that occurs when asphalt is exposed to air, and gradually causes bitumen to harden and lose its plasticity. Volatilization is the evaporation of lighter hydrocarbons from bitumen that causes it to lose its plasticity. Both mechanisms are temperature-dependent since the oxidation and volatilization rates double with every increase in temperature of 10°C above 100°C (Somayaji 2001). Chemical changes from both mechanisms could also reduce the binder volume and stiffen the pavement surface. The pavement becomes prone to cracking and reduction of asphalt stiffness.

The process starts when the bitumen comes into contact with oxygen and gradually becomes oxidized. Polar groups containing oxygen form and unite into micelles of higher micellar weight, thus increasing the viscosity of the bitumen. Subsequently, polar hydroxyl, carbonyl and carboxylic groups are formed to create more complex molecules resulting in harder and stiffer bitumen (Read and Whiteoak 2003). The oxidation process involves the loss of electrons and hydrogen, and the gaining of oxygen. The reactions are characterized as follows (Ricardson 2000):

$$C_xH_y + O \rightarrow C_xH_yO \quad (2\text{-}1)$$

$$C_xH_y + O \rightarrow C_xH_{y-2} + H_2O \quad (2\text{-}2)$$

$$C_xH_y + 2O \rightarrow C_{x-1}H_y + CO_2 \quad (2\text{-}3)$$

These reactions need greater amounts of activating heat and light to encourage the process. Reaction type 1 normally occurs at the exposed surface of bitumen. A protective skin forms on the outer surface, which can delay hardening. When the skin is not abraded and the exposure to oxygen is low, the oxygen reaction and evaporation of volatile oils may be modified.

Tests to determine the resistance of bitumen to hardening are aimed at measuring the effect of heat and air on bitumen during the production process. The thin-film oven test (TFOT) was initially used to simulate practical conditions in order to determine the degree of volatilization and susceptibility to oxidation of bitumen in service. In this test, the amount of bitumen hardening was claimed to be similar to that which occurs in practice. The rolling thin-film oven test (RTFOT) was introduced later to improve bitumen's lack of homogeneity when exposed to heat and air and the continuous movement performed by TFOT. The test was used to estimate the degree of bitumen hardening in asphalt production plants. The amount of hardening seen in the RTFOT correlates well with a conventional batch at full scale mixing in practice (Read and Whiteoak 2003).

Ageing causes functional damage to asphalt because it reduces the flexibility in service life. The RTFOT method is commonly used to simulate the short-term ageing of asphalt binder during production (mixing, transporting and paving) of hot asphalt mix. In this method, the asphalt binder is heated for 85 minutes at 165°C to represent ageing effects comparable to average field conditions. One study claimed that excessive ageing time in the RTFOT caused an increase in the high temperature viscosity of asphalt binders. The study employed gel permeation chromatography (GPC) to measure the molecular size distribution of asphalt (Lee et al. 2008). However, another study reported that ageing causes an increase in the complex modulus and a decrease in the phase angle (Gomez, Quintana and Lizcano 2013).

Thin bitumen is normally used for noise-reducing pavement on high traffic volume roads and streets. In fact, thin bitumen surfacing covers approximately 3000 km of Australia's road network. However, there is still no prediction available for thin asphalt stiffness, especially for asphalt in Western Australia. Hence, it is important to study asphalt stiffness to ensure its resistance to severe distress such as fatigue cracking and permanent deformation, for asphalt designed according to Main Roads specifications.

2.5.3 Asphalt Performance and Stiffness

Much of the research in pavement engineering over the past decade can be classified into three groups, namely materials, structures and construction. Materials research aims to develop innovative materials, mixtures and additives, and carry out chemical and material characterization. Research into structures investigates the use and development of advanced techniques, sensors, equipment and models to understand pavement structure and its components. Pavement construction research aims to develop faster and better construction through investigating new procedures and equipment, construction under difficult conditions, and recycled materials.

Material characterization is used to evaluate the properties of asphalt concrete and to predict its performance in the field under major distress mechanisms such as fatigue cracking and permanent deformation (rutting). The tests are also performed to measure the response of materials to load, deformation and environmental conditions such as temperature, moisture or freeze-thaw cycles. Stiffness or load-spreading ability, fatigue resistance or resistance to cracking and deformation resistance or resistance to rutting are some important mechanical properties of asphalt pavement. Stiffness and fatigue resistance are determined from dynamic modulus, resilient modulus and flexural modulus. Permanent deformation is determined

from the creep compliance test. This section briefly reviews the material characterization of asphalt pavement in terms of permanent deformation and fatigue cracking.

2.5.3.1 Creep

As one of the most important distress mechanisms, permanent deformation (rutting) may occur as a sudden failure. Several tests are used to characterize permanent deformation, ranging from fundamental tests such as the uniaxial/triaxial tests and shear loading test, empirical tests such as the Marshall test and Hveem test, and simulative tests such as wheel tracking and asphalt pavement analyser (Zhang et al. 2005). Creep is an example of a uniaxial/triaxial test and is carried out by applying a static load to hot mix asphalt specimens and measuring the permanent deformation. The test is considered to be simple performance test for unconfined and confined samples under static or dynamic mode. The output is the response of the material, such as instantaneous elastic (recoverable) and plastic (irrecoverable) components (time independent), and viscoelastic and viscoplastic deformations (Witczak et al. 2002). Rutting is measured as the deformations caused by the viscoelastic and viscoplastic behaviour which is dependent on temperature and time of loading.

A dynamic creep test with uni-axial pulsed loading using an unconfined specimen is undertaken in accordance with AS 2891.12.1-1995 (Standards Australia 1995c). The procedures provided by Austroads AP-T100/08 Testing Asphalt Guide can be used to determine creep in accordance with the Austroads Mix Design Procedures (Austroads 2008e). The results are interpreted as the relationship between the level of service of the road and the weighted mean annual pavement temperature (WMAPT) to the required minimum slope value. The minimum slope values are used to classify the level of service of the traffic. The typical minimum slope from the creep test and the levels of service determined from the creep values can be seen in Table 2.8.

The creep test is widely used to predict permanent deformation owing to its simplicity and the availability of the laboratory procedures. However, studies have highlighted some interesting facts about this test. A direct comparison cannot be made between indirect tensile strength and uniaxial tensile creep. Wen (2003) showed that discrepancies occurred due to the incorrect initial assumption that asphalt is a homogeneous and isotropic material. Anisotropicity is believed to be the cause of both differences in performance. Another study by Zofka and Yut (2011) resulted in the modification of the bending beam rheometer (BBR), or the AASHTO procedure for determining creep compliance based on indirect tension test (AASHTO 2010) to accommodate sample thickness in order to measure creep. Sample

thickness was a problem for thin layers since the indirect tension test can only be performed on relatively thick specimens. Thick samples also cannot be used to determine oxidation and volatilization. As an alternative, the bending beam rheometer (BBR) test was used to measure low creep temperature using thin beam specimens made from asphalt mixture due to its practicality, efficiency, simplicity and repeatability of the test results (Velasquez et al. 2011, Turos et al. 2012). Those findings are certainly an improvement in determining permanent deformation through the creep test. Despite the discrepancies from both studies, it is still important to determine rutting (permanent deformation), taking into consideration the great differences between day and night temperatures. Furthermore, there are issues with the asphalt thickness in Western Australian roads, which are assumed to be not stiff enough to resist premature rutting failure. It is therefore recommended that creep be investigated in order to predict the permanent deformation of asphalt pavement in Western Australia.

Table 2.8 Typical laboratory minimum dynamic creep slopes in μm/m/cycle (Austroads 2008e)

WMAPT (°C)	Traffic			
	Very Heavy	Heavy	Medium	Light
>30	< 0.5	0.5 to 3	> 3 to 6	
20 – 30	< 1	1 to 6	> 6 to 10	*Not applicable*
10 – 20	< 2	2 to 10	*Not applicable*	

Traffic Levels	**Explanation**
Very Heavy	Stop/start traffic, climbing lanes, slow-moving vehicles; Traffic > $5x10^6$ (>500 commercial vehicles per day per lane), or Free flowing traffic: > $2x10^7$ ESA (> 1000 commercial vehicles per day per lane)
Heavy	Stop/start traffic, climbing lanes, slow-moving vehicles: < $5x10^5$ to $5x10^6$ (100 to 500 commercial vehicles per day per lane) or Free flowing traffic: in the range $5x10^6$ to $2x10^7$ ESA (500 to 1000 commercial vehicles per day per lane)
Medium	Stop/start traffic, climbing lanes, slow-moving vehicles: < $5x10^5$ ESA (< 100 commercial vehicles per day per lane) or Free flowing traffic: $5x10^5$ to $5x10^6$ ESA (100 to 500 commercial vehicles per day per lane)
Light	Free flowing traffic: < $5x10^5$ ESA (< 100 commercial vehicles per day per lane)

2.5.3.2 Resilient Modulus

Resilient modulus is defined as the elastic modulus based on the recoverable strain under repeated loads (Huang 2004). Asphalt is not an elastic-type material that sustains permanent

deformation at each load application. The deformation under repetitive load is recoverable since the applied load is less than the strength of the material. Resilient modulus under repeated load is illustrated in Figure 2.20.

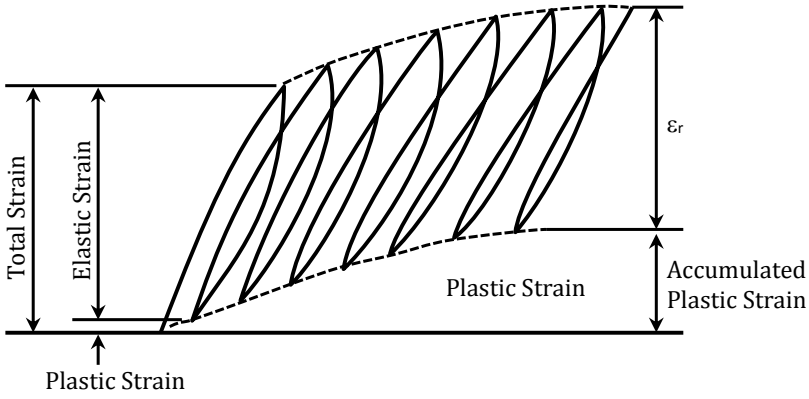

Figure 2.20 Strains under repeated load (Huang 2004)

It can be seen in Figure 2.20 that significant permanent deformation or plastic strain occurs at an early stage in the application of load. When there is an increase in the number of repetitions, a decrease in the plastic strain is observed. Normally, the strain is recoverable after 100 to 200 repetitions. The ratio of the amplitude of the repeated axial stress to the amplitude of the resultant recoverable axial strain is known as the resilient modulus (M_R). This ratio is defined as:

$$M_R = \frac{\sigma_d}{\varepsilon_t} \tag{2-4}$$

where

M_R = resilient modulus,

σ_d = axial stress in an unconfined compression test,

ε_r = plastic strain.

The resilient modulus test was developed by various researchers to obtain a rapid, low-cost and precise method. Schmidt (1972) proposed a direct method using the measurement of tensile strength/compressive tests in the laboratory. Barksdale et al. (1997) suggested using an extensive repeated load triaxial test to measure M_R for various base and subgrade materials. Later, MEPDG 2004 recommended the falling weight deflectometer (FWD) to measure in situ resilient modulus for subgrade materials. In the field, the M_R value can be determined by back-calculation procedures from measured surface deflections obtained from

FWD loading. Correction factors for the back-calculation were proposed to determine the equivalent laboratory resilient modulus values (Oh et al. 2011).

Several factors affect the resilient modulus values under cycling loading, such as material volumetric properties, test temperature, frequency of loading cycle, load magnitude, load duration, aggregate gradation and specimen dimensions (Law 2003, Saleh 2008, Shalaby, Liske and Kavussi 2004). Some of these factors can be explained as follows. The volumetric properties are determined by the asphalt density and air voids. As the air voids in the asphalt mix increase, the density and resilient modulus decrease. Using shorter load durations in testing results in a higher resilient modulus because the asphalt mixture has less time to perform a viscous response. It has been observed that mixtures with coarser gradation have a higher resilient modulus due to the increase of particle-to-particle contact in the aggregate structure. High resilient modulus values were also observed in thin and small specimens, which display a greater confinement effect of the aggregate particles than larger and thicker specimens.

The resilient modulus from indirect tensile test (ITT) was used to characterize asphalt concrete stiffness for decades. Since the development of the mechanistic-empirical design guide by NCHRP (2004b), the test is no longer used. By contrast, Austroads 2008 still includes the resilient modulus for pavement as the asphalt modulus value or design input at Stage 1 (Austroads 2008c). Table 2.9 shows the resilient modulus for dense graded asphalt mixes from the ITT test with 5% air voids. The values are used as a guide and presumptive values for design purposes for a range of mix sizes and binder types.

Table 2.9 Modulus (MPa) of typical Australian dense graded asphalts determined on laboratory-manufactured samples using the indirect tensile test procedure and standard test conditions and 5% air voids (Austroads 2008c)

Binder	Mix size (maximum particle size) (mm)					
	10		14		20	
	Range	Typical	Range	Typical	Range	Typical
Class 170	2000–6000	3500	2500–4000	3700	2000–4500	4000
Class 320	3000–6000	4500	2000–7000	5000	3000–7500	5500
Class 600	3000–6000	6000	4000–9000	6500	4000–9500	7000
Multigrade	3300–5000	4500	3000–7000	5000	4000–7000	5500
A10E	1500–4000	2200	2000–4500	2500	3000–7000	3000

Note: Standard test conditions are 40 ms rise time and 25°C test temperature (Standards Australia 1995a)

In addition, Table 2.10 presents the typical laboratory resilient modulus values for pavement application. The suggested values were applied for asphalt mixes with aggregates of

reasonable quality and about 70% of typical mixtures used in Australia (Austroads 2008e). Any variation in mixtures such as grading or fibre inclusion could possibly change the typical resilient modulus values.

Table 2.10 Typical laboratory resilient modulus values in MPa (Austroads 2008e)

Application	Class 170	Class 320	Multigrade or Class 600	A35P	AE10
Wearing course	2200	3000	4000	3000	2000
Intermediate layer or base course	3000	4000	5000	4000	2000
Fatigue course	2200	3000	4000	3000	2000

In one study, Loulizi et al. (2006) investigated the most accurate means of characterizing hot mix asphalt stiffness by comparing the resilient modulus with the dynamic modulus. Both tests were conducted for two typical mixes used in the Commonwealth of Virginia, USA. The results showed that the dynamic modulus is a better measure of stiffness than the resilient modulus because it can accommodate various temperatures and loading frequencies. Another study has confirmed that the resilient modulus test has low repeatability and high variability due to common experimental errors, which certainly does not support the use of resilient modulus in design calculations (Brown and Foo 1989).

Although MEPDG 2004 does not use the resilient modulus, this property is still considered essential for design input in Austroads 2008. However, an Austroads report has shown that it is inevitable that the great variability in resilient modulus measurements cannot represent actual conditions (Austroads 2006c). In one preliminary study on Western Australian asphalt mixtures, Rickards (2009) has suggested using the dynamic modulus as an alternative means of measuring stiffness, indicating that it performs better than ITT. He argued that the dynamic modulus is more accurate because the measurement method represents the actual load conditions on the road. His suggestion to use the dynamic modulus master curve and back-calculate the dynamic modulus from resilient modulus test data could be a solution for obtaining the values. Lee and Kim (2011) proposed back-calculation of dynamic modulus from resilient modulus test data to accommodate the practical measurement of stiffness using resilient modulus. The method is an attempt to back-calculate the existing resilient modulus values to obtain the dynamic modulus based on the theory of linear viscoelasticity. Further investigation is certainly necessary to obtain a clear explanation for this method.

2.5.3.3 Flexural Stiffness (Modulus)

Another method of characterizing asphalt stiffness is to obtain the flexural modulus from the flexural beam test, developed by the University of California, USA. This method is utilized to determine asphalt flexural stiffness, phase angle, dissipated energy per cycle, cycles to failure and cumulative dissipated energy upon asphalt failure. By applying simple elastic beam theory, the asphalt beam stiffness and the maximum strain level can be calculated to provide design data (Mallick and El-Korchi 2009). This test method is preferred because it is capable of reproducing the actual behaviour of an asphalt layer under traffic loading better than the other methods; consequently it is included in Report No 18 (APRG 2002) to check the performance of asphalt mixes (Austroads 2006b).

The flexural modulus value is needed for determining the fatigue life that is used as a design input parameter in mechanistic-empirical design. Inclusion of fatigue life is important in ensuring an efficient pavement structural design. Research shows that a relationship exists between the flexural fatigue and modulus or mixture stiffness. For a given thickness of asphalt when exposed to the same loading and temperature, a stiffer mix is more brittle and has reduced fatigue resistance. In an example given by Rickards (2009), increasing the modulus by about 10% (e.g. 5000 to 5500 MPa) reduces the critical tensile strain in asphalt by around 10%, theoretically increasing the fatigue life by about 60%. In practice, the consultant is pressed to translate this benefit into reduced asphalt thickness (10–15 mm).

The flexural fatigue test was used to verify and revise the asphalt modulus relationship in the Austroads 2008 (Austroads 2008c), i.e. the relationship between the ratio of the modulus at vehicle speed to the modulus from the standard indirect tensile test and design speed (Austroads 2008d). There has been little research, however, on utilizing the flexural fatigue test to characterize asphalt stiffness and correlate it with the indirect tensile test in Australia (Fakhri 1997, Pronk and Erkens 2002). The flexural fatigue test is necessary as it is a major input that can help predict fatigue life. It is also worth investigating the relationship of mix stiffness to fatigue characteristics in Western Australian mixes.

2.5.3.4 Dynamic Modulus

Dynamic Modulus and Phase Angle

The dynamic modulus is used to define the stress to strain relationship of viscoelastic material under a continuous sinusoidal loading (Witczak and Bari 2004). The stiffness of a particular mix over a wide range of temperatures and loading frequencies can certainly be determined through the dynamic modulus. The dynamic modulus or complex modulus $|E^*|$

is a complex number that expresses the relationship between stress and strain under sinusoidal loading for linear viscoelastic materials like asphalt mixtures. In theory, the dynamic modulus is measured by dividing the maximum stress by the peak recoverable axial strain for viscoelastic material under non-static load conditions, as shown in Figure 2.21.

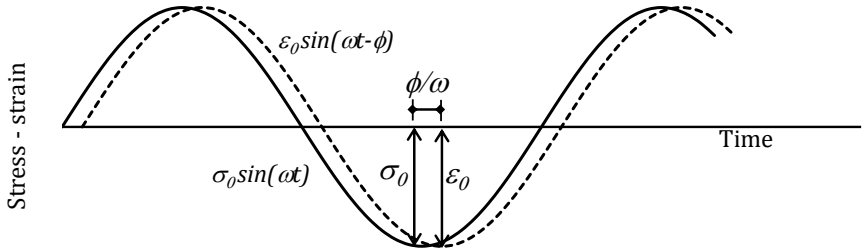

Figure 2.21 Dynamic modulus (Witczak and Bari 2004)

The complex dynamic modulus formula can be written as follows:

$$|E^*| = \frac{\sigma}{\varepsilon} = \frac{\sigma_0 e^{i\omega t}}{\varepsilon_0 e^{i(\omega t-\phi)}} = \frac{\sigma_0 \sin \omega t}{\varepsilon_0 \sin(\omega t - \phi)} \quad (2\text{-}5)$$

Where:

$|E^*|$ = complex dynamic modulus,

σ_0 = peak (maximum) stress,

ε_0 = peak (maximum) recoverable axial strain,

ϕ = phase angle (degrees),

ω = angular velocity (degrees per second),

t = time (seconds).

Hence, the dynamic modulus $|E^*|$ can be expressed as the absolute value of the complex modulus:

$$|E^*| = \frac{\sigma_0}{\varepsilon_0} \quad (2\text{-}6)$$

The phase angle (ϕ) indicates viscosity or elasticity of asphalt mixtures. In a viscoelastic material such as asphalt, there is a time lag where the corresponding strain occurs some time after the load has been applied. Since this linear viscoelastic material is time dependent, the pure elastic and pure viscous materials have different phase angle, which are $\phi = 0°$ and 90°, respectively. Other values between 0 and 90° can be seen in Figure 2.22, where three different viscoelastic responses are distinguished, i.e. ϕ = 0–5° is elastic, ϕ = 5–45° is

viscoelastic (typical of asphalt mixtures) and ϕ = 45–90° is predominantly viscous. Phase angle can be calculated as follows:

$$\phi = \frac{T_i}{T_p} \times 360^o \quad (2\text{-}7)$$

where:

T_i = time lag between stress and strain,

T_p = period of applied stress.

Phase angle is affected by various factors, such as aggregate gradation, asphalt cement content, air voids, effective binder volume, voids in mineral aggregates (VMA), voids filled with asphalt (VFA), binder characteristics (A and VTS), binder viscosity, test temperature and frequency of loading. In a recent study (Biligiri, Kaloush and Uzan 2010), the phase angle was investigated as a practical measurement of the noise-dampening characteristics of pavement in the field. A phase angle predictive equation was also developed from over 6510 data points in the study, and it was claimed to be a good parameter for predicting viscoelastic properties without the need for extensive experimentation.

Some factors affecting the dynamic modulus are specimen geometry, nominal aggregate size, loading time and test temperature. A study on 17 field/lab mixtures by Robinette et al. (2010) showed that maximum aggregate size, test temperature and binder grades influence the dynamic modulus variability. Kim, Momen and King (2005) noted that the asphalt source, grade and content were more influential on /*E**/ than aggregate source and gradation. Furthermore, mixtures with large size aggregates showed a high dynamic modulus /*E**/ or stiffness due to a strong aggregate interlock in the system (Mohammad et al. 2007). Inclusion of additives such ash styrene butadiene styrene (SBS) produced high /*E**/ mixes with regard to a decrease of energy loss at high temperature (Kumar and Veeraragavan 2011).

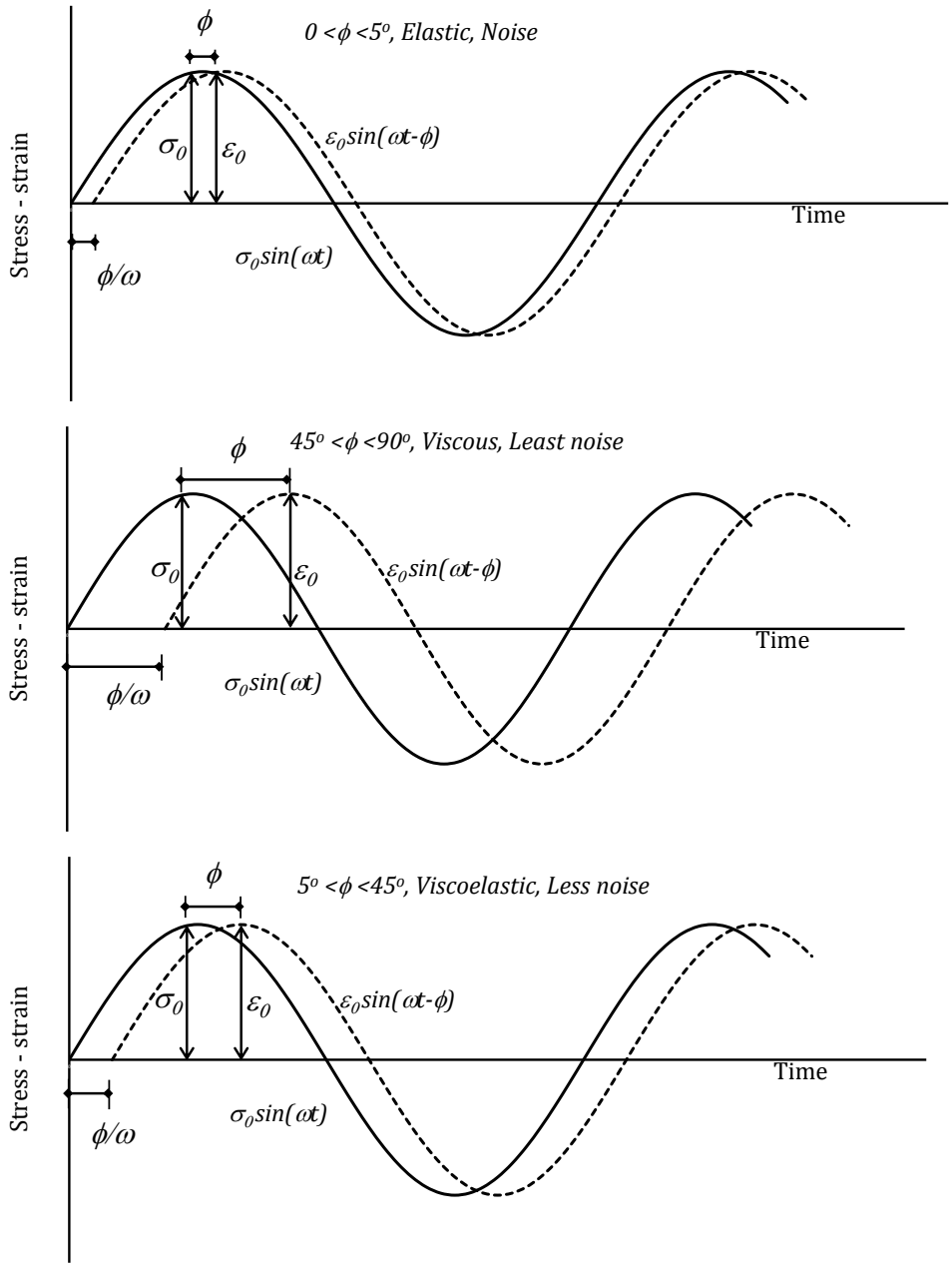

Figure 2.22 Asphalt mixture stress-strain responses under a sinusoidal load for different viscoelastic behaviour (Biligiri, Kaloush and Uzan 2010)

As discussed in section 2.4.2, there are three hierarchical levels of input in MEPDG 2004, and the dynamic modulus can be determined by various methods at each level. At Level 1, the dynamic modulus is taken in the laboratory at various temperatures and loading frequencies. The suggested temperatures and frequencies used in previous studies can be seen in Table 2.11. At this level, the master curve is developed to illustrate the time-temperature dependency of the mix response. In the second and third levels, an empirical

equation or predictive equation is employed to develop the master curve. The predictive equations were provided in anticipation of a lack of laboratory testing capabilities and the high cost of labour. At Level 3, the values used in the equation are performance grade, viscosity grade and penetration grade of the binder.

Table 2.11 Summary of temperature and frequencies used in some studies

Study	Temperature (°C)	Frequency (Hz)	Remarks
Fonseca and Witczak (1996)	-17.8, 4.4, 21.1, 37.8, 54.4	25, 10, 1, 0.1	Temperature is allowed to deviate ±0.5 from target
Di Benedetto et al. (2001, 2004)	10	10 Hz	Single temperature per specimen
Clyne et l. (2003).	-20, -10, 4, 20, 40, 54	25, 10, 1, 0.1, 0.01	
NCHRP (2004c)	-10, 4, 21, 37, 54	25, 10, 5, 1, 0.5, 0.1	Minimum recommended series
Kim et al. (2004)	-10, 10, 35	25, 10, 5, 1, 0.5, 0.1, 0.05, 0.01	
Rickards (2011)	5, 20, 35, 50	25, 10, 5, 1, 0.5, 0.1	Confinement at high temperatures is recommended

Although the predictive equation was designed by considering the material response, there are two conditions that significantly influence the stiffness of pavement (Zeghal and Mohammed 2008). Firstly, the dynamic modulus was unstable at two extreme temperatures. At a low temperature, the dynamic modulus was low and might under-predict low temperature cracking. Secondly, the dynamic modulus over-predicted and gave a false high stiffness at high temperature, thus disguising the potential for major distress such as rutting due to actual low stiffness. It is therefore recommended to use a Level 1 MEPDG 2004 predictive equation to reduce design errors at other levels.

Master Curve, Shift Factor and Sigmoidal Function

The master curve is a graph illustrating the viscoelastic behaviour of asphalt as a function of both temperature and loading frequency. It is generated from experimental dynamic modulus values at a range of temperatures and frequencies. The time-temperature superposition principle introduced by Witczak and Fonseca (1996) is applied to generate the master curves. This principle allows all dynamic modulus test data at various temperatures and frequencies to be shifted to a reference temperature or frequency to form a new single master curve. The horizontal translations are for $|E^*|$ values above and below the reference temperature, while the data at reference temperature remains unaffected. Some typical fitted master curves from one study (Zhu et al. 2011) are presented in Figure 2.23.

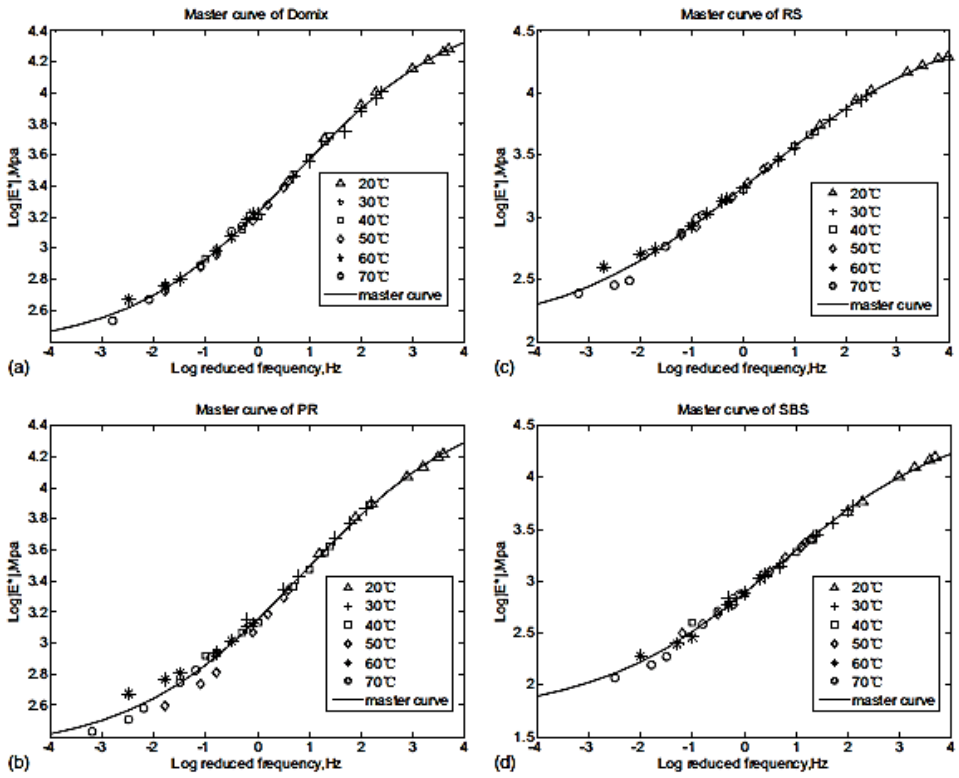

Figure 2.23 Samples of fitted master curve for various mixes used in the study (Zhu et al. 2011).

To construct the master curve and to enable shifting of data to the curve, a shift factor is used to shift dynamic modulus at various temperatures to the reference temperature. The shift factor is described as the required shift at a given temperature, and is equal to 1 at the reference temperature. It can be written as follows:

$$t_r = \frac{t}{a_T} \tag{2-8}$$

$$\log t_r = \log t - \log a_T \tag{2-9}$$

where:

t_r = time of loading at the reference temperature,

t = time of loading at a given temperature of interest,

a_T = shift factor as a function of temperature,

T = temperature of interest.

The shift factors are determined from binder viscosity for the age and temperature of interest. Binder effect in the master curve generation is incorporated through the viscosity-

temperature relationship. The asphalt viscosity-temperature relationship is determined by linear regression after log-log transformation of the viscosity data and log transformation of the temperature data:

$$\log\eta = \log^{(A+VTS\log T)} \tag{2-10}$$

where:

η = viscosity (cP),

T = temperature at which the viscosity was estimated (Rankine),

A, VTS = regression parameters,

A = regression intercept,

VTS = regression slope of viscosity temperature susceptibility.

The A and VTS parameters can be determined from the test in accordance with AASHTO T315-09: Determining the Rheological of Asphalt Binder using a Dynamic Shear Rheometer (DSR) (AASHTO 2009), or other tests to obtain viscosity, softening point and penetrations.

As the measured dynamic modulus $|E^*|$ values are shifted, the master curve is established. To improve the master curve by manipulating and processing, some mathematical functions or sigmoid functions are applied to the data. The sigmoid function is used by MEPDG 2004 to mathematically model the dynamic modulus master curve, and can be expressed as follows:

$$\log|E^*| = \delta + \frac{\alpha}{1+e^{\beta+\gamma\log t_r}} \tag{2-11}$$

where:

$|E^*|$ = dynamic modulus (psi),

t_r = time of loading at the reference temperature,

δ, α = fitting parameters, δ represents the minimum value of $|E^*|$ and $\delta+\alpha$ represents the maximum value of $|E^*|$,

β, γ = parameters describing the shape of the sigmoidal function.

Detailed equations to determine the fitting parameters are found elsewhere (NCHRP 2004a).

Both fitting parameters and shift factors are important for generating master curves. The fitting parameters used in master curves depend on some material properties. The δ is a function of aggregate gradation, the binder content and the air void content, while α only varies through aggregate gradation (NCHRP 2004a). The β and γ depend on the asphalt characteristics and magnitude of δ and α.

The dynamic modulus test has never been used for design purposes in Australia to determine stiffness. The Austroads method for pavement design uses indirect tensile strength, which cannot be precisely applied to viscoelastic materials like asphalt. The current test is limited in its ability to simulate actual traffic and local weather conditions, especially weather and traffic load in Western Australia. By applying the dynamic modulus test and its associated master curve for Western Australian pavement, it is possible to characterize the viscoelastic behaviour of asphalt mixtures under a wide range of temperatures and loading frequencies to minimize design complexity.

2.5.4 Asphalt Stiffness Prediction

2.5.4.1 Fatigue Life

The damage to asphalt pavements due to repetitive stresses and strains caused by traffic loading and environmental factors is called fatigue cracking. This behaviour is mainly affected by air voids, binder type, binder content, aggregate type, temperature and mode of loadings. Fatigue cracking is controlled by tensile strain at the bottom of the asphalt layer and compressive strain at the top of the subgrade. These main factors govern the mechanistic approach to designing flexible pavement by trying to limit strain values in order to increase fatigue resistance.

Fatigue life is defined as the number of traffic repetitions that the pavement can sustain before fatigue failure or the number of cycles to failure. Zaitsev (1994) defined fatigue life as the number of cycles required to reduce the flexural stiffness of an asphalt mix to half its initial value. Fatigue life is used to predict pavement performance by estimating the remaining life of the pavement due to cracking (Rajbongshi 2009). Generally, fatigue depends on the loading (load history, rate of application, wave form, type of specimen), mixture characteristics (air void content, stiffness, asphalt content, aggregate type and gradation, asphalt type and hardness), and environmental conditions (temperature, moisture).

There is also a difference between constant-strain and constant-stress modes of loading for both thin and thick layers (Rolt 2004, Romanoschi, Dumitru and Dumitru. 2006). When the asphalt layer is thin, the bases become load-bearing layers and the mode of loading is constant-strain. By contrast, when a thick asphalt layer acts as one of the main load-bearing layers, the mode of loading is closer to constant-stress. Fatigue life is measured differently for thick asphalt layers (>100 mm) and thin layers (<100 mm). The fatigue life for thick asphalt layers is characterized using stress-controlled tests with a small number of

specimens. In this case, the stiffness of the asphalt is proportional to fatigue life. Conversely, the characterization of the fatigue life of thin asphalt layers is done using strain-controlled tests with a large number of specimens due to the high variability of the test results. The strain in a thin asphalt layer depends solely on the underlying layers and the pavement layer is not the main load-carrying component. A reduction in layer stiffness could significantly reduce the fatigue life. Figure 2.24 shows the effect of asphalt layer thickness on the calculated fatigue life. A significant increase in fatigue life is observed when the thickness of the asphalt is changed from 100 mm to 235 mm (Said et al. 2011).

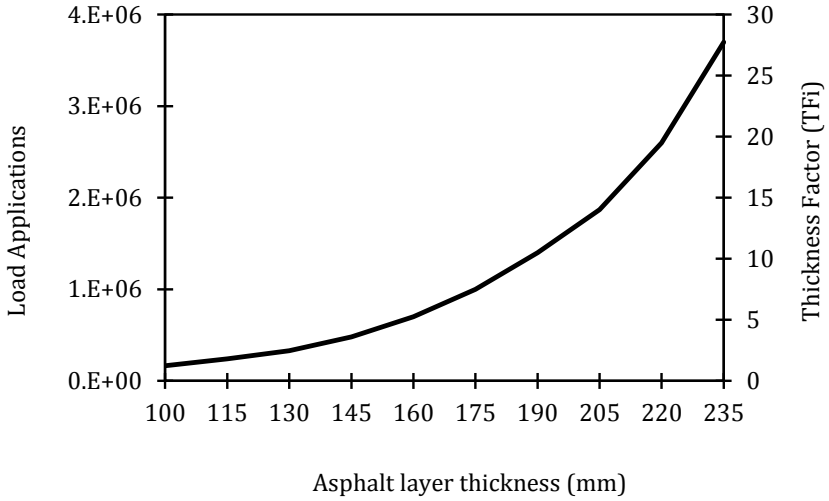

Figure 2.24 The influence of asphalt layer thickness on fatigue life (Said et al. 2011)

Fatigue Cracking Model

Some models of fatigue life have been developed according to various testing configurations used and materials tested. The models are a function of the tensile strain and mix stiffness (modulus), and are formed to predict the load repetitions leading to fatigue cracking. MEPDG 2004 (NCHRP 2004b) used the following model for fatigue characterization:

$$N_f = Ck_1\left(\frac{1}{\varepsilon_t}\right)^{k_2}\left(\frac{1}{E}\right)^{k_3} \tag{2-12}$$

$$N_f = \beta_{f1}k_1\varepsilon_t^{-\beta_{f2}k_2}E^{-\beta_{f3}k_3} \tag{2-13}$$

where:

N_f = number of repetitions of fatigue cracking

ε_t = tensile strain at the critical location

E = stiffness of the material

k_1, k_2, k_3 = laboratory regression coefficients

β_{f1}, β_{f2}, β_{f3} = calibration parameters

C = laboratory to field adjustment factor

The Asphalt Institutes model for predicting the number of load repetitions to fatigue cracking, which is based on constant stress, is as follows:

$$N_f = 0.00432\ C\left(\frac{1}{\varepsilon_t}\right)^{3.291}\left(\frac{1}{E}\right)^{0.854} \quad (2\text{-}14)$$

$$C = 10^M \quad (2\text{-}15)$$

$$M = 4.84\left(\frac{V_b}{V_a + V_b} - 0.69\right) \quad (2\text{-}16)$$

where:

N_f = number of repetitions to fatigue cracking

ε_t = tensile strain at the critical location

E = stiffness of the material

C = laboratory to field adjustment factor

V_b = effective binder content (%)

V_a = air voids (%)

In MEPDG 2004, the field fatigue characterization model was governed by numerical optimization and other modes of comparison to produce national calibration factors of:

β_{f1} $= k_1.\beta'_{f1}$

β'_{f1} $=1.0$

β_{f2} $=1.2$

β_{f3} $=1.5$

The following final model allows the prediction of fatigue cracking with top-down or bottom-up mode.

$$N_f = 0.00432 \cdot k'_1\, C\left(\frac{1}{\varepsilon_t}\right)^{3.9492}\left(\frac{1}{E}\right)^{1.281} \quad (2\text{-}17)$$

This equation uses the parameter k'_1, which is a correction for different asphalt layer thickness (h_{ac}) effects. The k'_1 is defined as follows:

a) For bottom-up cracking:

$$k'_1 = \left(\frac{1}{0.000398 + \frac{0.003602}{e^{11.02-3.49 \cdot hac}}} \right) \quad (2\text{-}18)$$

b) For top-down cracking:

$$k'_1 = \left(\frac{1}{0.01 + \frac{12.00}{1+e^{15.676-2.8186 \cdot hac}}} \right) \quad (2\text{-}19)$$

where:

h_{ac} = total thickness of the asphalt layers, in

Austroads 2008 (Austroads 2008c) uses one of Shell (1978) relationships showing a general relationship between the maximum tensile strains in asphalt produced by a specific load and the allowable number of repetitions of that load:

$$N = RF\left(\frac{6918 \cdot (0.856 V_b + 1.08)}{S_{mix}^{0.36} \cdot \varepsilon_\mu} \right)^5 \quad (2\text{-}20)$$

where:

N = allowable number of repetitions of the load

ε_μ = tensile strain produced by the load (microstrain)

V_B = percentage by volume of bitumen in the asphalt (%)

S_{mix} = asphalt modulus (MPa)

RF = reliability factor for asphalt fatigue (Table 2.12)

Table 2.12 Suggested reliability factors (RF) for asphalt fatigue (Austroads 2008c)

Desired project reliability				
80%	85%	90%	95%	97.5%
2.5	2.0	1.5	1.0	0.67

It was highlighted that the laboratory fatigue underestimates the field fatigue. This is due to the fact that laboratory fatigue does not simulate actual field conditions such as crack propagation time, effect of frequency of loading pulses, loading mode, ageing and healing effects (Said et al. 2011). The main differences between laboratory fatigue and field fatigue evaluation are shown in Figure 2.25. To overcome uncertainty in the prediction of fatigue

life, a shift factor is used as an adjustment factor or calibration of fatigue equation. The shift factor is the ratio of field fatigue life to laboratory fatigue life. The typical values could be constant such as 20–100 or 40–100 (Adhikari, Shen and You 2009, Said et al. 2011), or vary with parameters such as strain or dynamic modulus.

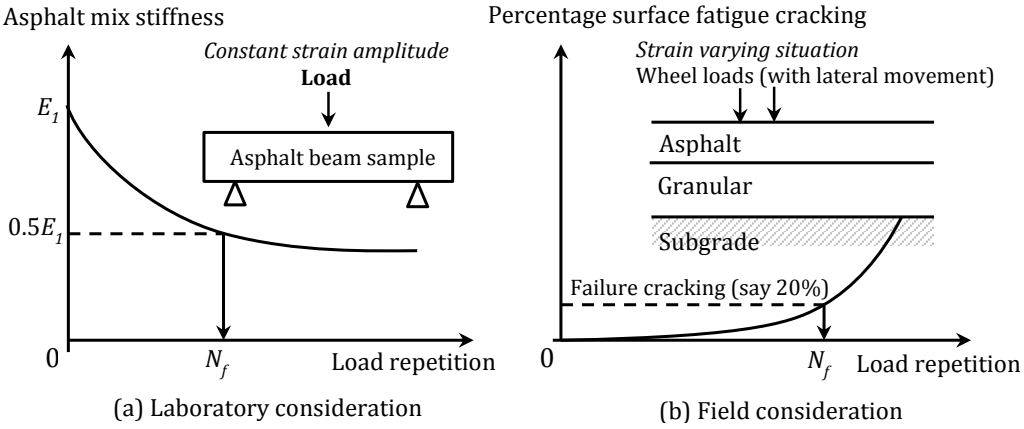

Figure 2.25 Laboratory fatigue and field fatigue considerations (Rajbongshi 2009)

Li and Metcalf (2004) support this argument because they have found that actual fatigue life was higher than the lab-based predictions on bending beam or indirect tensile fatigue tests. This may be due to the effect of sample dimensions on fatigue life measurement. In this research, the fatigue test was used to investigate crack initiation and propagation. Initially, it was suggested that the differences between laboratory and field fatigue life performance were due to variances of calculated versus measured strain, the state of stress in the field and in the laboratory, laboratory-compacted specimens and field compaction, traffic wander area and asphalt healing during the rest period (Vanelstraete, Leonard and Veys 2000).

The Austroads 2008 design method employs fatigue modelling to design heavy traffic roads and industrial pavements. However, it has been argued that using fatigue modelling to design pavement thickness results in overly conservative and wasteful designs for the traffic classes (Rickards 2011). Western Australia uses thin pavement layers that undergo constant strain under loading. From the above review, since fatigue life is a key factor in asphalt performance to predict the remaining pavement life, more data regarding this property at various layer temperatures and stiffnesses is strongly desirable.

2.5.4.2 Dynamic Modulus Predictive Models

An alternative means of estimating dynamic modulus is to use a predictive model. The model is based on an equation to calculate *E** from volumetric properties. The most common models used are the Shell Oil equation, the Witczak model and the Hirsch model. The Witczak model was established empirically by using 149 different mixtures to predict the dynamic modulus at a range of temperatures, rates of loading and ageing conditions. The dynamic modulus model is as follows (Lee et al. 2007, Witczak et al. 2002):

$$\log|E^*| = 1.249937 + 0.029232(P_{200}) - 0.001767(P_{200})^2 - 0.002841(P_4) - 0.058097(V_a) - \frac{0.802208V_{eff}}{V_{eff}+V_a}$$

$$+\frac{3.871977 - 0.0021(P_4) + 0.003958(P_{38}) - 0.000017(P_{38})^2 + 0.00547(P_{34})}{1+e^{(-0.603313 - 0.313351\log(f) - 0.393532\log\eta)}} \quad (2\text{-}21)$$

where:

$|E^*|$ = asphalt mix dynamic modulus, 10^5 psi

η = bitumen viscosity, 10^6 poise

f = load frequency, Hz

V_a = percent air voids in the mix, by volume

V_{eff} = percent effect bitumen content, by volume

P_{34} = percent retained on 19 mm sieve, by total aggregate weight (cumulative)

P_{38} = percent retained on 9.5 mm sieve, by total aggregate weight (cumulative)

P_4 = percent retained on 4.76 mm sieve, by total aggregate weight (cumulative)

P_{200} = percent retained on 0.075 mm sieve, by total aggregate weight

The Hirsch model is another means of predicting the dynamic modulus, and is as follows (Mohammad et al. 2007):

$$|E^*| = P_c\left[4200\left(1-\frac{VMA}{100}\right)+3|G^*|\left(\frac{VFA\times VMA}{10{,}000}\right)\right]+\frac{1-P_c}{\frac{1-VMA/100}{4{,}200{,}000}+\frac{VMA}{3\cdot VFA\cdot|G^*|}} \quad (2\text{-}22)$$

$$P_c = \frac{\left(20+\frac{VFA\times 3|G^*|}{VMA}\right)^{0.58}}{650+\left(\frac{VFA\times 3|G^*|}{VMA}\right)^{0.58}} \quad (2\text{-}23)$$

where:

$|E^*|$ = dynamic modulus for the asphalt mixture, psi

$|G^*|$ = complex shear modulus for the binder, psi

P_C = contact factor

VMA = void in the mineral aggregate, percent

VFA = void filled with asphalt, percent

Bari and Witczak (2007) suggested the modified model for $|G^*|$.

$$\left|G^*\right| = 0.0051 f_s \eta_{fs,T} \left(\sin \delta_b\right)^{7.1542 - 0.4929 f_s + 0.0211 f_s^2} \quad (2\text{-}24)$$

where:

$|G^*|$ = dynamic shear modulus (Pa), for calculated $|G^*|_{binder}$ > 1GPa, use $|G^*|_{binder}$ = 1GPa

f_s = dynamic shear loading frequency to be used with $|G^*|_{binder}$ and δ_b (Hz) =1/(2πt), t = loading time (s)

$\eta_{fs,T}$ = viscosity of asphalt binder as a function of both loading frequency (f_s) and temperature (T), cP

δ_b = phase angle, degree

Viscosity of asphalt binder ($\eta_{fs,T}$) is calculated using the following equations.

$$\log\log \eta_{f_s,T} = A' + VTS' \log T_R \quad (2\text{-}25)$$

$$A' = 0.9699\ f_s^{-0.0527} \times A \quad (2\text{-}26)$$

$$VTS' = 0.9668\ f_s^{-0.0575} \times VTS \quad (2\text{-}27)$$

where:

$\eta_{fs,T}$ = viscosity of asphalt binder as a function of both loading frequency (f_s) and temperature (T), (cP) (for calculated $\eta_{fs,T} > 3\text{x}10^{12}$ cP, use $\eta_{fs,T} = 3\text{x}10^{12}$ cP)

f_s = loading frequency in dynamic shear mode as used in the $|G^*|_{binder}$ testing (Hz) =1/(2πt), t = loading time (s)

A = regression intercept from the conventional ASTM A_i-VTS_i from Equation 2-10

VTS = slope from the conventional ASTM A_i–VTS_i from Equation 2-10

A' = adjusted A (adjusted from loading frequency)

VTS' = adjusted VTS (adjusted from loading frequency)

T_R = temperature in Rankine scale, (°R)

The phase angle of binder (δ_b) is determined using the following equation.

$$\delta_b = 90 + \left(b_1 + b_2\, VTS'\right) \times \log\left(f_s \times \eta_{fs,T}\right) + \left(b_3 + b_4\, VTS'\right) \times \left\{\log\left(f_s \times \eta_{fs,T}\right)\right\}^2 \quad (2\text{-}28)$$

where

δ_b = binder phase angle (deg) (for calculated δ_b > 90°, use δ_b = 90°),

VTS' = adjusted VTS from Equation 2-10

f_s = loading frequency in dynamic shear (Hz) =1/(2πt), t = loading time (s)

$\eta_{fs,T}$ = viscosity of asphalt binder as a function of both loading frequency (f_s) and temperature (T), (cP), and b_1, b_2, b_3, b_4 are fitting parameters = −7.3146, −2.6162, 0.1124, and 0.2029, respectively.

Some researchers have argued that the Witczak model tends to overemphasize the influence of temperature and understate the influence of other mixture characteristics at the very low and high temperature extremes (Apeagyei, Diafenderfer and Diafenderfer 2011, Ceylan et al. 2009). For example, in a study of Korean asphalt mixtures (Lee et al. 2007), slightly higher values at high test temperature and lower values at low temperature were observed from the predicted dynamic modulus. Although both models were mostly used in dynamic modulus prediction, the accuracy and robustness of the Witczak and Hirsch models are still debatable. The models might need to be modified to suit local aggregate gradations and shapes, and asphalt properties. An attempt was made to model the viscoelastic-based microstructure of hot mix asphalt, and there were found to be some discrepancies between the new and old models. As a result, the Witczak and Hirsch models were still popular (Shu and Huang 2008).

Witczak model prediction has been used in various studies to estimate dynamic modulus values for asphalt mixtures. It was found that the predictive equation and measured dynamic values were not significantly different. A study by Mohammad et al. (2007) on the measured and predicted dynamic modulus values for Louisiana asphalt mixtures showed good agreement with an R-square greater than 0.90. However, some studies did show great discrepancies between the measured and Witczak predicted dynamic values, which arose mainly from the type of mix, air voids and temperatures (Singh, Zaman and Commuri 2012a).

Austroads 2008 uses the resilient modulus to characterize the stiffness of hot mix asphalt. Typical binders with limited presumptive elastic modulus values are too weak to model a wide range of temperatures and loading rates. However, using the dynamic modulus with a master curve is a means of presenting stiffness characterization over a wide range of temperatures and loading frequencies in small increments, in order to produce precise values. These values may even be used with the Witczak and Hirsch models without undertaking the test, when the aggregate characteristics and asphalt properties are known. Therefore, it is important to compare the measured and predictive dynamic modulus values using both models. This may be a new approach to determining stiffness from well-known predictive equations and to investigating their validity for WA asphalt mixtures.

2.5.4.3 Statistical Assessment of Dynamic Modulus Predictive Models

The accuracy of the /*E**/ predictive model can be assessed using statistical analysis. Researchers use many statistical methods to assess the accuracy of the predictive models. The first method is to calculate the dynamic modulus values from both dynamic predictive models and compare them with the measured values in a proportionally distributed graph. It is common to assume that the predicted model has a good correlation when the matching points are fairly distributed around the equality line. This method has been used by many researchers such as Tran (2005), who calculated the values using statistical analysis. The correlation between the predicted and measured values was strong and the models were in agreement with the lab values. Another method employed in the accuracy assessment is to visually compare the master curve of the measured and predicted dynamic modulus values at a reference temperature.

Statistical methods using goodness-of-fit statistics, including the lack-of-fit statistic (S_e/S_y = the standard error of estimate/standard deviation), and the correlation coefficient (R^2) were employed in this research. The lack-of-fit statistic (S_e/S_y) is a measure of the improvement in the accuracy of prediction of the predictive model. The smaller the value, the better the prediction. The correlation coefficient (R^2) is a measure of the model accuracy, and is better used for linear models with a large sample size. The higher the value, the better the prediction. Both values of the lack-of-fit statistics and the correlation coefficient can be calculated using the following equations:

$$S_e = \sqrt{\frac{\sum (y - \hat{y})^2}{n - k}} \tag{2-29}$$

$$S_y = \sqrt{\frac{\sum (y - \bar{y})^2}{n - 1}} \tag{2-30}$$

$$R^2 = 1 - \frac{(n-k)(S_e)^2}{(n-1)(S_y)^2} \tag{2-31}$$

where:

S_e = standard error of estimate

S_y = standard deviation

R^2 = correlation coefficient

$\hat{y}$ = measured dynamic modulus

$\bar{y}$ = mean value of tested dynamic modulus

n = sample size

k = number of independent variables in the model

The method is used to determine the bias and precision of the predictive models. Bias is related to the difference between predicted and observed values, while precision is determined by the errors and other factors. To increase the precision/accuracy and to decrease the bias in modelling, it is imperative to minimize the sum of square of errors and sum of errors, respectively. Both concepts are illustrated in Figure 2.26.

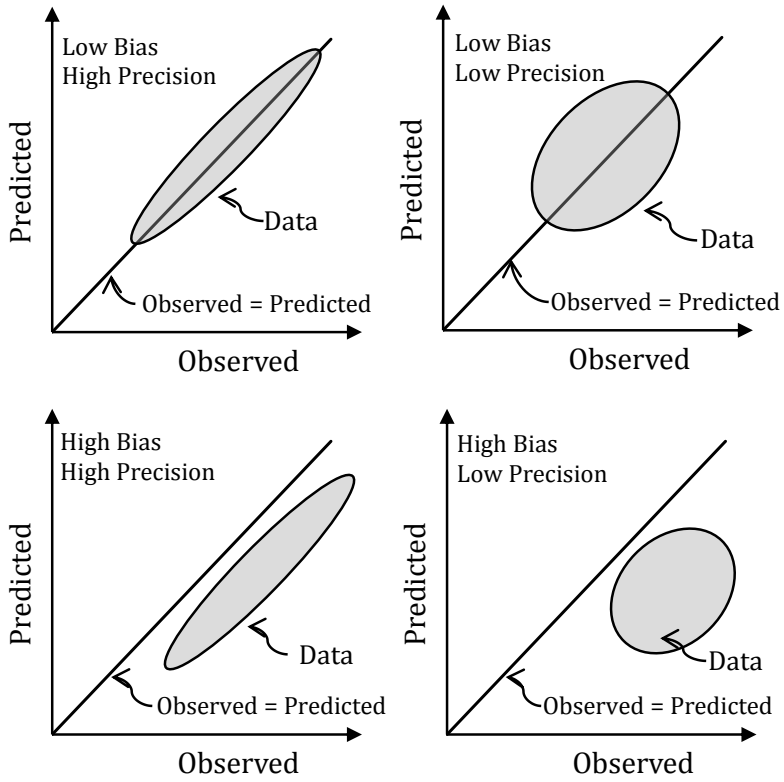

Figure 2.26 Illustration of bias and precision (Tran 2005)

The performance of the predictive models can be analysed using the criteria given in NCHRP Project 9-19 Task C (Witczak et al. 2002). The criteria for goodness of fit are presented in Table 2.13. Previous studies have reported various results for the criteria for goodness of fit. Most prediction errors were related to mixture properties, such as binder grade, volumetric properties and aggregate properties.

Table 2.13 Criteria for goodness of fit

Criteria	R^2	S_e/S_y
Excellent	≥ 0.90	≤ 0.35
Good	0.70 – 0.89	0.36 – 0.55
Fair	0.40 – 0.69	0.56 – 0.75
Poor	0.20 – 0.39	0.76 – 0.89
Very Poor	≤ 0.19	≥ 0.90

2.6 Summary

2.6.1 Research Needs

Increases in automobile technology have had an impact on traffic load, which is changing the role of conventional asphalt pavement. Asphalt is the most widely used material in transportation. The key challenge is to improve the quality of asphalt pavement by providing a stiffer material that can resist major distress mechanisms such as fatigue cracking and permanent deformation, so that it can fulfil the requirement of long life pavement with low cost maintenance. The stiffness measurement has been incorporated in the mechanistic-empirical structural pavement design in order to overcome sudden failure. At this stage, the stiffness measurement in Australia, particularly Western Australia, relies only on resilient modulus (indirect tensile strength) and does not accommodate local materials and environment conditions. Further research and development are needed into laboratory stiffness characterization in Western Australia including:

a) A systematic study of stiffness characterization under fatigue cracking, including all types of cracking, i.e. bottom-up and top-down, to obtain a precise measure of stiffness at various thicknesses of asphalt layers.
b) A systematic study of creep as a means of characterizing permanent deformation, including the occurrence of permanent deformation due to highly elevated temperatures during summer, especially since the Austroads 2008 does not accommodate this type of distress measurement due to difficulties in modelling the behavior. It is recommended to investigate creep in order to predict the permanent deformation of asphalt pavement in Western Australia.
c) A systematic study of stripping and thermal cracking as a means of characterizing major distresses. It is important to investigate stripping since asphalt mixtures in Western Australia use granite as a source of material, and the siliceous, low affinity and hydrophilic properties of granite may induce stripping. The development of thermal cracking as one of the major distress modes, which is relevant because of the contrast between day and night temperatures in Western Australia.

d) A study of resilient modulus of Western Australia asphalt mixtures using various parameters as indicative values for pavement design inputs. An inclusion of back calculation of dynamic modulus from resilient modulus test data is also more relevant to accommodate practical measurement of stiffness.
e) A systematic study on flexural fatigue to characterize asphalt stiffness and to predict fatigue life. An investigation of correlation between mix stiffness and fatigue characteristics in Western Australian mixes is necessary.
f) A systematic study of dynamic modulus /*E**/ under a wide range of loading frequencies and temperatures, dynamic modulus /*E**/ master curves construction, and analysis of some factors influencing the dynamic modulus.
g) A study of to compare between laboratory measured and predictive dynamic modulus values using Witczak and Hirsch model. An inclusion of statistical analysis is relevant to reduce bias and increase precision in modelling.

2.6.2 Research Objectives

The above literature review has identified various research gaps in the field. It is impossible to completely research all of the issues, so this thesis focuses on an investigation of the characterization of asphalt mixtures in Western Australia. The objectives are:

a) To measure creep values as a means of characterizing permanent deformation for typical Western Australian mixtures.
b) To investigate resilient modulus for typical Western Australian mixtures and compare the laboratory data to the modulus values listed in the Austroads 2008.
c) To determine flexural fatigue by measuring beam fatigue for typical Western Australian mixtures.
d) To establish the dynamic modulus /*E**/ values for typical asphalt mixes used in Western Australia by measuring the laboratory dynamic modulus and phase angle using normal and Rolling Thin Film Oven Test (RTFOT) aged binders. In addition, the /*E**/ master curves are generated and factors influencing the measured /*E**/ are evaluated.
e) To compare the predicted and measured dynamic modulus master curve using MEPDG Witczak and Hirsch's predictive models. Validation of the Witczak and Hirsch's model predicted data /*E**/ with laboratory /*E**/ is investigated. Statistical evaluation of Witzcak and Hirsch predictive equations is conducted.

3 RESEARCH METHODOLOGY

3.1 Introduction

This chapter presents the experimental procedure and modelling of asphalt stiffness. The experimental investigation aims to study the various means of stiffness characterization, such as creep, indirect tensile strength, beam fatigue, and dynamic modulus. In addition, dynamic modulus master curves will be established. Fatigue life will be modelled in order to predict asphalt performance by the MEPDG 2004 method. The asphalt mixes used will be designed according to Main Roads specifications. Figure 3.1 shows the layout of the research plan.

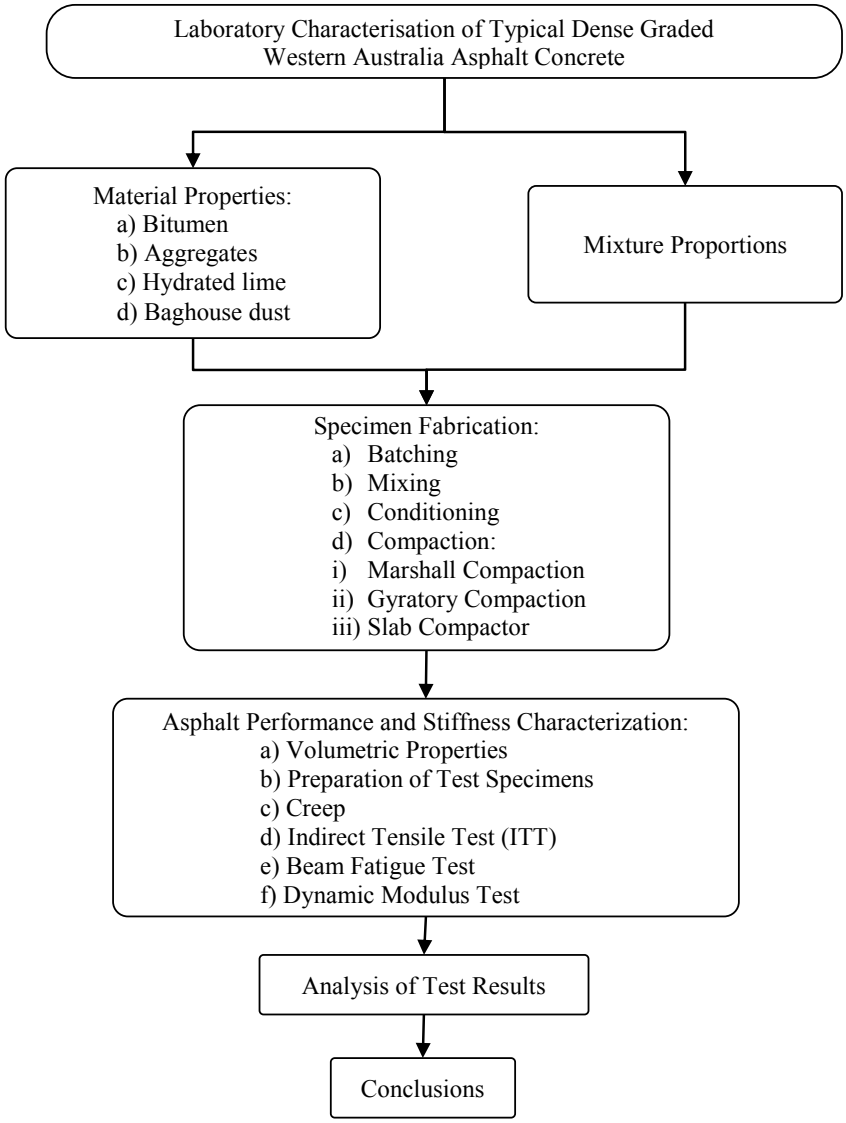

Figure 3.1 Layout of the research plan.

The research was carried out in three stages. The first was an investigation into material properties, mixture proportions and specimen fabrication. The properties of fine and coarse aggregates were investigated and a mix design for asphalt pavement was determined according to Main Roads Western Australia specifications. In the second stage, specimens were subjected to various methods of compaction including Marshall, gyratory and rolling compaction. In the third stage, stiffness was characterized using the creep test, indirect tensile strength test, beam fatigue test and dynamic modulus test. The analysis of test results and conclusions were determined after the laboratory characterization.

3.2 Material Properties

3.2.1 Bitumen

As a major component used in asphalt, bitumen is classified according to special requirements, as explained in section 2.2.1. In this research, BP residual bitumen Class 170 and 320 were used as the primary binder for the asphalt wearing course and full depth asphalt. The specified binders as specified in Guide to Pavement Technology Part 4F: Bituminous Binders (Austroads 2008b) meet the requirements of Main Roads WA Standard 71-06-135 (Main Roads Western Australia 2010a). Bitumen is a temperature-sensitive material and some major properties related to its consistency, such as viscosity at various temperatures and penetration, are listed in Table 3.1. Viscosity is a measure of the rate of flow of the bitumen. It is claimed to be a more accurate measurement than penetration to specify the temperature susceptibility and consistency of bitumen (Koole and Thagesen 2004). This is due to the rheology of bitumen, which changes with temperature to a certain degree. A measure of the hardness of bitumen at low temperatures is defined as penetration (Austroads 2006a). The penetration of bitumen depends on its class, with the highest grade bitumen usually displaying the lowest penetration. This property is obtained by measuring the depth/distance that a needle penetrates into the bitumen.

3.2.2 Aggregates

According to the specifications for full depth asphalt pavement, the coarse aggregate is defined as the material retained on a 2.36 mm Australian Standard Sieve, while fine aggregate is all of the material retained on a 75 micron and passing a 2.36 mm Australian Standard Sieve, and is in form of crushed rock material. Both types shall be crushed local granite aggregates used for asphalt manufactured in the Perth region. Coarse aggregates with a nominal maximum aggregate size (NMAS) of 10 mm, 14 mm, and 20 mm from Gosnells Quarry, Western

Australia, were used in the asphalt mixes. The typical aggregate mix sizes for dense graded wearing course, intermediate course and base course were given in Table 2.2 (section 2.2.2). Particle size distribution and some physical properties were investigated. In order to be used as full depth asphalt pavement, fine aggregates must comply with the requirement of AS 1141.5-2000 (Standards Australia 2000) for water absorption to be less than 2%. The coarse aggregates need to satisfy the physical properties requirements set out in Main Roads Western Australia Document No. 71/06/135 (Main Roads Western Australia 2006) (see Table 3.2).

Table 3.1 Physical and chemical properties of bitumen (Austroads 2008b)

Property	C170	C320
Viscosity at 60°C (Pa.s)	140–200	260–380
Penetration[1] at 25°C 100g, 5s (pu)	62 min	40 min
Viscosity at 135°C	0.25–0.45	0.40–0.65
Viscosity at 60°C after Rolling Thin Film Oven (RTFOT), test as a percentage of the original	300 max	300 max
Matter insoluble in toluene (% by mass)	1.0 max	1.0 max
Flashpoint (°C)	250 min	250 min
Loss on heating (% max)[1]	0.5 max	0.5 max
Appearance	black, solid material at 25°C	black, solid material at 25°C
Solubility in water	insoluble	insoluble
Vapour pressure	below 0.1 kPa @20°C	below 0.1 kPa @20°C
Vapour density (Air = 1)	heavier than air	heavier than air
Density	1.03 kg/L (AS 2341.7)	1.03 kg/L (AS 2341.7)
Flash point	>250°C (AS 2341.14)	>250°C (AS 2341.14)
Initial boiling point	250°C (thermal degradation) (ASTM D 86)	250°C (thermal degradation) (ASTM D 86)
Dynamic viscosity	170 Pa. s (0.32 m^2/s) @ 60°C (AS 2341.2)	320 Pa. s (0.32 m^2/s) @ 60°C (AS 2341.2)
Softening point	47°C (AS 2341.18)	52°C (AS 2341.18)

[1] Typical values only (not specified in AS 2008)
* Provided by manufacturer

Table 3.2 Physical properties of crushed aggregates (Main Roads Western Australia 2006)

Property	Requirement	Test Method
Los Angeles abrasion value		
Granite and other rock types	35% maximum	WA 220.1
Basalt	25% maximum	WA 220.1
Flakiness index	35% maximum	WA 216.1
Water absorption of fine and coarse aggregate	2% maximum	AS 1141.6.1 & AS 1141.5
Wet strength	100 kN min	AS 1141.22
Wet/dry strength variation	35% maximum	AS 1141.22
Stripping test value	10% maximum	AS 1141.20
Degradation factor	50 minimum	AS 1141.25.2
Secondary mineral content	25% maximum	AS 1141.26
Petrographic examination	Statement of suitability for use as an asphalt aggregate	

Table 3.3 Sieve analysis results for each nominal maximum aggregate size

Size Sieve (AS1152)	unit	20 mm	14 mm	10 mm	7 mm	WQS	BHD
26.5	mm	100	100	100	100	100	100
19	mm	85	100	100	100	100	100
13.2	mm	7.6	90.2	100	100	100	100
9.5	mm	1.1	27.3	89.7	100	100	100
6.7	mm	0.6	16.1	8.5	93.9	100	100
4.75	mm	0.5	1.2	1.4	49.3	99.5	100
2.36	mm	0.5	1.1	0.6	2.9	84.5	100
1.18	mm	0.4	0.9	0.4	1.7	54.0	100
0.6	mm	0.4	0.7	0.4	1.4	32.1	100
0.3	mm	0.3	0.5	0.3	1.0	16.5	100
0.15	mm	0.1	0.3	0.3	0.8	6.3	98
0.075	mm	0.0	0.1	0.1	0.4	2.6	95

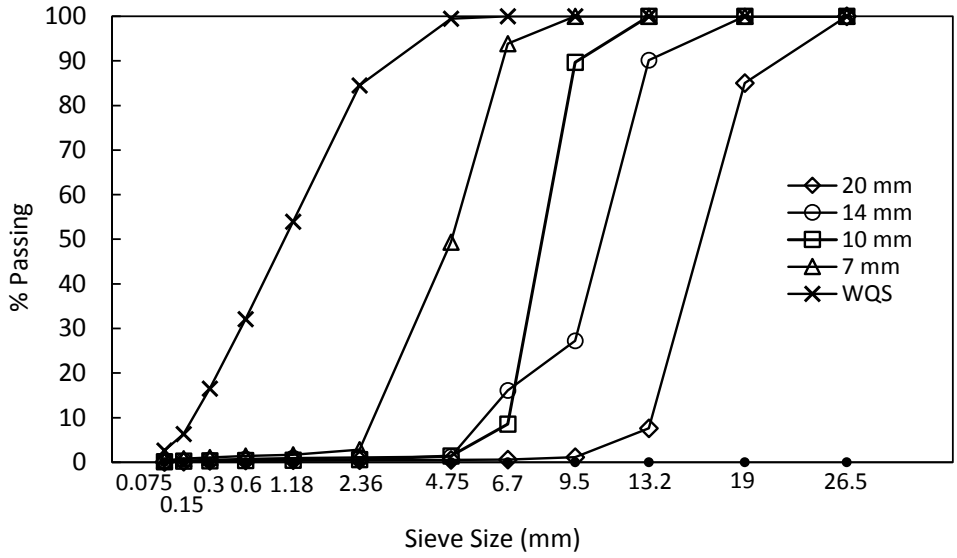

Figure 3.2 Grading curves of each nominal maximum aggregate size.

3.2.3 Hydrated Lime

Hydrated lime is mineral filler used to increase the stiffness of asphalt mix by filling voids and to reduce susceptibility to stripping by improving bitumen adhesion (Little, Epps and Sebaaly 2006). In this research, calcium hydroxide in the form of a fine powder with the commercial name Swan Hydrated Lime was included in the mixture. The physical and chemical properties of the hydrated lime are given in Table 3.4. This filler must comply with AS 1672.1-1997 (Standards Australia 1997), where the available lime limit (calculated as calcium hydroxide) is ≥65%.

Table 3.4 Physical and chemical properties of hydrated lime*

Physical and chemical properties	Proportion
Appearance	White amorphous powder
Specific gravity	2300 kg/m^3
Solubility in water	soluble
pH	Approximately 12
Calcium hydroxide ($Ca[OH]_2$)	80–90%
Magnesium hydroxide ($Mg[OH]_2$)	0–6%
Silicon dioxide (SiO_2)	2–6%
Aluminium oxide (Al_2O_3)	0.2–0.6%
Iron oxide (Fe_2O_3)	0.1–0.3%

*Provided by manufacturer

3.2.4 Baghouse Dust

Baghouse dust was used as mineral filler. The baghouse dust was collected from plant and varied in quality. This material had to pass a 0.075 mm Australian Standard sieve, and the particle size distribution of the dust was analysed according to AS 1411.11.1-2009 (Standards Australia 2009). In order to ensure quality, at least one particle size distribution test had to be carried out per 500 tonnes of production of each filler type (Roads and Traffic Authority New South Wales 2001). The reactivity of bag house dust was determined using the methylene blue value (MBV) test in accordance with International Slurry Surfacing Association Technical Bulletin No 145.1 (Roads and Traffic Authority New South Wales 2003).

3.3 Mixture Proportions

The compositions of the dense graded mixtures were designed according to specifications from Main Roads Western Australia (MRWA), namely Specification 504 Asphalt Wearing Course (Main Roads Western Australia 2010a) and Specification 510 Full Depth Asphalt Pavement (Main Roads Western Australia 2010b). The mixtures consisted of coarse aggregates, washed quarry sand, bitumen, hydrated lime and bag house dust. The nominal maximum aggregate sizes were 10, 14, and 20 mm for the mixtures designed using MRWA Specifications 504 and 510. The MRWA specifications are based on the Marshall mix design. This research did not follow the Australian Provisional Guide, APRG Report No. 18 (APRG 2002) since it focused only on Western Australian asphalt mixtures.

The mixtures were designed by selecting target aggregate grading within grading envelopes from the MRWA Specification 510 (Main Roads Western Australia 2010b). The target grading was located close to the midpoint of the grading envelope and was adjusted in order to determine the desirable volumetric properties. Table 3.5 shows the specifications for each nominal maximum aggregate size (NMAS) envelope and it is also illustrated in Figure 3.3. The

aggregate fraction quantities and filler were proportioned by trial and error based on a particle size distribution through sieve analysis in compliance with AS 1141.11.1-2009 (Standards Australia 2009).

Table 3.5 MRWA grading specification

Size Sieve (AS1152)	unit	MWRA 504 Spec Range	MRWA 504 Spec Range	MWRA 510 Spec Range
26.5	mm	100–100	100–100	100–100
19	mm	100–100	100–100	90–100
13.2	mm	100–100	93–100	75–85
9.5	mm	95–100	79–89	55–65
6.7	mm	78–88	63–73	45–55
4.75	mm	63–73	49–59	40–50
2.36	mm	40–48	33–41	28–38
1.18	mm	25–32	22–32	20–28
0.6	mm	18–24	15–23	13–19
0.3	mm	12–17	10–18	7–12
0.15	mm	8–12	6–11	4–8
0.075	mm	3–5	2–5	3–5

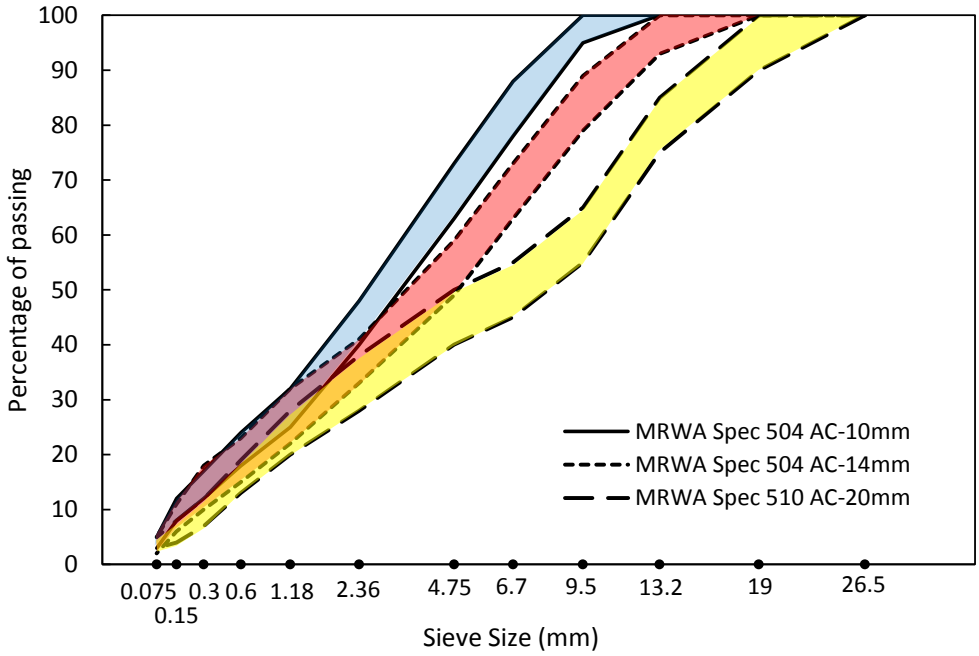

Figure 3.3 Grading envelopes of MRWA specifications

3.4 Specimen Fabrication

3.4.1 Batching

The proportion of a batch of asphalt mixture depends on the type of specimen. For example, one batch used for the Marshall and resilient modulus tests consists of three samples requiring 4 kg of materials. A batch of dynamic modulus samples uses approximately 6 kg of materials to produce only two specimens. Three batches of mixture at 6 kg each were used to fill a prismatic (slab) mould for the beam fatigue test. One prismatic slab can be cut into three beam samples.

3.4.2 Mixing

The preparation, mixing, quartering and conditioning of asphalt samples followed the procedures in Austroads Technical Report: Preparation of Asphalt Samples for Testing No. AP-T132/09 (Austroads 2009) and AS 2891.2.1-1995 (Standards Australia 1995a). To start with, the aggregates were preheated in the oven at 175°C and the bitumen at 155 to 160°C. The aggregates had to be heated overnight in order to reach the target temperature. The aggregate fractions were added and mixed individually for 15 minutes before being returned to the oven. Bitumen was heated for less than four hours to make it viscous. All mixing tools such as spatulas and mixing bowls were also heated in the oven at the same temperature as the bitumen to control heat loss during mixing.

The procedure started with a dummy mix being pre-mixed with a similar binder in order to wet the mixing bowl and obtains a thin coating of binder and fine particles on the bowl and mixing equipment. After the dummy mix had been discarded, the preheated aggregates were added to the mixing bowl followed by the preheated bitumen. The bowl was placed on a balance for the addition of bitumen, in order to ensure that exactly the right amount was added. The materials were then mixed for a maximum of three minutes using a planetary mixer (Figure 3.4) until the bitumen film coated the aggregates thoroughly (Figure 3.5).

Splitting is used to split materials into equal portions, prevent segregation and maintain the mix temperature. First the splitting equipment was preheated to 155°C and the material was then placed directly into a heated oven tray. According to the purpose or required specimen size, the mix was divided into several portions using a preheated steel plate, or left as it was. The divided samples for the indirect tensile test were placed on an individual oven tray, and later placed in the oven for conditioning. A dial thermocouple was located in the mix to check the actual temperature after mixing. Samples for the dynamic modulus and the beam

fatigue were not divided due to the specimen sizes needed; instead, the mixed material was put straight into the oven for conditioning.

Figure 3.4 Planetary mixer with 6 kg mixing capacity

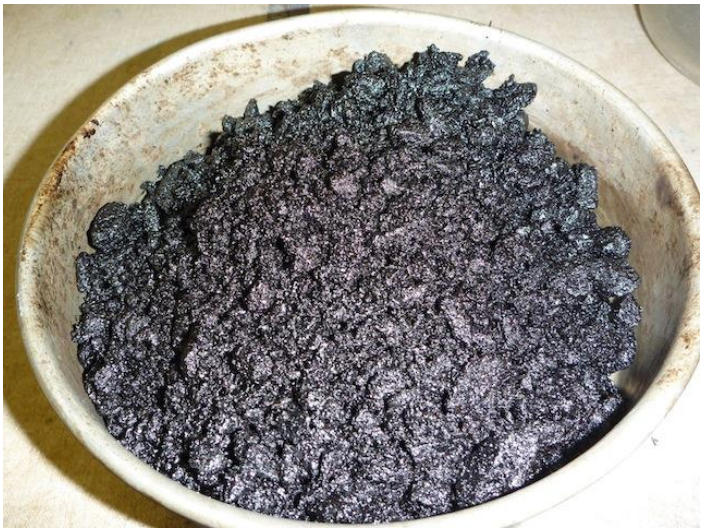

Figure 3.5 Loose asphalt concrete after mixing process

Figure 3.6 Splitting: (a) quartering mixtures, (b) quarter samples for conditioning

3.4.3 Conditioning

The Class 170 and Class 320 asphalt mixtures were conditioned in the oven at 155 to 160°C for one hour. This process was aimed to simulate the binder hardening and oxidation that happens during the manufacturing, transporting and placing of asphalt mixture at an early stage of the field service (Austroads 2006a, Austroads 2007). During the conditioning process, the mixes were placed in oven trays depending on the purpose of the tests. It is imperative to keep a consistent conditioning time to allow proportional comparison between the mixes. The quarter samples were taken after one hour of conditioning and were compacted immediately with a five-minute interval between samples.

3.4.4 Compaction

Compaction of standard binders should be carried out at 155± 5°C. In this research, three types of compaction, namely Marshall, gyratory and slab compaction, were used for volumetric and mechanical testing specimens. The temperature prior to compaction was measured using thermocouples.

3.4.4.1 Marshall Compaction

The Marshall procedure is commonly used to compact, assess the stability and examine the flow of asphalt mixtures. A cylinder-type specimen is required for stability and flow, in accordance with AS 2891.5-2004 (Standards Australia 2004) or test method WA731 (Main

Roads Western Australia 2004). This study used the Civilab Australia Dual Mechanical Compactor CL40525, manufactured by Double Rd Holdings, New South Wales.

The asphalt mix was placed in a preheated mould assembly with paper protective discs at the top and bottom. The specimens were put in the oven until the temperature reached 142±3°C for Class 170 or 150±3°C for Class 320 bitumen. The specimens were then positioned on the compaction pedestals and were compacted using 50 or 75 blows depending on the mix specification, with a blow rate of 60 to 70 blows per minute. The same number of blows was applied to the reverse side of the mould. The Marshall test rig and setup for stability and flow are illustrated in Figure 3.7.

The stability and flow tests were performed within 30 seconds after the specimen was removed from the water bath. The load was applied to the specimen until shear failure caused the load reading to decrease. The stability was calculated from the load at failure multiplied by the correction factor. The correction factors or factors to adjust the Marshall stability of specimen height were obtained from AS 2891.5-2004 (Standards Australia 2004). The flow at failure was calculated using the flow gauge reading or the recorder transducer reading and the applicable calibration factor.

Figure 3.7 Marshall Test: (a) Marshall test rig, (b) specimen under stability and flow test

3.4.4.2 Gyratory Compaction

Gyratory compaction is another procedure to produce cylindrical samples. This test is preferable because it is simple to operate, relatively inexpensive, represents the actual mechanical properties of field-placed material, and shows less variability in performance. Detailed descriptions of the laboratory asphalt compactor can be found in two Austroads Technical reports, i.e. No. AP-T94/08 and No. AP-T192-11 (Austroads 2008, Austroads 2011a). The instrument or gyratory compactor used was a Servopac from Industrial Process Controls Ltd (IPC), Australia. The device is capable of applying a vertical loading stress of 240 kPa to a specimen in the mould at a rate of 60±5 rpm. The gyratory compactor and mould for compaction are shown in Figure 3.8.

Figure 3.8 Gyratory compaction: (a) Gyratory compactor, (b) Gyratory mould

The gyratory compacted specimens were prepared in accordance with AS 2891.2.2-1995 (Standards Australia 1995b). The specimens were prepared for a dense graded asphalt mix with a nominal maximum aggregate size of 20 mm. The testing requirements are as follows: a) diameter of specimen is 100±2 mm, b) nominal height of specimen is 85 mm, c) gyratory angle of 3°, and d) the applied vertical loading stress is 240±10 kPa. The specimens were conditioned in the oven at 150±5°C before compacted. During compaction, the preheated specimen was placed in a cylindrical mould and a constant vertical loading stress was applied.

The specimen was subjected to shearing forces and rearrangement of aggregate particles when the mould rotated simultaneously about its longitudinal axis through a small angle of 2 or 3°.

The dynamic modulus test specimens were prepared for several target air voids. The target air void for all specimens was 3, 4, 5, 6 and 7% with an allowance of ±0.5%. The density and air voids were measured according to Main Roads Western Australia test method 733.1 (Main Roads Western Australia 2006). In this research, a trial compaction was required to determine the gyration cycles for the target air voids. Figure 3.9 shows an example of dynamic modulus trial compaction curves for 10, 14, and 20 mm mixtures.

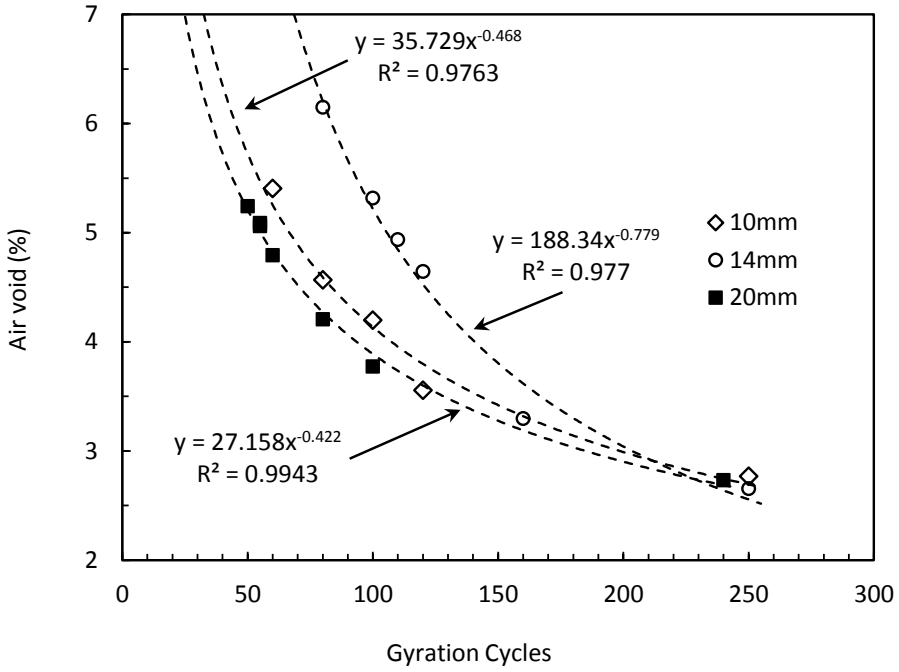

Figure 3.9 Variation of air voids with gyration cycles

The dynamic modulus samples were compacted directly in the Servopac gyratory compactor using 100 mm diameter moulds. After being compacted, the specimens were allowed to cool at room temperature for several hours, then the dynamic modulus samples were cut into cylinders 150 mm in height.

3.4.4.3 Slab Compactor

Specimens for the flexural fatigue test were prepared using the roller compactor produced by Cooper Research Technology Ltd, whose performance in particle orientation, uniformity of air voids and aggregate crushing satisfies the Australian standard procedure given in AG-

PT/T220 (Austroads 2005a). This device is a rolling wheel type completed with segmental wheel compactors and footpath rollers. Three batches of asphalt mix were prepared in accordance with AS 2891.2.1-1995 (Standards Australia 1995a).

The slab dimension is 400x280x70 mm, in accordance with Table 1 of AG-PT/T220 (Austroads 2005a) for mixes with a maximum NMAS of 20 mm. After conditioning for one hour in the oven at a temperature of 150–160°C, the mix was directly and uniformly spread in the mould to avoid segregation. The specimen was compacted to the required density. In order to achieve a comparable sample, the target air void of the asphalt mix for flexural fatigue specimens had to be similar to the air void in the gyratory compacted specimens. This makes it possible to compare the effects of compaction using the gyratory and roller compactors. Figure 3.10 shows the rolling compactor and the compacting process.

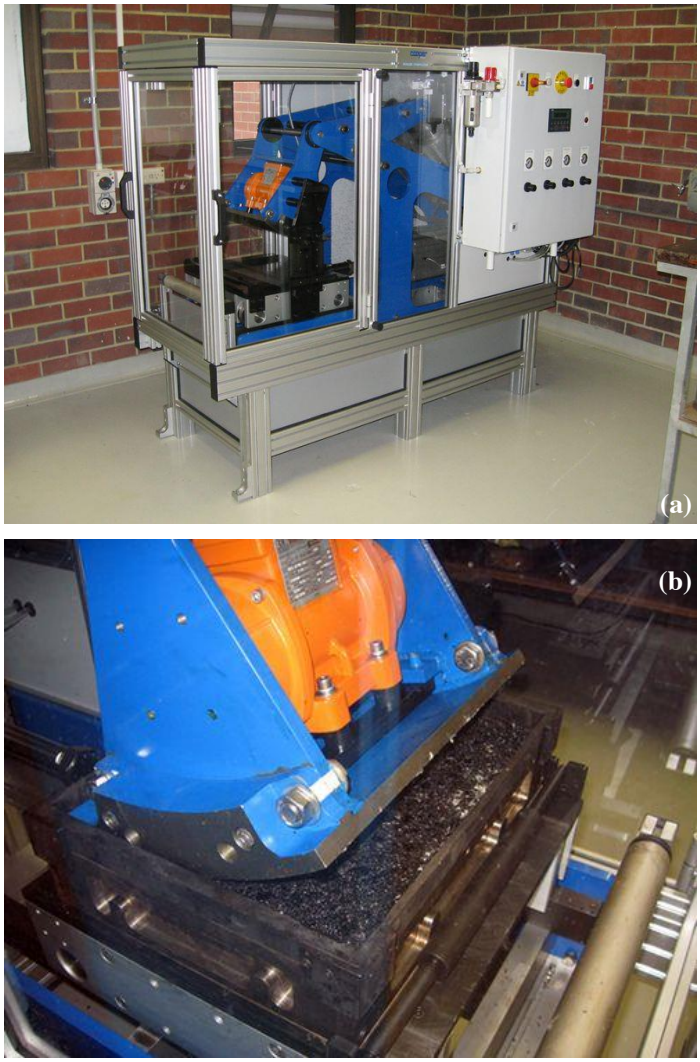

Figure 3.10 Slab compactor: (a) rolling compactor, (b) specimen under compaction

3.5 Asphalt Performance and Stiffness Characterization

3.5.1 Volumetric Properties

Western Australia relies on the Marshall test for its asphalt mix design. Volumetric properties of the compacted specimens such as air voids, Marshall stability, flow and bulk density were determined according to MRWA 504 and 510 (Table 3.6).

Table 3.6 Volumetric properties of Western Australian mix design

	AC10-170	AC10-320	AC14-320	AC20-320	AC20-320 BC
Blows	50	75	75		
Bit. Content (%) Class	5.4 ± 0.3 *C170 & 320*		4.7 ± 0.3 *C320*	4.5 ± 0.3 *C320*	5.1 ± 0.3 *C320*
Air voids (%)	4–6		4–7	3.5–5.5	1.5–3.5
VMA (%)	min. 15		min. 14		
Stability (kN)	min. 8				
Flow	2–4				
Hydrated Lime (%)	1.5 ± 0.5				

3.5.2 Experimental Design

The experimental design for laboratory test was consisted of three parts, i.e. material properties investigation, specimens compaction and stiffness characterization. The stiffness of asphalt is usually a main parameter to determine the performance of the material during a service life. The most important criteria of mechanical responses of the asphalt based on its service level. The stiffness was characterised from creep, indirect tensile test (ITT), beam fatigue, and dynamic modulus test. In application, the California Bearing Ratio and resilient modulus are the common methods used to determine stiffness of the asphalt pavement. In this study, another approach by determining a set of stiffness characteristics, such as creep, indirect tensile test (ITT), beam fatigue and dynamic modulus were used. This study would improve the conventional approach in determining stiffness of Western Australia mixes by providing resilient modulus (M_R), flexural modulus (S_{mix}), and dynamic modulus (|E*|) to provide input for the local database material performance.

The creep test was based on AS 2891.12.1-1995 and the objective is to determine the permanent compressive strain or dynamic creep of asphalt mixtures from Western Australia. The standard requires at least three specimens to be evaluated. The Indirect Tensile Test (ITT) was carried out in accordance to AS 2981.13.1-1995. The specimens number were three. The beam fatigue test using beam with at least three specimens and the test was conducted according to Austroads AG:PT/T233. The dynamic modulus test was taken based

on AASHTO T342-11 and three specimens were tested. Specimens of various sizes but complying with testing requirements were used in this research. All values were calculated as the average of three specimens. The specimen sizes and number are given in Table 3.7.

Table 3.7 Details of the test specimens

Type of test	Type of specimens	Size of specimens	Number of specimens
Creep	Cylinder	100±2 mm (dia), 50±5 mm (height)	3
Indirect tensile test	Cylinder	100±2 mm (dia), 75±15 mm (height)	3
Beam fatigue test	Beam	390x64x50 mm	3
Dynamic modulus test	Cylinder	100x150 mm	3

Fatigue testing specimens are rectangular cross section beams. The asphalt slabs were cut to size using an Autosaw machine (automated asphalt saw) with a blade speed of 1400–1680 rpm (50/60 Hz), manufactured by IPC Global. The beams were strictly cut to tolerances of ±2 mm to ensure repeatability of the test. The device and specimen types used in the beam fatigue test are shown in Figure 3.11.

In this research, the determination of important parameters, namely M_R, S_{mix}, $|E^*|$, and ϕ was used to characterize the stiffness of Western Australia asphalt mixtures. To determine the dynamic modulus of hot mix asphalt used in Australia and the USA, the tests were carried out according to current standard i.e. AASHTO T342-11 (AASHTO 2011). Other variables such as temperature, frequency, loading rate and stress/strain level were included to obtain the monitored parameters. Only mix AC 320 was used for creep, resilient modulus and fatigue tests since it is commonly used in asphalt manufacture in Australia. The binder is also stiffer than AC 170 in warmer climates like in Western Australia (warm temperate rainy, hot, dry summer). Mixes AC 170 and AC 320 were used for the dynamic modulus test to investigate various traffic applications. The test program is presented in Table 3.8.

Table 3.8 Test program for characterization of asphalt stiffness

Test Method	Parameters monitored	Standard/ Protocol	Temp. (°C)	Frequency (Hz)	Stress/ Strain Level
Creep	Minimum slope (μm/m/c)	AS 2891.12.1	50±0.5	0.5	
Indirect tensile test (ITT)	M_R (Resilient Modulus, MPa)	AS 2891.13.1	25±0.5	n/a	50 με
Beam fatigue test	S_{mix} (Flexural Stiffness, MPa)	Austroads AG: PT/T233	20±0.5	10	400 με
Dynamic modulus test	$\|E^*\|$, ϕ	AASHTO T 342-11	4, 20, 40, 55	25, 10, 5, 1, 0.5, 0.1	LVE*

*Linear viscoelastic region

Figure 3.11 Beam fatigue test: (a) Autosaw machine, (b) beam samples

3.5.3 Creep Test

The creep test was taken in accordance with AS 2891.12.1-1995 (Standards Australia 1995c) using UTM25 manufactured by IPC. The UTM is used to apply repeated stress pulse to asphalt specimens measuring the vertical deformation with the Linear Variable Displacement Transducer (LVDTs). The specimens were located in the temperature controlled cabinet at 50±0.5°C. The temperature in the specimen must be in equilibrium. The rectangular pulse wave stress/load of 1.571 kN was applied to the specimen at frequency of 0.5Hz. The peak load (F) is applied using the following equation:

$$F = 1.571 \times D^2 \times 10^{-4} \quad (3\text{-}1)$$

where:

F = the peak load to be applied (kilo newtons)

D = the mean diameter of the specimen (mm)

The load cycles were applied to the specimen. Some measurements were taken such as the temperature inside the dummy specimen, the deformation or strain accumulated from the commencement of the test. The software stopped the test until the maximum accumulated strain reached 30000 micro strain or 40000 cycles has been reached. The dynamic creep specimen set up and typical test results can be seen in Figure 3.12 and Figure 3.13, respectively.

Figure 3.12 Creep test set up

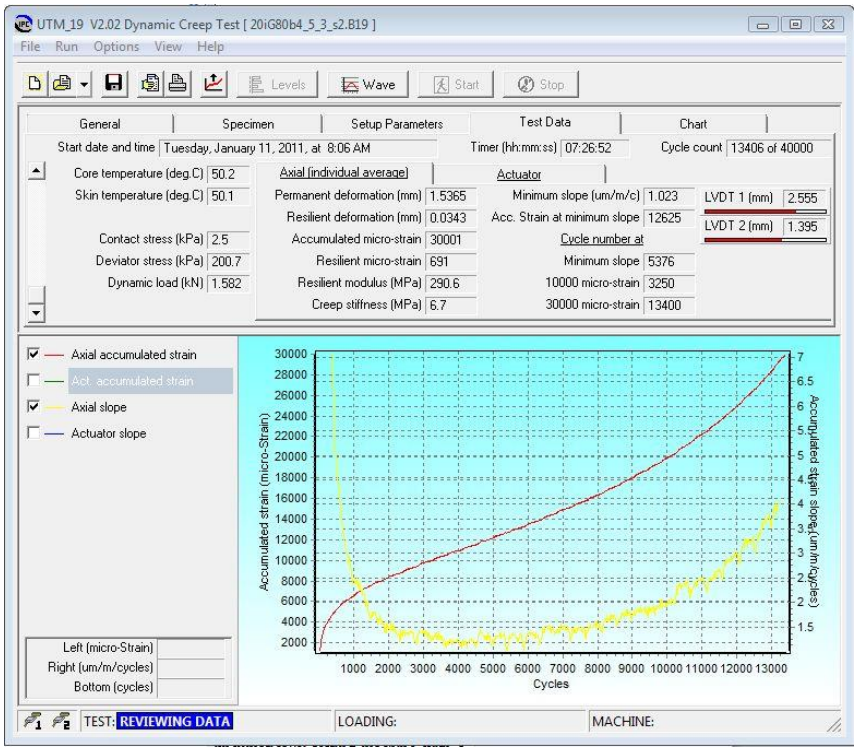

Figure 3.13 Typical creep test result.

3.5.4 Indirect Tensile Test (ITT)

The resilient modulus of asphalt samples was determined using the indirect tensile test, according to AS 2891.13.1-1995 (Standards Australia 1995d). A universal testing machine 14P (UTM 14P) manufactured by IPC and an environmental chamber were used to test specimens (Figure 3.14). The UTM 14P is a servo-pneumatically testing machine with a capacity of 14 kN. The machine is equipped with Control Data Acquisition System (CDAS) and IPC UTS software. The testing conditions were set to the standard reference, i.e. at 25±0.5°C temperature, 0.04±0.005 s rise time (10 to 90%), 3.0±0.005 s of pulse repetition period (10% to 10%), and 50±20 με recovered horizontal strain.

The specimens were placed in a temperature-controlled cabinet at 25°C for approximately two hours. This allowed the specimens to reach the targeted temperature. A dummy sample with two temperature probes attached to the side and in the centre of the sample was used to check the targeted temperature. After conditioning, one specimen at a time was placed into the loading jig. The flat surfaces of the specimen were anchored in place using clamp bolts tightened to a torque of 250 mN. The resilient modulus specimen set up is shown in Figure 3.15.

Figure 3.14 Indirect tensile test; IPC UTM-14 apparatus and environmental chamber

Figure 3.15 Indirect tensile (resilient modulus) test set up

The standard reference test conditions for at least one set of specimens consists of a test temperature of 25±0.5°C, rise time of 0.04±0.005 s, pulse repetition period of 3.0±0.005 s and recovered horizontal strain of 50±20 με. A repeated vertical compressive force was applied acting parallel to and along the vertical diametrical plane of the sample, and

horizontal displacements were measured mid-height through the horizontal diameter (APRG 2002. Using the MATTA apparatus, a procedure detailed in AS 2891.13.1-1995 (Standards Australia 1995d) will be performed to determine the resilient modulus of the optimum asphalt mixtures. The resilient modulus (E) is taken as the average of three specimens with a variability of less than ±15% from the average E. For each specimen the resilient modulus can be calculated as (Austroads 2008e):

$$E = P\frac{(\nu + 0.27)}{H \times h_c} \tag{3-2}$$

where:

E = resilient modulus (MPa)

P = peak load (Newtons)

ν = Poisson ratio (assumed to be 0.4)

H = recovered horizontal deformation of specimen after application of load (mm)

h_c = height of specimen (mm)

The required information, such as the specimen number and measurements, was entered into the test software. The software applied the first five load pulses as a calibration process to obtain the proper loading magnitudes. After this calibration step, the software applied five more test pulses. The test procedure was repeated for each specimen and all types of asphalt mix. A typical ITT result from the software is illustrated in Figure 3.16.

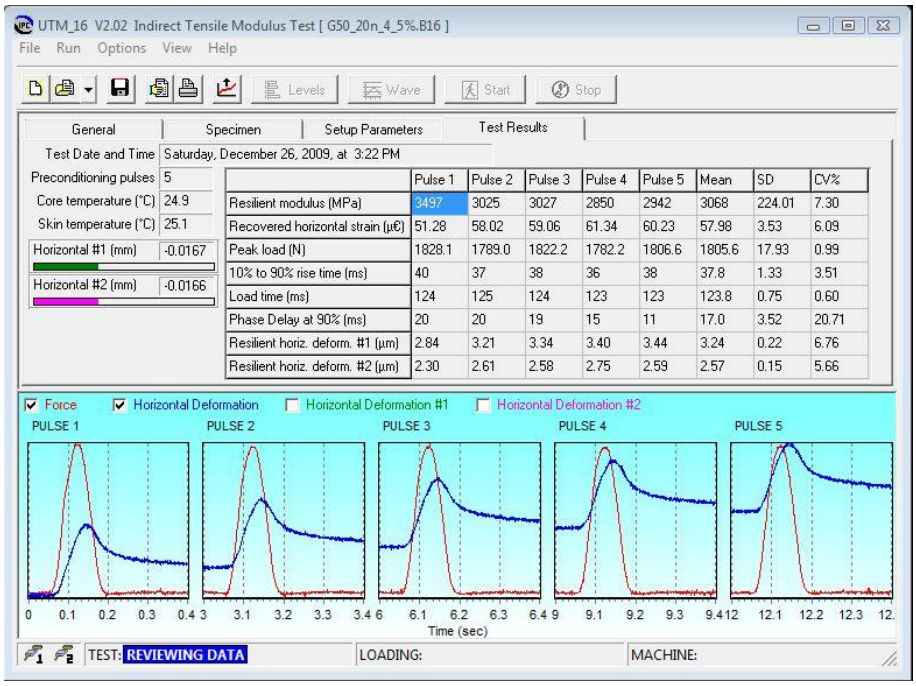

Figure 3.16 Typical indirect tensile test result

The resilient modulus value was included in Level 2 of the performance-related APRG Report No 18 mix design (APRG 2002). The results could be compared directly with the typical Australian dense graded modulus listed in the Austroads Guide as described in section 2.5.3.2 (Austroads 2008c).

3.5.5 Beam Fatigue Test

The beam fatigue test was applied to evaluate the resistance of an asphalt mixture to fatigue cracking in accordance with the Austroads AG PT/T233 procedure (Austroads 2005b). The test output is a flexural modulus value that can be used to estimate fatigue life. A servo-pneumatic testing machine manufactured by IPC was used to determine the flexural modulus. Some test conditions were applied according to Austroads AG PT/T233 (Austroads 2005b), such as a test temperature of 20±0.5°C, loading frequency of 10±0.1 Hz, continuous haversine mode of loading with peak tensile strain for the 50th and subsequent cycles at 400 με, and triplicate specimens for each batch.

The test principle was based on the application of a repeated haversine load to a beam specimen at a frequency of 10 Hz. The beam was subjected to a MATTA four point bending with free rotation and horizontal translation at the support reaction points. The load was applied at one-third distances from the ends of the beam and a uniform bending moment occurred at the centre of the specimen. The deflection was recorded using a linear variable differential transducer (LVDT) at the beam mid-span for each load cycle. The beam fatigue test apparatus, specimens and test set up are shown in Figure 3.17.

The test started with the application of a loading sequence of 50 load cycles on the beam and the initial flexural stiffness was calculated at this point. The beam was then subjected to further loading cycles until the specimen failed. At this stage, failure or the number of cycles to failure was defined as a 50% reduction of the initial beam stiffness (at the 50th cycle). This was where the specimen had achieved its fatigue life. The flexural stiffness was calculated using the equations:

$$S_{mix} = \frac{1000 \times \sigma_t}{\varepsilon_t} \tag{3-3}$$

where:

S_{mix} = flexural stiffness (MPa)

σ_t = peak tensile stress (kPa)

ε_t = peak tensile strain (mm/mm)

$$\sigma_t = \frac{LP}{wh^2} \times 10^6 \tag{3-4}$$

where:

σ_t = peak tensile stress (kPa)

L = beam span (mm)

P = peak for excursion (kN)

w = beam width (mm)

h = beam height (mm)

$$\varepsilon_t = \frac{108\,\delta \times \sigma_t}{23\,L^2} \tag{3-5}$$

where:

ε_t = peak tensile strain (mm/mm)

δ = peak tensile strain (microstrain)

Typical output of the test is shown in Figure 3.18.

Figure 3.17 Beam fatigue test set up

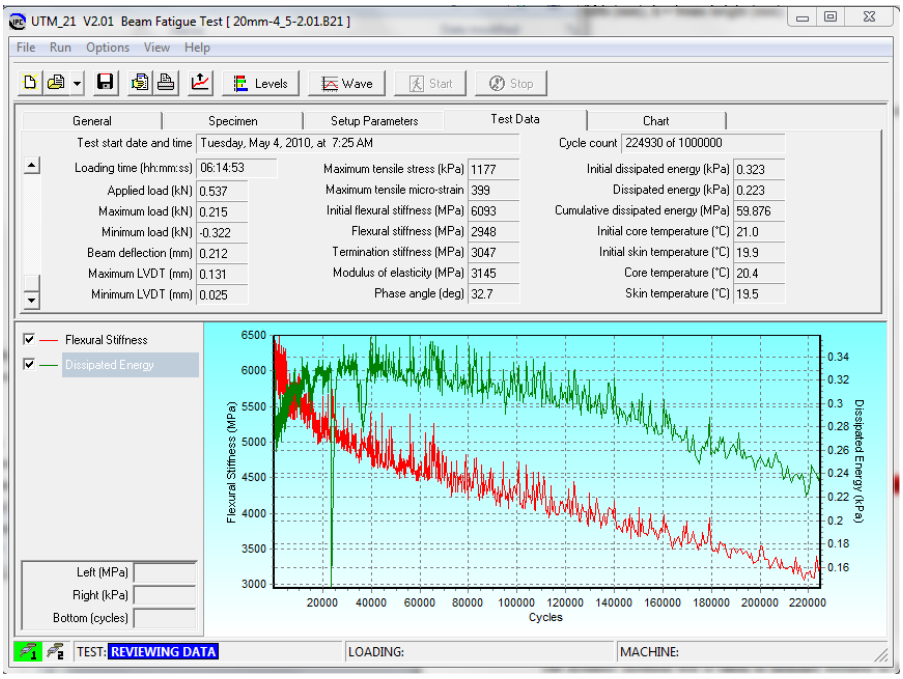

Figure 3.18 Typical result of beam fatigue test

3.5.6 Dynamic Modulus Test

The dynamic modulus test is taken to measure the stiffness of asphalt mixture by assuming the material has linear viscoelastic properties. In this investigation, only aggregate size 10mm was used for AC 170, since this size is suitable for general purpose wearing course in light and medium traffic applications. The test was carried out using AASHTO T342-11 (AASHTO 2011). The device used was an IPC UTM-25 testing machine comprised of a loading frame integrally mounted with a 25 kN servo hydraulic actuator system, a load cell and a displacement transducer. This system includes an integrated multi-axis control system (IMACS) and a computer, to provide force or displacement waveform generation and to control the automatic sequencing of test procedures. In order to simulate climatic conditions, an environmental chamber rated -15 to 60°C was used.

The experiment was started by placing the specimens in the environmental chamber overnight at 4°C to ensure temperature equilibrium. A dummy sample with a temperature probe in the centre to enable target temperature checking was located close to the tested specimen. Each specimen was examined for 24 combinations of temperature and frequency, comprised of four different temperatures (4, 20, 40 and 55°C) and six loading frequencies (25, 10, 5, 1, 0.1 and 0.05 Hz). The protocol test AASHTO T 342-11 (AASHTO 2011) requires testing at -10°C, however, this temperature was not adopted because the temperature

is too low for Western Australian conditions. After the entire cycle of frequencies was completed at 4°C, the environmental chamber was set to the next higher temperature. After several hours of conditioning, the load frequency sweep was repeated, and the complete process repeated until the modulus had been measured at the highest temperature level. The strain level was kept within the range of 50 to 150 microstrain, which was automatically controlled by the software. The specimens that underwent unrecoverable axial strains exceeding 1500 microstrain were discarded.

The test rig, as shown in Figure 3.19, used a set of three on-specimen LVDTs separated 120° from each other to measure the deformations produced during the dynamic modulus test. In order to eliminate potential error of misalignment, a special clamp was used as shown in Figure 3.20 to ensure the proper position of gauges.

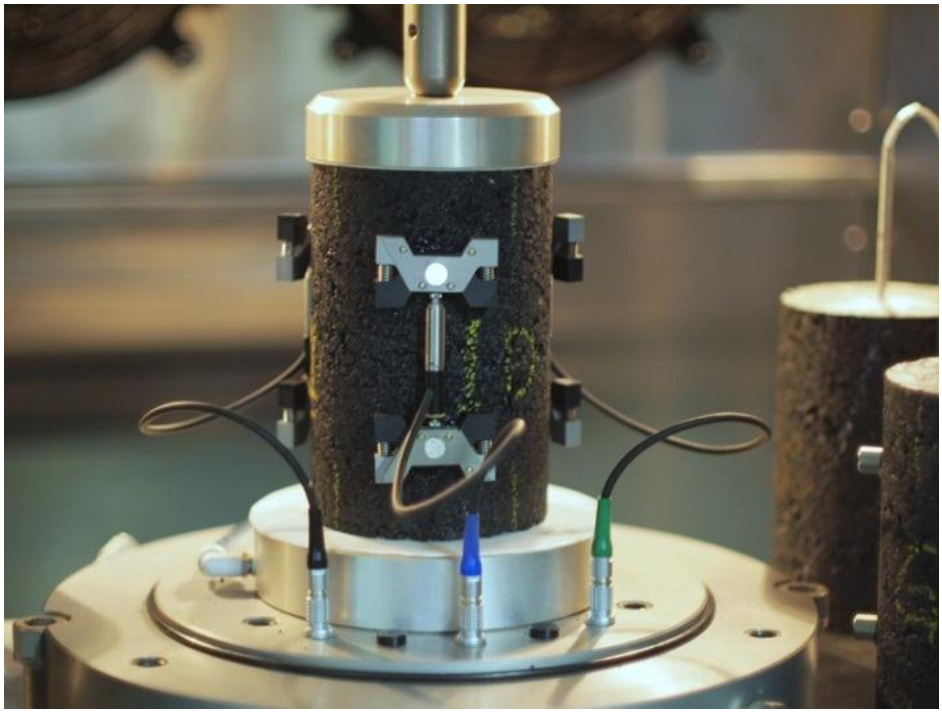

Figure 3.19 Dynamic modulus test set up with three on-specimen LVDTs

Two fundamental parameters were determined in this test, namely the dynamic modulus $|E^*|$ and phase angle (ϕ). The test frequencies, conditioning time, target temperature, target confining stress, initial modulus, axial gauge length and specimen dimensions were defined in the setup menu of the IPC SPT software. The applied stress, temperature and resulting axial strain from the three on-specimen LVDTs were measured as a function of time and

then used to calculate the dynamic modulus and other required values, such as phase angle, average temperature, average confining pressure and a number of data quality measurements, as illustrated in Figure 3.21.

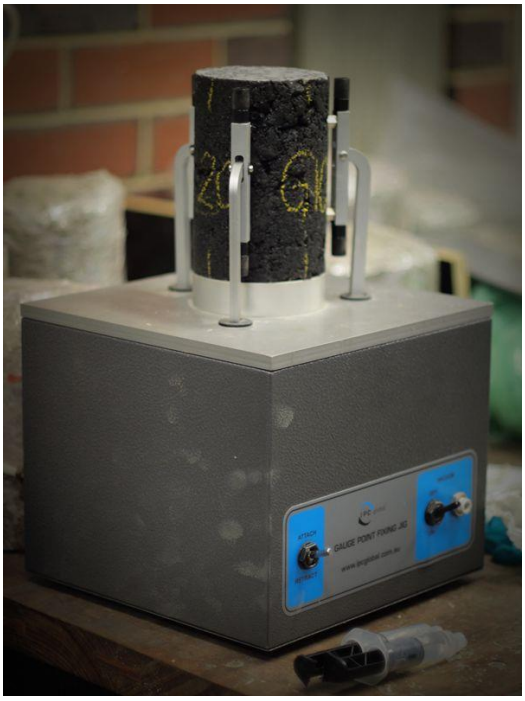

Figure 3.20 Dynamic modulus gauge point fixing jig

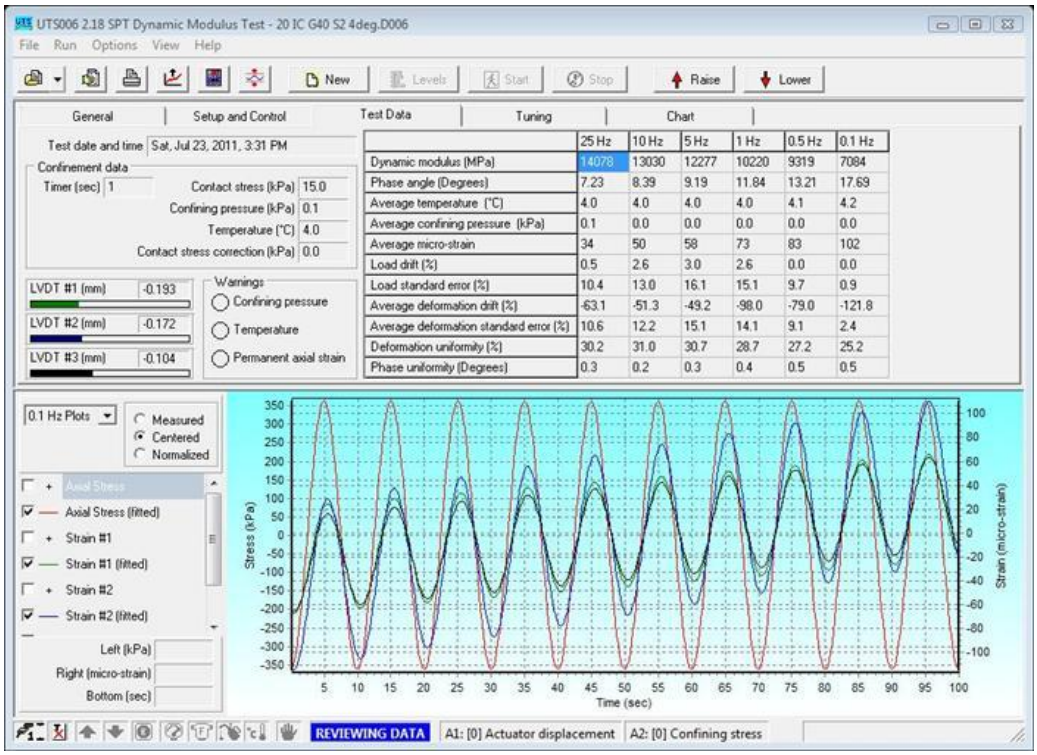

Figure 3.21 Example of dynamic modulus test result

Dynamic Modulus Calculation and Master Curve Generation

The following steps were used to determine the dynamic modulus and to produce a master curve to determine |*E**| values. A set of values for the dynamic modulus |*E**| at various temperatures and loading frequencies from the dynamic modulus test was used to generate the master curve. The theoretical details of master curve generation were explained in section 2.5.3.4. Master curves were generated from the dynamic modulus by simplifying the features of the data at a reference temperature. The curves were superimposed to form a single continuous curve by means of horizontal translations only. The reference temperature becomes a starting point for shifting the data from higher/lower temperature and the data is unchanged. The test data measured at temperatures above the reference temperature are shifted horizontally to the right or to the lower frequencies, while the data obtained at temperatures below the reference temperature are shifted to the left or to the higher frequencies.

AASHTO PP 61 (AASHTO 2010b) provides a modified version of the dynamic modulus master curve equation included in the MEPDG as explained in Section 2.5.4.2. The general form of |*E**| is as follow.

$$\log|E^*| = \delta + \frac{\left(|E^*|_{Max} - \delta\right)}{1 + e^{\beta+\gamma \log f_r}} \tag{3-6}$$

where:

|*E* *| = the dynamic modulus, psi;

δ, β, and γ = the fitting parameters;

$|E^*|_{max}$ = the limiting maximum modulus, psi; and

f_r = the reduced/shifted frequency, Hz.

The shifted frequency (f_r) is computed using the Arrhenius equation.

$$\log f_r = \log f + \log a_T \tag{3-7}$$

$$\log a_T = \frac{\Delta E_a}{19.14714}\left(\frac{1}{T} - \frac{1}{T_r}\right) \tag{3-8}$$

where:

f_r = the reduced frequency at the reference temperature, Hz;

f = the loading frequency at the test temperature, Hz;

ΔE_a = the activation energy (treated as a fitting parameter);

T = the test temperature, °K; and

T_r = the reference temperature, °K.

a_T = the shift factor at temperature T;

The maximum limiting modulus ($|E^*|_{Max}$) is estimated from asphalt concrete volumetric properties based on Hirsch model as in Equation 2-22 (Christensen, Pellinen, and Bonaquist 2003).

$$|E^*|_{\max} = P_c\left[4200\left(1-\frac{VMA}{100}\right)+435{,}000\left(\frac{VFA\times VMA}{10{,}000}\right)+\frac{1-P_c}{\frac{1-VMA/100}{4{,}200{,}000}+\frac{VMA}{435{,}000\,VFA}}\right] \quad (3\text{-}9)$$

$$P_c = \frac{\left(20+\frac{435{,}000\,VFA}{VMA}\right)^{0.58}}{650+\left(\frac{435{,}000\,VFA}{VMA}\right)^{0.58}} \quad (3\text{-}10)$$

where

$|E^*|_{max}$ = the limiting maximum HMA dynamic modulus, psi;

VMA = the voids in the mineral aggregate, %; and

VFA = the voids filled with asphalt, %.

Another way to construct the dynamic modulus master curve is explained in AASHTO PP 62 (AASHTO 2010c). The $|E^*|$ uses the following expression.

$$\log|E^*| = \delta + \frac{\alpha}{1+e^{\beta+\gamma\log f_r}} \quad (3\text{-}11)$$

where:

$|E^*|$ = the dynamic modulus, psi;

$\alpha, \beta, \delta,$ and γ = the fitting parameters;

f_r = the shifted frequency, Hz.

The shift factors (a_T) are calculated using the following equation.

$$\log a_T = c\left(\log\eta - \log\eta_{T_R}\right) \quad (3\text{-}12)$$

where:

f = the loading frequency at the test temperature;

c = a fitting coefficient;

η = the viscosity of the binder at the test temperature, cP;

T_R = the reference temperature, °R; and

η_{TR} = the viscosity of the binder at the reference temperature, cP.

Viscosities are determined using Equation 2-10 in Section 2.5.4.2

The typical dynamic modulus data at various temperatures and frequencies before and after shifting is illustrated in Figure 3.22.

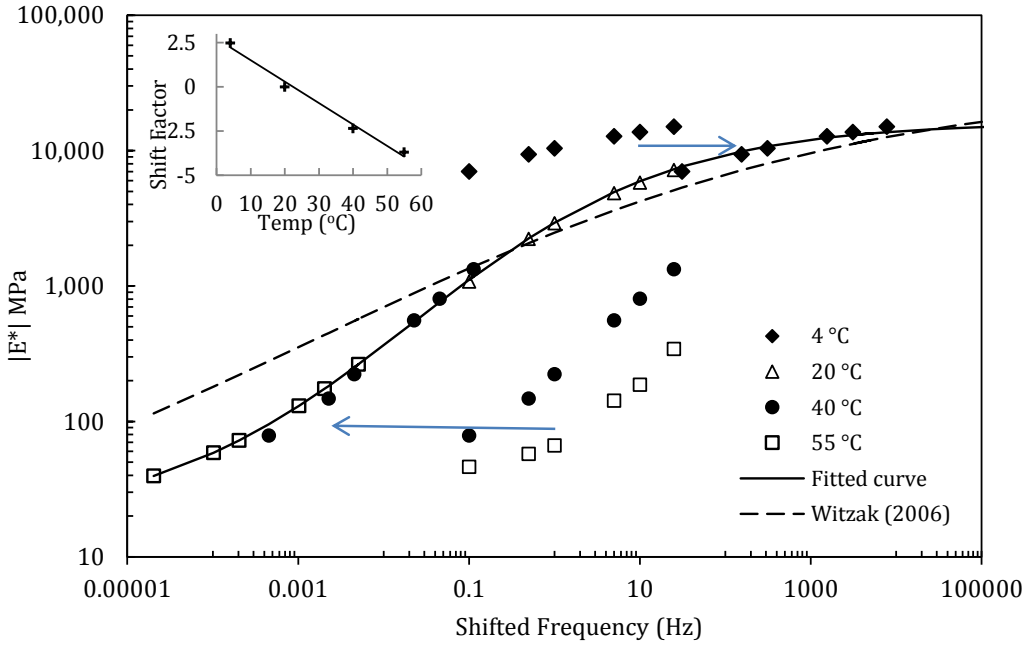

Figure 3.22 Typical dynamic modulus data at various temperature and loading frequencies

4 RESULTS AND DISCUSSION

4.1 Introduction

This chapter presents the results and discussion of the aggregate properties tests, volumetric properties tests, and asphalt stiffness characterization. The objectives outlined in Chapter 1 were achieved by the experimental methods described in Chapter 3. The Western Australian asphalt mixtures were evaluated to determine their creep, resilient modulus and flexural fatigue. The dynamic modulus test was also conducted and the comparison between the measured $|E^*|$ and predicted $|E^*|$ was taken. The effect of various parameters and their correlation are also discussed.

4.2 Aggregate Properties

The materials used in this study are representative of mixtures typically used in Western Australia. Asphalt mixtures were produced using fine aggregates and coarse aggregates with nominal maximum sizes of 7, 10, 14 and 20 mm. Both the physical properties and gradation of fine and coarse aggregates were studied.

4.2.1 Physical Properties

Crushed granites from Perth region were used as coarse aggregates with a diameter size of 7, 10, 14 and 20 mm. The fine aggregate was uncrushed yellow sand. The properties of coarse aggregates were studied, including particle density, oven dry specific gravity, SSD specific gravity, apparent specific gravity, and absorption. The physical properties of coarse and fine aggregates are given in Table 4.1.

Table 4.1 Physical properties of coarse and fine aggregates

Property	Values					Standard/ Method
	7 mm	10 mm	14 mm	20 mm	Sand	
Particle density (t/m^3)	2.64	2.65	2.70	2.67	1.86	AS1141.6.1/ AS1141.5
Oven dry basis bulk relative density	2.54	2.60	2.61	2.63	2.59	
SSD basis bulk relative density	2.58	2.62	2.65	2.65	2.61	
Apparent relative density	2.65	2.65	2.71	2.67	-	
Absorption (%)	1.60	0.74	1.42	0.58	0.8	

The particle density of the aggregate is defined as the mass per unit volume of particles. This property is useful in asphalt mix design calculations. The particle density of the coarse aggregates studied was in the range of 2.64-2.70 t/m^3, which is greater than the 2.3 t/m^3 specified for asphalt (Austroads 2007). Compared to the oven-dried specific gravity, the saturated surface dry (SSD) specific gravity is normally used in a concrete mix design calculation to represent an ideal condition of the aggregate used in the mixture. The SSD specific gravity values of the coarse aggregate were 2.58–2.6. Coarse granite usually has an SSD specific gravity of 2.6–3.0. Absorption determines the porosity of asphalt aggregates. The absorption of the coarse aggregates varied with a range of 0.58–1.60%, which is less than the maximum specified value of 2–2.5% (Austroads 2007). Based on these values, the coarse aggregates were suitable for asphalt production.

4.2.2 Gradation

Aggregate grading determines the type, proportions of material components and air void content in asphalt production. The Western Australian mixtures were designed by proportioning aggregate quantity based on a particle size distribution obtained through sieve analysis in compliance with AS 1141.11.1-2009 (Standards Australia 2009). The aggregate grading combinations are shown in Table 4.2, and their gradation curves are shown in Figure 4.1, Figure 4.2, and Figure 4.3. There were two types of AC20-320 mixtures, i.e. the Intermediate Course (IC) and Base Course (BC) used in this research. As mentioned in section 2.2.2, IC layer is placed underneath the Wearing Course (WC), while the BC layer is located under the IC layer. The combinations comply with the grading requirements for dense graded asphalt as in Table 2.2. Grading curves for single aggregate sizes are presented in Figure 3.2.

Table 4.2 Aggregate grading combinations

	7 mm	10 mm	14 mm	20 mm	WQS	BHD	H-lime
AC10-170 &320	32.9%	16%			47.2%	2.3%	1.5%
AC14-320	21%	14%	22%		39.5%	2%	1.5%
AC20-320	8%	7%	25%	21%	35.5%	2%	1.5%

WQS (washed quarry sand), BHD (baghouse dust), H-lime (hydrated lime)

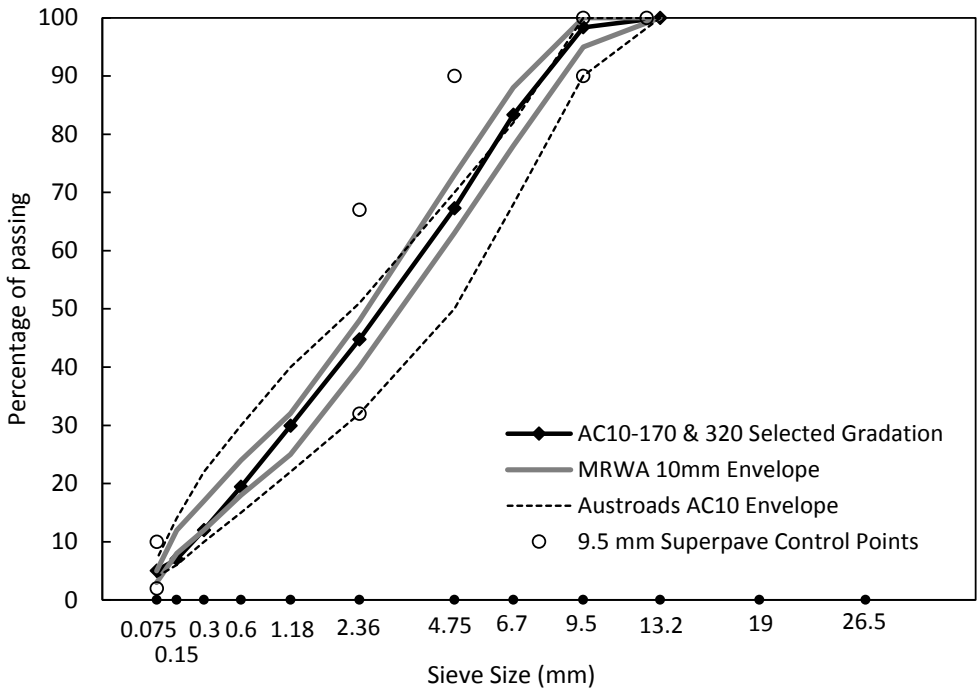

Figure 4.1 Grading of AC10-170 and AC10-320

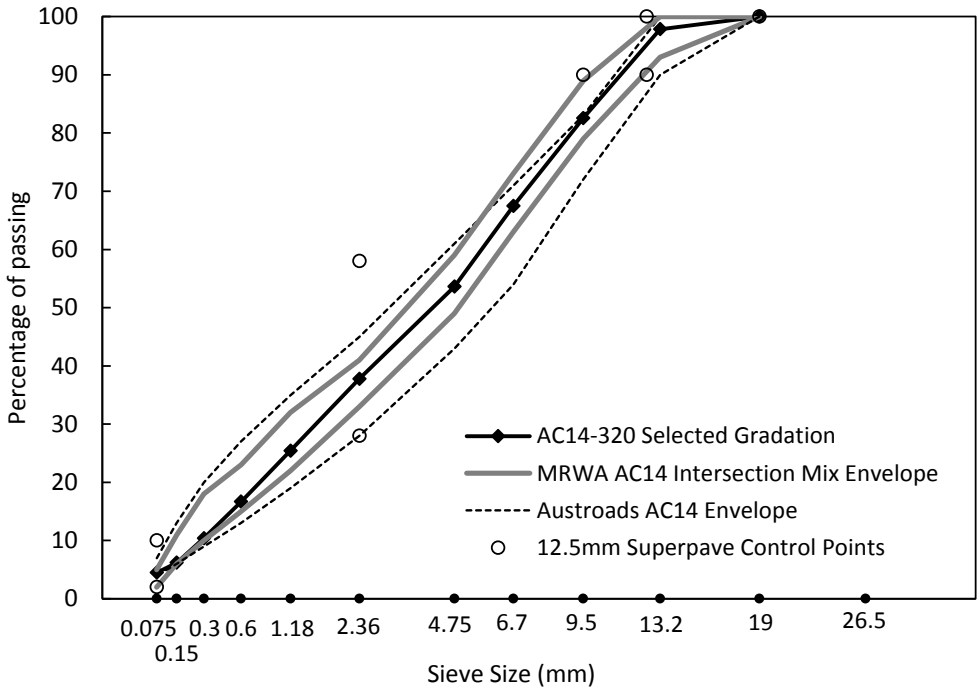

Figure 4.2 Grading of AC14-320

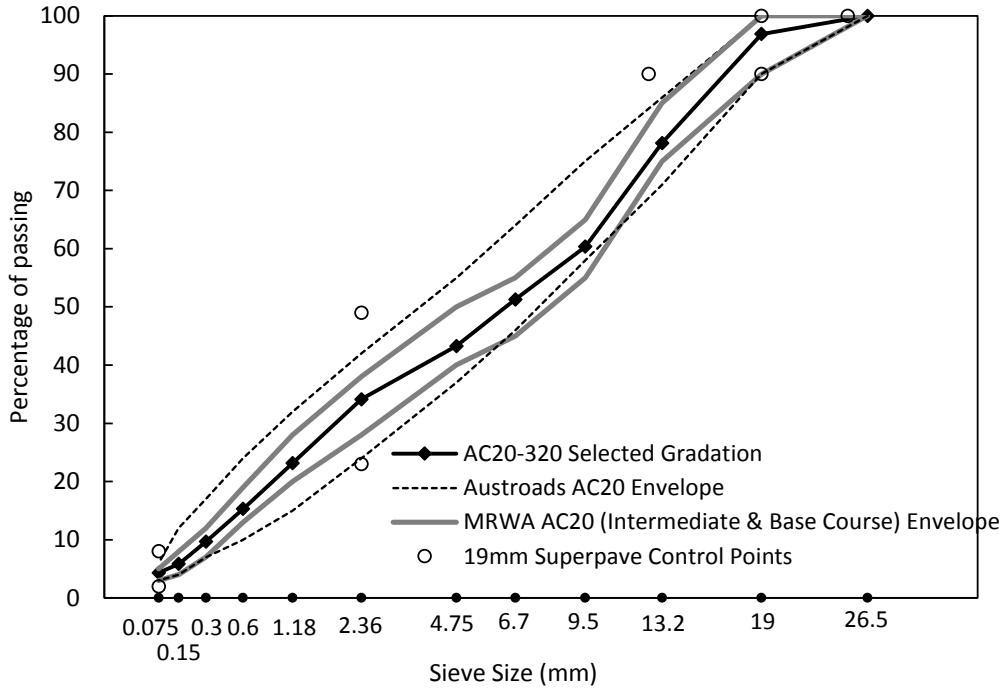

Figure 4.3 Grading of AC20-320

4.2.3 Volumetric Properties

The volumetric properties of the Western Australian mix were determined according to and compared to the Main Roads specifications. The volumetric properties were used for Witzcak and Hirsch dynamic modulus predictive models in section 2.5.4.2. The design standards for the Western Australian mixture require that for wearing course design, a nominal maximum aggregate size (NMAS) of 10 mm should be used, voids in mineral aggregate (VMA) should be 15.0% minimum while the specification range for voids filled with asphalt (VFA) is between 65% and 75%. Table 4.3 shows the VMA and air void content trends with respect to the binder content in the asphalt mixture. The general trend indicates that as the air voids increase, the binder content decreases, then VMA increases. It is believed that the increase in air voids causes the absorption of some of the asphalt in the mix due to the surface pores on the mixture. This absorption thus reduces the effective asphalt content in the asphalt mixture.

Table 4.3 Volumetric properties of Western Australian mixtures

Mix design properties	AC10-170	AC10-320	AC14-320	AC20-320	AC20-320 BC
Bitumen content (%)	5.4 (5.4 ± 0.3) *Bitumen classes 170 & 320*	5.4	4.7 (4.7 ± 0.3) *Class 320*	4.5 (4.5 ± 0.3) *Class 320*	5.1 (5.1 ± 0.3) *Class 320*
Air voids (%)	4.9 (4–6)	4.5	4.8 (4–7)	4.4 (3.5–5.5)	2.2 (1.5–3.5)
VMA (%)	17.3 (min. 15)	16.9	15.9	14.8 (min. 14)	14.3
Stability (kN)	11.8	13.2	14.5 (min. 8)	18.7	19
Flow (mm)	3.5	3.6	3.4 (2–4)	2.8	3.0
Hydrated lime (%)			1.5 (1.5 ± 0.5)		

*MRWA criteria in brackets

4.3 Asphalt Performance and Stiffness Characterization

4.3.1 Creep

The dynamic creep test is a test to assess the resistance of asphalt to permanent deformation by applying repeated pulse uniaxial stress to the specimen. In this test, the values were derived from the dynamic creep curves with the point of inflection (minimum slope). The minimum slope becomes the indicator of the mixture's susceptibility to repeated load or the deformation resistance of the asphalt mixtures (He and Wong 2008). A mix with a small minimum slope has better deformation resistance. In addition, Austroads (2008e) provides a relationship between the minimum slope values and the road's service level. Three traffic categories, i.e. very heavy, heavy and medium can be determined from the minimum slope values of asphalt mixtures.

Table 4.4 lists the results of the dynamic creep test of the three mixes used in this research. It is noted that the initial permanent deformation varied in the range of (1.494–1.564 mm) and tended to decrease with the compaction level. There was a difference between the values; hence variation of permanent deformation of the three mixes was reported negligible. Furthermore, Austroads (2008e) stipulates minimum slope values to assess the susceptibility of mixtures to permanent deformation. In general, it can be seen that the minimum slope decreased with an increase in maximum aggregate size and decrease in bitumen content in the mixes. The AC10-320 mixes compacted with 120 gyration cycles showed the highest minimum slope of 8.570 μm/m/c, while the AC20-320 mixes with similar compaction

displayed the lowest slope (1.873 μm/m/c). Asphalt mixtures become less resistant to permanent deformation when the minimum slope is larger.

Table 4.4 Summary of dynamic creep results

Mix type	Gyration cycles	Bitumen content (%)	Strain to min. slope	Permanent deformation (mm)	Creep stiffness (MPa)	Minimum slope (μm/m/cycle)	Cycles to min. slope
AC10-320	100	5.4	13067	1.494	6.66	8.546	1068
	120		12844	1.496	6.68	8.570	864
AC14-320	100	4.7	13764	1.511	6.65	4.832	1244
	120		20075	1.483	6.64	4.302	2624
AC20-320	100	4.5	12151	1.564	6.69	2.971	1568
	120		13966	1.541	6.63	1.873	3248

Figure 4.4 shows the traffic classification indicated by creep values for the mixtures AC10-320, AC14-320 and AC20-320 for various air void contents. Only one type of binder was used for the creep study, namely, AC-320, which is commonly used in asphalt manufacture in Australia. There is a linear relationship between the minimum slope and the percentage of air voids, where the minimum slope increases with an increase of air voids. The standard reference condition of air void was 5 ± 0.5%. This value was considered critical as the creep value increases as the air void decreases.

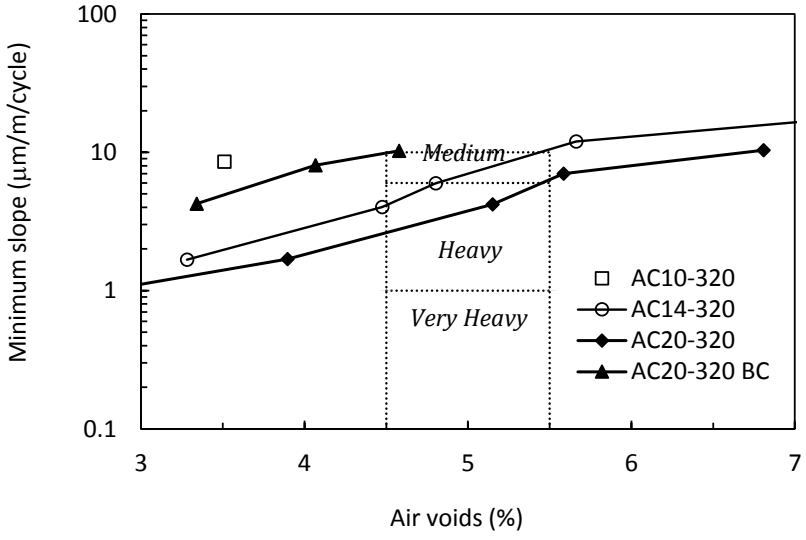

Figure 4.4 Plot of average minimum slopes and cycles at minimum slope with variation of air voids

Moreover, the variation in minimum slope is quite small and the values could be used to determine the traffic categories for the mixtures used in this research. The traffic categories based on the creep test interpretation from Austroads (2008) can be seen in section 2.5.3.1. The Weighted Mean Annual Pavement Temperature (WMAPT) was 25^{o}C in Perth based on annual data. It is noted that mix AC20-320 for intersection course with a minimum slope of less than 3 μm/m/c can be used as asphalt mixture for heavy traffic roads with commercial vehicles/lane/day of 500–1000. On the other hand, mix AC14-320 can be used for medium traffic, where the commercial vehicles/lane/day number 100–500.

4.3.2 Resilient Modulus

Resilient modulus (M_R) is the material property used to measure the stiffness of a material for the required pavement thickness calculation. The value is required as a design input in the Level 2 Austroads mix design procedure (Austroads 2008b). The three mixtures studied in this research, namely AC10-320, AC14-320 and AC20-320, were investigated at a reference temperature of 25°C for various air voids. The reference temperature of 25°C is the temperature where the state of asphalt is resistant to fatigue.

Figure 4.5 shows the effect of the nominal maximum aggregate size (NMAS) and air voids on the resilient modulus. A comparison of resilient modulus values showed that the values for mix AC20-320 were considerably higher than for mixes AC10-320 and AC14-320. As explained in section 2.5.3.2, maximum aggregate size greatly affects the performance of the mixtures. The higher the nominal aggregate size, the coarser the aggregate gradation. This increases the stiffness of the asphalt mix due to the higher particle-to-particle contact in the coarse aggregate structure. Some studies have made similar findings related to factors affecting resilient modulus (Lim and Tan 1995, Saleh 2008).

Figure 4.5 also shows the variation of the resilient modulus values with air voids for mixes AC10-320, AC14-320 and AC20-320, respectively. The resilient modulus value obtained for mix AC20-320 with 3% air voids is the highest followed by that obtained for the AC14-320 and AC10-320 mixtures. This also indicates that the effect of air voids is significant because the lower air void content results in a higher resilient modulus, due to the high density of the mixtures.

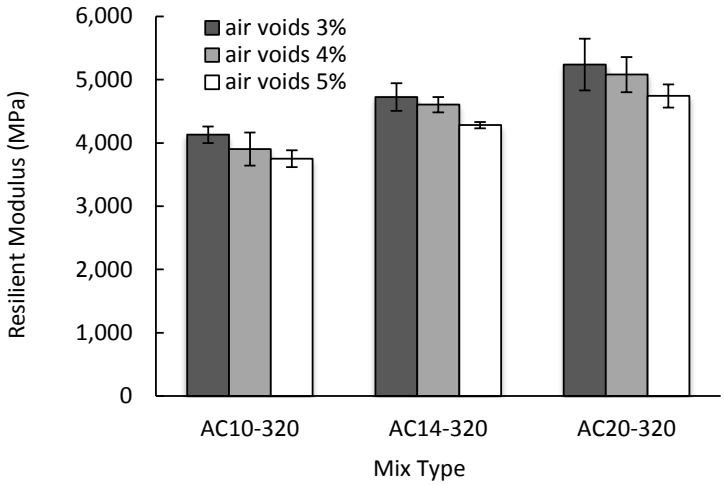

Figure 4.5 Resilient modulus values with various maximum aggregate sizes and air void contents

The resilient modulus values were taken from triplicate samples. Statistical analysis using standard deviation shows some variability in the mixtures. On average, the variability occurred mostly in the mixes with 3–4% air void content. The highest variability was observed in mixture AC20-320 with 3% air voids. It is argued that the resilient modulus test showed the highest variability in test results, with a reproducibility of approximately 40% of gross mean value (Austroads 2006c). The great discrepancies in results were thought to arise from several factors, such as variability in the software and hardware of the MATTA devices, procedural matters, and the interpretation of test procedures.

Table 4.5 shows the variation in resilient modulus values for all mixtures at a reference testing temperature of 25°C. The resilient moduli of mix AC10-320 varied from 3483–3768 MPa, while the mix AC20-320 showed higher values in the range of 4087–4860 MPa. Mix AC20-320 had the highest resilient modulus values of the included mixes. The average resilient modulus of mix AC10-320 with 3% air voids was 3768 MPa. This value reached 4860 MPa for mix AC20-320 samples, i.e., a 28.98% increase in resilient modulus value. The average resilient modulus for the samples with 5% air voids increased from 3483 MPa for mix AC10-320 to 4089 MPa for mixes AC20-320. It is obvious that mix AC20-320 showed the lowest deformation or the highest resilient modulus of the three mixes.

The typical presumptive modulus values (Table 2.7, section 2.5.3.2), and the values obtained from the current testing cannot be directly compared due to the differences in the results for the 5% air voids mixes. The resilient modulus values with 5% air voids differed from the

typical values by between 5.8% and 34.5%. The resilient modulus results obtained from the laboratory testing were typically in the lower part of the range of the Austroads presumptive values (Austroads 2008c). Previous research into a mix similar to AC10 has confirmed a comparable trend. The resulting modulus for the mixtures was in the range of 2596 to 3585 MPa (Julaihi 2010). The values obtained in this research are relevant for designing full depth dense-graded flexible pavement in Western Australia, due to the recommendation of the MRWA that the resilient modulus values used in the mechanistic procedure must not exceed the Austroads recommended typical dense-graded asphalt values (Main Roads Western Australia 2008). This might be to accommodate the practicalities of asphalt manufacture using the locally available bitumen and aggregate sources. In conclusion, the resilient modulus values from this research could be used as indicative values for pavement design inputs in Western Australia.

Table 4.5 Resilient modulus results from laboratory tests (test temperature of 25^{O}C)

Mix type	Air voids (%)	Peak load (N)	Total recovered strain (με)	VMA (%)	VFA (%)	Resilient modulus (MPa)	Austroads presumptive values (5% air voids, in MPa)*	Typical values (5% air voids, in MPa)*
	3	52.3	2171.7	15.3	79.4	4130		
AC10-320	4	55.3	2097.2	16.4	75.8	3905	3000–6000	4500
	5	**54.0**	**1998.1**	**17.2**	**71.5**	**3751**		
	3	52.4	2406.5	13.9	78.0	4725		
AC14-320	4	53.5	2403.3	15.3	71.8	4606	2000–7000	5000
	5	**54.9**	**2251.9**	**15.7**	**69.4**	**4281**		
	3	51.2	2776.7	13.6	77.9	5239		
AC20-320	4	51.5	2603.0	14.7	71.0	5080	3000–7500	5500
	5	**51.6**	**2411.5**	**15.2**	**68.5**	**4744**		

*Austroads (2008c)

4.3.3 Flexural Fatigue

The flexural modulus/stiffness was determined as another characteristic of asphalt stiffness. This value is used to to measure fatigue life. Due to limited data in this research, the results are emphasized on flexural stiffness values. There were three mixtures measured in this research, i.e. mix AC10-320, mix AC14-320, and mix AC20-320..Each mix has different bitument content within range of 4.5-5.4%. As mentioned in section 3.5.5, the repeated loading was continued until the flexural stiffness reduced to 50% of the initial flexural stiffness in this test. Fatigue life is taken as the number of load cycles to achieve the 50% of the initial stiffness.

Figure 4.7 shows an example of the beam fatigue results of AC10-320 mixes tested at 400με. There was an initial stiffness gradual decrease, which is likely caused by some increase in temperature during testing. In that stage, the damage was due to accumulation in the micro-crack formation. It was confirmed by Di Benedetto, Soltani and Chaverot (1996) that an increase in temperature of 1.3ºC for classical fatigue testing could reduce the modulus up to 15%.

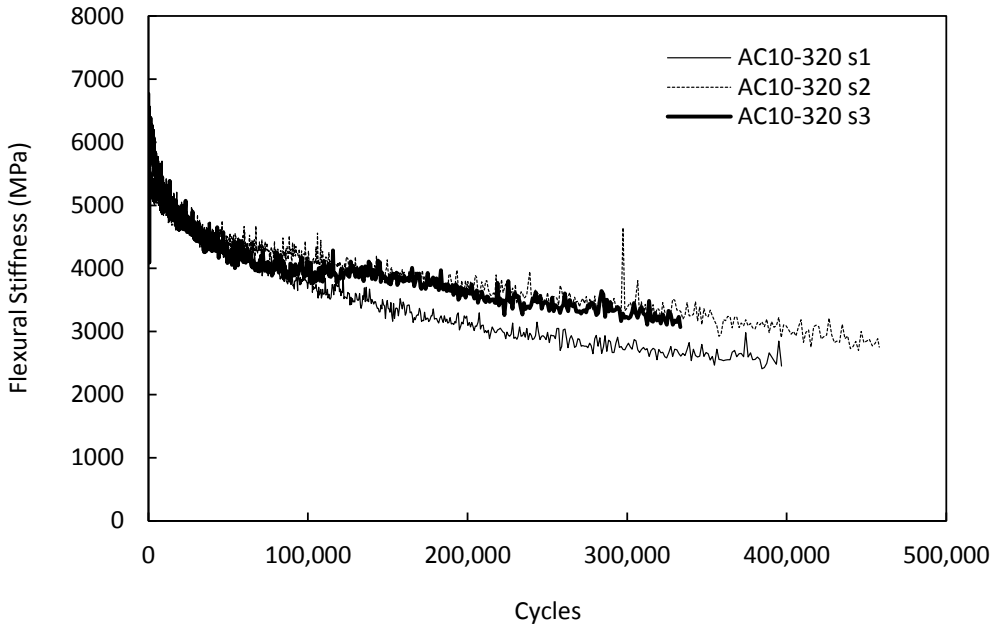

Figure 4.6 Flexural stiffness vs loading cycles for mix AC10-320

Table 4.6 presents a summary of the beam fatigue results for those mixtures. The results for all mixes are shown in Appendix D. There was a dramatic decrease of bending repetition with the increase of loading amplitude. It can be seen that the higher binder content increased the fatigue resistance of WA mixes. Specimens with 5.4% binder content (AC10-320) showed higher fatigue life than those with 4.5% binder content (AC20-320). This could be due to the ability of thicker binder films to resist breakdown of the mix stiffness under increasing numbers of strain repetitions. Previous studies confirmed similar findings (Liu and Liu 2010, Peploe 2008).

The test also indicate that the number of load cycles to 'failure' were independent of the NMAS variation. There was a gradual increase in fatigue life from mixes AC10-320 to AC20-320. This is a considerably contradicting data given that the fatigue tests were carried out under controlled strain conditions (400με). It was stated that (Austroads 2004), an increase in asphalt modulus (resilient modulus) results in a decrease in fatigue life under

controlled strain loading conditions. There is a linear correlation between resilient modulus in section 4.3.2 with the flexural stiffness. It is unclear why this behaviour was not observed in the test results. In one study (Mogawer et al. 2011), it was observed that flexural stiffness was inconsistent with regard to aggregate gradation or NMAS, and showed considerable variability. The high variability in the original test data and limited number of data available, confirmed that more tests need to be performed to confirm these trends.

Table 4.6 Summary of beam fatigue test

Properties	Mixtures		
	AC10-320	AC14-320	AC20-320
Bitumen content (%)	5.4	4.7	4.5
Air void (%)	5.3	5.4	6.1
Number of cycles	396,060	282,613	195,477
Maximum tensile (μm)	397.2	397.2	414.3
Initial flexural stiffness (MPa)	5587	5682	5613
Termination stiffness (MPa)	2793	2944	2751

4.3.4 Dynamic Modulus (*|E*|*) of Western Australian Asphalt Mixture

Dynamic modulus is a stiffness property that relates laboratory test results to field performance. The test offers a broad loading range and temperature spectrum compared to the resilient modulus test. The dynamic modulus (*|E*|*) has not been specified in Austroads as a performance measurement, hence, this research sought to determine the dynamic modulus for Western Australian asphalt mixtures. Some measurements from the Austroads materials specifications were adjusted.

A number of parameters were investigated in this research, including binder conditioning, asphalt grade, nominal maximum aggregate size and air void content. There were two types of binder conditioning considered in this study, namely original binder and RTFOT (rolling thin film oven temperature). The first type was conditioned without any treatment, while the latter was treated for several minutes in the oven at 165°C before moulding to imitate the actual mixing temperature in the field. The second parameter was the type of asphalt grade. In this case, only one mix (AC10) was considered, with varied asphalt grades, namely Class 170 and Class 320. The third parameter was the nominal maximum aggregate size, including 10 mm, 14 mm and 20 mm. The fourth parameter was the air void content. The air voids determine the volumetric properties and density of asphalt mixtures which in turn determine the asphalt content, degree of compaction needed and stiffness characteristics. Master curves were generated for each variable, the dynamic modulus values were calculated, and the predicted and measured dynamic modulus values were compared. The dynamic modulus was

also compared with the resilient modulus and flexural modulus values. Statistical assessment was used to evaluate the accuracy of dynamic modulus predictions for Western Australian asphalt mixtures.

4.3.4.1 Dynamic Modulus

Typical dynamic modulus |E| and phase angle (ϕ)*

The dynamic modulus of Western Australian asphalt mixtures was determined for each specimen that was tested at six different loading frequencies and four different temperatures. There were 48 responses (|*E**| and phase angle) in total. Each dynamic modulus test provided two responses simultaneously, namely dynamic modulus |*E**| and phase angle (ϕ). The phase angle indicates the elastic and viscous properties of the mix. Typical values for the dynamic modulus |*E**| and the associated phase angle for mixes AC10-170 and AC10-320 specimens are listed in Table 4.7 and Table 4.8. The results for all mixes are shown in Appendix E. It can be seen from Table 4.7 and Table 4.8 that the dynamic modulus of both mixes followed a general trend, increasing with an increase in loading frequency and decreasing as the temperatures increased. The effect of air voids and binder grade are quite significant. For example, mixes with an air void content of 3% showed higher dynamic modulus than mixes with an air void content of 4% and 7%. The AC10-320 mix with a higher grade binder yielded better dynamic modulus values than the mix with a lower grade asphalt.

The phase angle showed a different trend to the dynamic modulus. Initially the phase angle decreased as the loading frequency increased from 4°C to 20°C. At 40°C and 55°C, the behaviour of the phase angle as a function of frequency seemed more complex. At higher temperatures, the phase angle increased with an increase in frequency to 10Hz, after which the values decreased at the highest loading frequency. The complex behaviour of the phase angle at higher temperatures or at lower frequencies may be attributed to the predominant effect of the aggregate interlock. Other studies have confirmed that similar elastic behaviour of aggregate at high temperature and low frequency determines the response of the specimen. It can be observed from the tables that the phase angle values for the mix AC10-320 were considerably lower than those for mix AC10-170. This is attributed to the better quality asphalt grade used in mix AC10-320 which contributed to the low phase angle.

The type of binder also has an impact on dynamic modulus values. In this research, two types of binder, namely original and RTFOT (rolling thin film oven test) were investigated.

The RTFOT specimens were original binders aged by the rolling thin film oven (RTFO) procedure. Table 4.9 compares the typical dynamic modulus values for both types of mixture. It appears that the dynamic modulus of RTFOT binder is slightly higher than that of the original binder for all air void variations at test temperatures of 4 and 20°C. This indicates the effect of aging since the binder became stiffer and the dynamic modulus became higher than the original binder. At high temperatures (40 and 50°C), there is no difference between the dynamic modulus of the original and RTFOT binders. It seems the effect of aging (RTFOT) is not significant at high temperatures.

Table 4.7 Typical values of dynamic modulus $|E^*|$ and phase angle (ϕ) for each different air void content of mix AC10-170

		Mix AC10-170											
		3%				5%				7%			
t °C	f Hz	Dynamic Modulus		Phase Angle		Dynamic Modulus		Phase Angle		Dynamic Modulus		Phase Angle	
		$\|E^*\|$ MPa	CV %	ϕ °	Sy	$\|E^*\|$ MPa	CV %	ϕ °	Sy	$\|E^*\|$ MPa	CV %	ϕ °	Sy
4	0.1	7070	8.84	20.7	3.07	6986	8.13	20.1	0.65	5419	3.31	22.2	0.06
4	0.5	9477	6.16	15.1	1.07	9365	5.44	15.5	0.55	7564	3.48	17.1	0.08
4	1	10627	4.27	13.6	1.47	10347	4.25	14.0	0.47	8504	3.48	15.3	0.03
4	5	13043	2.93	9.4	0.66	12700	2.91	11.0	0.36	10720	3.29	12.0	0.01
4	10	14043	2.79	8.0	0.63	13674	2.77	10.0	0.30	11622	2.65	10.8	0.02
4	25	15410	2.80	5.8	0.10	15004	2.78	8.7	0.26	12790	2.23	9.4	0.08
20	0.1	1096	8.13	39.3	4.54	1078	8.07	37.8	0.29	777	8.45	39.0	0.67
20	0.5	2260	8.54	34.4	4.10	2221	8.57	34.5	0.35	1666	9.13	35.9	0.64
20	1	2950	8.56	31.9	3.97	2901	8.56	32.5	0.37	2208	9.45	34.1	0.71
20	5	4924	7.94	24.6	1.47	4840	7.95	27.0	0.46	3801	9.10	28.5	0.59
20	10	5897	7.28	22.9	2.24	5797	7.28	24.7	0.46	4582	8.58	26.1	0.54
20	25	7306	6.27	19.9	2.15	7182	6.28	21.5	0.47	5732	7.40	22.6	0.41
40	0.1	110	4.52	28.5	1.84	79	3.69	28.3	1.47	50	0.42	28.2	0.95
40	0.5	196	7.60	35.7	0.88	147	1.54	37.2	1.17	95	1.41	36.8	0.97
40	1	258	4.39	39.0	0.86	223	4.25	38.4	0.11	135	1.57	40.4	1.10
40	5	697	3.35	39.5	1.11	555	2.59	40.5	0.31	381	0.32	41.2	0.80
40	10	965	1.10	40.3	1.73	802	1.13	41.4	0.10	544	0.61	43.1	0.88
40	25	1476	6.32	37.5	3.52	1328	1.54	39.5	0.66	951	1.34	41.2	1.63
55	0.1	48	20.6	26.8	0.79	46	3.07	20.0	0.98	52	30.2	25.2	1.10
55	0.5	73	0.00	25.3	4.27	58	10.9	22.5	0.23	51	2.65	22.2	3.23
55	1	88	5.66	27.0	1.36	66	18.4	26.6	0.81	49	26.2	27.4	0.42
55	5	175	5.66	35.0	4.74	142	2.69	31.9	0.37	127	18.6	32.0	0.27
55	10	232	2.44	38.5	2.02	186	2.70	36.5	0.82	157	23.6	38.6	0.04
55	25	379	1.49	39.7	6.02	342	2.03	36.3	1.29	296	16.4	35.6	0.04

Table 4.8 Typical values of dynamic modulus $|E^*|$ and phase angle (ϕ) for each different air void content of mix AC10-320

t °C	f Hz	Mix AC10-320											
		4%				5%				7%			
		Dynamic Modulus		Phase Angle		Dynamic Modulus		Phase Angle		Dynamic Modulus		Phase Angle	
		$\|E^*\|$ MPa	CV %	ϕ °	Sy	$\|E^*\|$ MPa	CV %	ϕ °	Sy	$\|E^*\|$ MPa	CV %	ϕ °	Sy
4	0.1	8255	7.47	17.6	1.32	7488	7.47	19.2	1.44	6384	3.32	22.0	0.36
4	0.5	11180	6.09	12.3	0.75	10141	6.09	14.1	0.86	8911	3.48	16.8	0.11
4	1	12288	3.79	10.5	0.40	11146	3.79	12.3	0.47	10019	3.48	13.7	1.25
4	5	15122	3.27	7.0	0.23	13716	3.27	8.2	0.27	12629	3.29	10.6	0.53
4	10	16304	2.61	4.8	0.13	14788	2.61	6.8	0.18	13691	2.65	8.8	0.41
4	25	17829	2.80	3.5	0.10	16171	2.80	6.9	0.19	15067	2.22	5.8	1.10
20	0.1	1455	5.79	33.0	1.91	1332	5.84	39.2	2.29	955	8.44	39.0	4.23
20	0.5	3055	8.96	31.3	2.80	2797	8.95	32.2	2.88	2047	9.16	35.0	3.21
20	1	3981	8.65	29.0	2.51	3646	8.67	29.3	2.54	2713	9.44	33.4	1.72
20	5	6643	8.04	23.0	1.85	6083	8.04	23.8	1.91	4669	9.09	25.7	3.01
20	10	7951	6.81	18.2	1.24	7281	6.81	19.7	1.34	5630	8.58	24.1	1.36
20	25	9871	5.71	13.6	0.78	9039	5.71	17.4	0.99	7042	7.41	19.7	2.20
40	0.1	126	5.61	31.0	1.74	101	5.60	32.5	1.82	90	7.86	31.3	2.46
40	0.5	232	1.22	36.0	0.44	187	1.51	37.3	0.56	118	3.01	32.8	1.78
40	1	343	3.92	40.1	1.57	284	4.24	39.5	1.68	168	3.80	35.9	1.46
40	5	753	2.91	43.0	1.25	703	2.82	39.3	1.11	487	1.16	39.4	2.26
40	10	1094	0.71	37.0	0.26	1021	0.69	39.3	0.27	696	0.61	40.8	0.34
40	25	1738	7.04	37.0	2.61	1623	7.02	35.9	2.52	1216	2.85	38.2	1.58
55	0.1	53	16.01	19.0	3.04	51	15.4	26.4	4.07	43	3.29	20.5	1.06
55	0.5	70	3.05	22.0	0.67	66	5.40	27.6	1.49	61	2.32	26.7	0.62
55	1	81	3.49	32.0	1.12	77	3.67	31.4	1.15	71	3.01	26.9	3.04
55	5	179	1.58	35.0	0.55	184	2.70	36.3	0.98	155	17.3	36.8	7.17
55	10	229	0.31	37.0	0.11	242	1.75	38.9	0.68	191	23.7	37.6	8.91
55	25	387	1.10	39.0	0.43	441	2.41	40.4	0.97	360	16.5	40.9	7.52

Table 4.9 Typical values of dynamic modulus /*E**/ for each mixture (origin and RTFOT)

Temp (°C)	Freq (Hz)	/*E**/ Mix AC10-320 (MPa)					
		4%		5%		7%	
		Origin	RTFOT	Origin	RTFOT	Origin	RTFOT
4	0.1	9,372	9,494	8,195	8,309	6,589	6,690
4	0.5	12,074	12,135	10,832	10,890	9,325	9,387
4	1	13,079	13,110	11,797	11,827	10,394	10,431
4	5	14,974	14,940	13,571	13,541	12,454	12,431
4	10	15,610	15,551	14,146	14,094	13,148	13,103
4	25	16,303	16,215	14,757	14,680	13,901	13,828
20	0.1	1,423	1,429	1,169	1,174	791	792
20	0.5	2,969	2,976	2,617	2,623	1,843	1,844
20	1	3,902	3,906	3,523	3,527	2,553	2,552
20	5	6,562	6,550	6,142	6,132	4,804	4,792
20	10	7,826	7,804	7,380	7,359	5,961	5,940
20	25	9,498	9,457	8,990	8,953	7,550	7,514
40	0.1	117	117	102	101	84	83
40	0.5	236	235	209	208	159	158
40	1	332	330	300	298	221	220
40	5	763	759	730	726	518	516
40	10	1,091	1,086	1,070	1,065	760	757
40	25	1,718	1,710	1,735	1,727	1,246	1,241
55	0.1	48	48	45	45	42	42
55	0.5	73	73	68	69	60	60
55	1	92	92	86	86	73	74
55	5	175	176	169	170	134	134
55	10	241	242	237	239	183	184
55	25	379	382	387	390	289	291

4.3.4.2 Construction of /*E**/ master curve

Shift factor and sigmoidal function

Master curves for all mixtures were generated from the dynamic modulus at a reference temperature. This curve presents a wide range of stiffness for an asphalt mixture at all temperatures and loading frequencies. Details of the master curve calculation can be seen in section 3.5.5. In order to construct the master curve, a shift factor must be calculated. Figure 4.7 shows the typical shift factors for different mixes (AC10-320, AC14-320 and AC20-320) with various types of binder conditioning (original and RTFOT).

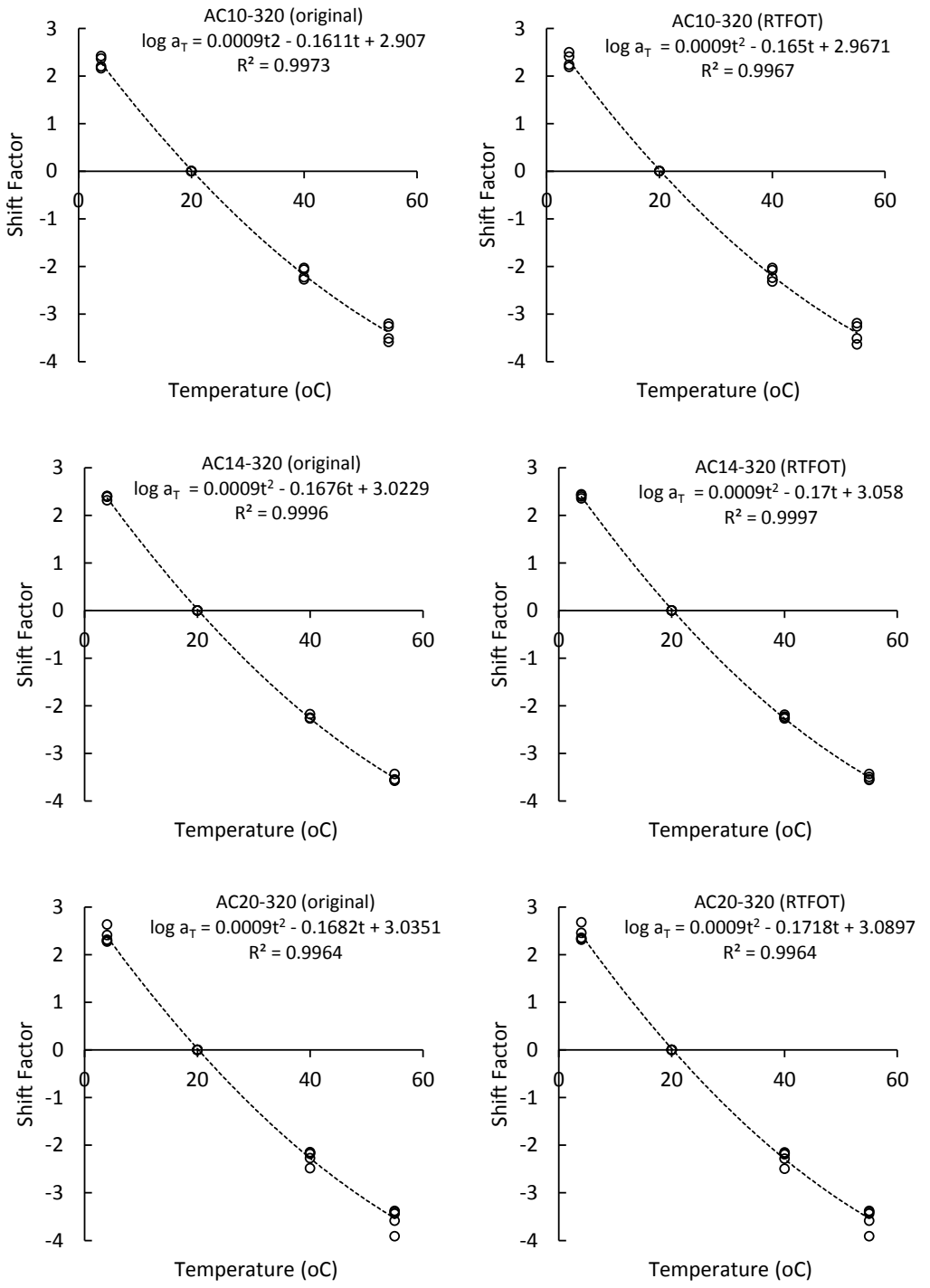

Figure 4.7 Typical shift factors for mixes AC10-320, AC14-320 and AC20-320

To construct the master curve, a shift factor was used to shift the dynamic modulus at various temperatures to the reference temperature. The shift factor was calculated by dividing the shifted temperature with the reference temperature. The correlation coefficient

(R^2), which is a measure of accuracy showed that all typical shift factors were higher than 0.90. Maximum aggregate size also affected the shift factor slope. The higher the aggregate size the higher the shift factor slope.

Combined shift factor regressions and their R^2 for all mixes are summarized in Table 4.10 to 4.12. Overall, the values are just slightly varied.

Table 4.10 Shift factor regressions (AASHTO 2010a)

Mix	Shift factor regression	R^2
AC10-170	$\log a_T = 0.0003t^2 - 0.1231\ t + 2.3313$	0.9998
AC10-320	$\log a_T = 0.0003t^2 - 0.1259\ t + 2.3836$	0.9985
AC14-320	$\log a_T = 0.0004t^2 - 0.1272\ t + 2.4091$	0.9999
AC20-320	$\log a_T = 0.0004t^2 - 0.1293\ t + 2.4484$	0.9959
AC20-320 BC	$\log a_T = 0.0003t^2 - 0.1250\ t + 2.3660$	0.9995

The shift factors were calculated using Eq. 3-8

Table 4.11 Shift factor regressions for original binder (AASHTO 2010b)

Mix	Shift factor regression	R^2
AC10-170	$\log a_T = 0.0008t^2 - 0.1546\ t + 2.7876$	0.9993
AC10-320	$\log a_T = 0.0009t^2 - 0.1611\ t + 2.907$	0.9973
AC14-320	$\log a_T = 0.0009t^2 - 0.1676\ t + 3.0229$	0.9996
AC20-320	$\log a_T = 0.0009t^2 - 0.1682\ t + 3.0351$	0.9964
AC20-320 BC	$\log a_T = 0.0009t^2 - 0.1638\ t + 2.9363$	0.9994

The shift factors were calculated using Eq. 3-12

Table 4.12 Shift factor regressions for RTFOT binder (AASHTO 2010b)

Mix	Shift factor regression	R^2
AC10-170	$\log a_T = 0.0009t^2 - 0.1591\ t + 2.8565$	0.9992
AC10-320	$\log a_T = 0.0009t^2 - 0.165\ t + 2.9671$	0.9967
AC14-320	$\log a_T = 0.0009t^2 - 0.1676\ t + 3.0229$	0.9996
AC20-320	$\log a_T = 0.0009t^2 - 0.17t + 3.058$	0.9997
AC20-320 BC	$\log a_T = 0.0009t^2 - 0.1672t + 3.0078$	0.9993

The shift factors are calculated using Eq. 3-12

The shift factor regressions in Table 4.11 and 4.12 use binder viscosity in the form of the A-VTS viscosity temperature relationship. Both of the values A (regression intercept) and VTS (viscosity-temperature susceptibility) must be determined according to the default values as suggested by the MEPDG 2004 (NCHRP 2004a). Since there is no precise equipment available to determine A and VTS for the two bitumen classes used, the values were derived and interpolated from Australian bitumen survey data (Austroads 2011b). The calculated

values for the original binder for Class 170 are 10.95 for A and -3.68 for VTS, and the values of Class 320 are 10.89 for A and -3.65 for VTS (Table 4.13). The values for RTFOT binder are given in Table 4.14. The tables also present the source data for asphalt bitumen properties at various temperatures for original and RTFOT binders.

Table 4.13 Asphalt bitumen properties at various temperatures (original binder)

t (°C)	Viscosity at temperature – Pa.s				A	VTS
	25	45	60	135		
C170	184,077	2831	175	0.390	10.95	-3.68
C320	349,945	5957	301	0.519	10.89	-3.65

Table 4.14 Asphalt bitumen properties at various temperatures (RTFOT)

t (°C)	Viscosity at temperature – Pa.s				A	VTS
	25	45	60	135		
C170	386,367	5598	310	n/a	11.88	-4.01
C320	762,079	11298	595	n/a	11.49	-3.86

The master curves were modelled using the sigmoidal functions as expressed in Equation 3-6 and 3-11 (Section 3.5.6). The sigmoidal models are used in MEPDG 2004 and are quite popular for generating a smooth master curve. Some coefficients had to be determined in order to run the function, namely α, β, δ, γ and c. The sigmoidal functions were used to justify the stiffness of asphalt mixtures under low and high temperature. Table 4.15 and 4.17 show all of the sigmoidal function parameters obtained for the original binder and RTFOT binder.

Table 4.15 Sigmoidal function coefficients for $|E^*|$ master curve (AASHTO 2010b)

Mix	Air void	E_{max}	δ	β	γ	ΔE_a	R^2	S_e/S_y
AC10-170	3%	3.52	0.44	-0.88	-0.64	180144	0.99	0.11
	5%	3.51	0.43	-0.88	-0.67	182009	0.98	0.15
	7%	3.49	0.47	-0.65	-0.70	176370	0.95	0.24
AC10-320	4%	3.52	0.52	-1.06	-0.68	189092	1.00	0.03
	5%	3.51	0.47	-1.00	-0.71	177203	0.96	0.13
	7%	3.49	0.52	-0.79	-0.71	176876	0.93	0.19
AC14-320	5%	3.52	0.49	-1.44	-0.72	184042	0.99	0.12
	6%	3.51	0.30	-1.28	-0.65	185526	0.99	0.13
	7%	3.50	0.10	-1.22	-0.60	184082	0.98	0.15
AC20-320	4%	3.53	0.49	-1.44	-0.69	188052	0.99	0.10
	5%	3.52	0.20	-1.40	-0.64	179637	0.99	0.13
	6%	3.52	0.32	-1.27	-0.64	182881	0.99	0.13
	7%	3.51	0.24	-1.15	-0.62	182040	0.99	0.12
AC20-320 BC	3%	3.53	0.66	-1.24	-0.72	177777	0.98	0.14
	4%	3.52	0.34	-1.22	-0.65	181805	0.98	0.14
	5%	3.51	0.05	-1.30	-0.61	186952	0.99	0.12

The coefficients were determined using Eq. 3-6

Table 4.16 Sigmoidal function coefficients for |*E**| master curve for original binder (AASHTO 2010b)

Mix	Air void	α	β	δ	γ	c	R^2	S_e/S_y
AC10-170	3%	2.96	-1.02	0.45	-0.69	0.98	0.99	0.06
	5%	2.87	-1.05	0.49	-0.77	1.13	0.99	0.09
	7%	2.69	-0.89	0.57	-0.87	1.07	0.97	0.18
AC10-320	4%	2.93	-1.19	0.51	-0.71	1.16	0.99	0.07
	5%	2.86	-1.18	0.53	-0.79	1.07	0.99	0.09
	7%	2.84	-0.93	0.54	-0.78	1.05	0.96	0.14
AC14-320	5%	3.06	-1.55	0.42	-0.70	1.17	0.99	0.07
	6%	3.20	-1.41	0.25	-0.65	1.17	0.99	0.09
	7%	3.13	-1.42	0.23	-0.69	1.13	0.99	0.10
AC20-320	4%	3.07	-1.56	0.42	-0.69	1.18	0.99	0.09
	5%	3.29	-1.54	0.16	-0.66	1.12	0.99	0.08
	6%	3.10	-1.43	0.33	-0.68	1.13	0.99	0.10
	7%	3.03	-1.34	0.34	-0.71	1.11	0.99	0.08
AC20-320 BC	3%	2.95	-1.32	0.56	-0.69	1.10	0.99	0.09
	4%	3.32	-1.31	0.18	-0.62	1.13	0.99	0.10
	5%	3.33	-1.47	0.08	-0.65	1.16	0.99	0.10

The coefficients were determined using Eq. 3-11

Table 4.17 Sigmoidal function coefficients for |*E**| master curve for RTFOT binder (AASHTO 2010b)

Mix	Air void	α	β	δ	γ	c	R^2	S_e/S_y
AC10-170	3%	2.96	-1.03	0.45	-0.69	0.98	1.00	0.06
	5%	2.87	-1.07	0.48	-0.77	0.98	0.99	0.09
	7%	2.69	-0.90	0.57	-0.87	0.93	0.97	0.17
AC10-320	4%	2.92	-1.20	0.50	-0.71	1.04	1.00	0.03
	5%	2.85	-1.18	0.52	-0.79	0.97	0.98	0.09
	7%	2.83	-0.93	0.53	-0.78	0.95	0.96	0.13
AC14-320	5%	3.06	-1.56	0.41	-0.70	1.06	1.00	0.07
	6%	3.20	-1.42	0.24	-0.65	1.05	0.99	0.09
	7%	3.13	-1.43	0.22	-0.69	1.02	0.99	0.10
AC20-320	4%	3.07	-1.57	0.41	-0.69	1.07	0.99	0.09
	5%	3.29	-1.56	0.15	-0.66	1.01	0.99	0.08
	6%	3.10	-1.44	0.33	-0.68	1.02	0.99	0.10
	7%	3.03	-1.35	0.34	-0.71	1.00	0.99	0.08
AC20-320 BC	3%	2.95	-1.33	0.55	-0.69	0.99	0.99	0.09
	4%	3.31	-1.32	0.18	-0.61	1.04	0.99	0.09
	5%	3.33	-1.48	0.07	-0.65	1.05	0.99	0.10

The coefficients were determined using Eq. 3-11

4.3.4.3 Evaluation of factors influencing measured /*E**/ values

The effect of air voids on dynamic modulus values

Master curves were generated from three samples at each target air void content. Figure 4.8 and 4.9 show the master curves with a reference temperature of 20°C for two types of asphalt (Class 170 and Class 320) at various air void contents (3–7%). In general, it can be seen that increasing the air voids led to a decrease in the dynamic modulus value at different frequencies for both mixtures. Increasing the air voids by 2% for each mix decreases the dynamic modulus values gradually. Similar findings have been confirmed in other studies (Mohammad et al. 2007, Singh et al. 2011). Air void content in an asphalt mixture considerably changes the dynamic modulus /*E**/ because the voids determine the volumetric properties and the bitumen content. The effects of air void changes were inconsistent for the AC10-170 mix. At low temperatures, the /*E**/ master curves of mixes with 3% and 7% air voids showed little overlap. The small overlap of /*E**/ was also observed between mixes with 5% and 7% at high temperature. The higher the temperature the more softer the bitumen and the greater the effect of the air voids that could be distinguished. However, there was no significant effect observed at low temperatures because the asphalt state was elastic. Both mixes (C170 and C320) show similar patterns in the effect of the air voids on the dynamic modulus.

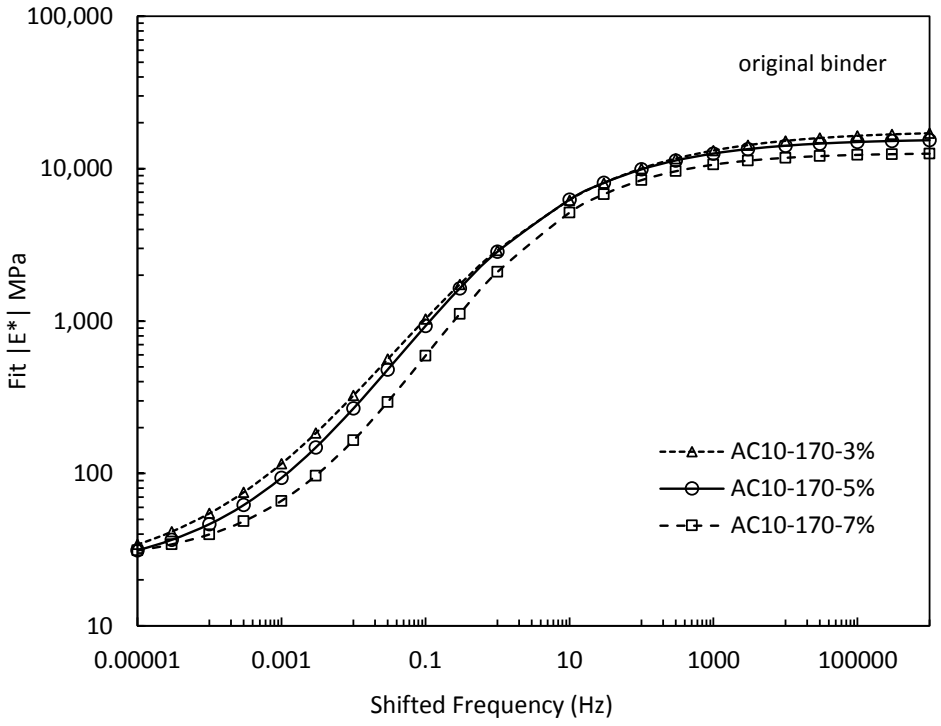

Figure 4.8 Effect of air voids on dynamic modulus for mix AC-170

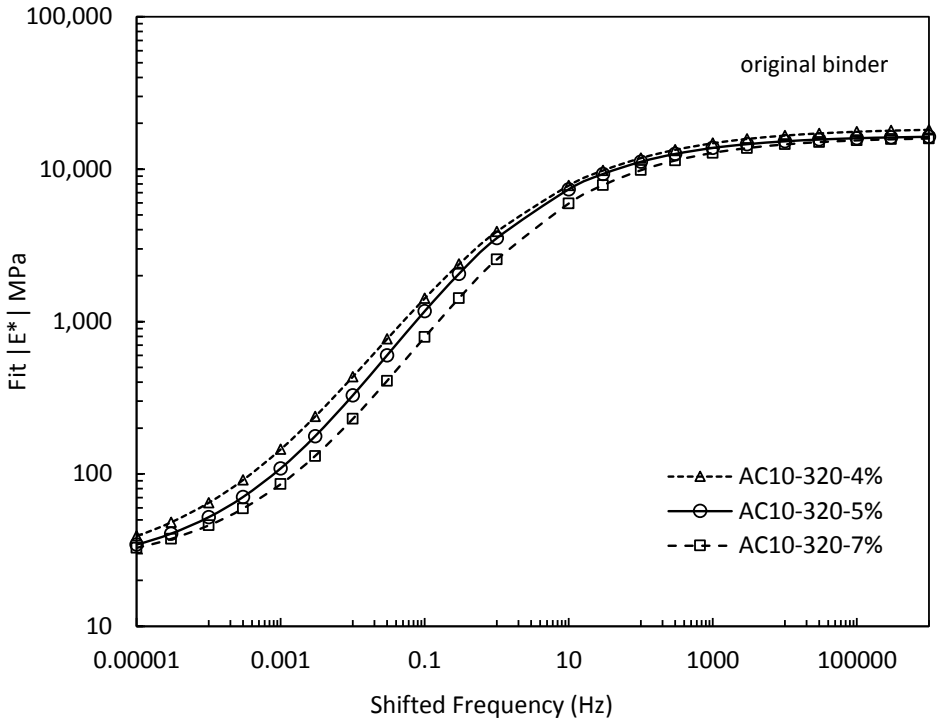

Figure 4.9 Effect of air voids on dynamic modulus for mix AC10-320

Effect of nominal maximum aggregate size on |E| master curve*

Three maximum aggregate sizes were used in the asphalt mixtures for this research, namely 10 mm, 14 mm and 20 mm. As a general hypothesis, the dynamic modulus increases with the maximum size of the aggregates. Mixtures with a maximum aggregate size of 10 mm showed a lower dynamic modulus. The increase in dynamic modulus is due to a stronger stone-to-stone contact between the aggregate particles (aggregate interlock) in mixtures with larger aggregates (Mohammad et al. 2007). This can certainly increase the overall stiffness of asphalt mixtures. Figure 4.10 and Figure 4.11 show that there is a discrepancy between the dynamic modulus for the AC14 and AC20 mixes with 5% air voids and similar mixes with 7% air voids. The general hypothesis regarding an increase of |*E**| with an increase in aggregate size was only applicable for mixes with 7% air voids. Interestingly, the AC14-320 mix with 5% air voids displayed the highest dynamic modulus. Although the difference is not significant, the discrepancy still contributes to the |*E**|. The discrepancy could be due to the finer gradation of the AC14 mixes with 5% air voids or the variability of specimens produced in this research.

The effect of binder type on |E| master curve*

Binder type certainly has an effect on the dynamic modulus of asphalt mixtures. In general, mixtures with Class 170 asphalt grade show a lower dynamic modulus than mixtures using Class 320. It can be seen from Figure 4.10**Error! Reference source not found.** and Figure 4.11 that the mixes using Class 170 asphalt had the lowest dynamic modulus of all variations (aggregate size, air voids and binder condition). As discussed in section 2.5.2, the binder type influences the stiffness and deformation properties of asphalt mixtures. Austroads (2006a) has specified that bitumen Class 170 should be used for low traffic applications and cool climate zones.

The effect of binder conditioning on |E| master curve*

Figure 4.10 and Figure 4.11 display the comparison between original (un-aged) and RTFOT (aged) binder for all mixtures with 5% air voids. It can be seen that aging had quite a significant impact on the dynamic modulus |*E**| at all air void levels. The |*E**| was higher for all RTFOT mixtures. The oxidation process resulting from aging increases the asphalt stiffness due to the increased amount of asphalthenes that can form solid structures in the asphalt binder (Liu et al. 1998a, 1998b). As discussed in section 2.5.2, aging also causes a decrease in asphalt stiffness in the long term and makes the pavement more prone to fatigue cracking. The increase in |*E**| caused by aging and dependent upon the aggregate and air void content has been studied by Singh, Zaman and Commuri (2012b) for recycled aggregate pavement. Gomez, Quintana, and Lizcano (2013) confirmed that aging increases the complex modulus of normal binder. It was noticed that the mixtures with high air void content aged more when compared to mixes with lower air void content. The effect of air voids in aggregates is to allow free circulation of air inside the specimen, which causes more hardening and changes the stiffness of the binder. Although there is no obvious difference between RTFOT-aged mixes with 5% and 7% air voids in this study, the effect of aging on the dynamic modulus |*E**| of the binders is acknowledged.

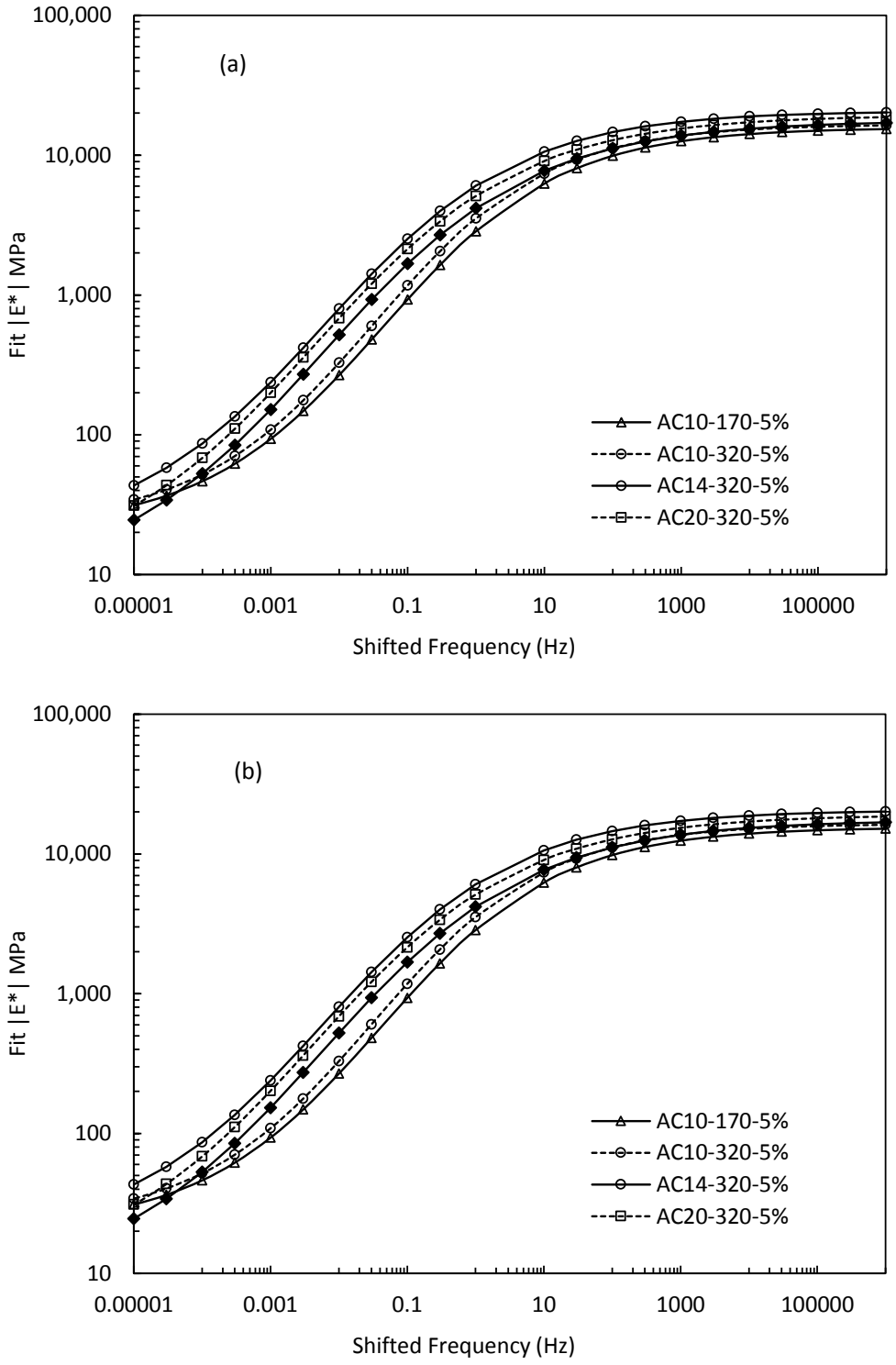

Figure 4.10 Effect of maximum aggregate size, binder type and binder conditioning on dynamic modulus for 5% air voids mixtures a) Original binder, b) RTFOT binder

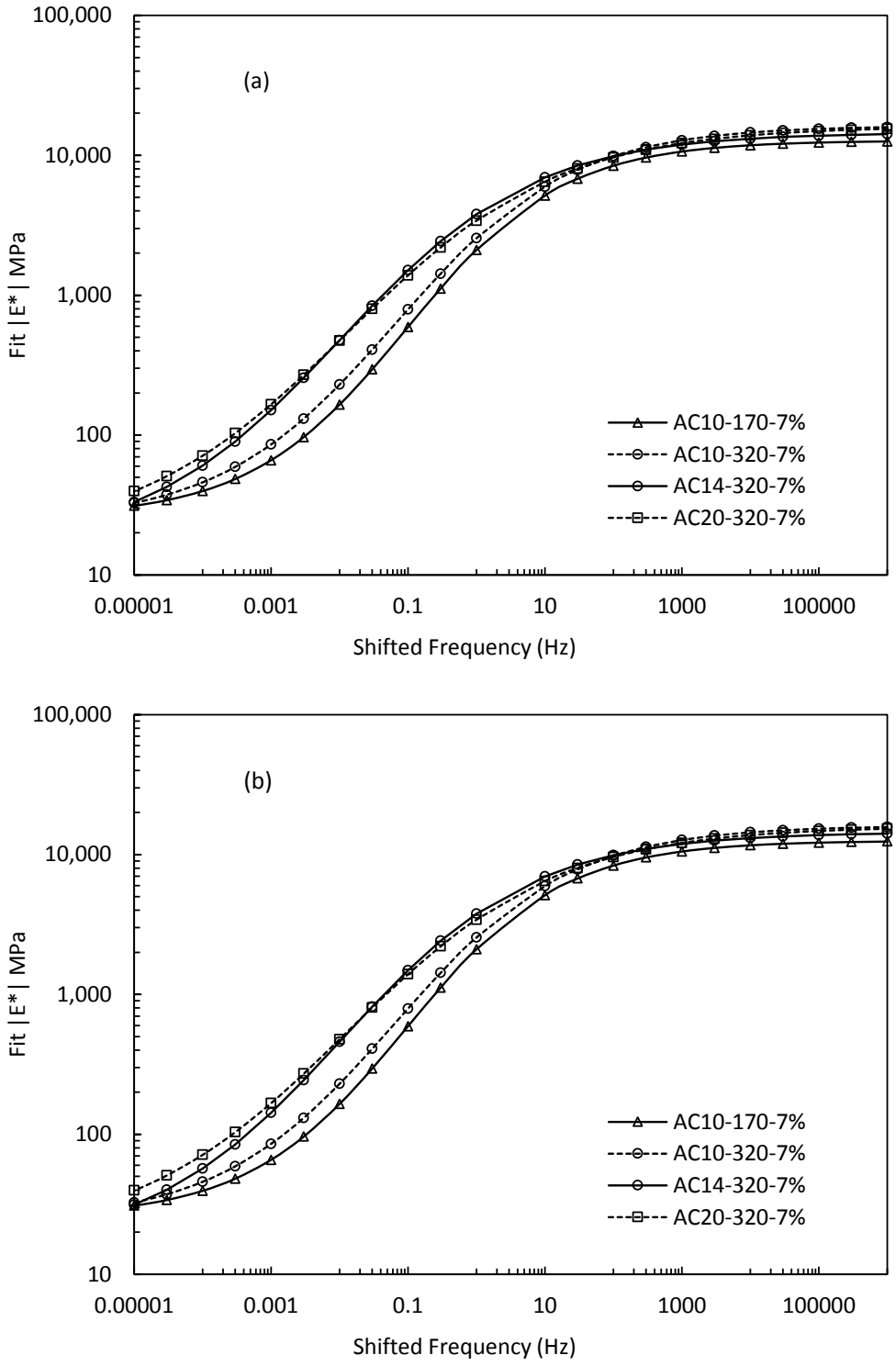

Figure 4.11 Effect of maximum size, aggregate binder type and binder conditioning on dynamic modulus for 7% air voids mixtures a) Original binder, b) RTFOT binder

4.3.4.4 Phase angle and black space

Phase angle

The phase angle indicates the dominant component of the elastic and viscous properties of the asphalt mixture. Figure 4.13 and Figure 4.14 Black space diagram for all mixtures show the measured phase angle for mixtures with an air void content of 5% and 7%, respectively. The data shows a smooth trend, especially at frequencies higher than 0.01Hz. It can be seen that the phase angle increased with the increase in frequency, reached a peak (breakpoint) and then decreased. The phase angle slope increased from 15° to just under 45° at 0.01Hz. In this state, the material was viscoelastic, and typical asphalt mixtures are viscoelastic when the phase angles fall between 5° and 45° (Biligiri, Kaloush, and Uzan 2010). From the figure it can also be seen that, after the breakpoint, the phase angle decreased to 5° at a loading frequency of 10,000Hz. The material is elastic. A previous study has confirmed that the material is linear viscoelastic at low frequencies of less 0.1Hz, while at higher frequencies the mix acts as a granular nonlinear elastic material (Christensen 1998).

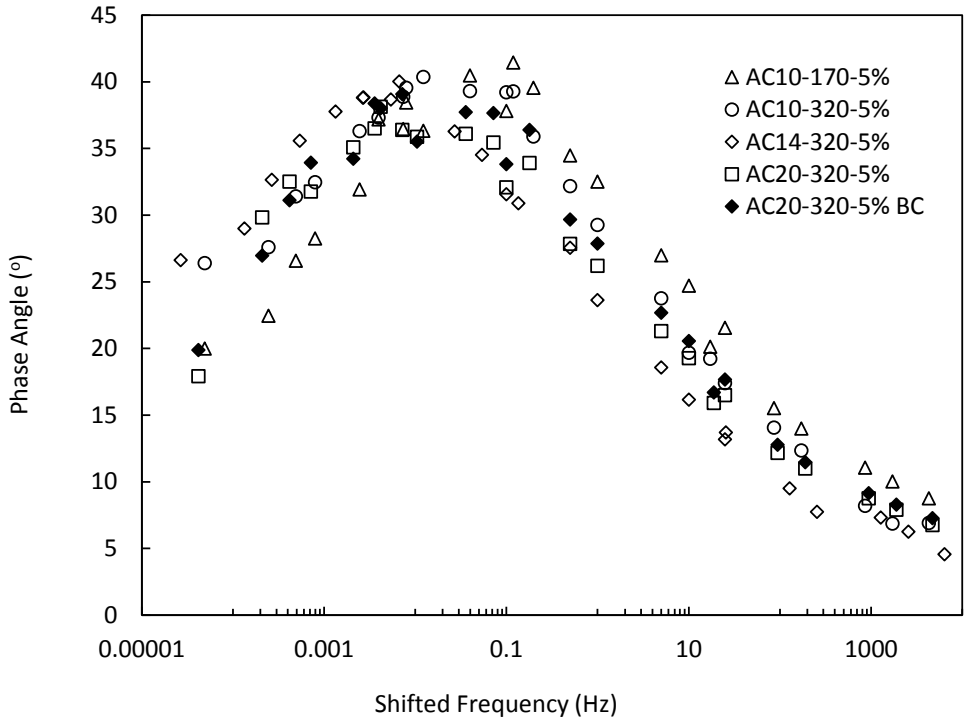

Figure 4.12 Measured phase angle master curves for 5% air void content

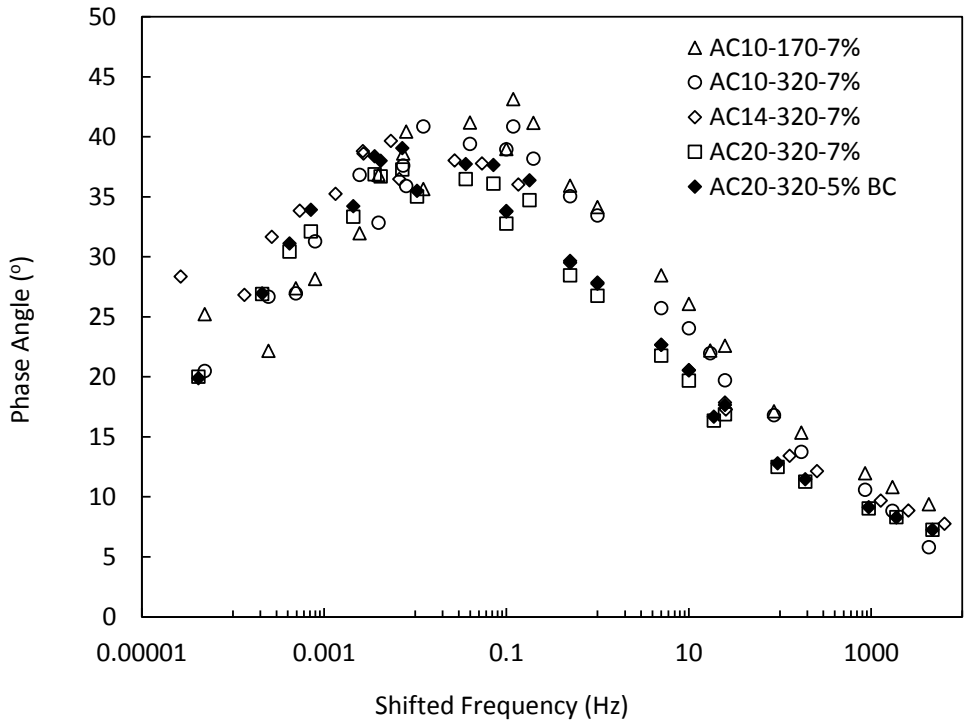

Figure 4.13 Measured phase angle master curves for 7% air void content

In general, the phase angles for both with mixes 5% and 7% air voids followed a relatively similar pattern. The AC10-170 mix exhibited a higher phase angle than the other mixes for frequencies of more than 0.1Hz, implying that the effect of aggregate size was to significantly decrease the resistance of the mixtures. In this state, the viscosity of asphalt is more dominant than the effect of aggregate. Mixes containing an asphalt grade of C320 showed a higher phase angle before reaching a peak, and a lower phase angle after the peak. However, when mixtures containing AC10-320 asphalt were compared after changing the phase angle slope at 0.01Hz, the phase angles were considerably lower than for the AC10-170 mixtures. This is because the asphalt binder mainly governs the phase angle at high frequency. At low frequencies, the AC10-320 mix had a lower phase angle than the AC14-320 and AC20-320 mixes. Aggregate size has more dominant effect on phase angle; hence the viscous state of the asphalt is overpowered by the mechanical response of the aggregate skeleton at low frequency (Pellinen and Witzcak 2002). It is interesting to note that soon after the breakpoint had been achieved, the AC10-320 mix showed a higher phase angle than the other two mixes. The asphalt viscosity seems to be more dominant in this state.

Black space

Figure 4.14 displays the black space diagram for all of the mixtures. This diagram is plotted from the average values of the /*E**/ and phase angle for each set of laboratory data. The black space plot is used to identify testing variability, nonlinearity or both in the behaviour of the material (Pellinen 2001). The diagram indicates that either nonlinearity or measurement error was occurring at the intermediate-to-higher test temperatures for the 9.5 mm mix. Intermediate and higher test temperatures were represented toward the middle and left side of the curves, respectively. In this study, variability in phase angle was slightly greater at lower frequencies and higher temperatures.

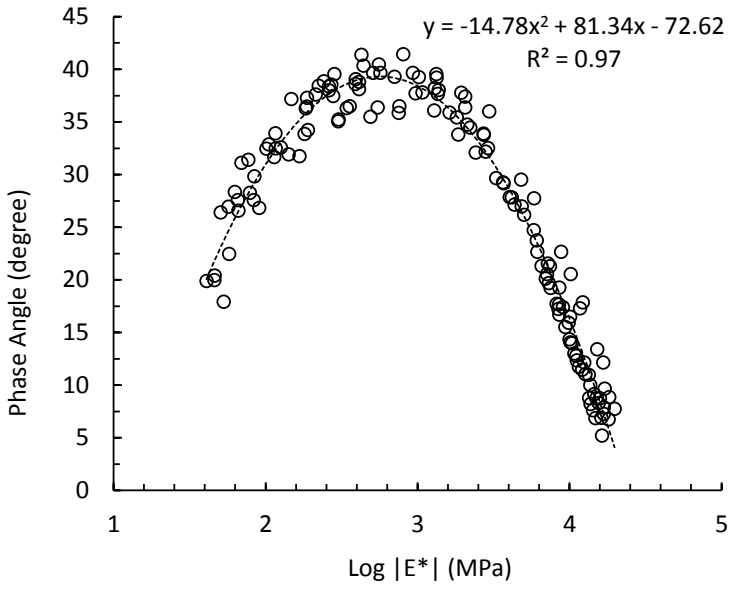

Figure 4.14 Black space diagram for all mixtures

4.3.4.5 Comparison of predicted and measured dynamic modulus master curve

This section presents the dynamic modulus master curve for the mixtures investigated in this research. The information reported includes the dynamic modulus master curve for each air void variation and dynamic modulus predictive model. As discussed in section 2.4.2, MEPDG 2004 employs three levels of design. In the second and third levels, the dynamic modulus values can be determined from predictive equations using the input parameters from material specifications. In this research, the /*E**/ master curves of the Witczak and Hirsch models were used and compared with the laboratory /*E**/ master curve.

Comparison with MEPDG Witczak's predictive model

Figure 4.15 to Figure 4.18 show the master curves plotted for the AC-170, AC10-320, AC14-320 and AC20-320 mixes respectively. In general, it can be seen that the laboratory master curves were clustered together. It was observed that the dynamic modulus values of mixes with lower air void content were slightly higher than those with higher air void content. The effect of air voids on the dynamic modulus was discussed in section 4.3.4.3.

The dynamic modulus showed that loading frequency and test temperature dictate the performance of the asphalt mixtures. Mixes become stiffer at the lowest temperature and highest frequency, but the mixes have the lowest /*E**/ at highest temperature and lowest frequency. It was noted that in all figures, in the upper region where the stiffness is calculated from the lower temperature, the master curves tended to be smaller than the Witczak predictive /*E**/ master curve. At an intermediate temperature, the master curves overlapped with the predictive model, except for the AC10-170 and AC10-320 mixes (original and RTFOT aged). Those mixes were assumed to be slightly stiffer at that temperature than shown in the predictive model. High levels of discrepancy and divergence in the master curve were observed at high temperature. The predictive and laboratory measured /*E**/ for all mixtures were not in good agreement, particularly for the aged RTFOT binder.

In Figures 4.15 to 4.18 it can be seen that the master curves clustered together at low temperatures and diverged at intermediate and higher temperatures. The Witczak predicted /*E**/ values were generally comparatively higher at high temperatures and slightly lower at low temperatures. The Witczak predictive model had an /*E**/ master curve higher than those of Western Australian asphalt mixtures at the intermediate and higher test temperatures. The discrepancy at high temperature and low frequency region were also reported in many studies. The Witczak's model tends to overemphasize the influence of high and very low temperatures on dynamic modulus |E*| (Lee et al. 2007, Ceylan et al. 2009, Apeagyei and Diefenderfer 2011). This is because the inability of the model to characterize performance of various mixtures with different aggregate and asphalt properties than the US specifications at high temperature (Schwartz 2005).

In one study to predict dynamic modulus of typical Australian asphalt mixtures, Yousefdoost et al. (2013) compared four different models, namely Witczak 1999, Witczak 2006, Hirsch and Al Khateeb. The models were not supported the measured dynamic modulus and it was suggested to modify the models accordingly based on the properties of the origin materials.

The binder type, aging condition, aggregate size, type and gradation, shear modulus and dynamic modulus set up (equipment, temperature and loading rate), specimen size, mix design, compaction method, and volumetric properties are some factors that responsible to the divergence of |E*| at high temperature. A research conducted for Western Australia dynamic modulus prediction, also revealed that the Witczak model as overestimated the values, particularly at high temperatures. The model are lined above the experimental curve for all temperature variations (Kumlai et al. 2014).

In this research, the effect of aggregate gradation could be one reason of the discrepancy of dynamic modulus |E*| at high temperatures. Aggregate used, i.e. granite, based on MRWA specification has different properties to the aggregate used in the US specification. Besides, at high temperatures, the asphalt mixture is more dependent on the aggregate structure. The binder changes its state of viscosity, becomes more elastic and does not hold the aggregate particles together. At this stage, the shape and angularity of aggregates are important to ensure interlocking and friction among particles to maintain the structure stability. At low temperatures, the binder is more viscous and the aggregate particles are immobilized to produce better dynamic modulus (Singh, et al. 2012c).

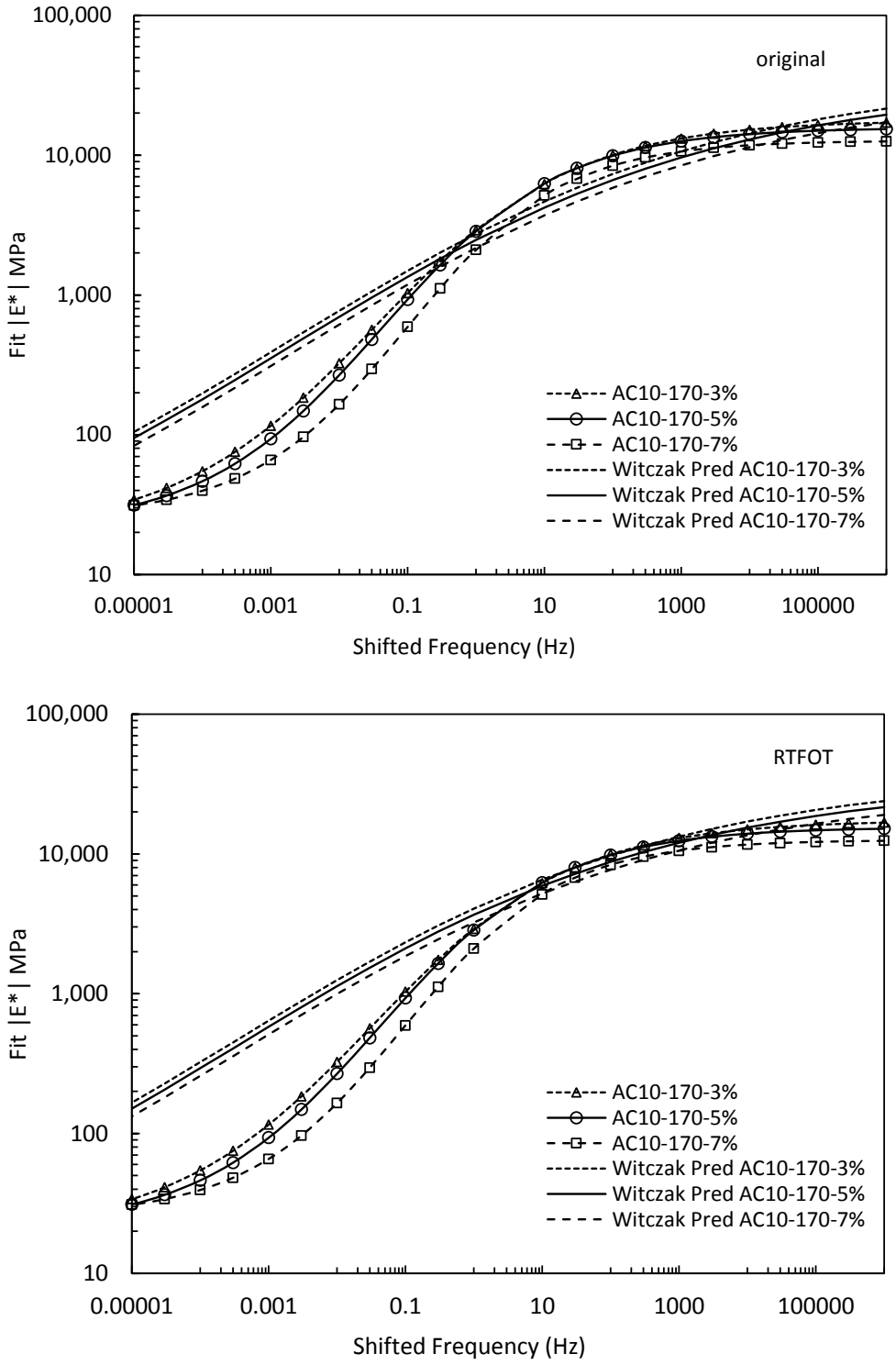

Figure 4.15 Comparison of developed master curves with Witczak's predictive equation for mixes AC10-170

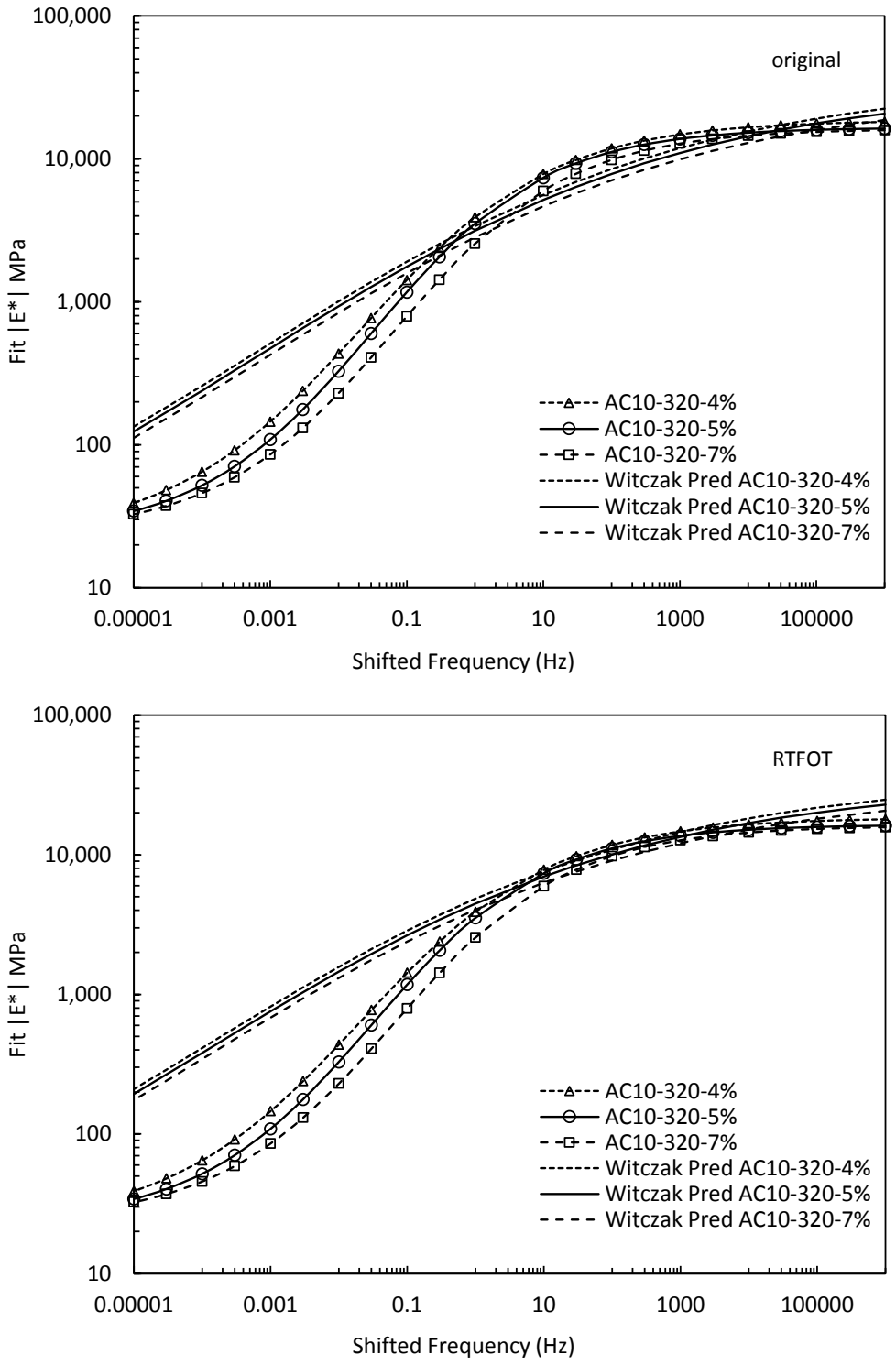

Figure 4.16 Comparison of developed master curves with Witczak's predictive equation for mixes AC10-320

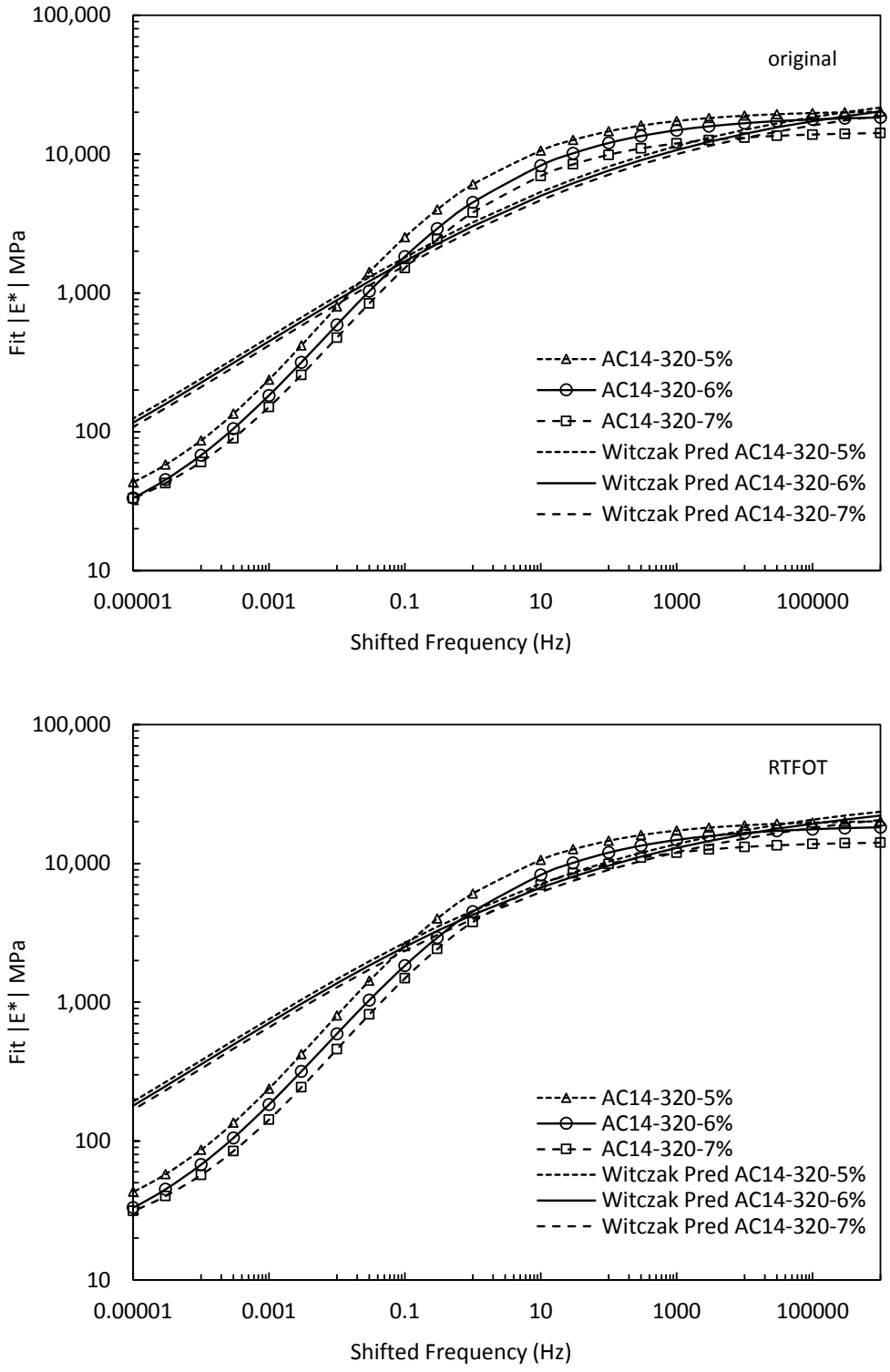

Figure 4.17 Comparison of developed master curves with Witczak's predictive equation for mixes AC14-320

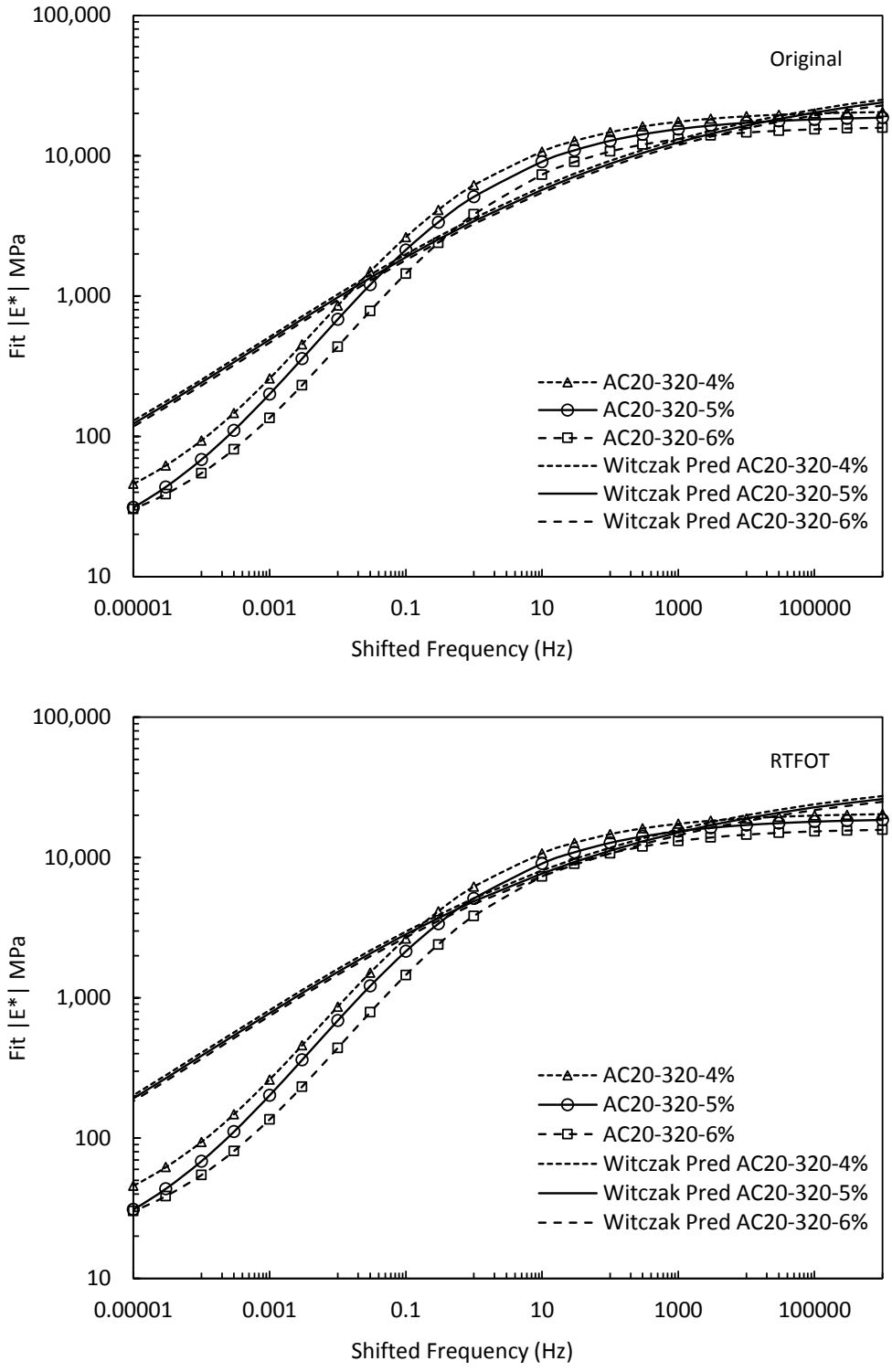

Figure 4.18 Comparison of developed master curves with Witczak's predictive equation for mixes AC20-320

Comparison with MEPDG Hirsch's predictive model

Figure 4.19 to Figure 4.22 show the plotted master curves for all mixes with the Hirsch predictive model. There was a discrepancy between the lower temperature and higher temperature for all mixtures. At low temperature, the |*E**| master curves for mixes AC10-170 and AC10-320 were lower than |*E**| master curve for Hirsch model. A higher gap on the comparison was observed for mix AC10-320. The asphalt performance became interesting at intermediate temperature. All mixes showed a considerable discrepancy of |*E**| with the predictive model, except mix AC10-170 and AC10-320 aged RTFOT binder which were nearly overlap with the model. However, at high temperature, all mixes tend to have a large discrepancy with the predictive model.

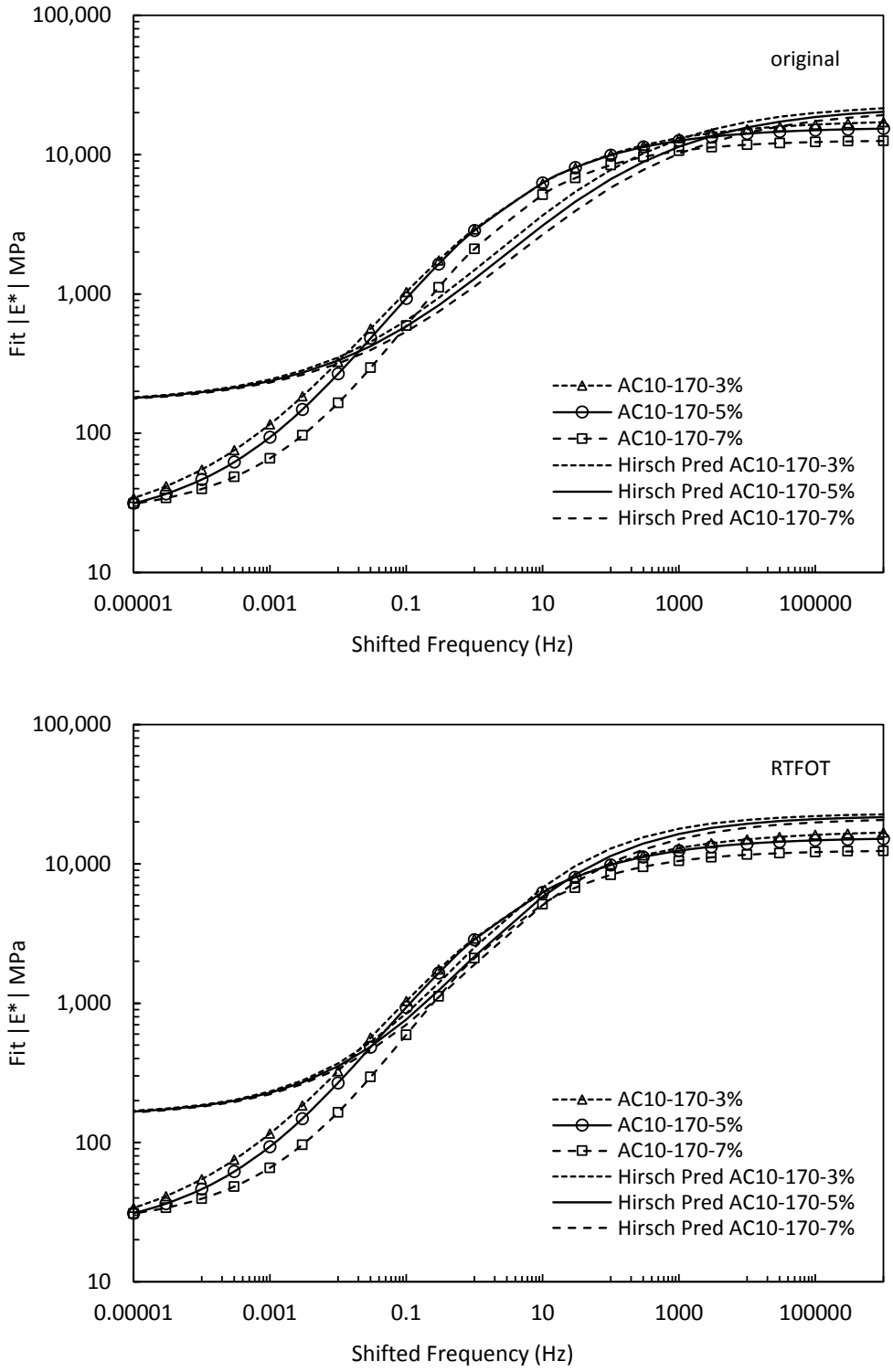

Figure 4.19 Comparison of developed master curves with Hirsch's predictive equation for mixes AC10-170

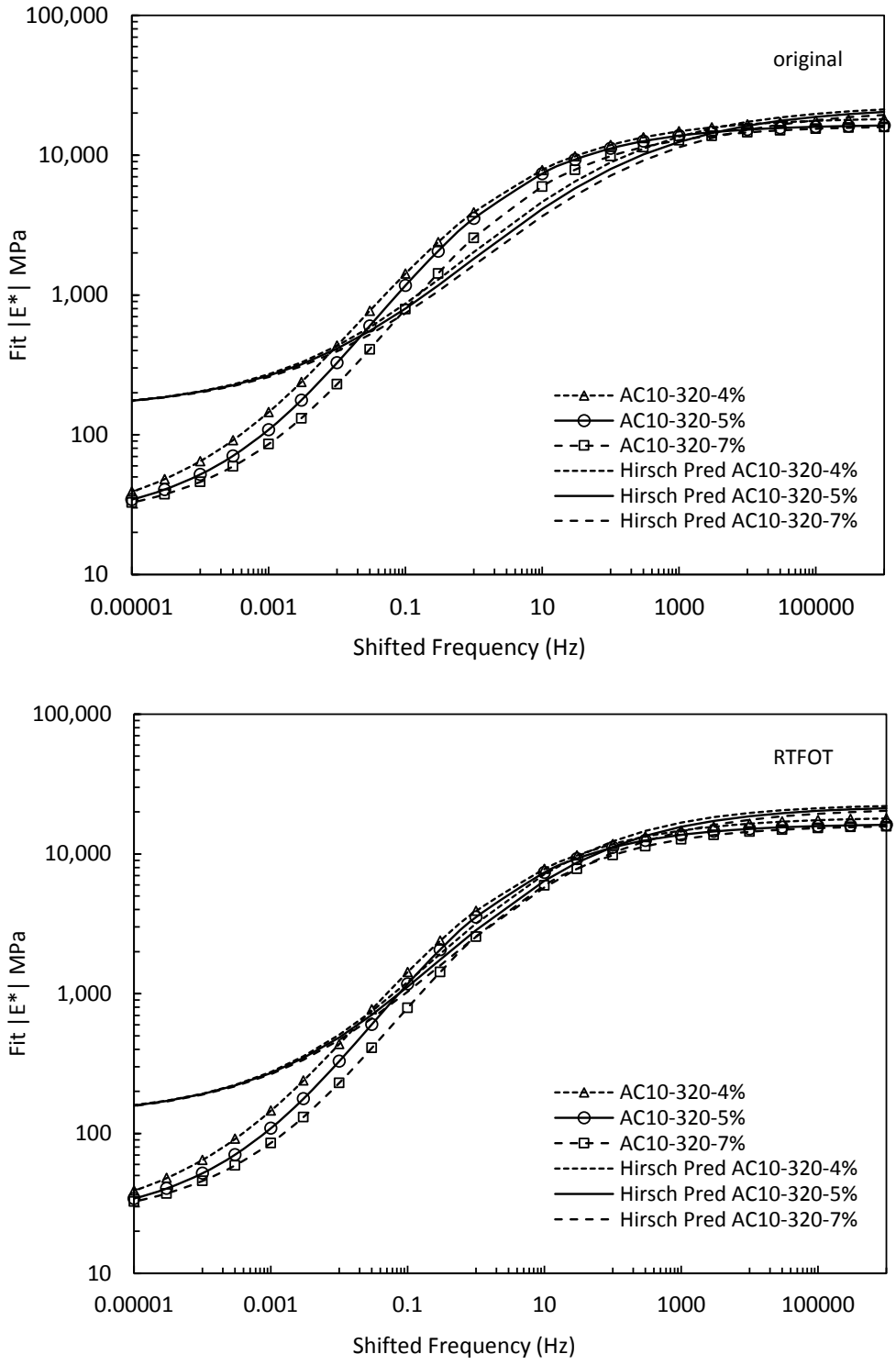

Figure 4.20 Comparison of developed master curves with Hirsch's predictive equation for mixes AC10-320

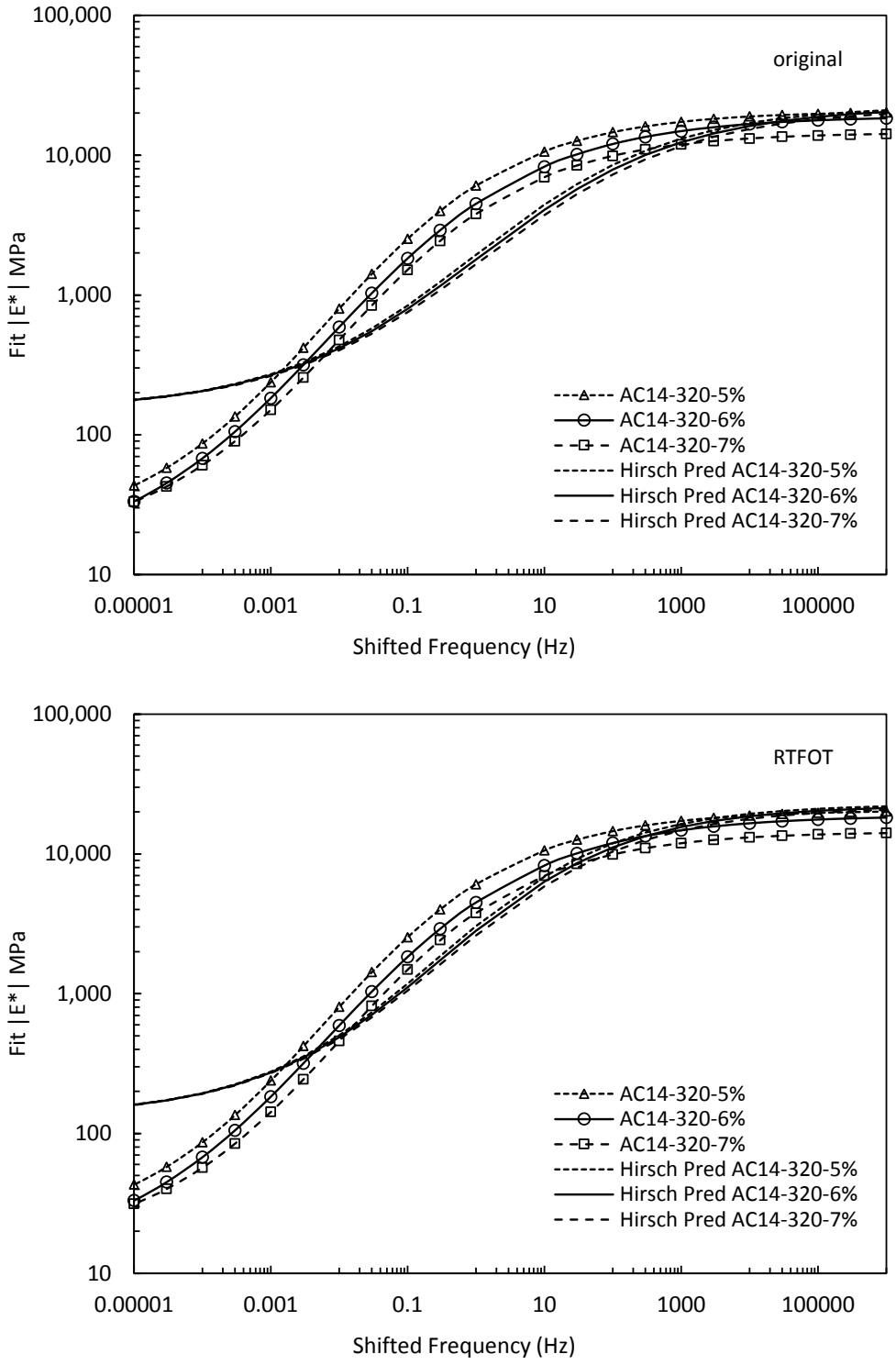

Figure 4.21 Comparison of developed master curves with Hirsch's predictive equation for mixes AC14-320

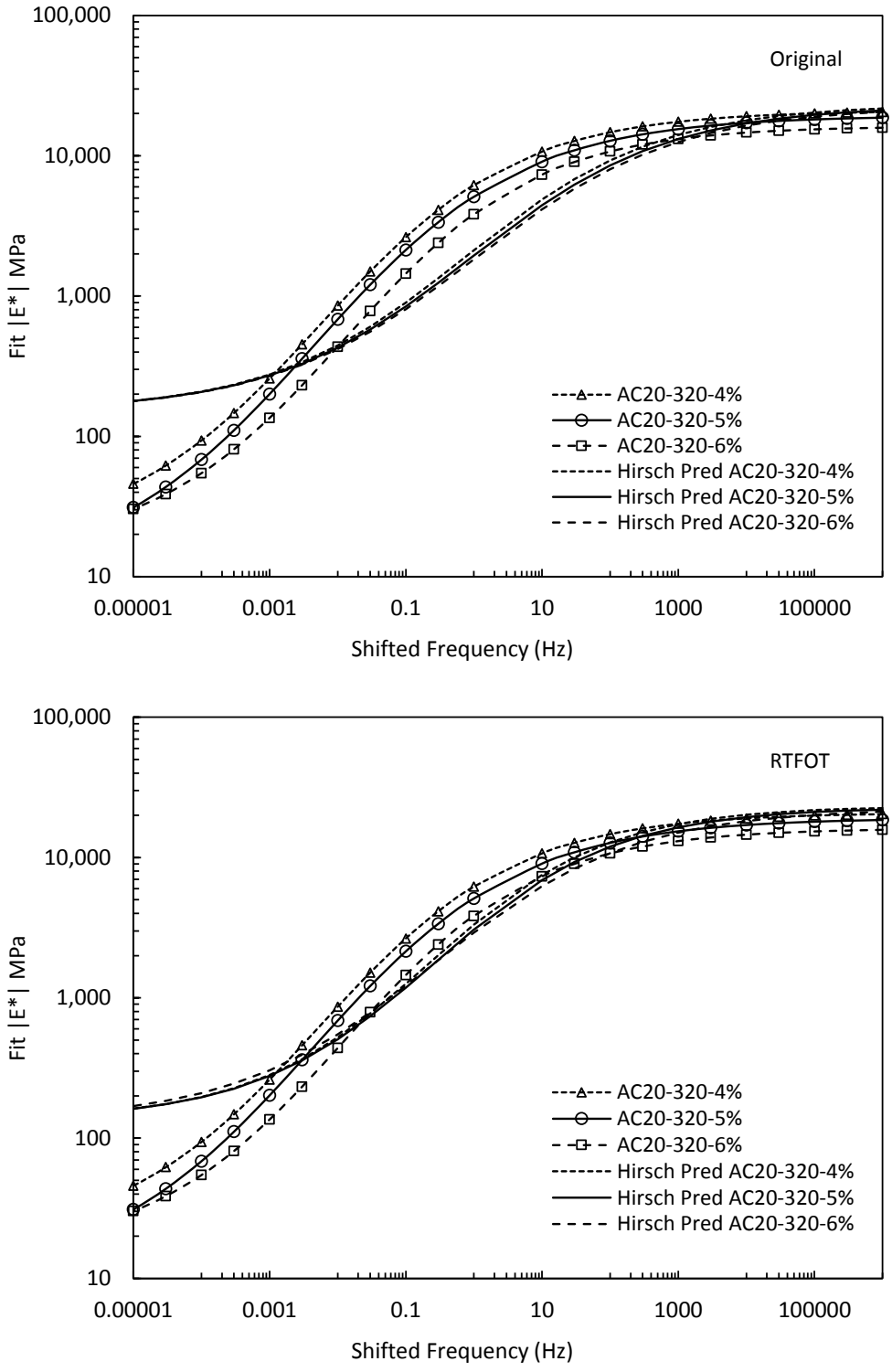

Figure 4.22 Comparison of developed master curves with Hirsch's predictive equation for mixes AC20-320

4.3.4.6 Statistical analysis of predicted and measured values of dynamic modulus

The Witczak predictive equation and the Hirsch model were employed to calculate the predictive values of the dynamic modulus for the Western Australian asphalt mixture. The comparison was established by plotting both predicted and measured values of the dynamic modulus on the same graph. A good correlation between the matching points is obtained when the points are distributed around the equity line, as discussed in section 2.5.4.4. In this section the bias and precision of the predicted and measured values will be analysed by statistical means and discussed.

Validation of Witczak Model Predicted E data with laboratory E* data*

Figure 4.23 presents a comparison of the predicted dynamic modulus using the Witczak equation and the measured dynamic modulus of all mixes for the original and RTFOT-aged binder. Overall, there is a good correlation with a coefficient of correlation (R^2) greater than 0.90 between the predicted and measured $|E^*|$, except for the AC14-320 mix. The discrepancy is quite distinct. It can be observed that the predicted values were lower than the measured values between low and intermediate temperatures, which contributed to the lower R^2 value for this particular mix. Other mixes consistently showed slightly higher predicted dynamic modulus values at high temperatures and slightly lower values at low temperatures than the measured $|E^*|$. The predicted values were also higher than the measured values with the variation of nominal maximum aggregate size and binder type.

There are some potential reasons for the discrepancies in the model. The Witczak predictive model tends to overestimate dynamic modulus $|E^*|$ at high temperatures (Schwartz 2005). At high temperatures, the model is insensitive to various asphalt mixtures, because at high temperatures the asphalt performance depends largely on the aggregate structure (Harran and Shalaby 2009). Instead of differences in the applied micro strain level in $|E^*|$ test, it is suggested that the discrepancies were mostly due to different aggregate gradations, aggregate types and asphalt sources than the United States specifications. The Witczak model was developed to simplify dynamic modulus calculation based on volumetric properties and binder grades of asphalt mixtures. The models certainly do not accommodate other material properties outside the US. A few studies have highlighted this issue and tried to modify the predictive equation to match local material conditions, such as by reconstructing the predictive equation using a nonlinear regression analysis for 540 dynamic modulus data in Korea (Cho et al. 2010). Another attempt was made to develop a model based on improvement of the material gradation by using finer-graded materials to encourage better aggregate interlock at high temperatures (Harran and Shalaby 2009). It is certainly a

challenge to modify the dynamic modulus predictive equation for use in Western Australian asphalt mixture.

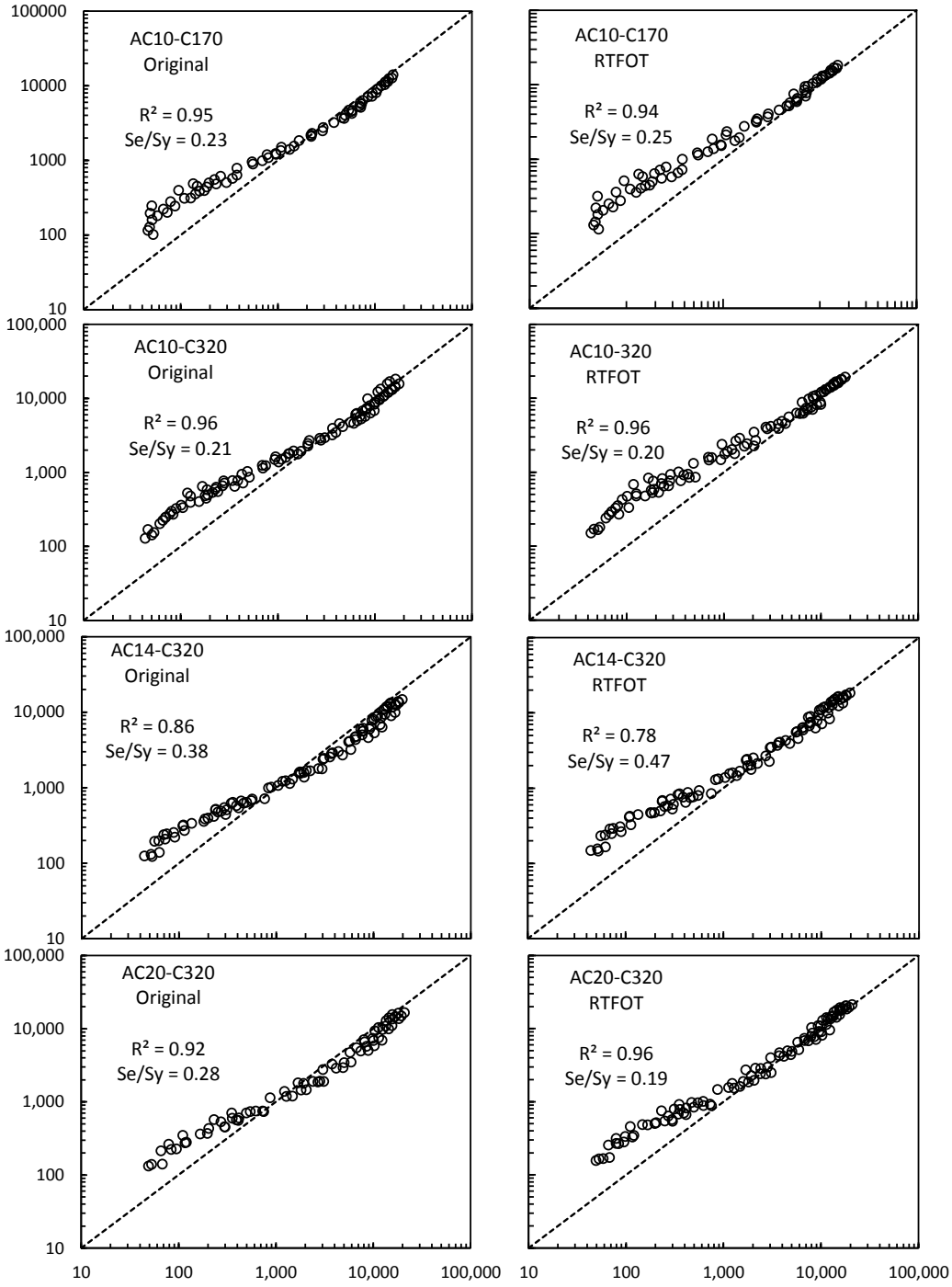

Figure 4.23 Comparison of measured and predicted dynamic modulus by Witczak equation

Modified Witczak predicted model

Based on the master curve |E*| data, a new dynamic modulus predictive model was developed. The model is a revised version of the existing Witczak predictive model by including the properties of aggregate and asphalt binder used in Western Australia. The hot mix asphalt (HMA) used is designed using Main Road WA guideline. This mix uses AC10, AC14, AC20 12.5mm dense-graded HMA with at least 75% of the coarse aggregate. The asphalt input (A and VTS) for the new model was from Table 4.13. The aggregate gradation of the Western Australia asphalt mixtures used in the modified Witczak predictive equation is presented in Table 4.18. The gradation is displayed in the form of percent retaining for 19.0 mm (P_{34}), 9.5 mm (P_{38}), and 4.75 mm (P_4) sieves. Sieve size of 0.074 mm or No. 200 (P_{200}) is given in percent passing.

Table 4.18 Input aggregate gradation for the Witczak predictive model

Mixture/ Gradation	P_{34} % retained	P_{38} % retained	P_4 % retained	P_{200} % retained	Gsb
AC10-10mm	0	1.9	36.7	5.7	2.65
AC14-14mm	0	17.4	49.0	4.5	2.65
AC20-20mm	6	42.8	61.4	4.3	2.65

Based on the regression analysis of test results, the modified predictive equation is

$$\log|E^*| = 5.924485 - 0.022472(P_{200}) - 0.003558(P_{200})^2 + 0.000383(P_4) - 0.148753(V_a) - 2.244106\left(\frac{V_{beff}}{V_{beff}+V_a}\right)$$

$$+\frac{2.981461 + 0.000603(P_4) + 0.001822(P_{38}) - 0.000045(P_{38})^2 - 0.011555(P_{34})}{1+e^{(-0.513068-0.714007\log f-0.798338\log\eta)}} \quad (4\text{-}1)$$

where

$|E^*|$ = asphalt mix dynamic modulus, 10^5 psi
η = bitumen viscosity, 10^6 poise
f = load frequency, Hz
V_a = percent air voids in the mix, by volume
V_{eff} = percent effect bitumen content, by volume
P_{34} = percent retained on 19 mm sieve, by total aggregate weight (cumulative)
P_{38} = percent retained on 9.5 mm sieve, by total aggregate weight (cumulative)
P_4 = percent retained on 4.76 mm sieve, by total aggregate weight (cumulative)
P_{200} = percent retained on 0.075 mm sieve, by total aggregate weight

The master curve obtained |E*| and the laboratory measured |E*| are presented in Figure 4.24 The new model produced master curves with improved R^2. There appears to be close agreement between the new Witczak model with master curve from Australian asphalt mixtures. These modified Witczak model predicted |E*| and the laboratory measured |E*| can

produce well-fitted results when compared to laboratory |E*| test data. Hence, for practical purposes, the modified Witczak predictive model is applicable for dynamic modulus prediction of Western Australia asphalt mixture.

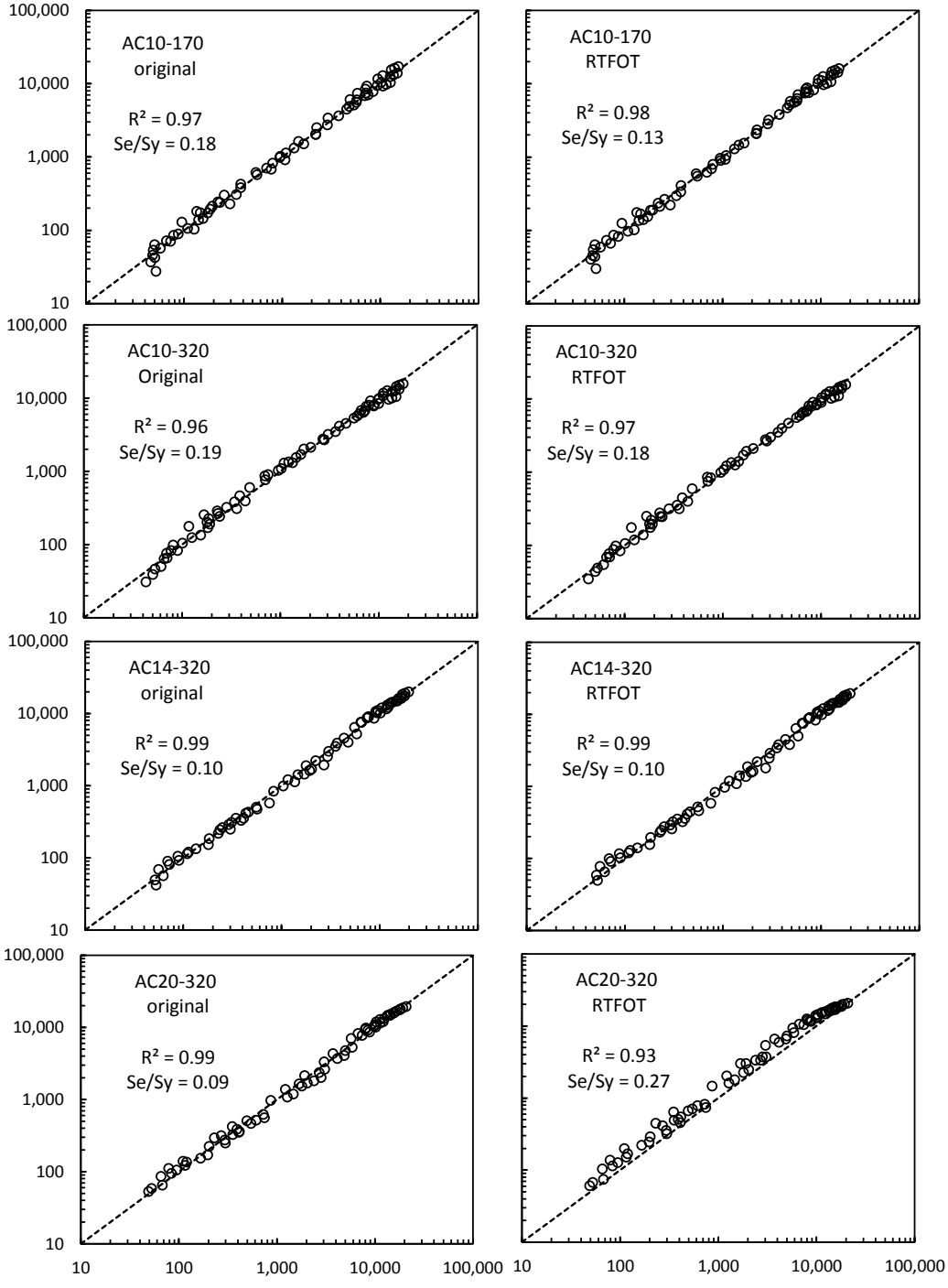

abscissa = measured /*E**/ (MPa); ordinate = modified Witczak predictive /*E**/ (MPa)

Figure 4.24 Comparison of measured and predicted dynamic modulus by modified Witczak equation

Validation of Hirsch model predicted |E| data with laboratory |E*| data*

Figure 4.25 shows the comparison of the predicted and measured |*E**| using the Hirsch model. There was generally a good correlation between the values, with an R^2 greater than 0.78. However, the R^2 from this predictive model was slightly lower than for the values calculated using the Witczak model. It is noted for all mixes calculated using original binder property, the predicted dynamic modulus values generally overlapped with the line of equity at low temperatures, fell beneath the line of equity at intermediate temperatures, and were higher than the line at high temperatures. This behaviour is fairly consistent with variations in nominal maximum aggregate size and caused a noticeable discrepancy between the predicted and measured |*E**|. By contrast, the mixes with aged RTFOT binder property showed good correlation, with R^2 in the range of 0.94–0.99. The predicted values were in agreement with the measured values for low and intermediate temperatures, but then slightly higher at high temperatures.

The Hirsch predictive model is claimed to be more accurate in estimating dynamic modulus at a broad range of values and variables than the Witczak model (Dongre et al. 2005, Obulareddy 2006). This is because of the small margin between the predicted and measured |*E**| for the asphalt mixtures. However, in this research there was a large discrepancy between the measured values and the predicted |*E**| values.

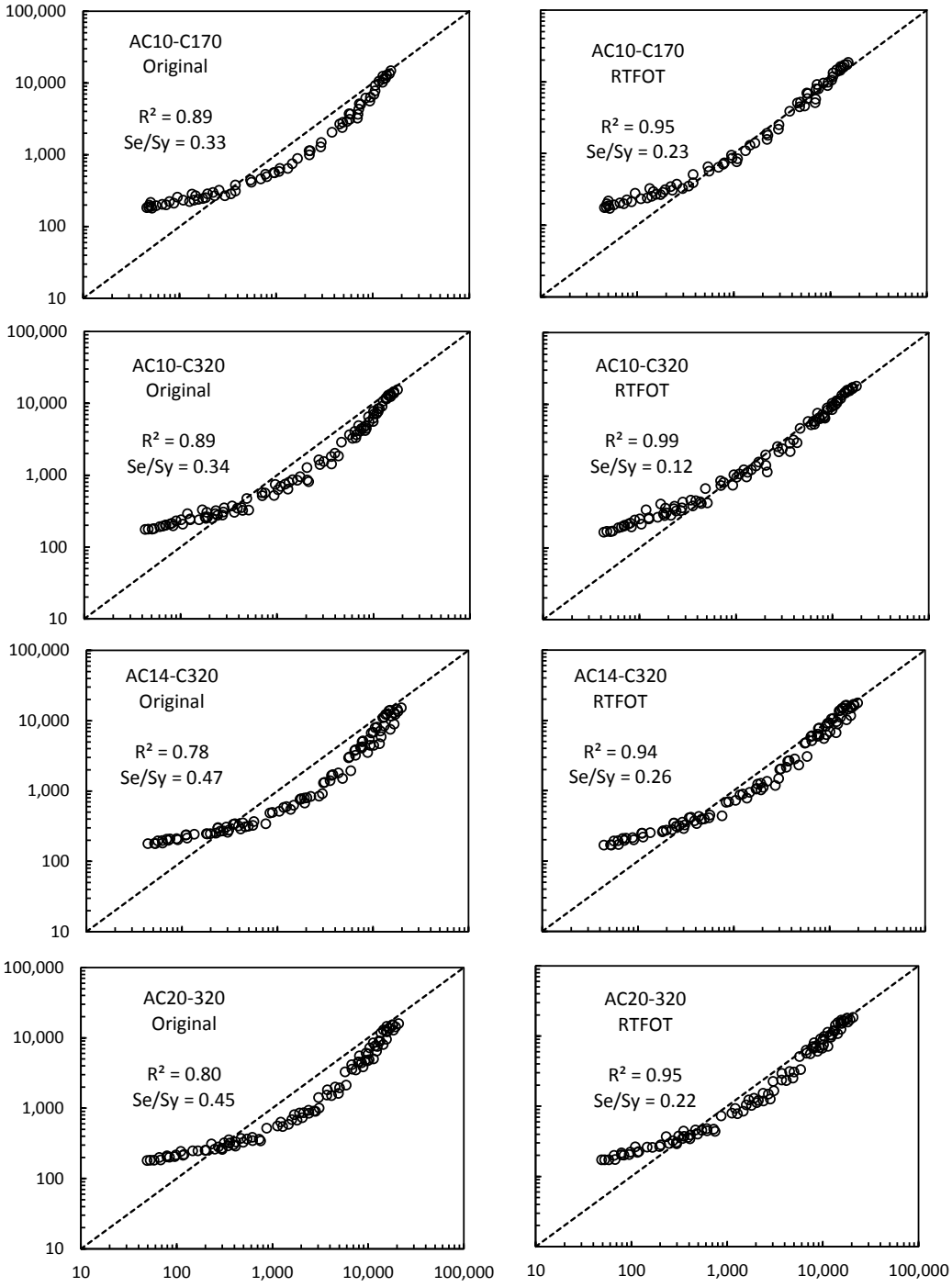

abscissa = measured /*E**/ (MPa); ordinate = Hirsch predictive /*E**/ (MPa)

Figure 4.25 Comparison of measured and predicted dynamic modulus by Hirsch equation

Statistical evaluation of Witczak and Hirsch predictive equations

The accuracy and reliability of the dynamic modulus calculated from the Witczak and Hirsch predictive models with the laboratory-measured data were evaluated using goodness-of-fit statistics criteria. The criteria were based on standard error of estimate/standard deviation (S_e/S_y) and coefficient correlation (R^2) as discussed in section 2.5.4.4. The bottom line of these criteria is that a good model has a high R^2 and a small S_e/S_y. Tables 4.18 and 4.19 present the performance analysis of Western Australian mixtures using the Witczak and Hirsch equations.

In general, it can be seen from Table 4.19 that most of the predicted dynamic moduli showed excellent correlation with the measured values. Both surface layer mixes (AC10-170 and AC10-320) showed excellent correlation with R^2 in the range of 0.94 and 0.96 and an S_e/S_y ratio of 0.20–0.25. The only good correlation was rated for the intersection mix i.e. AC14-320 (original binder), which had an R^2 of 0.86 and an S_e/S_y ratio of 0.38. It is noted that the effect of mixture aging is the dominant factor in improving the accuracy and reliability of the model. The reliability of the Witczak model decreases as the nominal maximum aggregate size increases for the original binder, while for the aged RTFOT binder, the reliability of the Witczak model tends to increase as the nominal maximum aggregate size increases.

Table 4.20 shows that the goodness-of-fit-criteria for original mixtures predicted using Hirsch's equation were 'good'. Most of the correlations (R^2) fell within the range of 0.78–0.89, with an S_e/S_y ratio of 0.33–0.47. When the values of the original mixes were compared with the RTFOT-aged binder, the effect of aging seemed to be quite significant in improving the correlation with the predictive models. The reliability of the Hirsch model tends to fluctuate as the nominal maximum aggregate size increases for the RTFOT-aged binder. Moreover, the reliability of the Hirsch model decreases as the nominal maximum aggregate size increases for the original binder.

Overall, in this research the results of the Witczak and Hirsch predictive equations fitted well with the dynamic modulus $|E^*|$ data. In comparing both models, the Witczak predictive model seemed to be more suitable than the Hirsch model for use with the dynamic modulus data for Western Australian asphalt mixtures. Many researchers have found slight discrepancies on using Witczak and Hirsch's predictive models due to the variability of material characteristics in many states inside and outside the US (Mohammad et al. 2007). However, the predictive model is still useful despite laborious efforts required to determine the aggregate volumetric properties and binder shear modulus from various mixtures as a

major input for the models, then modify and simplify the equations to suit local material conditions and modified binder specifications due to discrepancies at low, intermediate or high temperatures. These factors are discussed in detail in the literature (Cho Y-H et al. 2010, Hassan and Al-Shamsi 2010, Lee et al. 2007, Zhu et al. 2011).

Table 4.19 Performance analysis of mixtures predicted using Witczak's equation

Mixtures	R^2	S_e/S_y	Ranking
AC10-170			
Original binder	0.95	0.23	Excellent
RTFOT-aged	0.94	0.25	Excellent
AC10-320			
Original binder	0.96	0.21	Excellent
RTFOT-aged	0.96	0.20	Excellent
AC14-320			
Original	0.86	0.38	Good
RTFOT-aged	0.97	0.17	Excellent
AC20-320			
Original	0.92	0.28	Excellent
RTFOT-aged	0.96	0.19	Excellent
AC20-320 BC			
Original	0.93	0.26	Excellent
RTFOT-aged	0.98	0.14	Excellent

Table 4.20 Performance analysis of mixtures predicted using Hirsch's equation

Mixes	R^2	S_e/S_y	Ranking
AC10-170			
Original binder	0.89	0.33	Good
RTFOT-aged	0.95	0.23	Excellent
AC10-320			
Original binder	0.88	0.35	Good
RTFOT-aged	0.99	0.11	Excellent
AC14-320			
Original	0.78	0.47	Good
RTFOT-aged	0.94	0.26	Excellent
AC20-320			
Original	0.80	0.45	Good
RTFOT-aged	0.95	0.22	Excellent
AC20-320 BC			
Original	0.83	0.41	Good
RTFOT-aged	0.97	0.17	Excellent

A study on the dynamic modulus predictive models for Australian asphalt mixtures has confirmed that both the Witczak and Hirsch models had high level of biases and errors when used for predicting Australian mixtures (Yousefdoost et al. 2013). The binder properties caused limited confidence in applying the Witczak and Hirsch models directly to Australian

asphalt mixtures. Furthermore, the sensitivity analysis confirmed that the binder properties including viscosity, complex shear modulus and binder phase angle are major parameters in determining the dynamic modulus predicted values. Sullivan et al. (2013) also argued there is no need to use the Witczak and Hirsch predictive models in assessing Australian asphalt mixtures. The data can be evaluated by grouping all data statistically and determining the R^2 and S_e/S_y. This is to overcome the large variability due to variations in binder and aggregate characteristics and offers practicality for application.

Therefore, despite their limitations the Witczak and Hirsch predictive models can be used as an evaluation tool for the dynamic modulus of Western Australian asphalt mixture.

4.3.4.7 Comparison of dynamic modulus with resilient modulus

There are fundamental differences in the testing methods for dynamic modulus and resilient modulus, including loading frequency and test temperature. Despite these differences, the resilient modulus is still used in the Austroads 2008 (Austroads 2008c) to indicate the stiffness of asphalt mixture. Many researchers have investigated the relationship between the dynamic modulus and resilient modulus to find a practical means of obtaining the dynamic modulus for application purposes (Birgisson et al. 2004, Loulizi et al. 2006). This was not only done through laboratory experimentation but also through back calculation of the dynamic modulus from resilient modulus or vice versa (Lee and Kim 2011).

In this research, the resilient modulus data was calculated to adjust the frequency of the dynamic modulus data. Both values were greatly comparable and the comparison could be analysed. Figure 4.26 shows the comparison between resilient and dynamic modulus at similar loading frequencies. The linear regression analysis revealed that the dynamic modulus increased with an increase in total resilient modulus. The dynamic modulus values were quite divergent below the line of equity, but there were some matching points overlapping with the line, i.e. 3600 MPa, 4200 MPa and 5200 MPa. Judging with the goodness of fit criteria, the correlation between the modulus values was classified as ‘fair’ with $R^2 = 0.65$ and $S_e/S_y = 0.58$. The current coefficient of correlation was considerably lower than the previous study on empirical correlation between resilient and complex modulus, in which the R^2 correlation was 0.89–0.90. The study suggested a simple method to establish the dynamic modulus and resilient modulus correlation by developing the regression correlation (Ping and Xiao 2011).

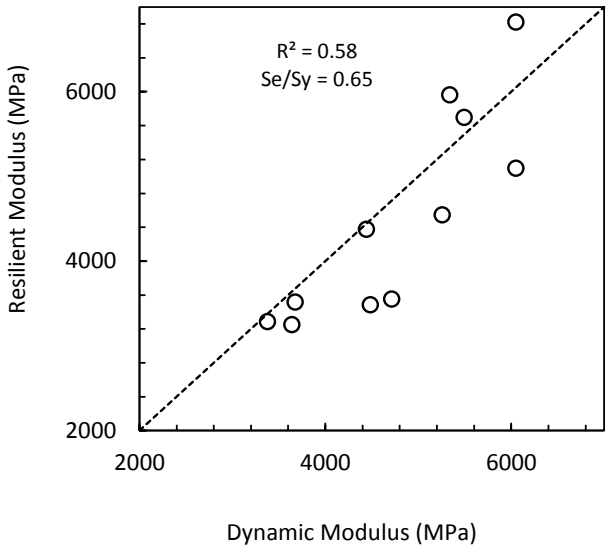

Figure 4.26 Comparison between resilient modulus and dynamic modulus

5 CONCLUSIONS AND RECOMMENDATIONS

5.1 Introduction

This chapter concludes the findings on the laboratory stiffness of the Western Australian asphalt mixtures described in Chapter 4. Recommendations are also made regarding future work. This research has contributed to the present body of knowledge on the stiffness characterization of Western Australian asphalt mixtures. Creep, resilient modulus, flexural modulus and dynamic modulus characterize the stiffness of asphalt pavement. Statistical analysis was also reported to validate the dynamic modulus prediction for wider application in determining the dynamic modulus of asphalt in Western Australia. The main findings are given below.

5.2 Conclusions

5.2.1 Creep

a) The initial permanent deformation was in the range of 1.494–1.564 mm. The values decreased with an increase in compaction level.
b) The minimum slope of asphalt mixtures generally decreased with an increase in maximum aggregate size and decrease of the bitumen content in the mixes.
c) The AC10-320 mix displayed the highest minimum slope (8570 um/m/c), while the AC20-320 mix showed the lowest minimum slope (1873 um/m/c). The larger the minimum slope, the less resistant the mixture to permanent deformation.
d) Based on minimum slope values, both the AC14-320 and AC20-320 mixes can be used in designing roads with medium and heavy traffic, respectively.

5.2.2 Resilient Modulus

a) The analysis proved that the resilient modulus significantly decreases when the nominal maximum aggregate size increases. The AC20-320 mix had considerably higher resilient modulus values than the AC10-320 and AC14-320 mixes. The higher particle-to-particle contact increases the stiffness of asphalt mixtures.
b) The AC20-320 mix with 3% air voids had the highest resilient modulus. The resilient modulus values vary with air voids because lower air void content in the mixes results in an increase in density.
c) The resilient moduli of the Western Australian mixtures were in the range of 3483–4860 MPa at the 25^{O}C test temperature. The values were still within the range of the Austroads presumptive values, but precisely in the lower part of the range.

d) The resilient modulus values for mixes in this research are acceptable and could be used as indicative values for design inputs in Western Australian pavement design.

5.2.3 Flexural Fatigue

The flexural modulus test was carried out with limited specimens from mixes AC10-320, AC14-320 and AC20-320.

a) It can be reported that the higher binder content increased the fatigue resistance of WA mixes.
b) There was a gradual increase in fatigue life which was contradicting to the resilient modulus-flexural stiffness correlation.
c) There was a considerable variability in the test results that requires more data validation with other flexural moduli for similar mix design.

5.2.4 Dynamic Modulus

a) The dynamic modulus test provides a better characterization of hot mix asphalt than the resilient modulus because it provides full characterization of the mix over temperature and loading frequencies.
b) The dynamic modulus data followed a general trend, increasing with an increase in the loading frequency and decreasing as the temperatures increased.
c) The phase angle displayed a different trend to the dynamic modulus. The phase angle behavior became complex as the loading frequencies were increased. This is attributed to the predominant effect of aggregate interlock at high temperatures.
d) The aged RTFOT binder had a higher dynamic modulus than the original binder at test temperatures of 4° and 20°C. There was no difference between the dynamic modulus of original and RTFOT binder at high temperatures.
e) Shift factor is determined by many parameters, including maximum aggregate size. The accuracy of shift factor is higher than 0.90.
f) The effect of air voids is significant in determining the dynamic modulus since the voids determine the volumetric properties and bitumen content.
g) The nominal maximum aggregate size can increase the stiffness. Higher dynamic modulus results from large aggregate size which promotes aggregate interlock in the mixtures. The $|E^*|$ test was sensitive to nominal maximum aggregate size (NMAS) in a mixture. Mixtures with larger aggregate size in combination tend to have high $|E^*|$ values at high temperatures.
h) Mixes with higher binder grade (Class 320) showed a higher dynamic modulus. The binder type is influenced by the stiffness and deformation properties of the asphalt mixtures.

i) Test temperature, NMAS and binder performance grade are significant factors in affecting the variability of the dynamic modulus test results.

j) The AC10-170 mix showed a higher phase angle than the other mixes for lower frequency. This is attributed to the effect of the aggregate size in decreasing the mixture's resistance to pavement distress.

k) Black space analysis indicated a high variability in phase angle at low frequencies.

l) The Witczak predictive /*E**/ master curve was higher at low temperatures (upper region). At intermediate temperatures, the master curves overlapped with the predictive model except for the AC10-170 and AC10-320 mixes. At high temperatures, a high discrepancy was observed, leading to a low correlation between the measured and predictive values.

m) The Hirsch model showed large discrepancies at high and low temperatures. The mixes overlapped with the Hirsch model at intermediate temperatures.

n) The Witczak model showed excellent correlation with the laboratory-measured dynamic modulus. However, this model tends to overestimate the dynamic modulus at high temperatures. This is because the model is insensitive to aggregate gradation, type and asphalt source than the specifications outside the US.

o) The Hirsch model established a good correlation with the Western Australian mixtures. The predicted dynamic modulus showed a noticeable discrepancy between the predicted and measured /*E**/ at nominal maximum aggregate size.

p) The results of the Witczak and Hirsch predictive equations fitted well when compared with the laboratory-measured /*E**/ data. In this research the Witczak model is more suitable than the Hirsch model for use with Western Australian asphalt mixture data.

q) Both the Witczak and Hirsch models were able to predict the dynamic modulus /*E**/ values with excellent reliability. The use of these prediction models can be a valuable tool in approximately estimating the dynamic modulus /*E**/ value of asphalt mixtures.

r) The correlation between the dynamic modulus and resilient modulus values according to goodness-of-fit criteria was classified 'fair' with $R^2 = 0.65$ and $S_e/S_y = 0.5$.

5.3 Recommendations

The following recommendations can be used for future study:

a) Laboratory study on resilient modulus and dynamic modulus indicated that the asphalt mixtures designed using Main Road Western Australia specifications have fulfilled the asphalt stiffness characteristics. It is recommended that to investigate the influence of various parameters such as gradation (open and dense graded), and asphalt grade (AC 600, synthetic binder) to give more data for application. In parallel to laboratory

investigation, mixtures used in the field should also be investigated and compared to obtain the correlation between laboratory and application.

b) The dynamic modulus predictive model is a practical approach to determine (E*) values without laboratory measurement. From both predictive models used in this thesis, the Witczak calculation was more suitable for Western Australia's asphalt mixtures. However, it is recommended to use various statistical methods to analyze the dynamic modulus and efficiently eliminate the outlier data.

c) The predictive model could be successfully applied to characterize dynamic modulus of Western Australia mixtures. It is also recommended to develop other predictive models to predict some influential asphalt characteristics used in Western Australia, such as permanent deformation (rutting), resilient modulus and fatigue life to accommodate practical measurement of material properties.

6 REFERENCES

AASHTO 2009. *Standard Method of Test for Determining the Rheological Properties of Asphalt Binder Using a Dynamic Shear Rheometer (DSR)*. AASHTO T315-09. Washington D.C.: American Association of State Highway and Transportation Officials.

AASHTO 2010a. *Determining the Flexural Creep Stiffness of Asphalt Binder Using the Bending Beam Rheometer (BRR)*. AASHTO T313-10. Washington D.C.: American Association of State Highway and Transportation Officials.

AASHTO 2010b. *Developing Dynamic Modulus Master Curves for Hot Mix Asphalt (HMA) Using the Asphalt Mixture Performance Tester (AMPT)*. AASHTO PP 61. Washington D.C.: American Association of State Highway and Transportation Officials.

AASHTO 2010c. *Developing Dynamic Modulus Master Curves for Hot Mix Asphalt (HMA)*. AASHTO PP 62. Washington D.C.: American Association of State Highway and Transportation Officials.

AASHTO 2011. *Standard Method of Test for Determining Dynamic Modulus of Hot Mix Asphalt (HMA)*. AASHTO T342-11. Washington D.C.: American Association of State Highway and Transportation Officials.

Adhikari, S., S. Shen, and Z. You. 2009. Evaluation of fatigue models of hot-mix asphalt through laboratory testing. *Journal of the Transportation Research Board* 2127(1): 36-42.

Al-Khateeb, G., and Basheer, I. A three-stage rutting model utilizing rutting performance data from the Hamburg Wheel-Tracking Device (WTD). *Road & Transport Research* 18(3): 12-25.

Apeagyei, A.K., B.K. Diefenderfer, and S.D. Diefenderfer. 2011. Development of dynamic modulus master curves for hot-mix asphalt with abbreviated testing temperatures. *International Journal of Pavement Engineering* 13(2): 98-109.

APRG. 2002. *Selection & design of asphalt mixes: Australian provisional guide*. APRG Report No 18. Austroads Technical Report AP-T20/02. Haymarket: Austroads/AAPA/ARRB Transport Research Ltd.

Arambula, E., E. Masad, and A.E. Martin. 2007. Influence of air void distribution on the moisture susceptibility of asphalt mixes. *Journal of Materials in Civil Engineering* 19(8): 655-664.

Austroads. 2002. *Selection & Design of Asphalt Mixes: Australian Provisional Guide*. Sydney: Austroads Incorporated.

Austroads. 2004. *Pavement design – a guide to the structural design of road pavements*. AP-G17/04. Sydney: Austroads Incorporated.

Austroads. 2005a. *Sample preparation- Compaction of asphalt slabs suitable for characterisation*. No. AG: PT/T220. Sydney: Austroads Incorporated.

Austroads. 2005b. *Fatigue life of compacted bituminous mixes subject to repeated flexural bending*. No. AG: PT/T233. Sydney: Austroads Incorporated.

Austroads. 2006a. *Austroads Technical Report: Introduction to Asphalt Mix Design*. No. AP-T62/06. Sydney: Austroads Incorporated.

Austroads. 2006b. *Austroads Technical Report: Asphalt Characterisation for Pavement Design*. No. AP-T63/06. Sydney: Austroads Incorporated.

Austroads. 2006c. *Austroads Technical Report: Proficiency Exercise: Resilient Modulus*. No AP-T57/06. Sydney: Austroads Incorporated.

Austroads. 2007. *Guide to Pavement Technology Part 4B: Asphalt*. No. AGPT04B/07. Sydney: Austroads Incorporated.

Austroads. 2008. *A Review of Austroads Gyratory Compaction Research*. No. AP-T94/08. Sydney: Austroads Incorporated.

Austroads. 2008a. *Australian and International Bituminous Binder Specifications*. No. AP/T113/08. Sydney: Austroads Incorporated.

Austroads. 2008b. *Guide to Pavement Technology Part 4F: Bituminous Binders*. No. AGPT04F/08. Sydney: Austroads Incorporated.

Austroads. 2008c. *Guide to Pavement Technology Part 2: Pavement Structural Design*. No. AGPT02/08. Sydney: Austroads Incorporated.

Austroads. 2008d. *Technical Basis of Austroads Guide to Pavement Technology Part 2: Pavement Structural Design*. No. AP-T98/08. Sydney: Austroads Incorporated.

Austroads, 2008e. *Testing Asphalt in Accordance with the Austroads Mix Design Procedures*. No. AP-T100/08. Sydney: Austroads Incorporated.

Austroads. 2009. *Austroads Technical Report: Preparation of Asphalt Samples for Testing*. No. AP-T132/09. Sydney: Austroads Incorporated.

Austroads. 2011a. *Selection of a Laboratory Asphalt Compactor for Australasia*. No. AP-T192-11. Sydney: Austroads Incorporated.

Austroads. 2011b. *Second National Survey of Australian Bitumen*. No. AP-T182. Sydney: Austroads Incorporated.

Bae, A., S. Stoffels, T. Clyne, B. Worel, G.R. and Chehab. 2007. Direct effects of thermal cracks on pavement roughness. *Journal of the Association of Asphalt Paving Technologist* 76: 59-83.

Bari, J. and M.W. Witczak. 2007. New predictive models for viscosity and complex shear modulus for use with Mechanistic-Empirical Pavement Design Guide. *Journal of the Transportation Research Board* 2001/2007 Bituminous Paving Mixtures 2007: 9-19.

Barksdale, R.D., J. Alba, N.P. Khosla, R. Kim, P.C. Lambe, and M.S. Rahman. 1997. *Laboratory Determination of Resilient Modulus for Flexible Pavement Design*. NCHRP Web Document Issue Number 14. NCHRP Project 1-28. Washington DC: Transportation Research Board.

Berthelot, C., A. Anthony, C. Wandzura, and B. Marjerison. 2010. Triaxial frequency sweep characterization of asphalt-aggregate adhesion in Saskatchewan asphaltic mixes. *Journal of Transportation Engineering* 136(2): 158-164.

Biligiri, K.P., K. Kaloush, and J. Uzan. 2010. Evaluation of asphalt mixtures viscoelastic properties using phase angle relationships. *International Journal of Pavement Engineering* 11(2): 143-152.

Birgisson, B., R. Roque, J. Kim, and L. Pham. 2004. *The use of complex modulus to characterize the performance of asphalt mixtures and pavements in Florida*. Final Report. Report No. 4910-4504-784-12. Florida: Florida Department of Transportation.

Brown, E.R., and K.Y. Foo. 1989. *Evaluation of variability in resilient modulus test results* (ASTM D4123). NCAT Report No 91-6. Alabama: National Centre for Asphalt Technology of Auburn University.

Brown, E.R. 1990. Density of asphalt concrete- how much is needed? *The 69th Annual Meeting of the Transportation Research Board* Washington D.C.: Transportation Research Board.

Brown, E.R., and C.E. Basset. 1990. *Effects of maximum aggregate size on rutting potential and other properties of asphalt aggregate mixtures*. Transportation Research Record. No 1259. pp. 107-119.Brown, S. 2000. Function and properties of road layers. In *Asphalts in Road Construction*, ed. R.N. Hunter. London: Thomas Telford.

Bureau of Infrastructure, Transport and Regional Economics Public. 2009. *Road-related Expenditure and Revenue in Australia 2008 update*. Information Sheet 29.

Butcher, M., and H. van Loon. 2003. A review of the determination of asphalt modulus for pavement design. *The 12th AAPA International Flexible Pavements Conference*. Melbourne, Victoria: Australian Asphalt Pavement Association.

Ceyland, H., C.W. Schwartz, K. Sunghwan, and G. Kasthurirangan. 2009. Accuracy of predictive models for dynamic modulus of hot-mix asphalt. *Journal of Materials in Civil Engineering* 21(6): 286-293.

Cho, Y-H., Park, D-W., and S-D. Hwang. 2010. A predictive equation for dynamic modulus of asphalt mixtures used in Korea. *Construction and Building Materials* 24: 513-519.

Christensen, D.W. 1998. Analysis of creep data from indirect tension test on asphalt concrete. *Journal of the Association of Asphalt Paving Technologist* 67: 458-492.

Christensen, D.W., and R. Bonaquist. 2002. Use of strength tests for evaluating the rut resistance of asphalt concrete. *Journal of the Association of Asphalt Paving Technologist* 71: 692-711.

Christensen, D. W., T. K. Pellinen, and R. F. Bonaquist. 2003. Hirsch Model for Estimating the Modulus of Asphalt Concrete. *Journal of the Association of Asphalt Paving Technologists* 67.

Clyne, T.R., X. Li, M.O. Marasteanu, and E.L. Skok. 2003. *Dynamic and Resilient modulus of Mn/DOT asphalt mixtures*. Report No. MN/RC-2003-09. Minnesota: Minnesota Department of Transportation.

Cominsky, R.J., B.M. Killingsworth., R.M. Anderson., D.A. Anderson., and W.W. Crockford. 1998. *Quality control and acceptance of superpave-designed hot mix asphalt*. National Cooperative Highway Research Project (NCHRP) Report No. 409. Washington D.C.: Transportation Research Board.

Di Benedetto, H., A.A. Soltani, and P. Chaverot. 1996. Fatigue damage for bituminous mixtures: a pertinent approach. *Journal of the Association of Asphalt Paving Technologists* 65: 142-158.

Di Benedetto, H.D., M.N. Partl, L. Francken, and C. de La Roche. 2001. Stiffness testing for bituminous mixtures. *Materials and Structures* 34: 66-70.

Di Benedetto, H.D., C. de La Roche, H. Baaj, A. Pronk and R. Lundstrom. 2004. Fatigue of bituminous mixtures. *Materials and Structures* 37(3): 202-216.

Dongre, R., L. Myer, J. D'Angelo, C. Paugh, and J. Gudimettla. 2005. Field evaluation of Witczak and Hirsch models for predicting dynamic modulus of hot mix asphalt. *Journal of the Association of Asphalt Paving Technologist* 74: 381-442.

Fakhri, M. 1997. Characterisation of asphalt pavement materials. PhD dissertation. University of New South Wales.

Fonseca, O.A., and M.W. Witczak. 1996. A prediction methodology for the dynamic modulus of in placed aged asphalt mixtures. *Journal of the Association of Asphalt Paving Technologists* 74: 381-442.

Ghareib, H., and S. Ahmed. 2009. Improving the prediction of the dynamic modulus of fine-graded asphalt concrete mixtures at high temperatures. *Canadian Journal of Civil Engineering* 36(2): 180-190.

Gomez, W.D.F., H.R. Quintana, and F.R. Lizcano. 2013. A review of asphalt and asphalt mixture aging. *Ingenieria E Investigacion* 33(1): 5-12.

Haas, R., and S. Tighe. 2007. *Annual Conference of Transportation Association of Canada: Mechanistic-empirical pavement design: evolution and future challenges*. Saskatoon: Transportation Association of Canada.

Harran, G., and A. Shalaby. 2009. Improving the prediction of the dynamic modulus of fine-graded asphalt concrete mixtures at high temperatures. *Canadian Journal of Civil Engineering* 36: 180-190.

Hassan, H.F., and K. Al-Shamsi. 2010. Characterisation of asphalt mixes containing MSW ash using the dynamic modulus |E*| test. *International Journal of Pavement Engineering* 11(6): 575-582.

He, G-P. and W-G. Wong. 2008. Effects of moisture on strength and permanent deformation of foamed asphalt mix incorporating RAP materials. *Construction and Building Materials* 22(1): 30-40.

Hossain, M., and J.Z. Chen. 2002. Optimization of Superpave mixture volumetric properties. *International Journal of Pavement Engineering* 3(2): 63-69.

Hossain, Z., M. Zaman, and K. Hobson. 2010. Effects of liquid anti-stripping additives on rheological properties of performance grade binders. *International Journal of Pavement Research and Technology* 3(4): 160-170.

Hu, X., and L.F. Walubita. 2009. Modelling tensile strain response in asphalt pavements, bottom-up and/or top-down fatigue crack initiation. *Road Materials and Pavement Design* 10(1): 125-154.

Huang, B., X. Shu, Q. Dong, and J. Shen. 2010. Laboratory evaluation of moisture susceptibility of hot mix asphalt containing cementitious fillers. *Journal of Materials in Civil Engineering* 7(22): 667-673.

Huang, Y.H. 2004. *Pavement Analysis and Design*. Second Edition. New Jersey: Pearson Prentice Hall.

Hubner, D., and G. Jameson. 2008. *Technical Basis of Austroads Guide to Pavement Technology Part 2: Pavement Structural Design*. Austroads No. AP-T98/08. Sydney: Austroads Incorporated.

Isacsson, U., and H. Zeng. 1998. Low temperature cracking of polymer-modified asphalt. *Materials and Structures* 31:58-63.

Jitsangiam, P., H.R. Nikraz, and C. Leek. 2010. Development of hot-mix asphalt layer thickness design for longer-life asphalt pavements. *The 6th PATREC Research Forum*. Fremantle: Planning & Transport Research Centre.

Julaihi, A.H. 2010. Determination and comparison of resilient and flexural modulus in asphalt concrete layer. Final Year Project Report. Curtin University.

Kaloush, K.E., M.W. Witczak, and H.V. Quintus. 2002. Pursuit of the simple performance test for asphalt mixture rutting. *Journal of the Association of Asphalt Paving Technologist* 71: 783-810.

Kim, Y.R., S. Youngguk, M. King, and M. Momen. 2004. Dynamic modulus testing of asphalt concrete in indirect tension mode. *Journal of the Transportation Research Board* 1891: 163-173.

Kim, Y.R., M. Momen, and M. King. 2005. *Typical dynamic moduli for North Carolina asphalt concrete mixtures*. FWHA Report NC/2005-03. Raleigh: North Caroline State University.

Kim, Y.R., H.M. Park, F.T.S. Aragao, and J.E.S. Lutif. 2009. Effects of aggregate structure on hot-mix asphalt rutting performance in low traffic volume local pavements. *Construction and Building Materials* 23(6): 2177-2182.

Koole, R., and B. Thagesen. 2004. *Asphalt pavement materials*. In Road Engineering for Development. Robinson, eds. R. Koole and B. Thagesen. London: Spon Press.

Kumar, S.A., and A. Veeraragavan. 2011. Dynamic mechanical characterization of asphalt concrete mixes with modified asphalt binders. *Materials Science and Engineering: A* 528(21): 6445-6454.

Kumlai, S., P. Jitsangiam, and H. Nikraz. 2014. An investigation into dynamic modulus of Western Australia hot mix asphalt. In *Asphalt Pavement*, ed. Y.R. Hunter. Leiden: CRC Press/Balkema.

Lancaster, I. 2000. Bitumens. In *Asphalts in road construction*, ed. R.N. Hunter. London: Thomas Telford.

Law, T.L. 2003. Resilient modulus of asphalt concrete mixtures. Master thesis. University of Manitoba.

Lee, H.S., and J. Kim. 2011. Backcalculation of dynamic modulus from resilient modulus test data. *Canadian Journal of Civil Engineering* 38: 582-592.

Lee, K., H. Kim, N. Kim, and Y. Kim. 2007. Dynamic modulus of asphalt mixtures for development of Korean pavement design guide. *Journal of Testing and Evaluation* 35(2): 1-8.

Lee, S.J., Amirkhanian, S.N., K. Shatanawi, and K.W. Kim. 2008. Short-term aging characterization of asphalt binders using gel permeation chromatography and selected Superpave binder tests. *Construction and Building Materials* 22: 2220-2227.

Li, Y., and J.B. Metcalf, 2004. Fatigue characteristics of asphalt concrete from asphalt slab tests. *Journal of Materials in Civil Engineering* 16(4): 306-314.

Li, Q., D.X. Xiao, K.C.P. Wang, K.D. Hall, and Y. Qiu. 2011. Mechanistic-empirical pavement design guide (MEPDG): a bird's-eye view. *Journal of Modern Transportation* 19: 114-133.

Lim, C.T. and Tan, S.A. 1995. Specimen size effects on the diametrical mechanical testing of cylindrical asphalt mixes. *Journal of Testing and Evaluation*. 23: 436-441.

Little, D.N., J.A. Epps, and P.E. Sebaaly. 2006. *The Benefits of Hydrated Lime in Hot Mix Asphalt*. National Lime Association.

Liu, M., M.A. Ferry, R.R. Davidson, C.J. Glover, and J.A. Bullin. 1998a. Oxygen uptake as correlated to carbonyl growth in aged asphalts and asphalt Corbett fractions. *Industrial and Engineering Chemistry Research* 37(12): 4669-4674.

Liu, M.M., M.S. Lin, J.M. Chaffin, R.R. Davison, C.J. Glover, and J.A. Bullin. 1998b. Oxidation kinetics of asphalt Corbett fractions and compositional dependence of asphalt oxidation. *Petroleum Science and Technology* 167(7-8): 827.

Liu, P., and J. Liu. 2010. *Characterization of asphalt treated base course material*. Research Report No. 107049. Alaska: Department of Civil and Environmental Engineering University of Alaska.

Loulizi A, G.W. Flinthsch, I.L. Al-Qadi, and D. Mokarem, 2006. Comparing resilient modululs and dynamic modulus of hot-mix asphalt as material properties for flexible pavement design. *Journal of the Transportation Research Board* 1970: 161-170.

Lytton, R.L. 2009. Comprehensive overview of the stiffness characterization of asphalt concrete. In *Modeling of asphalt concrete*, ed. Y.R. Kim. Virginia: American Society of Civil Engineers.

Main Roads Western Australia. 2004. *Stability and Flow of Asphalt: Marshall Method*. Test Method WA 731.1. Perth: Main Roads Western Australia.

Main Roads Western Australia. 2006. *Materials for Bituminous Treatments*. Document No. 71/06/135. Perth: Main Roads Western Australia.

Main Roads Western Australia. 2008. *Procedure for the Design of Flexible Pavements*. Engineering Road Note 9. Perth: Main Roads Western Australia.

Main Roads Western Australia. 2010a. *Specification 504 Asphalt Wearing Course*. Document 04/10112. Perth: Main Roads Western Australia.

Main Roads Western Australia. 2010b. *Specification 510 Full Depth Asphalt Pavement*. Document 07/5856. Perth: Main Roads Western Australia.

Mallick, R.B., and El-Korchi, T. 2009. *Pavement Engineering- Principles and Practice*. Boca Raton: CRC Press Taylor & Francis Group.

Mamlouk, M., and J.P. Zaniewski. 1999. *Materials for Civil and Construction Engineers*. London: Longman.

McCann, M., and Sebaaly, P. 2003. Evaluation of moisture sensitivity and performance of lime in hot-mix asphalt: resilient modulus, tensile strength, and simple shear tests. Transportation Research Record: *Journal of the Transportation Research Boar* 1832: 9-16.

McDaniel, R.S., V.L. Gallivan, G.A. Huber, D.H. Andrewski, and M. Miller. 2005. Use of HMA stiffness results as a referee test in Indiana. *Journal of ASTM International* 2(4): 1-5.

Merril, D., A. Van Dommelen, and L. Gaspar. 2006. A review of practical experience throughout Europe on deterioration in fully-flexible and semi-rigid long-life pavements. *International Journal of Pavement Engineering* 7(2): 101-109.

Mogawer, W.S., A.J. Austerman, J.S. Daniel, F. Zhou, and T. 2011. Bennert. Evaluation of the effects of hot mix asphalt density on mixture fatigue performance, rutting performance and MEPDG distress predictions. *International Journal of Pavement Engineering* 12(2): 161-175.

Moghaddam, T.B., M.R. Karim, and M. Abdelaziz. 2011. A review on fatigue and rutting performance of asphalt mixes. *Scientific Research and Essays* 6(4): 670-682.

Mohammad, L.N., S. Saadeh, S. Obulareddy, and S. Cooper. 2007. Characterization of Louisiana asphalt mixtures using simple performance tests. *Journal of Testing and Evaluation* 36(1): 1-12.

Monismith, C.L, J.A. Epps, and F.N. Finn. 1985. Improved asphalt mix design. *Journal of Association of Asphalt Paving Technologists* 54: 347-406.

NCHRP. 2004a. *Guide for Mechanistic-Empirical Design of New and Rehabilitated Pavement Structures*. *Part 2 Design Inputs*. *Chapter 2 Material Characterization*. Illinois: National Cooperative Highway Research Program.

NCHRP. 2004b. *Guide for Mechanistic-Empirical Design of New and Rehabilitated Pavement Structures*. *Part 3 Design Analysis*. *Chapter 3 Design of New and Reconstructed Flexible Pavements*. Illinois: National Cooperative Highway Research Program.

NCHRP. 2004c. 2002 Design Guide: *Design of New and Rehabilitated Pavement Structures*. NCHRP 1-37A Final Report. Washington D.C.: Ara Inc. and ERES Consultants Division.

Nunn, M.E., A. Brown, D. Weston, and Nicholls, J.C. 1997. *Design of long-life flexible pavements for heavy traffic*. TRL Report TRL 250. London: Transport Research Laboratory.

Nunn, M.E. 1998. Structural design of long life flexible roads for heavy traffic. *Proceedings of Institution of Civil Engineers (Transportation)* 129 (3): 126-133.

Obulareddy, S. 2006. Fundamental characterization of Louisiana HMA mixtures for the 2002 Mechanistic-Empirical Design Guide. MSc Thesis. Lousiana State University.

Oh, J.H., E.G. Fernando, C. Holzschuher, and D. Horhota. 2011. Comparison of resilient modulus values for flexible mechanistic-empirical pavement design. *International Journal of Pavement Engineering* 13(5): 472-484.

Pellinen, T. 2001. Investigation of the use of dynamic modulus as an indicator of hot-mix asphalt performance. PhD dissertation. Arizona State University.

Pellinen, T.K. and M.W. Witczak. 2002. *Use of stiffness of hot mix asphalt as a simple performance test*. Transportation Research Record no 1789. Washington D.C.: Transportation Research Board.

Pellinen, T.K. 2004. Conceptual performance criteria for asphalt mixtures. *Journal of the Association of Asphalt Paving Technologists*. 73: 337-366.

Pellinen, T.K., and S. Xiao. 2006. *Stiffness of Hot-Mix Asphalt*. FHWA/IN/JTRP-2005/20. Joint Transportation Research Program. Indiana: Indiana Department of Transportation and Purdue University.

Pellinen, T.K. 2009. Complex modulus characterization of asphalt concrete. In *Modeling of asphalt concrete*, ed. Y.R. Kim. Sydney: ASCE Press- McGraw-Hill Construction.

Peploe, R.J. 2008. *Flexural modulus of typical New Zealand structural asphalt mixes*. Research Report No. 334. Wellington: Land Transport New Zealand.

Ping, W.V., and Y. Xiao. 2011. Empirical correlation of indirect tension resilient modulus and complex modulus test results for asphalt concrete mixtures. *Road Materials and Pavement Design* 9(1): 177-200.

Pronk, A., and S. Erkens. 2002. A note on fatigue bending tests using a haversine loading. *Road Materials and Pavement Design* 3(1): 95-106.

Prowell, B.D., J. Zhang, and E.R. Brown. 2005. *Aggregate properties and the performance of Superpave-Designed Hot Mix Asphalt*. National Cooperative Highway Research Program (NCHRP) Report 539. Washington D.C.: Transportation Research Board.

Powell, W.D, J.F. Potter, H.C. Mayhew, and M.E. Nunn. 1984. *The Structural Design of Bituminous Roads*. Crowthorne: TRL.

Rajbongshi, P. 2009. A critical discussion on mechanistic-empirical fatigue evaluation of asphalt pavements. *International Journal of Pavement Research Technology* 2(5): 223-226.

Read, J., and D. Whiteoak. 2003. *The Shell Bitumen Handbook*. Fifth Edition. London: Thomas Telford Publishing.

Ricardson, J. 2000. Function and Properties of Road Layers. In: *Asphalts in Road Construction*, ed. R.N. Hunter. London: Thomas Telford.

Rickards, I. 2009. The application of laboratory derived performance measures at project level. *AAPA 13th International Flexible Pavements Conference, October 11-14 2009*. Sydney: Australian Asphalt Pavement Association.

Rickards, I. 2011. Asphalt pavement solutions- for life implementation project update. *AAPA 14th International Flexible Pavements Conference, September 25-28 2011*. Sydney: Australian Asphalt Pavement Association.

Roads and Traffic Authority New South Wales. 2001. *QA Specification R116. Asphalt (Dense Graded and Open Graded)*. Sydney: Roads and Traffic Authority of New South Wales.

Roads and Traffic Authority New South Wales. 2003. *QA Specification R123. Thin Open Graded Asphalt Surfacing*. Sydney: Roads and Traffic Authority of New South Wales.

Robinette, C.J., T.M. Breakah, R.C. Williams, and J.P. Bausano. 2010. Evaluation of the variability of E* with field procured hot mix asphalt concrete mixtures. *Road Materials and Pavement Design* 11(3): 559-582.

Rolt, J. 2004. Structural design of asphalt pavement. In *Road engineering for development*, eds. R. Robinson, R and B. Thagesen. London: Spoon Press.

Romanoschi, S.A., N.I. Dumitru, and O. Dumitru. 2006. *Resilient Modulus and the Fatigue Properties of Kansas Hot Mix Asphalt Mixes*. Research Report. The Kansas Department of Transportation Topeka. Kansas: Kansas State University.

Said, S.F., H. Hakim, H. Carlsson, and L.G. Wiman. 2011. Fatigue life evaluation of flexible pavement. *International Journal of Pavement Research Technology* 4(2): 80-88.

Saleh, M. 2008. *Hot mix asphalt stiffness moduli: laboratory versus field*. 6th International Conference on Road and Airfield Pavement Technology, Sapporo 20-23 July 2008. *Sapporo: Japan Society of Civil Engineers*.

Schmidt, R.J. 1972. *A practical method for measuring the resilient modulus of asphalt-treated mixes*. Highway Research Record No. 404. Washington D.C.: Highway Research Board.

Shell. 1978. *Shell Pavement Design Manual: Asphalt pavements and overlays for road traffic*. London: Shell International Petroleum Company.

Shalaby, A., Liske, T., and Kavussi, A. 2004. Comparing back-calculated and laboratory resilient moduli of bituminous paving mixtures. *Canadian Journal of Civil Engineering* 31: 988-996.

Shu, X. and B. Huang. 2008. Dynamic modulus prediction of HMA mixtures based on the viscoelastic micromechanical model. *Journal of Materials in Civil Engineering* 20(8): 530-538.

Singh, D., Beainy, F.N., Mai, A.T., Commuri, S. and Zaman, M. 2011. In-situ assessment of stiffness during the construction of HMA pavements. *Journal of Pavement Research and Technology* 4(3):131-139.

Singh, D., M. Zaman, and S. Commuri. 2012a. Evaluation of dynamic modulus of modified and unmodified asphalt mixes for different input levels of the MEPDG. *International Journal of Pavement Research Technology* 5(1): 1-11.

Singh, D., M. Zaman, and S. Commuri. 2012b. A laboratory investigation into the effect of long term oven aging on RAP mixes using dynamic modulus test. *International Journal of Pavement Research and Technology* 5(3): 142-152.

Singh, D., M. Zaman, and S. Commuri. 2012c. Inclusion of aggregate angularity, texture, and form in estimating dynamic modulus of asphalt mixes. *Road Materials and Pavement Design* 13(2): 327-344.

Somayaji, S. 2001. *Civil Engineering Materials*. New Jersey: Prentice-Hall.

Sousa, J.B., J. Craus, and C.L. Monismith. 1991. *Permanent Deformation in Asphalt Concrete*. Summary Report. Strategic Highway Research Program SHRP-A-318. Washington D.C.: Institute of Transportation Studies.

Schwartz, C.W. 2005. Evaluation of the Witczak dynamic modulus prediction model. *Proceedings 84th Annual Meeting of the Transportation Research Board*. Paper no. 05-2112. Washington D.C.: Transportation Research Board of the National Academies.

Standards Australia. 1995a. *Methods of sampling and testing asphalt*. *Method 2.1: Sample preparation- Mixing quartering and conditioning of asphalt in the laboratory*. AS 2891.2.1-1995. Standards Australia Online: http://www.saiglobal.com (accessed April 27, 2009).

Standards Australia. 1995b. *Methods of sampling and testing asphalt*. *Method 2.2: Sample preparation-Compaction of asphalt test specimens using a gyratory compactor*. AS 2891.2.2-1995. Standards Australia Online: http://www.saiglobal.com (accessed March 02, 2009).

Standards Australia. 1995c. *Methods of sampling and testing asphalt*. *Method 12.1: Determination of the permanent compressive strain characteristics of asphalt- Dynamic creep test*. AS. 2891.12.1-1995. Standards Australia Online: http://www.saiglobal.com (accessed September 25, 2009).

Standards Australia. 1995d. *Methods of sampling and testing asphalt*. *Method 13.1: Determination of the resilient modulus of asphalt- Indirect tensile method*. AS 2891.13.1-1995. Standards Australia Online: http://www.saiglobal.com (accessed March 02, 2009).

Standards Australia. 1997. *Limes and Limestones: for Building*. AS 1672.1-1997. Standards Australia Online: http://www.saiglobal.com (accessed September 02, 2009).

Standards Australia. 2000. *Method for sampling and testing aggregates*. *Method 5: Particle density and water absorption of fine aggregate*. AS 1141.5-2000. Standards Australia Online: http://www.saiglobal.com (accessed April 13, 2009).

Standards Australia. 2004. *Methods of sampling and testing asphalt*. *Method 5: Determination of stability and flow- Marshall procedure*. AS 2891.5-2004. Standards Australia Online: http://www.saiglobal.com (accessed March 02, 2009).

Standards Australia. 2005. *Hot mix asphalt- a guide to good practice*. AS 2150-2005. Standards Australia Online: http://www.saiglobal.com (accessed Jan 21, 2009).

Standards Australia. 2009. *Method for sampling and testing aggregates- Particle size distribution- Sieving method*. AS1141.11.1-2009 Standards Australia Online: http://www.saiglobal.com (accessed September 07, 2009).

Sullivan, B., I. Rickards, S. Yousefdoost. 2013. Interconversion of laboratory measured modulus results to field modulus and strain. *AAPA 15th International Flexible*

Pavements Conference, September 22-25 2013. Sydney: Australian Asphalt Pavement Association.

Sybilski, D., and W. Bankowski. 2002. Asphalt pavement design using results of laboratory fatigue tests of asphalt mixtures. *Road Materials and Pavement Design* 3(2): 183-194.

Tashman, L., and M.A. Elangovan. 2007. *Dynamic modulus test- laboratory investigation and future implementation in the state of Washington*. Report No. WA-RD 704.1. Seattle: Washington State Transportation Center (TRAC).

Tran, N.H. 2005. Characterizing and predicting dynamic modulus of hot mix asphalt for mechanistic-empirical design guide. Master Thesis. University of Arkansas.

Turos, M.I., A.C. Falchetto, G. Tebaldi, M.O. Marasteanu. 2012. The flexural strength of asphalt mixtures using the bending beam rheometer. In *7th RILEM International Conference on Cracking in Pavements*, eds. A. Scarpas et al. Heidelberg: Springer.

Urbaez, E. and J. Erskine. 2011. Project level Australian methodology for flexible pavement design. *AAPA's 14th International Flexible Pavements Conference, Sydney 25-28 September 2011*. Sydney: Australian Asphalt Pavement Association.

Vanelstraete, A., D. Leonard, and J. Veys. 2000. *Structural design of roads with steel reinforcing nettings*. Proceedings of the 4th International RILEM Conference-Reflective Cracking in Pavements. Ontario: E&FN Spoon.

Velasquez, R., A. Zofka, M. Turos, M.O. Marasteanu. 2011. Bending beam rheometer testing of asphalt mixtures. *International Journal of Pavement Engineering* 12(5): 461-474.

Villiers, C., Y. Mehta, M. Tia, R. Roque, and B. Dietrich. 2008. The importance of mineral filler on construction specifications. *International Journal of Pavement Engineering* 9(5): 343-353.

Walubita, L.F., A.E. Martin, S.H. Jung, C.J. Glover, E.S. Park, A. Chowdhury, and R.L. Lytton. 2004. *Comparison of fatigue analysis approaches for two Hot Mix Asphalt Concrete (HMAC) mixtures*. 2004. FHWA/TX-05/0-4468-2. Texas Transportation Institute. Texas: The Texas A&M University System.

Wang, J.N., T.W. Kennedy, and R.B. McGennis. 2000. Volumetric and mechanical performance properties of superpave mixtures. *Journal of Materials in Civil Engineering* 12(3): 238-244.

Wen, H. 2003. Investigation of effects of testing methods on characterization of asphalt concrete. *ASTM Journal of Testing and Evaluation* 31:507-513.

Witczak, M.W., K. Kaloush, T. Pellinen, M. El-Basyouny, and H. Von Quintus. 2002. *Simple Performance Test for Superpave Mix Design*. NCHRP Report 465. Transportation Research Board National Research Council. Washington D.C.: National Academy Press.

Witczak, M.W., and O.A. Fonseca. 1996. Revised predictive model for dynamic (complex) modulus of asphalt mixtures. *Journal of the Transportation Research Board* 1540: 15-23.

Witczak, M.W., K. Kaloush, T. Pellinen, M. El-Basyouny, and H. Von Quintus, 2002. *Simple Performance Test for Superpave Mix Design*. NCHRP Report 465. Transportation Research Board-National Research Council. Washington D.C.: National Academy Press.

Witczak, M.W., and J. Bari. 2004. *Development of a master curve (E*) database for lime modified asphaltic mixtures*. Arizona State University Research Report. Tempe: Arizona State University.

Xue, Y., H. Hou, S. Zhu, and J. Zha. 2009. Utilization of municipal solid waste incineration ash in stone mastic asphalt mixture: pavement performance and environmental impact. *Construction and Building Materials* 23: 989-996.

Yaghoubi, E., and A. Mansourkhaki. 2010. Effect of "n" exponent in Fuller Equation of gradation on hot mixes asphalt resistance of permanent deformation. *International Journal of Pavement Research and Technology* 3(6): 336-343.

Yin, H., G.R. Chehab, and S.M. Stoffels. 2006. *Sensitivity of thermal cracking prediction to AC mixture properties using the M-E pavement design guide*. *The 10th International Conference on Asphalt Pavement August 12-17*. Quebec: International Society for Asphalt Pavements.

Yin, H., G.R. Chehab, S.M. Stoffels, T. Kumar, and L. Premkumar. 2010. Use of creep compliance interconverted from complex modulus for thermal cracking prediction using the M-E pavement design guide. *International Journal of Pavement Engineering* 11(2): 95-105.

Yousefdoost, S., B. Vuong, I. Rickards, P. Armstrong, and B. Sullivan. 2013. Evaluation of dynamic modulus predictive models for typical Australian asphalt mixes. *AAPA 15th International Flexible Pavements Conference, September 22-25 2013*. Sydney: Australian Asphalt Pavement Association.

Zaitsev, J.W. 1994. *Fatigue response of asphalt-aggregate*. Report SHRP-A-404. National Research Council.

Zeghal, M., and E.H. Mohammed. 2008. Assessment of analytical tools used to estimate the stiffness of asphalt concrete. *Canadian Journal of Civil Engineering* 35: 268-275.

Zhang, J., E.R. Brown, P.S. Kandhal, and R. West. 2005. An overview of fundamental and simulative performance tests for hot mix asphalt. *Journal of ASTM International* 2(5): 1-15.

Zhou, F., D-H. Chen, T. Scullion, and J. Bilyeu, 2003. Case study: Evaluation of laboratory test methods to characterize permanent deformation properties of asphalt mixtes. *International Journal of Pavement Engineering* 4(3): 155-164.

Zhu, H., Sun, L., Yang, J., Chen, Z., and G. Wenjun. 2011. Developing master curves and predicting dynamic modulus of polymer-modified asphalt mixtures. *Journal of Materials in Civil Engineering* 23(2): 131-137.

Zofka, A., and I. Yut. 2011. Alternative procedure for determination of hot mix asphalt creep compliance. *Journal of Testing and Evaluation* 39(1): 39-49.

Appendix A – Aggregate Grading

A.1 Individual Aggregate Grading

Sieve (AS1152)	20 mm	14 mm	10 mm	7 mm	WQS	BHD	H-lime
26.5	4.37	100	100	100	100	100	100
19	3.76	85	100	100	100	100	100
13.2	3.19	7.6	90.2	100	100	100	100
9.5	2.75	1.1	27.3	89.7	100	100	100
6.7	2.35	0.6	16.1	8.5	93.9	100	100
4.75	2.02	0.5	1.2	1.4	49.3	99.5	100
2.36	1.47	0.5	1.1	0.6	2.9	84.5	100
1.18	1.08	0.4	0.9	0.4	1.7	54.0	100
0.6	0.79	0.4	0.7	0.4	1.4	32.1	100
0.3	0.58	0.3	0.5	0.3	1.0	16.5	100
0.15	0.43	0.1	0.3	0.3	0.8	6.3	98
0.075	0.31	0.0	0.1	0.1	0.4	2.6	95

WQS (washed quarry sand), BHD (baghouse dust), H-lime (hydrated lime)

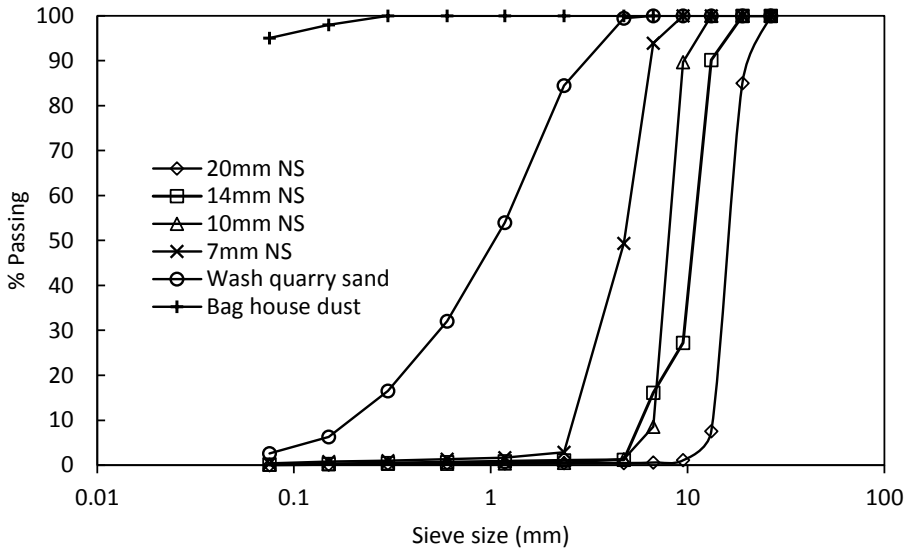

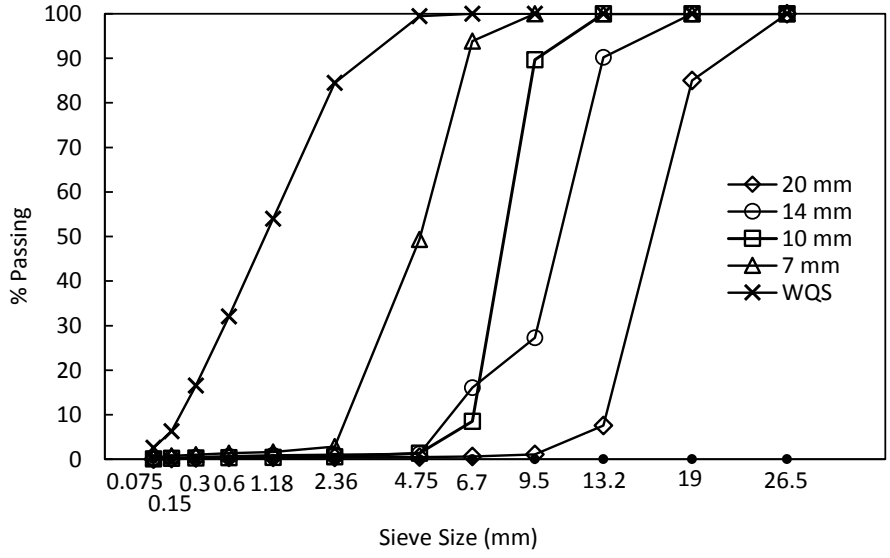

A.2 Grading AC10-170 and AC10-320

Sieve (AS1152)	20 mm 0%	14 mm 0%	10 mm 18.0%	7 mm 30.0%	WQS 47.5%	BHD 3.0%	H-lime 1.5%	Mix 100%	Spec Range
26.5									
19									
13.2			100	100	100	100	100	100	100-100
9.5			89.7	100	100	100	100	98.1	90-100
6.7			8.5	93.9	100	100	100	81.7	73-87
4.75			1.4	49.3	99.5	100	100	66.8	60-74
2.36			0.6	2.9	84.5	100	100	45.6	41-53
1.18			0.4	1.7	54.0	100	100	30.7	29-39
0.6			0.4	1.4	32.1	100	100	20.2	19-27
0.3			0.3	1.0	16.5	100	100	12.7	12-20
0.15			0.3	0.8	6.3	98	100	7.7	7-12
0.075			0.1	0.4	2.6	95	98.0	5.7	3-7

WQS (washed quarry sand), BHD (baghouse dust), H-lime (hydrated lime)

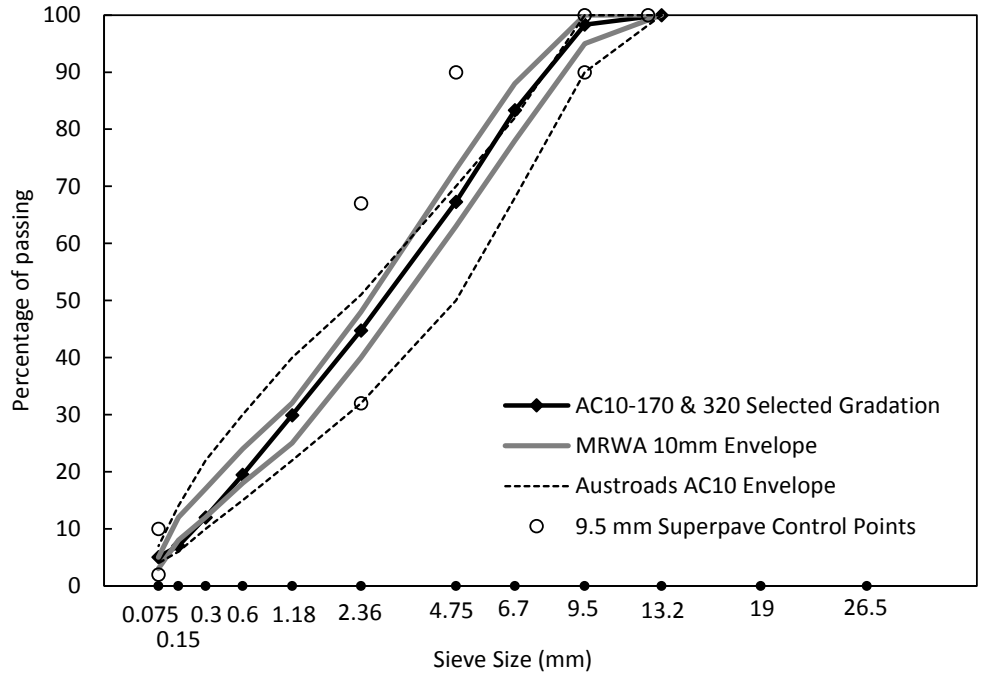

P_{200} = 5.7% (passing 0.074 mm)
P_4 = 36.7% (retained 4.36 mm)
$P_{3/8}$ = 1.9% (retained 9.5 mm)
$P_{3/4}$ = 0% (retained 19 mm)

A.3 Grading AC14-320

Sieve (AS1152)	20 mm 0%	14 mm 0%	10 mm 18.0%	7 mm 30.0%	WQS 47.5%	BHD 3.0%	H-lime 1.5%	Mix 100%	Spec Range
26.5									
19		100	100	100	100	100	100	100	100-100
13.2		90.2	100	100	100	100	100	97.8	93-100
9.5		27.3	89.7	100	100	100	100	82.6	79-89
6.7		16.1	8.5	93.9	100	100	100	67.5	63-73
4.75		1.2	1.4	49.3	99.5	100	100	53.6	49-59
2.36		1.1	0.6	2.9	84.5	100	100	37.8	33-41
1.18		0.9	0.4	1.7	54.0	100	100	25.4	22-32
0.6		0.7	0.4	1.4	32.1	100	100	16.7	15-23
0.3		0.5	0.3	1.0	16.5	100	100	10.4	10-18
0.15		0.3	0.3	0.8	6.3	98	98	6.2	6-11
0.075		0.1	0.1	0.4	2.6	95	95	4.5	2-5

WQS (washed quarry sand), BHD (baghouse dust), H-lime (hydrated lime)

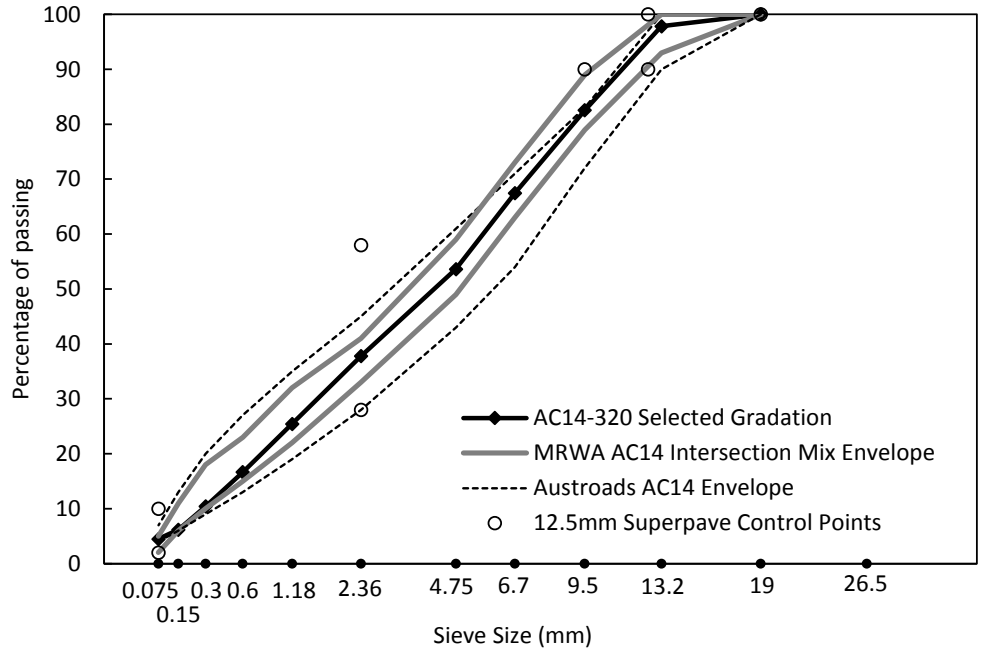

P_{200} = 4.5% (passing 0.074 mm)
P_4 = 49.0% (retained 4.36 mm)
$P_{3/8}$ = 17.4% (retained 9.5 mm)
$P_{3/4}$ = 0% (retained 19 mm)

A.4 Grading AC20-320

Sieve (AS1152)	20 mm 0%	14 mm 0%	10 mm 18.0%	7 mm 30.0%	WQS 47.5%	BHD 3.0%	H-lime 1.5%	Mix 100%	Spec Range
26.5	100	100	100	100	100	100	100	100	100-100
19	85.0	100	100	100	100	100	100	97	90-100
13.2	7.6	90.2	100	100	100	100	100	78	75-85
9.5	1.1	27.3	89.7	100	100	100	100	60	55-65
6.7	0.6	16.1	8.5	93.9	100	100	100	51	45-55
4.75	0.5	1.2	1.4	49.3	99.5	100	100	43	40-50
2.36	0.5	1.1	0.6	2.9	84.5	100	100	34	28-38
1.18	0.4	0.9	0.4	1.7	54.0	100	100	23	20-28
0.6	0.4	0.7	0.4	1.4	32.1	100	100	15	13-19
0.3	0.3	0.5	0.3	1.0	16.5	100	100	10	7-12
0.15	0.1	0.3	0.3	0.8	6.3	98	98	6	4-8
0.075	0.0	0.1	0.1	0.4	2.6	95	95	4	3-5

WQS (washed quarry sand), BHD (baghouse dust), H-lime (hydrated lime)

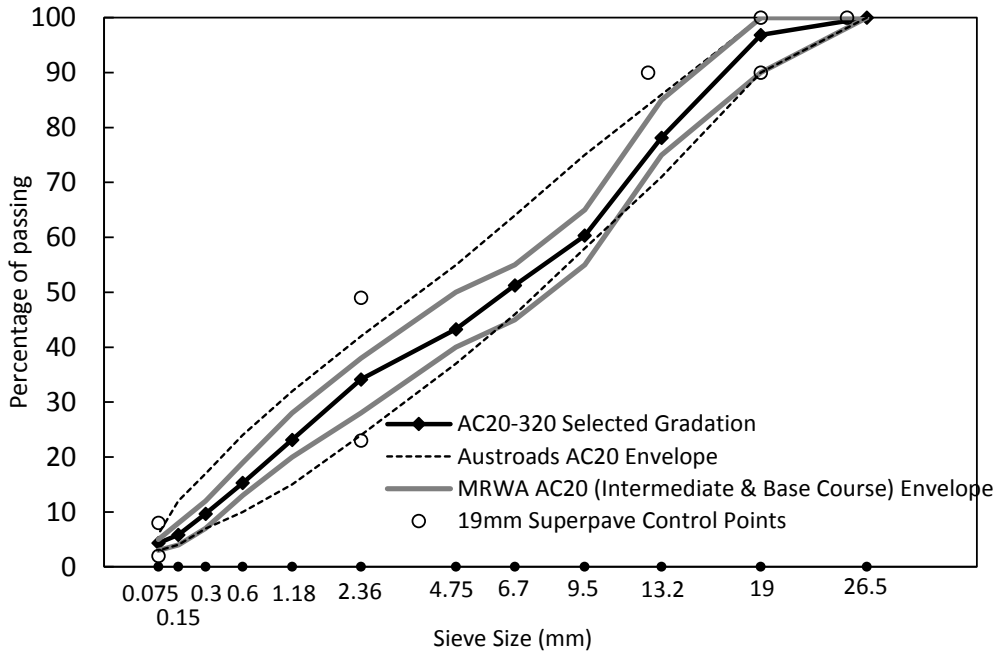

P_{200} = 4.3% (passing 0.074 mm)
P_4 = 61.4% (retained 4.36 mm)
$P_{3/8}$ = 42.8% (retained 9.5 mm)
$P_{3/4}$ = 6% (retained 19 mm)

Appendix B – Bitumen Properties

B.1 Bitumen Class 170

Source bitumen	Viscosity (Pa.s)								
	un-aged (original)					RTFOT			
	135°C	60°C	45°C	25°C	TSP60-25	60°C	45°C	25°C	TSP60-25
BP Kwinana	0.39	175	2831	184077	0.086	310	5598	386367	0.088

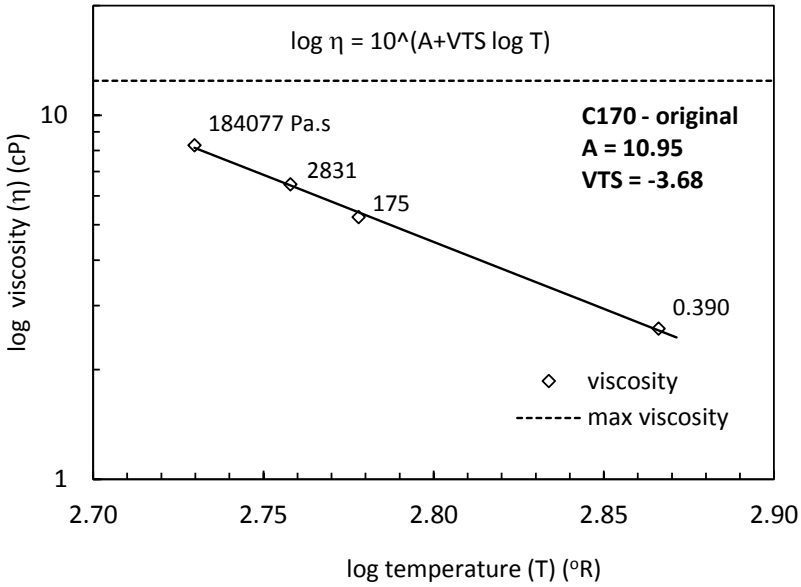

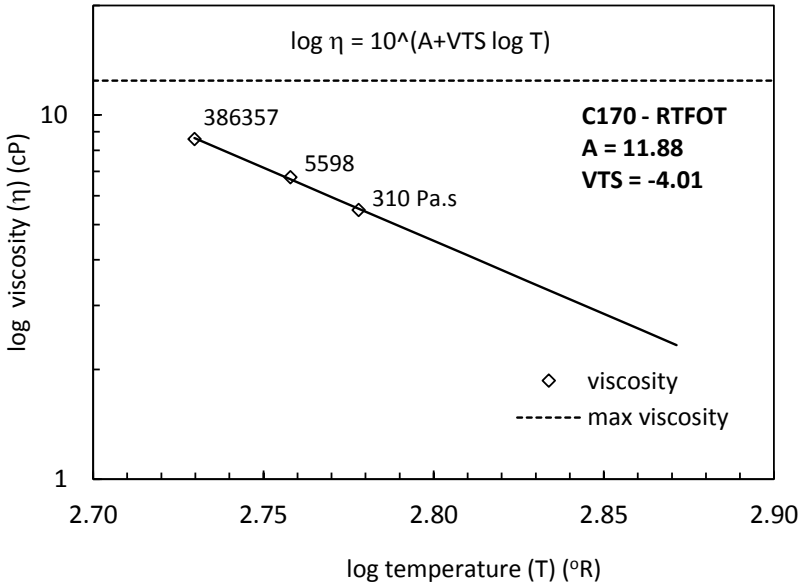

B.1 Bitumen Class 320

Source bitumen	Viscosity (Pa.s)								
	un-aged (original)					RTFOT			
	135°C	60°C	45°C	25°C	TSP60-25	60°C	45°C	25°C	TSP60-25
BP Kwinana	0.519	301	5957	349945	0.088	595	11298	762079	0.089

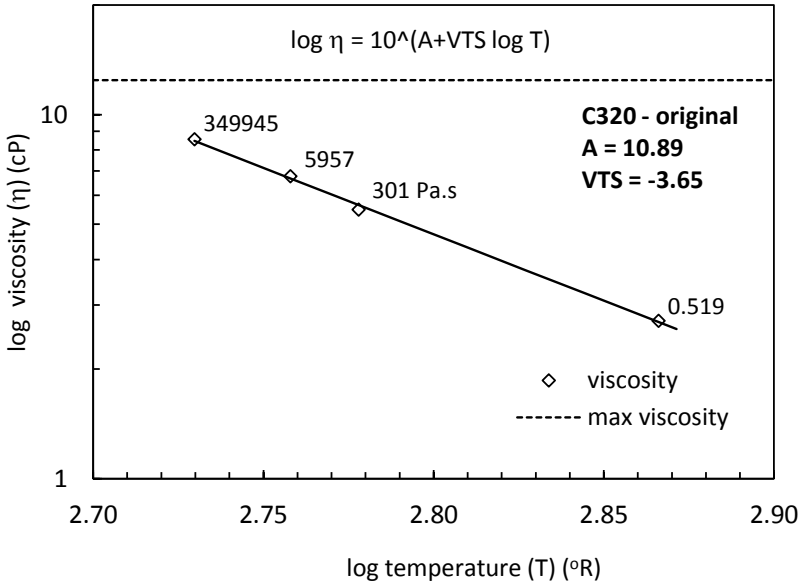

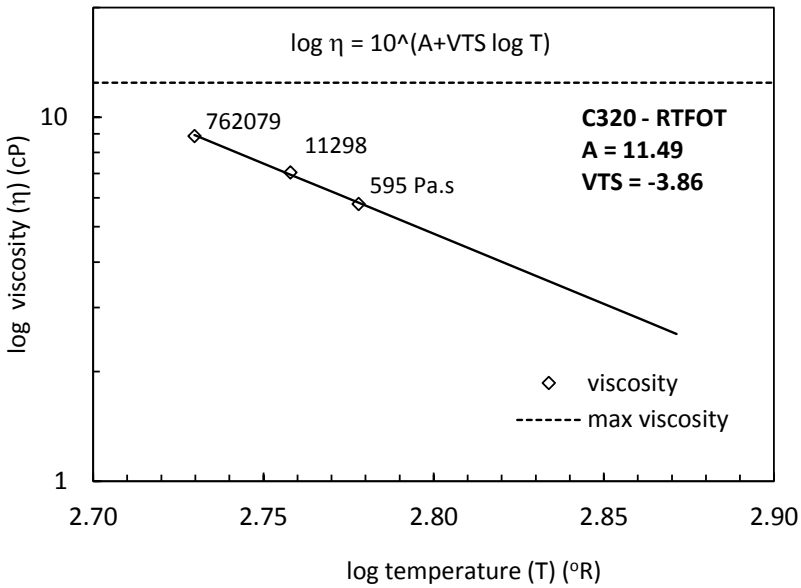

Appendix C - Resilient Modulus Test Results

Mixes	Air void (%)	Bit. Volume (%)	VMA (%)	VFA (%)	Modulus M_R	recovered strain (με)	Peak load (N)
AC10-320	2.8	12.6	15.3	82.0	4216	52.6	2170.4
	3.4	11.9	15.3	77.7	3978	51.7	2108.5
	3.3	11.9	15.2	78.5	4196	52.4	2236.3
	3.1	*12.1*	*15.3*	*79.4*	***4130***	*(average)*	
	3.6	12.5	16.0	77.8	4168	55.7	2090.9
	4.2	12.4	16.6	74.7	3463	58.5	1983.7
	4.2	12.4	16.6	74.8	4183	51.7	2217.0
	4.0	*12.4*	*16.4*	*75.8*	***3938***		
	4.8	12.3	17.1	72.0	3612	52.7	1907.4
	4.9	12.3	17.2	71.6	3766	54.7	2002.4
	5.0	12.2	17.2	71.0	3875	54.7	2084.4
	4.9	*12.3*	*17.2*	*71.5*	***3751***		
AC14-320	3.2	10.4	13.7	76.2	4953	53.1	2586.0
	3.3	11.0	14.3	77.0	4701	50.9	2307.7
	2.7	11.1	13.8	80.7	4521	53.3	2325.9
	3.1	*10.9*	*13.9*	*78.0*	***4725***		
	4.4	11.0	15.4	71.5	4476	53.7	2372.3
	4.0	11.0	15.1	73.2	4626	54.1	2451.8
	4.5	10.9	15.4	70.7	4716	52.8	2385.9
	4.3	*11.0*	*15.3*	*71.8*	***4606***		
	4.9	10.9	15.8	69.0	4221	54.9	2237.1
	4.6	10.9	15.5	70.1	4309	56.0	2283.8
	4.8	10.9	15.7	69.2	4313	53.7	2234.7
	4.8	*10.9*	*15.7*	*69.4*	***4281***		
AC20-320	2.7	10.6	13.3	79.5	5648	52.0	2993.4
	3.1	10.6	13.6	77.6	4832	51.2	2561.0
	3.2	10.6	13.8	76.5	5237	50.3	2775.6
	3.0	*10.6*	*13.6*	*77.9*	***5239***		
	4.2	10.4	14.7	71.2	5016	50.1	2455.3
	4.3	10.4	14.7	70.8	4841	52.3	2550.8
	4.3	10.4	14.7	71.0	5384	52.0	2802.8
	4.3	*10.4*	*14.7*	*71.0*	***5080***		
	4.6	10.4	15.0	69.6	4938	50.6	2483.0
	4.7	10.4	15.1	68.8	4574	53.1	2346.8
	5.0	10.4	15.4	67.2	4720	51.2	2404.8
	4.8	*10.4*	*15.2*	*68.5*	***4744***		
AC20-320 BC	2.8	12.0	14.8	80.9	4308	53.6	2380.6
	3.2	11.9	15.2	78.7	5382	51.8	2769.2
	3.4	11.9	15.3	77.7	5530	52.7	2869.5
	3.4	11.9	15.3	77.7	4218	56.2	2353.8
	3.2	*11.9*	*15.1*	*78.8*	***4860***		
	3.9	11.8	15.7	75.4	4379	53.0	2276.2
	4.2	11.8	16.0	73.9	4880	53.3	2586.6
	4.2	11.8	16.0	73.9	4367	55.2	2340.2
	4.1	*11.8*	*15.9*	*74.4*	***4542***		

Appendix D - Beam Fatigue Test Results

D.1 Beam Fatigue Test AC10-320

	Sample 1	Sample 2	Sample 3	Average	Sy
Air voids (%)	5.1	5.3	5.5	5.3	0.20
Number of cycles	396,840	457,920	333,420	396,060	62254
Maximum tensile micro-strain	397.1	397.1	397.5	397.2	0.21
Initial flexural stiffness (MPa)	4996	5515	6250	5587	630
Termination stiffness (MPa)	2498	2757	3125	2793	315

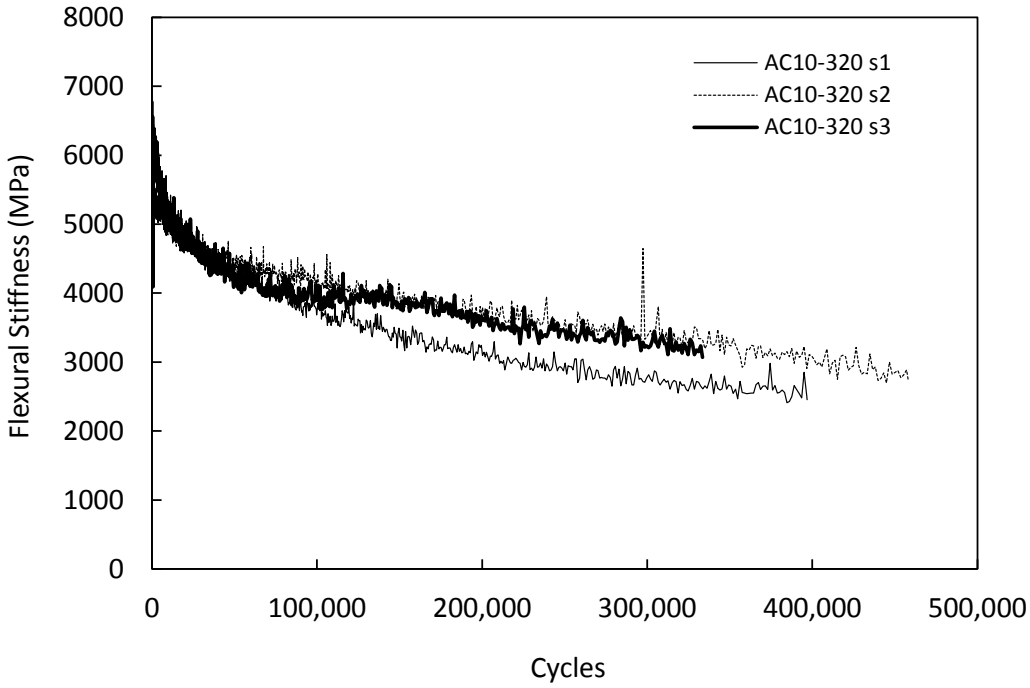

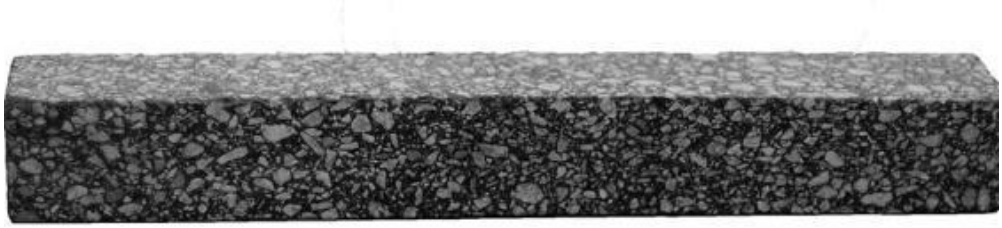

D.2 Beam Fatigue Test AC14-320

	Sample 1	Sample 2	Sample 3	Average	Sy
Air voids (%)	5.3	5.6	5.3	5.4	0.13
Number of cycles	232,000	398,610	217,230	282,613	100727
Maximum tensile micro-strain	397.1	396.9	397.4	397.2	0.28
Initial flexural stiffness (MPa)	4567	6039	6441	5682	987
Termination stiffness (MPa)	2789	2972	3072	2944	144

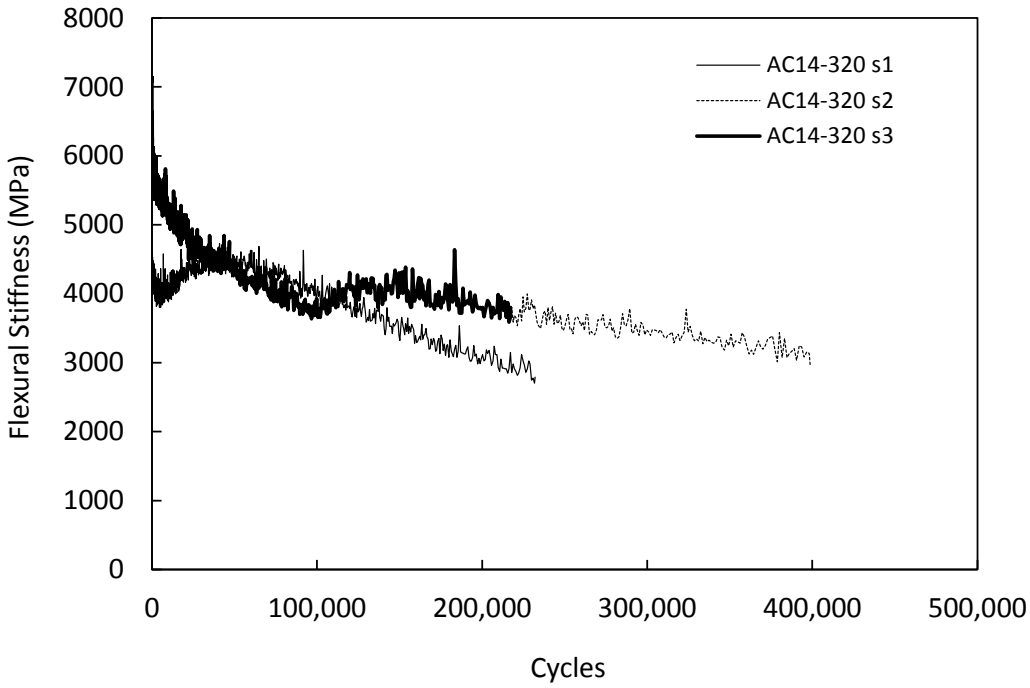

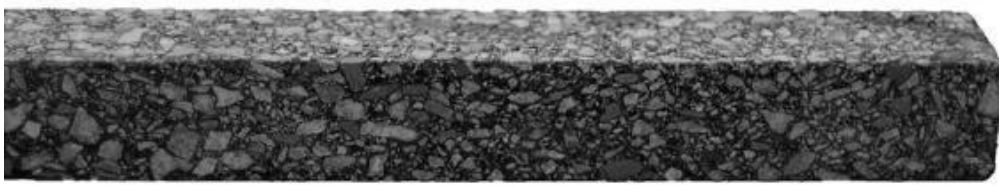

D.3 Beam Fatigue Test AC20-320

	Sample 1	Sample 2	Sample 3	Average	S_y
Air voids (%)	6.1	6.5	5.8	6.1	0.32
Number of cycles	224,930	181,600	179,810	195,447	25549
Maximum tensile micro-strain	413.8	419.7	409.2	414.3	5.26
Initial flexural stiffness (MPa)	6093	5064	5681	5613	518
Termination stiffness (MPa)	2948	2464	2840	2751	254

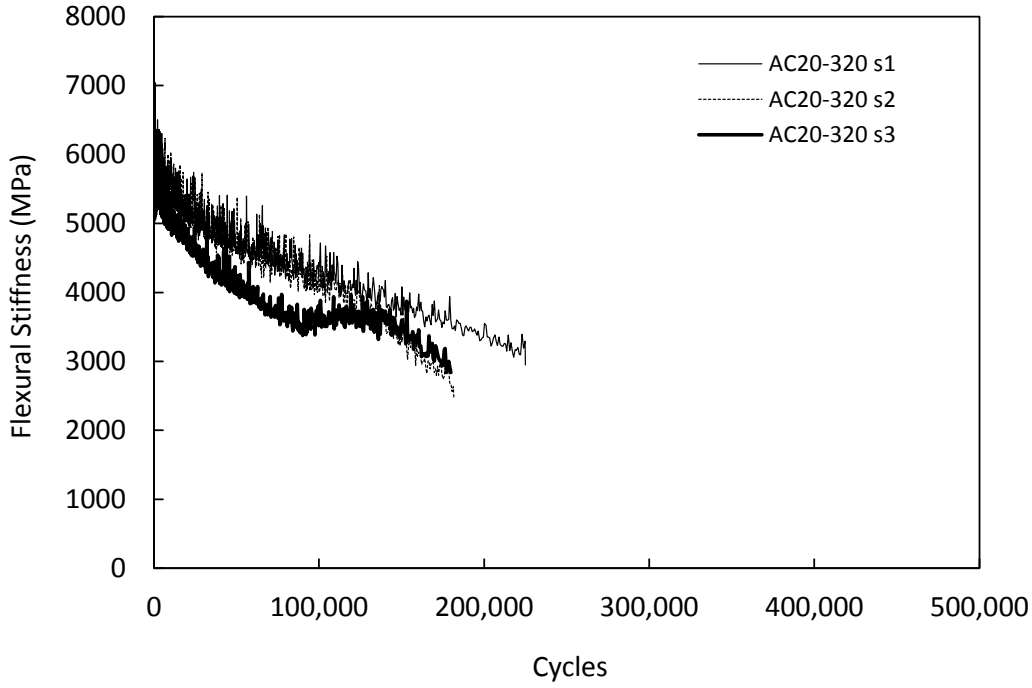

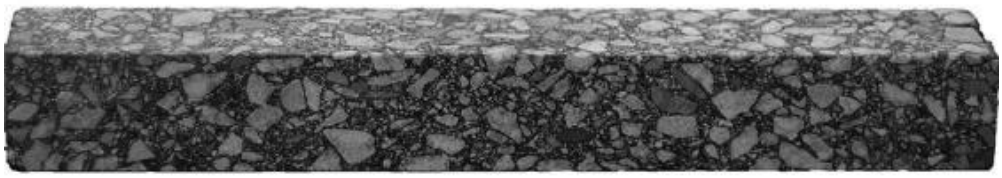

D.4 Typical beam fatigue test report from IPC UTM21 Software

FileName: D:\Experiment Data\UTM_21 BF\Data\Afiq\Beam1.B21

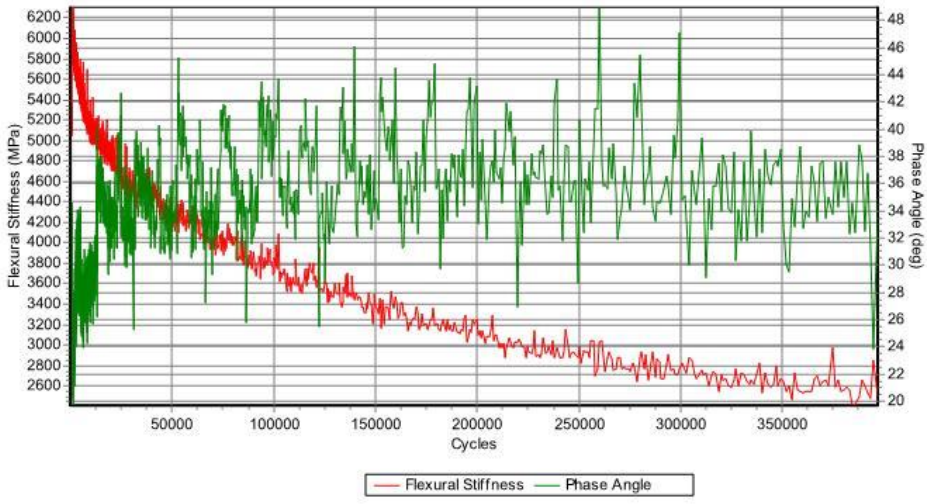

Test start date and time: Saturday, June 26, 2010, at 11:44 AM

Cycle count: 396840 of 1000000

Loading time (hh:mm:ss):	11:01:24	Maximum tensile stress (kPa):	969	Initial dissipated energy (kPa):	0.216
Applied Load (kN):	0.440	Maximum tensile micro-strain:	395	Dissipated energy (kPa):	0.191
Maximum load (kN):	0.137	Initial flexural stiffness (MPa):	4996	Cumulative dissipated energy (MPa):	86.731
Minimum load (kN):	-0.303	Flexural stiffness (MPa):	2455	Initial core temperature (°C):	20.3
Beam deflection (mm):	0.211	Termination stiffness (MPa):	2498	Initial skin temperature (°C):	20.2
Maximum LVDT (mm):	0.106	Modulus of elasticity (MPa):	2616	Core temperature (°C):	23.2
Minimum LVDT (mm):	0.001	Phase angle (deg):	34.9	Skin temperature (°C):	23.3

Operator: Afiq

Notes/comments: Beam 1, Mix 10mm Heavy Duty, Standard Test

Specimen Information

Identification: 10mm_beam1

Core/Sample Number: 1

Dimensions	Point 1	Point 2	Point 3	Point 4	Point 5	Average	Std Dev.
Width (mm)	63.51	64.05	64.27	63.94	63.86	63.926	0.2789803
Height (mm)	49.82	50.07	50.19	50.46	50.61	50.23	0.313289
Length (mm)	400					400	

Cross-Sectional Area: 25570.4

Volume: 1284401

Comments/Properties: Mix 10mm Heavy Duty, Beam 1 - Standard test

Setup Parameters

Gauge lengths		Loading conditions		Termination conditions	
Inside clamps (mm):	118.5	Control Mode:	Haversine strain	Termination stiffness (MPa):	2498
Outside clamps (mm):	355.5	Pulse width (ms):	100	Stop test after cycle:	1000000
		Peak to peak micro-strain:	400		
Default Poisson ratio:	0.4	Conditioning cycles:	200		

Calibration Information

Channel description	Filename	Transducer description	Span	Units	Date	Linearised
A: Axial Force	Y12346.CAR	STC5000 S/N: Y12346 +/-20kN	40	kN	07/12/05	No
B: Actuator LVDT	941C-340.CAR	AC-15 S/N: M992941C-340 +/-15mm	30	mm	07/12/05	No
C: On Specimen LVDT		Default Auxiliary LVDT	1	mm		No
D: Core Temperature	507.car	PT100 S/N: 507 -15 to +85 0 deg = 0 bits	100	Deg.C	13/12/06	Yes
E: Skin Temperature	506.car	PT100 S/N: 506 -15 to +85 0 deg = 0 bits	100	Deg.C	13/12/06	Yes

30/04/2014 8:40:17 AM **UTM_21 V2.01 Beam Fatigue Test**

Appendix E – Dynamic Modulus Test Results

E.1 Dynamic Moduli AC10-170

AC10-170													
Air void		3.2%				5.3%				7.3%			
V_{beff}		11.5				11.3				11.0			
VMA		15.8				17.6				19.4			
VFA		79.6				69.8				62.1			
		Dynamic Modulus		Phase Angle		Dynamic Modulus		Phase Angle		Dynamic Modulus		Phase Angle	
t °C	f Hz	|E*| MPa	*CV* %	ϕ °	*Sy*	|E*| MPa	*CV* %	ϕ °	*Sy*	|E*| MPa	*CV* %	ϕ °	*Sy*
4	0.1	7070	8.84	20.7	3.07	6986	8.13	20.1	0.65	5419	3.31	22.2	0.06
4	0.5	9477	6.16	15.1	1.07	9365	5.44	15.5	0.55	7564	3.48	17.1	0.08
4	1	10627	4.27	13.6	1.47	10347	4.25	14.0	0.47	8504	3.48	15.3	0.03
4	5	13043	2.93	9.4	0.66	12700	2.91	11.0	0.36	10720	3.29	12.0	0.01
4	10	14043	2.79	8.0	0.63	13674	2.77	10.0	0.30	11622	2.65	10.8	0.02
4	25	15410	2.80	5.8	0.10	15004	2.78	8.7	0.26	12790	2.23	9.4	0.08
20	0.1	1096	8.13	39.3	4.54	1078	8.07	37.8	0.29	777	8.45	39.0	0.67
20	0.5	2260	8.54	34.4	4.10	2221	8.57	34.5	0.35	1666	9.13	35.9	0.64
20	1	2950	8.56	31.9	3.97	2901	8.56	32.5	0.37	2208	9.45	34.1	0.71
20	5	4924	7.94	24.6	1.47	4840	7.95	27.0	0.46	3801	9.10	28.5	0.59
20	10	5897	7.28	22.9	2.24	5797	7.28	24.7	0.46	4582	8.58	26.1	0.54
20	25	7306	6.27	19.9	2.15	7182	6.28	21.5	0.47	5732	7.40	22.6	0.41
40	0.1	110	4.52	28.5	1.84	79	3.69	28.3	1.47	50	0.42	28.2	0.95
40	0.5	196	7.60	35.7	0.88	147	1.54	37.2	1.17	95	1.41	36.8	0.97
40	1	258	4.39	39.0	0.86	223	4.25	38.4	0.11	135	1.57	40.4	1.10
40	5	697	3.35	39.5	1.11	555	2.59	40.5	0.31	381	0.32	41.2	0.80
40	10	965	1.10	40.3	1.73	802	1.13	41.4	0.10	544	0.61	43.1	0.88
40	25	1476	6.32	37.5	3.52	1328	1.54	39.5	0.66	951	1.34	41.2	1.63
55	0.1	48	20.6	26.8	0.79	46	3.07	20.0	0.98	52	30.2	25.2	1.10
55	0.5	73	1.72	25.3	4.27	58	10.9	22.5	0.23	51	2.65	22.2	3.23
55	1	88	5.66	27.0	1.36	66	18.4	26.6	0.81	49	26.2	27.4	0.42
55	5	175	5.66	35.0	4.74	142	2.69	31.9	0.37	127	18.6	32.0	0.27
55	10	232	2.44	38.5	2.02	186	2.70	36.5	0.82	157	23.6	38.6	0.04
55	25	379	1.49	39.7	6.02	342	2.03	36.3	1.29	296	16.4	35.6	0.04

E.2 Dynamic Moduli AC10-320

AC10-320													
Air void		3.8%				5.4%				7.0%			
V_{beff}		11.4%				11.3%				11.1%			
VMA		16.3%				17.7%				19.1%			
VFA		76.5%				69.5%				63.2%			
		Dynamic Modulus		Phase Angle		Dynamic Modulus		Phase Angle		Dynamic Modulus		Phase Angle	
t °C	f Hz	|E*| MPa	CV %	ϕ °	Sy	|E*| MPa	CV %	ϕ °	Sy	|E*| MPa	CV %	ϕ °	Sy
4	0.1	8255	7.47	17.6	1.32	7488	7.47	19.2	1.44	6384	3.32	22.0	0.36
4	0.5	11180	6.09	12.3	0.75	10141	6.09	14.1	0.86	8911	3.48	16.8	0.11
4	1	12288	3.79	10.5	0.40	11146	3.79	12.3	0.47	10019	3.48	13.7	1.25
4	5	15122	3.27	7.0	0.23	13716	3.27	8.2	0.27	12629	3.29	10.6	0.53
4	10	16304	2.61	4.8	0.13	14788	2.61	6.8	0.18	13691	2.65	8.8	0.41
4	25	17829	2.80	3.5	0.10	16171	2.80	6.9	0.19	15067	2.22	5.8	1.10
20	0.1	1455	5.79	33.0	1.91	1332	5.84	39.2	2.29	955	8.44	39.0	4.23
20	0.5	3055	8.96	31.3	2.80	2797	8.95	32.2	2.88	2047	9.16	35.0	3.21
20	1	3981	8.65	29.0	2.51	3646	8.67	29.3	2.54	2713	9.44	33.4	1.72
20	5	6643	8.04	23.0	1.85	6083	8.04	23.8	1.91	4669	9.09	25.7	3.01
20	10	7951	6.81	18.2	1.24	7281	6.81	19.7	1.34	5630	8.58	24.1	1.36
20	25	9871	5.71	13.6	0.78	9039	5.71	17.4	0.99	7042	7.41	19.7	2.20
40	0.1	126	5.61	31.0	1.74	101	5.60	32.5	1.82	90	7.86	31.3	2.46
40	0.5	232	1.22	36.0	0.44	187	1.51	37.3	0.56	118	3.01	32.8	1.78
40	1	343	3.92	40.1	1.57	284	4.24	39.5	1.68	168	3.80	35.9	1.46
40	5	753	2.91	43.0	1.25	703	2.82	39.3	1.11	487	1.16	39.4	2.26
40	10	1094	0.71	37.0	0.26	1021	0.69	39.3	0.27	696	0.61	40.8	0.34
40	25	1738	7.04	37.0	2.61	1623	7.02	35.9	2.52	1216	2.85	38.2	1.58
55	0.1	53	16.01	19.0	3.04	51	15.4	26.4	4.07	43	3.29	20.5	1.06
55	0.5	70	3.05	22.0	0.67	66	5.40	27.6	1.49	61	2.32	26.7	0.62
55	1	81	3.49	32.0	1.12	77	3.67	31.4	1.15	71	3.01	26.9	3.04
55	5	179	1.58	35.0	0.55	184	2.70	36.3	0.98	155	17.3	36.8	7.17
55	10	229	0.31	37.0	0.11	242	1.75	38.9	0.68	191	23.7	37.6	8.91
55	25	387	1.10	39.0	0.43	441	2.41	40.4	0.97	360	16.5	40.9	7.52

E.3 Dynamic ModuliAC14-320

AC14-320													
Air void		5.1%				6.2%				7.3%			
V_{beff}		9.8%				9.7%				9.6%			
VMA		15.9%				16.9%				17.9%			
VFA		68.1%				63.5%				59.3%			
		Dynamic Modulus		Phase Angle		Dynamic Modulus		Phase Angle		Dynamic Modulus		Phase Angle	
t °C	f Hz	|E*| MPa	CV %	ϕ °	Sy	|E*| MPa	CV %	ϕ °	Sy	|E*| MPa	CV %	ϕ °	Sy
4	0.1	11732	10.47	13.7	0.58	9342	5.03	16.1	0.46	7418	2.40	17.3	0.06
4	0.5	15174	10.58	9.5	0.45	11939	4.89	12.4	0.54	9594	2.29	13.4	0.04
4	1	16674	10.59	7.7	0.12	13095	4.84	11.2	0.54	10542	2.28	12.1	0.02
4	5	17062	3.41	7.3	0.04	15615	4.37	8.9	0.43	12666	2.03	9.7	0.13
4	10	18250	2.95	6.3	0.12	16613	4.01	8.1	0.39	13550	2.49	8.9	0.20
4	25	19782	2.35	4.6	0.39	17923	4.09	7.2	0.45	14690	3.10	7.7	0.21
20	0.1	2722	12.73	31.6	0.81	2035	2.54	33.2	0.06	1719	0.12	33.8	0.28
20	0.5	4793	12.46	27.5	0.47	3568	2.24	28.9	0.03	3027	0.40	29.5	0.35
20	1	5844	12.48	23.6	0.25	4354	2.10	27.2	0.06	3690	0.38	27.8	0.34
20	5	8805	12.18	18.6	0.65	6546	1.63	22.2	0.05	5561	0.69	22.7	0.33
20	10	10187	11.89	16.2	0.46	7623	1.01	20.2	0.02	6436	0.98	20.6	0.33
20	25	12214	11.78	13.2	0.45	9136	0.26	17.5	0.01	7716	1.08	17.9	0.32
40	0.1	180	14.26	35.6	0.46	135	5.02	33.4	0.75	110	1.42	33.9	0.23
40	0.5	390	12.35	38.8	0.51	291	5.92	38.3	0.81	237	0.51	38.6	0.16
40	1	567	11.96	38.7	0.34	435	3.62	38.5	0.18	345	0.90	39.7	0.13
40	5	1374	11.66	36.3	0.08	1047	3.31	37.4	0.18	835	1.20	38.0	0.28
40	10	1934	11.65	34.5	0.55	1475	2.54	36.8	0.23	1164	1.21	37.8	0.09
40	25	2960	11.16	30.9	0.21	2241	1.58	35.0	0.58	1782	1.71	36.0	0.01
55	0.1	63	4.33	26.6	0.47	52	0.41	19.3	0.23	53	44.4	28.3	11.5
55	0.5	91	1.64	29.0	1.13	72	0.98	26.7	0.01	56	14.5	26.8	0.59
55	1	114	2.20	32.6	0.76	88	2.80	30.9	0.57	70	10.7	31.7	1.21
55	5	302	4.94	37.8	0.52	228	2.45	34.6	0.65	184	7.94	35.2	1.48
55	10	412	4.11	38.8	0.47	310	2.14	38.0	0.64	252	8.77	38.8	1.94
55	25	757	7.46	40.0	0.21	554	0.65	36.3	0.18	462	5.42	36.5	0.73

Moduli AC20-320

4.1%				5.2%				6.1%				6	
10.0%				9.9%				9.8%				9	
14.6%				15.5%				16.3%				1	
71.8%				66.5%				62.9%				5	
Dynamic Modulus		Phase Angle		Dynamic Modulus		Phase Angle		Dynamic Modulus		Phase Angle		Dynamic Modulus	
*E**| Pa	CV %	ϕ °	S_y	|*E**| MPa	CV %	ϕ °	S_y	|*E**| MPa	CV %	ϕ °	S_y	|*E**| MPa	CV %
387	6.43	16.3	0.59	9871	1.50	15.9	0.16	8004	16.3	17.4	0.45	6733	4.6
376	3.94	12.5	0.19	12481	2.50	12.2	0.01	10355	14.2	13.2	0.02	9445	1.1
557	2.43	11.3	0.09	13394	3.17	11.0	0.06	11333	13.9	11.9	0.01	11011	8.2
337	1.77	9.0	0.04	15826	3.43	8.8	0.09	13599	13.7	9.3	0.18	13450	1.7
415	1.63	8.3	0.00	16817	3.15	7.9	0.16	14483	14.2	8.5	0.13	14595	1.6
899	1.21	7.3	0.14	18105	3.34	6.8	0.40	15633	14.1	7.4	0.21	15710	1.2
834	0.84	32.8	0.18	2408	0.91	32.1	0.39	1692	12.9	33.9	0.37	1614	1.0
904	1.59	28.5	0.15	4165	0.44	27.8	0.37	3044	14.4	30.0	0.02	2842	1.0
913	2.34	26.8	0.16	5031	0.84	26.2	0.43	3759	14.6	28.3	0.01	3465	1.0
857	2.79	21.8	0.18	7436	1.21	21.3	0.41	5758	14.7	23.1	0.06	5436	1.0
220	2.77	19.7	0.21	8548	1.75	19.3	0.41	6736	15.3	21.0	0.08	6418	1.0
281	2.62	16.9	0.15	10078	1.58	16.5	0.26	8147	15.5	18.1	0.16	7695	1.0
198	2.66	32.1	0.48	167	5.03	31.8	0.95	111	18.1	31.0	3.00	101	5.2
417	1.66	36.9	1.08	357	4.97	36.5	1.27	232	15.6	36.9	2.74	176	6.0
619	0.59	37.3	0.88	546	8.22	36.4	0.04	352	11.6	37.1	1.25	289	2.2
478	0.76	36.5	0.81	1286	8.36	36.1	0.23	871	9.6	36.9	0.42	621	0.7
058	1.84	36.1	0.64	1810	8.32	35.4	0.47	1227	10.3	36.7	0.02	836	0.7
091	2.64	34.7	0.53	2709	8.22	33.9	0.76	1924	8.3	34.9	0.93	1284	0.7
68	6.11	20.0	0.15	53	34.3	17.9	2.71	49	15.6	19.2	2.72	43	1.0
95	8.37	26.9	0.48	84	21.4	29.8	3.40	66	10.5	25.9	2.92	60	6.1
120	11.2	30.4	0.60	116	15.9	32.5	2.65	79	9.19	30.0	2.62	84	4.6
296	6.77	33.3	0.91	300	13.2	35.1	2.18	204	7.07	32.9	1.99	141	2.8
393	2.51	36.7	0.59	412	12.3	38.1	1.57	273	5.53	36.9	1.90	169	1.7
730	1.16	35.0	0.62	752	6.09	35.9	0.02	496	4.66	35.2	0.54	268	5.3

E.5 Dynamic Moduli Test AC20-320 BC

AC20-320 BC													
Air void		2.9%				4.3%				5.0%			
V_{beff}		10.9%				10.7%				10.7%			
VMA		14.9%				16.1%				16.7%			
VFA		80.4%				73.3%				70.0%			
		Dynamic Modulus		Phase Angle		Dynamic Modulus		Phase Angle		Dynamic Modulus		Phase Angle	
t °C	f Hz	|E*| MPa	CV %	ϕ °	Sy	|E*| MPa	CV %	ϕ °	Sy	|E*| MPa	CV %	ϕ °	Sy
4	0.1	10780	7.85	16.1	0.52	9054	1.05	17.3	0.51	8569	2.79	16.7	0.26
4	0.5	13801	9.23	12.4	0.26	11979	0.96	13.7	0.30	11063	2.86	12.8	0.13
4	1	15071	9.29	11.3	0.24	13316	0.39	12.0	0.23	12110	2.86	11.5	0.06
4	5	18073	8.96	9.1	0.17	16355	0.57	10.0	0.38	14498	3.33	9.1	0.01
4	10	19271	9.29	8.3	0.18	17641	0.41	8.7	0.27	15514	3.51	8.3	0.11
4	25	20879	9.64	7.3	0.01	19161	0.24	7.7	0.12	16765	3.90	7.3	0.27
20	0.1	2404	2.59	32.7	0.29	1952	1.85	33.7	0.52	1852	4.73	33.8	0.56
20	0.5	4280	4.18	28.7	0.66	3460	1.17	29.4	0.78	3288	2.41	29.7	0.66
20	1	5217	4.97	27.0	0.79	4231	2.36	27.6	0.77	4027	1.95	27.9	0.59
20	5	7805	6.43	21.9	0.81	6388	4.21	22.5	0.75	6123	1.11	22.7	0.47
20	10	9032	6.95	19.8	0.80	7438	5.36	20.4	0.75	7110	1.02	20.5	0.50
20	25	10841	7.44	17.2	0.73	8955	7.28	17.6	0.72	8533	0.73	17.7	0.63
40	0.1	187	9.44	30.3	0.28	132	7.29	32.0	0.13	116	2.69	33.9	1.30
40	0.5	364	9.88	36.6	0.56	282	6.22	36.7	0.43	261	0.92	38.4	0.99
40	1	548	10.69	36.4	0.48	414	4.39	37.7	0.00	391	0.02	39.1	1.26
40	5	1311	9.49	36.4	0.33	998	4.34	37.3	0.62	969	0.70	37.7	0.95
40	10	1859	9.63	35.8	0.28	1398	3.69	36.9	0.78	1361	0.47	37.6	0.78
40	25	2822	9.60	34.5	0.08	2117	2.77	35.3	1.12	2060	0.48	36.4	0.45
55	0.1	81	7.55	18.8	0.08	52	9.23	20.0	0.40	41	0.87	19.9	0.57
55	0.5	113	5.70	25.3	0.30	75	6.92	26.9	0.54	57	0.12	27.0	0.13
55	1	139	8.21	29.2	0.18	92	5.69	30.9	0.83	69	0.20	31.1	0.01
55	5	335	8.64	32.7	0.06	239	2.60	33.6	0.87	190	3.13	34.2	0.56
55	10	450	6.73	36.0	0.24	328	2.57	37.0	0.87	261	4.11	38.0	0.52
55	25	775	5.72	34.9	0.27	588	3.48	34.7	0.38	488	7.18	35.5	0.18

E.6 Typical dynamic modulus test report from IPC UTS 006 Software

Data file name: D:\Experiment Data\UTS 006 DMT\Data\20IC MRWA\G60\20 IC G60 S2 20deg.D006
Project name: 20mm MRWA Intermediate Course
Target test temperature (°C): 20
Operators name: GW
Target confining stress (kPa): 0
Loading Rates: 25 Hz,10 Hz,5 Hz,1 Hz,0.5 Hz,0.1 Hz
Comments: 20IC MRWA Gyration 60cycles 20 degrees - sample 2

Specimen Information

Identification: 20 IC G60 S2
Conditioning time: 4 hours
Properties/Comments: 20IC MRWA Gyration 60c

Dimensions	Point 1	Point 2	Point 3	Point 4	Point 5	Point 6	Average	Std Dev.
Diameter (mm)	100.5	100.2	100.0	100.8	100.4	100.5	100.4	0.276
Height (mm)re	150.5m	150.9	150.8	151.0	150.6	150.5	150.7	0.214

Cross-sectional area (mm²): 7916.9

Test Data [0.1 Hz Plots]

Test date and time: Sat, Jul 23, 2011, 9:03 PM
Dynamic modulus (MPa): 2392
Phase angle (degrees): 32.35
Average temperature (°C): 20.4
Average confining pressure (kPa): 0.1
Warnings:

Drift for the applied load (%): 0.0
Standard error for the applied load (%): 0.6
Average drift for the deformations (%): -213.1
Average standard error for the deformations (%): 2.8
Uniformity coefficient for the deformations (%): 27.0
Uniformity coefficient for the deformation phase angles (degrees): 1.3

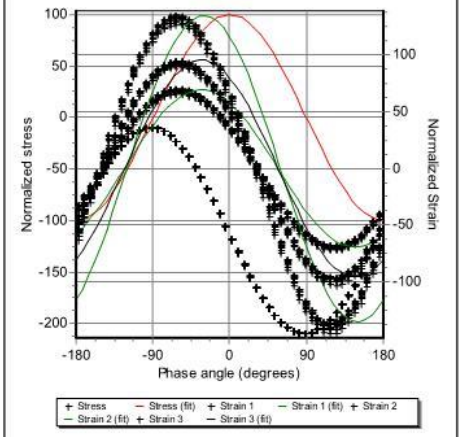

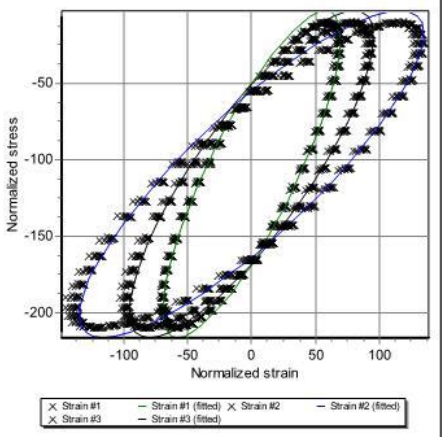

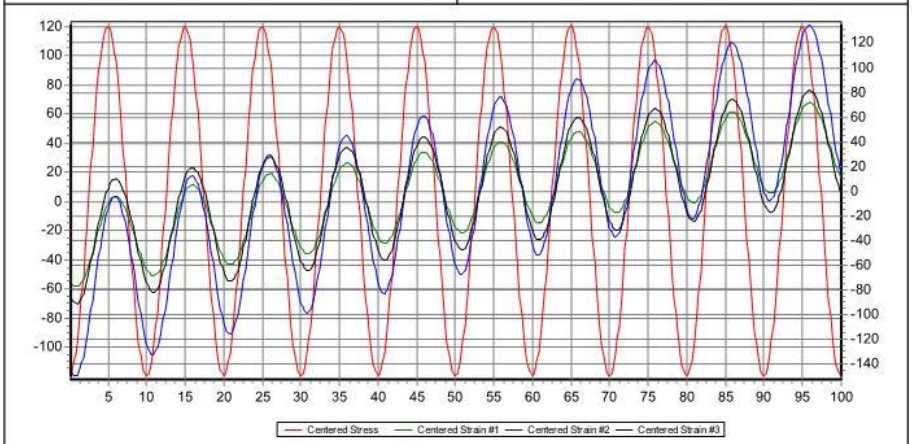

UTS006 2.18 SPT Dynamic Modulus Test
Print date: 30/04/2014 8:51:57 AM

Data file name: D:\Experiment Data\UTS 006 DMT\Data\20IC MRWA\G60\20 IC G60 S2 20deg.D006

Project name: 20mm MRWA Intermediate Course — Target test temperature (°C): 20

Operators name: GW — Target confining stress (kPa): 0

Loading Rates: 25 Hz,10 Hz,5 Hz,1 Hz,0.5 Hz,0.1 Hz

Comments: 20IC MRWA Gyration 60cycles 20 degrees - sample 2

Specimen Information

Identification: 20 IC G60 S2

Conditioning time: 4 hours

Properties/Comments: 20IC MRWA Gyration 60cycles 20 degrees - sample 2

Dimensions	Point 1	Point 2	Point 3	Point 4	Point 5	Point 6	Average	Std Dev.
Diameter (mm)	100.5	100.2	100.0	100.8	100.4	100.5	100.4	0.276
Height (mm)	150.5	150.9	150.8	151.0	150.6	150.5	150.7	0.214

Cross-sectional area (mm²): 7916.9

Tabulated Results Summary

	25 Hz	10 Hz	5 Hz	1 Hz	0.5 Hz	0.1 Hz
Dynamic modulus (MPa)	9965	8442	7372	5001	4152	2392
Phase angle (Degrees)	16.67	19.56	21.58	26.49	28.09	32.35
Average temperature (°C)	20.3	20.3	20.3	20.3	20.4	20.4
Average confining pressure (kPa)	0.1	0.1	0.1	0.1	0.1	0.1
Average micro-strain	41	67	79	88	94	100
Load drift (%)	1.3	1.0	1.8	1.2	-0.3	0.0
Load standard error (%)	5.3	3.6	3.7	4.5	5.1	0.6
Average deformation drift (%)	-314.2	-248.8	-233.1	-300.0	-245.3	-213.1
Average deformation standard error (%)	8.6	5.9	5.6	6.6	6.3	2.8
Deformation uniformity (%)	40.5	34.3	31.2	29.6	28.1	27.0
Phase uniformity (Degrees)	1.3	1.0	0.9	0.8	0.8	1.3

E.7 Examples of dynamic modulus master curve generation

Data: AC10-320 5% air void

	Specimen 1	*Specimen 2*	*Specimen 3*	average	
Air void (%)	5.2	5.2	5.0	**5.2**	
Bit.Content (%)	5.4	5.4	5.4	**5.4**	
Bit.Volume (%)	12.26	12.27	12.29	**12.27**	V_{beff} = **11.60**
VMA	17.5	17.47	17.31	**17.43**	
VFA	70.05	70.20	70.98	**70.41**	

temp	freq	$\|E^*\|$	ϕ	$\|E^*\|$	ϕ	$\|E^*\|$	ϕ	*average* $\|E^*\|$		*average* ϕ	
°C	Hz	MPa	deg	MPa	deg	Mpa	deg	MPa	*CV*	deg	*Sy*
4	0.1	8660	17.65	8563	17.45	8135	16.58	8453	3.3	17.2	0.57
4	0.5	10590	12.83	11097	13.44	10542	12.77	10743	2.9	13.0	0.37
4	1	11818	12.06	11641	11.88	11059	11.28	11506	3.5	11.7	0.41
4	5	13704	8.96	13624	8.91	12943	8.47	13424	3.1	8.8	0.27
4	10	14621	7.81	14411	7.70	13691	7.31	14241	3.4	7.6	0.26
4	25	16825	5.35	16606	5.28	15610	4.97	16347	4.0	5.2	0.20
20	0.1	1843	30.15	2634	43.08	1894	30.98	2124	20.8	34.7	7.24
20	0.5	3130	24.85	4615	36.64	3279	26.03	3675	22.3	29.2	6.49
20	1	3672	23.01	5443	34.10	3882	24.32	4332	22.3	27.1	6.06
20	5	5560	18.09	8011	26.06	6090	19.81	6554	19.7	21.3	4.19
20	10	8742	18.84	8495	18.31	7410	15.97	8216	8.6	17.7	1.53
20	25	10094	14.51	9974	14.34	9872	14.19	9980	1.1	14.3	0.16
40	0.1	127	32.83	115	29.73	136	35.15	126	8.4	32.6	2.72
40	0.5	274	36.91	269	36.24	291	39.20	278	4.1	37.5	1.55
40	1	408	39.48	427	41.32	448	43.35	428	4.7	41.4	1.94
40	5	868	36.93	890	37.87	1039	44.21	932	10.0	39.7	3.96
40	10	1177	34.70	1232	36.32	1477	43.55	1295	12.3	38.2	4.71
40	25	2057	37.50	1974	35.98	2126	38.75	2052	3.7	37.4	1.39
55	0.1	56	24.69	43	19.25	39	17.29	46	18.8	20.4	3.83
55	0.5	75	24.80	81	26.79	94	31.09	83	11.7	27.6	3.21
55	1	96	30.03	103	32.22	116	36.29	105	9.7	32.8	3.18
55	5	217	38.22	231	40.68	193	33.90	214	9.1	37.6	3.43
55	10	378	53.74	223	31.65	213	30.23	271	34.2	38.5	13.18
55	25	538	41.88	516	40.17	474	36.90	509	6.4	39.7	2.53

E.7.1 Sigmoidal function based on AASHTO PP 61 (AASHTO 2010a)

Limiting maximum modulus $|E^*|_{max}$

$$P_c = \frac{\left(20 + \frac{435{,}000\,VFA}{VMA}\right)^{0.58}}{650 + \left(\frac{435{,}000\,VFA}{VMA}\right)^{0.58}} = \frac{\left(20 + \frac{435{,}000 \times 17.43}{70.41}\right)^{0.58}}{650 + \left(\frac{435{,}000 \times 17.43}{70.41}\right)^{0.58}} = 0.8654$$

$$|E^*|_{max} = P_c\left[4200\left(1-\frac{VMA}{100}\right)+435{,}000\left(\frac{VFA\times VMA}{10{,}000}\right)+\frac{1-P_c}{\frac{1-VMA/100}{4{,}200{,}000}+\frac{VMA}{435{,}000\,VFA}}\right]$$

$$= 0.8654\left[4200\left(1-\frac{17.43}{100}\right)+435{,}000\left(\frac{17.43\times 70.41}{10{,}000}\right)+\frac{1-P_c}{\frac{1-17.43/100}{4{,}200{,}000}+\frac{17.43}{435{,}000\,(17.43)}}\right]$$

$|E^*|_{max}$ 3220.8 ksi = 22206.5 MPa; Log $|E^*|_{max}$ = 3.508 ksi

Reference Temperature (T_r) = 20°C = 293.15 °K

Numerical Optimisation

Initial fitting parameters

δ = 0.5
β = -1
γ = -0.5
ΔE_a = 200,000

Fitting parameters (solved using Solver function in MS Excel)

δ = 0.27
β = -1.25
γ = -0.61
ΔE_a = 190968

S_e = 0.09
S_y = 0.66
S_e/S_y = 0.13
R^2 = 0.97

$$\log f_r = \log f + \log a_T \qquad \log a_T = \frac{\Delta E_a}{19.14714}\left(\frac{1}{T}-\frac{1}{T_r}\right) \qquad \log|E^*| = \delta + \frac{\left(|E^*|_{Max}-\delta\right)}{1+e^{\beta+\gamma\log f_r}}$$

T °C	f Hz	T °K	log fr Hz	fr Hz	Log a_T Hz	measured $\|E^*\|$ MPa	predicted $\|E^*\|$ MPa	log $\|E^*\|$ sq. error
4	0.1	277.15	1.0	9.21E+00	1.964	8453	7968.8	0.001
4	0.5	277.15	1.7	4.60E+01	1.964	10743	11003.7	0.000
4	1	277.15	2.0	9.21E+01	1.964	11506	12265.8	0.001
4	5	277.15	2.7	4.60E+02	1.964	13424	14911.3	0.002
4	10	277.15	3.0	9.21E+02	1.964	14241	15895.4	0.002
4	25	277.15	3.4	2.30E+03	1.964	16347	17041.3	0.000
20	0.1	293.15	-1.0	1.00E-01	0.000	2124	1682.1	0.010
20	0.5	293.15	-0.3	5.00E-01	0.000	3675	3276.7	0.002
20	1	293.15	0.0	1.00E+00	0.000	4332	4206.5	0.000
20	5	293.15	0.7	5.00E+00	0.000	6554	6846.3	0.000
20	10	293.15	1.0	1.00E+01	0.000	8216	8123.4	0.000
20	25	293.15	1.4	2.50E+01	0.000	9980	9857.0	0.000
40	0.1	313.15	-3.2	6.72E-04	-2.173	126	154.4	0.008
40	0.5	313.15	-2.5	3.36E-03	-2.173	278	326.9	0.005
40	1	313.15	-2.2	6.72E-03	-2.173	428	459.4	0.001
40	5	313.15	-1.5	3.36E-02	-2.173	932	1012.2	0.001
40	10	313.15	-1.2	6.72E-02	-2.173	1295	1403.4	0.001
40	25	313.15	-0.8	1.68E-01	-2.173	2052	2110.5	0.000
55	0.1	328.15	-4.6	2.35E-05	-3.629	46	45.7	0.000
55	0.5	328.15	-3.9	1.18E-04	-3.629	83	76.6	0.001
55	1	328.15	-3.6	2.35E-04	-3.629	105	99.5	0.001
55	5	328.15	-2.9	1.18E-03	-3.629	214	198.7	0.001
55	10	328.15	-2.6	2.35E-03	-3.629	271	275.2	0.000
55	25	328.15	-2.2	5.88E-03	-3.629	509	430.2	0.005
							Σ=	0.044

E.7.2 Sigmoidal function based on AASHTO PP 62 (AASHTO 2010b)

Binder characteristic C320 (original)
A = 10.89
VTS= -3.65

Reference Temperature (T_r) = 20°C = 527.67 °R

$$\log\eta = \log^{(A+VTS\log Tr)} = \log^{(10.89-3.65\log 527.67)} = 9.008 \text{ cP}$$

Numerical Optimization

Initial fitting parameters

α = 3000
β = -1
δ = 0.5
γ = -0.5
c = 1

Fitting parameters (solved using Solver function in MS Excel)

α = 2.97
β = -1.46
δ = 0.40
γ = -0.70
c = 1.18

S_e = 0.05
S_y = 0.58
S_e/S_y = 0.08
R^2 = 0.99

$$\log a_T = c\left(\log\eta - \log\eta_{T_R}\right)$$

$$\log\eta = \log^{(A+VTS\log T)} \qquad \log f_r = \log f + \log a_T \qquad \log|E^*| = \delta + \frac{\alpha}{1+e^{\beta+\gamma\log f_r}}$$

T °C	f Hz	T °F	log η cP	log fr Hz	fr Hz	measured $\|E^*\|$ MPa	predicted $\|E^*\|$ MPa	log $\|E^*\|$ sq. error
4	0.1	39.2	11.05	1.0	2.61E+01	8453	9396.2	0.002
4	0.5	39.2	11.05	1.7	1.31E+02	10743	11466.4	0.001
4	1	39.2	11.05	2.0	2.61E+02	11506	12205.0	0.001
4	5	39.2	11.05	2.7	1.31E+03	13424	13565.0	0.000
4	10	39.2	11.05	3.0	2.61E+03	14241	14012.7	0.000
4	25	39.2	11.05	3.4	6.54E+03	16347	14497.2	0.003
20	0.1	68	9.01	-1.0	1.00E-01	2124	1829.8	0.004
20	0.5	68	9.01	-0.3	5.00E-01	3675	3522.7	0.000
20	1	68	9.01	0.0	1.00E+00	4332	4455.2	0.000
20	5	68	9.01	0.7	5.00E+00	6554	6892.0	0.000
20	10	68	9.01	1.0	1.00E+01	8216	7968.2	0.000
20	25	68	9.01	1.4	2.50E+01	9980	9332.2	0.001
40	0.1	104	7.08	-3.2	5.29E-04	126	137.5	0.001
40	0.5	104	7.08	-2.5	2.65E-03	278	295.6	0.001
40	1	104	7.08	-2.2	5.29E-03	428	421.5	0.000
40	5	104	7.08	-1.5	2.65E-02	932	966.5	0.000
40	10	104	7.08	-1.2	5.29E-02	1295	1359.9	0.000
40	25	104	7.08	-0.8	1.32E-01	2052	2071.7	0.000
55	0.1	131	5.97	-4.6	2.58E-05	46	47.6	0.000
55	0.5	131	5.97	-3.9	1.29E-04	83	78.3	0.000
55	1	131	5.97	-3.6	2.58E-04	105	101.7	0.000
55	5	131	5.97	-2.9	1.29E-03	214	207.3	0.001
55	10	131	5.97	-2.6	2.58E-03	271	291.8	0.000
55	25	131	5.97	-2.2	6.44E-03	509	466.9	0.003
							Σ=	0.017

Data shifting

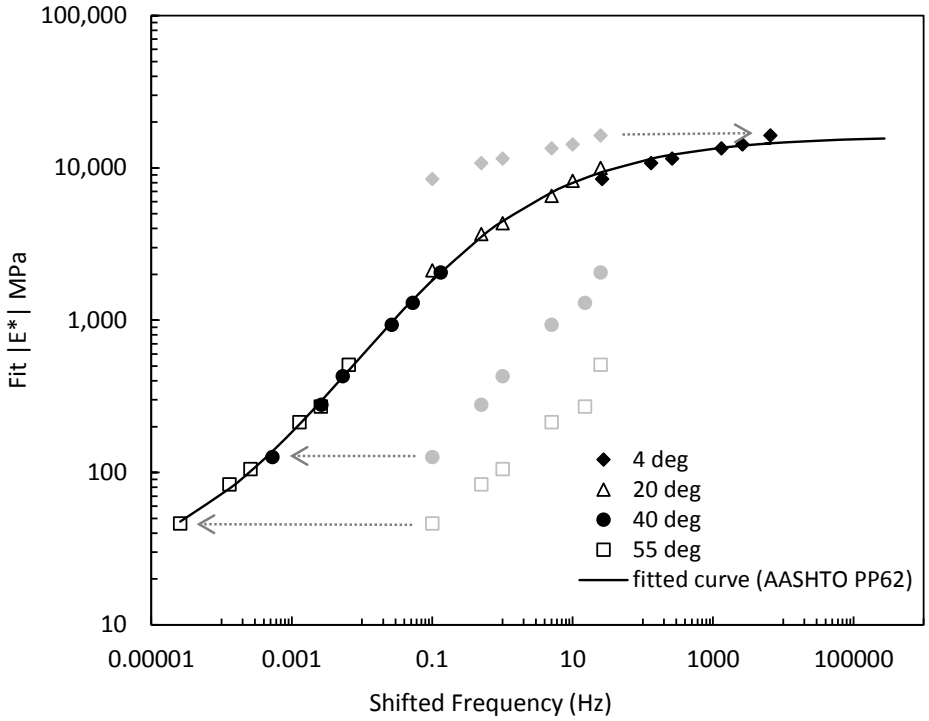

Comparison between the two methods of master curve generation

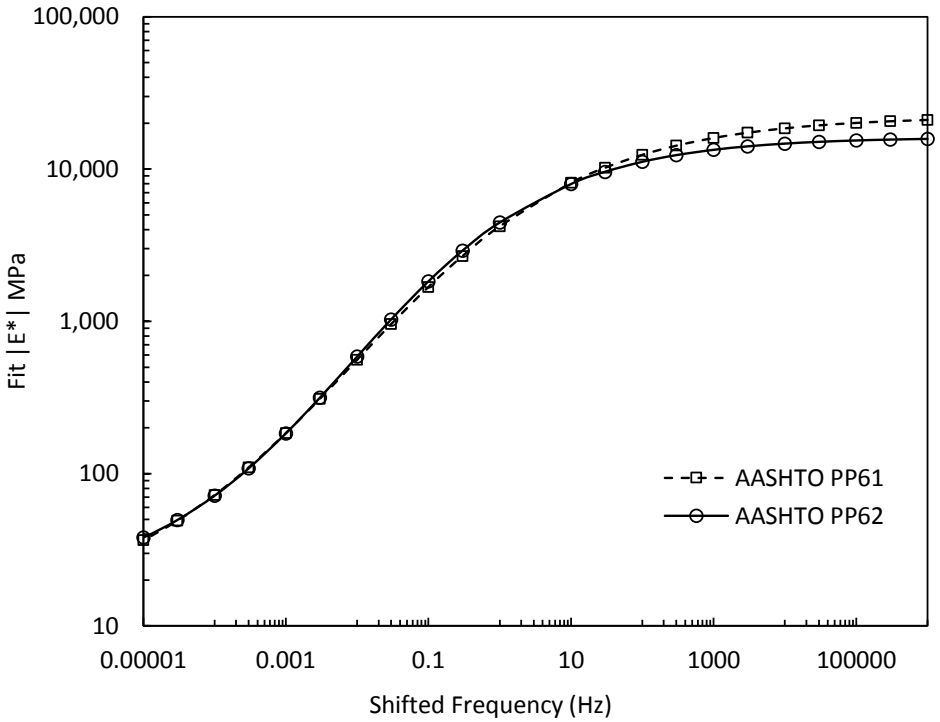

E.7.3 Witczak's predicted |*E**| calculation

Volumetric and aggregate properties:
V_a = 5.2%
V_{beff} = 11.6%
P_{200} = 5.7%
P_4 = 36.7%
$P_{3/8}$ = 1.9%
$P_{3/4}$ = 0%

Bitumen (C320) properties:
A = 10.89
VTS = -3.65

$$\log|E^*| = 1.249937 + 0.029232(P_{200}) - 0.001767(P_{200})^2 - 0.002841(P_4) - 0.058097(V_a) - \frac{0.802208V_{eff}}{V_{eff}+V_a}$$

$$+\frac{3.871977 - 0.0021(P_4) + 0.003958(P_{38}) - 0.000017(P_{38})^2 + 0.00547(P_{34})}{1+e^{(-0.603313 - 0.313351\log(f) - 0.393532\log\eta)}}$$

$$\log\eta = \log^{(A+VTS\log T)}$$

T	f	log η	log f_r	f_r	log |*E**|	|*E**|
°F	Hz	cP	Hz	Hz	ksi	MPa
4	0.1	11.05	1.570	3.72E+01	**2.994**	6793.7
4	0.5	11.05	2.269	1.86E+02	**3.110**	8880.1
4	1	11.05	2.570	3.72E+02	**3.155**	9849.2
4	5	11.05	3.269	1.86E+03	**3.248**	12209.0
4	10	11.05	3.570	3.72E+03	**3.284**	13253.4
4	25	11.05	3.968	9.29E+03	**3.327**	14640.8
20	0.1	9.01	-1.000	1.00E-01	**2.419**	1808.4
20	0.5	9.01	-0.301	5.00E-01	**2.597**	2726.5
20	1	9.01	0.000	1.00E+00	**2.669**	3218.4
20	5	9.01	0.699	5.00E+00	**2.824**	4601.5
20	10	9.01	1.000	1.00E+01	**2.886**	5301.9
20	25	9.01	1.398	2.50E+01	**2.962**	6320.9
40	0.1	7.08	-3.420	3.80E-04	**1.722**	363.8
40	0.5	7.08	-2.721	1.90E-03	**1.930**	587.1
40	1	7.08	-2.420	3.80E-03	**2.019**	720.3
40	5	7.08	-1.721	1.90E-02	**2.221**	1146.2
40	10	7.08	-1.420	3.80E-02	**2.305**	1391.2
40	25	7.08	-1.022	9.50E-02	**2.413**	1783.5
55	0.1	5.97	-4.815	1.53E-05	**1.317**	143.0
55	0.5	5.97	-4.116	7.65E-05	**1.517**	226.6
55	1	5.97	-3.815	1.53E-04	**1.605**	277.7
55	5	5.97	-3.116	7.65E-04	**1.813**	448.0
55	10	5.97	-2.815	1.53E-03	**1.902**	550.5
55	25	5.97	-2.417	3.82E-03	**2.020**	721.6

Fitted curve of the predicted results is determined using the same procedure as E.7.2

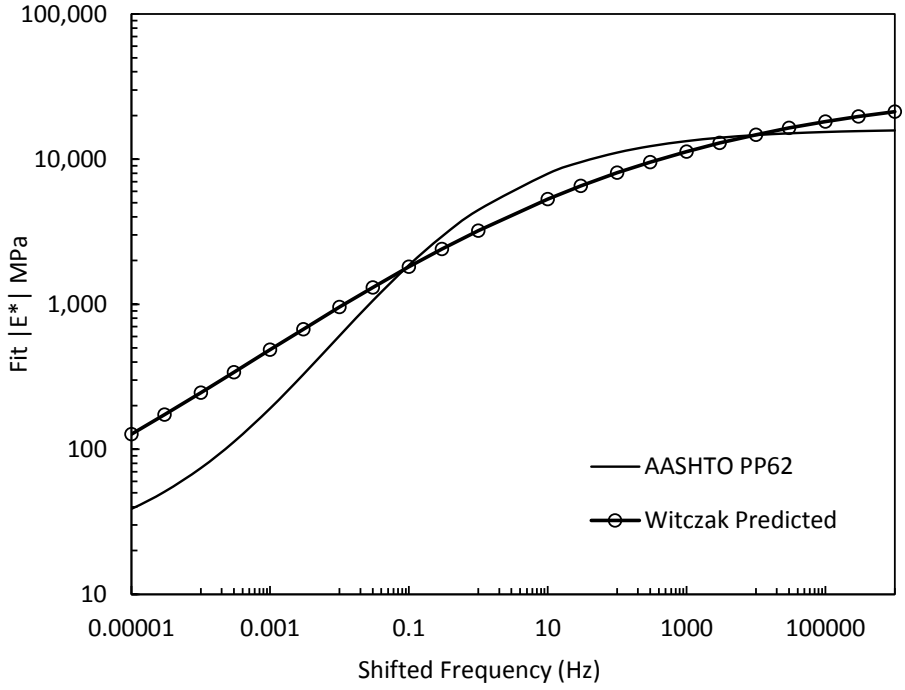

E.7.4 Hirsch's predicted /*E/ calculation**

Bitumen (C320) properties:
A =10.89
VTS =-3.65

The following expressions, as explained in Section 2.5.4.2, are used to calculate |*E**/.

$$\log\log\eta_{f_s,T} = A' + VTS'\log T_R \qquad A' = 0.9699\, f_s^{-0.0527} \times A$$

$$VTS' = 0.9668\, f_s^{-0.0575} \times VTS$$

$$\delta_b = 90 + (b_1 + b_2\, VTS') \times \log(f_s \times \eta_{f_s,T}) + (b_3 + b_4\, VTS') \times \{\log(f_s \times \eta_{f_s,T})\}^2$$

$$|G^*| = 0.0051 f_s \eta_{f_s,T} (\sin\delta_b)^{7.1542 - 0.4929\, f_s + 0.0211\, f_s^2}$$

$$P_c = \frac{\left(20 + \frac{VFA \times 3|G^*|}{VMA}\right)^{0.58}}{650 + \left(\frac{VFA \times 3|G^*|}{VMA}\right)^{0.58}}$$

$$|E^*| = P_c\left[4200\left(1 - \frac{VMA}{100}\right) + 3|G^*|\left(\frac{VFA \times VMA}{10{,}000}\right)\right] + \frac{1 - P_c}{\frac{1 - VMA/100}{4{,}200{,}000} + \frac{VMA}{3 \cdot VFA \cdot |G^*|}}$$

	T °R	A'	VTS'	$\eta_{fs,T}$ cP	δ_b °	$\|G^*\|$ Pa	$\|G^*\|$ Psi	Pc	$\|E^*\|$ ksi	lo
2	498.87	13.13	-4.47	2.90E+11	58.1	7,339,639	1065	0.2713	949.7	
8	498.87	12.06	-4.08	2.77E+11	48.2	13,911,372	2018	0.3503	1230.0	
6	498.87	11.63	-3.92	2.35E+11	44.8	15,909,673	2308	0.3682	1293.9	
0	498.87	10.69	-3.57	1.21E+11	38.4	19,612,408	2845	0.3968	1396.3	
9	498.87	10.30	-3.43	8.26E+10	36.3	23,188,537	3363	0.4203	1480.4	
8	498.87	9.82	-3.26	4.61E+10	34.0	37,714,707	5470	0.4901	1732.7	
2	527.67	13.13	-4.47	8.26E+08	81.0	61,324	8.9	0.0250	86.8	
8	527.67	12.06	-4.08	1.26E+09	71.1	344,600	50	0.0605	210.1	
6	527.67	11.63	-3.92	1.33E+09	67.1	606,730	88	0.0814	283.1	
0	527.67	10.69	-3.57	1.17E+09	58.9	1,671,353	242	0.1367	476.3	
9	527.67	10.30	-3.43	1.01E+09	55.9	2,425,646	352	0.1641	572.2	
8	527.67	9.82	-3.26	7.62E+08	52.1	4,185,873	607	0.2120	740.5	
2	563.67	13.13	-4.47	4.33E+06	90.0	352	0.051	0.0089	30.8	
8	563.67	12.06	-4.08	8.97E+06	85.1	3,548	0.515	0.0102	35.3	
6	563.67	11.63	-3.92	1.11E+07	81.7	8,360	1.21	0.0119	41.4	
0	563.67	10.69	-3.57	1.46E+07	73.8	45,011	6.5	0.0217	75.2	
9	563.67	10.30	-3.43	1.51E+07	70.5	83,596	12.1	0.0291	100.9	
8	563.67	9.82	-3.26	1.46E+07	66.3	181,863	26.4	0.0432	150.1	
2	590.67	13.13	-4.47	2.42E+05	90.0	20	0.0028	0.0088	30.3	
8	590.67	12.06	-4.08	5.55E+05	90.0	225	0.033	0.0088	30.6	
6	590.67	11.63	-3.92	7.32E+05	87.4	590	0.09	0.0090	31.2	
0	590.67	10.69	-3.57	1.15E+06	80.4	4,243	0.62	0.0105	36.2	
9	590.67	10.30	-3.43	1.30E+06	77.2	8,953	1.30	0.0121	42.1	
8	590.67	9.82	-3.26	1.42E+06	73.2	22,540	3.27	0.0162	56.3	

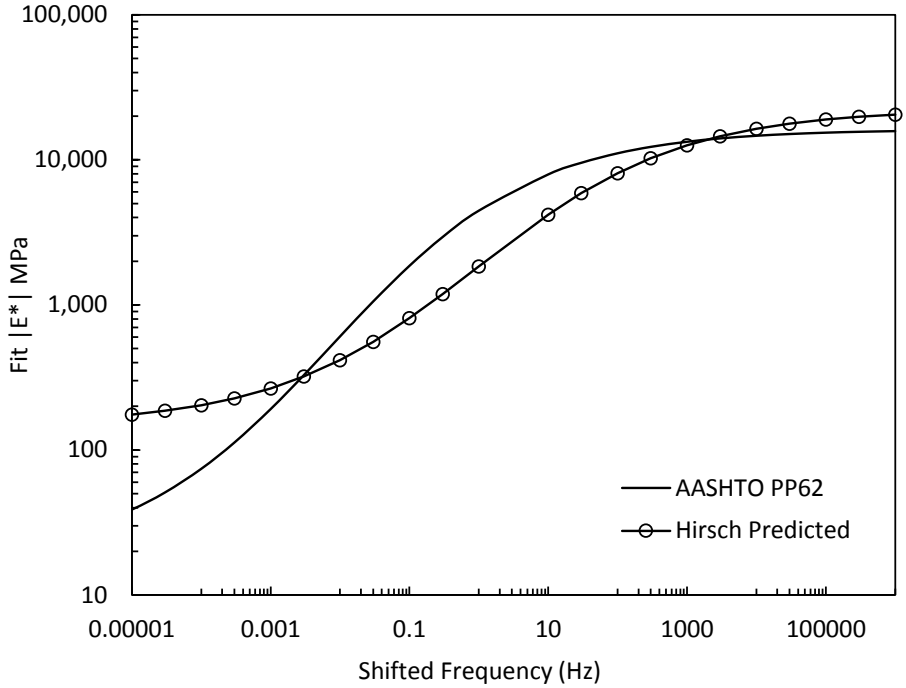
100,000
10,000
1,000
100
10
Fit |E*| MPa
0.00001
0.001
0.1
10
1000
100000
Shifted Frequency (Hz)
AASHTO PP62
Hirsch Predicted